

BIOCHEMICAL AND CELLULAR CHARACTERIZATION OF
REPLICATION FACTOR A (RFA) DURING MEIOSIS AND THE DNA DAMAGE
RESPONSE IN *SACCHAROMYCES CEREVISIAE*

A Dissertation
Submitted to the Graduate Faculty
of the
North Dakota State University
of Agriculture and Applied Science

By

Angela Marie Adsero

In Partial Fulfillment of the Requirements
for the Degree of
DOCTOR OF PHILOSOPHY

Major Program:
Cellular and Molecular Biology

January 2021

Fargo, North Dakota

North Dakota State University
Graduate School

Title

THE BIOCHEMICAL AND CELLULAR CHARACTERIZATION OF
REPLICATION FACTOR A (RFA) DURING MEIOSIS AND THE DNA
DAMAGE RESPONSE IN *SACCHAROMYCES CEREVISIAE*

By

Angela Marie Adsero

The Supervisory Committee certifies that this *disquisition* complies with North Dakota
State University's regulations and meets the accepted standards for the degree of

DOCTOR OF PHILOSOPHY

SUPERVISORY COMMITTEE:

Stuart Haring

Chair

John Wilkinson

Katie Reindl

Yagna Jarajapu

Gary Secor

Approved:

1/14/2021

Date

Katie Reindl

Department Chair

ABSTRACT

Replication Factor A (RFA) is an essential heterotrimeric single-stranded DNA (ssDNA) binding complex, comprised of Rfa1, Rfa2, and Rfa3 in *Saccharomyces cerevisiae*. RFA is required for DNA replication, repair, recombination, and cell cycle regulation. RFA acts as a sensor of ssDNA, a common intermediate of these processes, and coordinates these processes through recruitment of proteins. For example, during the DNA damage response (DDR), RFA-coated ssDNA is necessary for the recruitment and activation of the sensor kinase Mec1. Additional checkpoint proteins, also recruited by RFA, are necessary for the downstream recruitment and activation of the effector kinase Rad53 that ultimately leads to cell cycle arrest. Thus, RFA acts as a bridge to recruit the proteins required for checkpoint regulation in response to DNA damage.

Importantly, cell cycle resumption is contingent on Rad53 deactivation. There are two known scenarios in which Rad53 is deactivated: (1) checkpoint recovery, in which cells resume the cell cycle after DNA repair or (2) checkpoint adaptation, in which cells proceed with the cell cycle despite the continued presence of irreparable DNA damage.

Previous work has demonstrated that cells undergoing checkpoint adaptation display late Rfa2 N-terminal (NT) phosphorylation that is correlated with the inactivation (dephosphorylation) of Rad53. Additionally, the use of *rfa2* NT mutations consistently demonstrate that a negatively charged NT promotes adaptation in all adaptation-deficient strain backgrounds investigated. Interestingly, Rfa2 NT phosphorylation also occurs early during meiosis.

This work demonstrates that: (1) Rfa1-DBD-F participates in protein-protein interactions that are sensitive to DNA damage, (2) Rfa2 phosphorylation increases the DNA damage sensitivity of mutants with deficient DNA damage checkpoints, (3) the Rfa2 NT is required for proper progression through meiosis that appears to be unrelated to RFA functions in replication or DNA repair by homologous recombination (HR), and (4) Rfa2 phosphorylation may regulate Mec1 checkpoint signaling during the DDR to control checkpoint exit and cell cycle resumption. A mechanism is proposed that considers both Rfa1 DBD-F and the Rfa2 NT involvement to initiate HR repair that essentially allows for the continuation of the cell cycle by the delocalization of Mec1.

ACKNOWLEDGEMENTS

I am grateful for the experiences, the challenges presented, and the support from the Haring laboratory that has shaped me into the scientist I have become.

Firstly, I would like to thank my advisor Dr. Stuart Haring and my committee members: Dr. John Wilkinson, Dr. Katie Reindl, Dr. Yagna Jarajapu, and Dr. Gary Secor. My ideas were challenged on numerous occasions and even though sometimes frustrating, this increased my critical thinking and scientific communication skills. I especially would like to thank Stuart for journal clubs, which often involved delving into hypotheses that kept alive an excitement for ongoing research and continued scientific literary investigation.

Secondly, I would like to thank Dr. Timothy Wilson, for providing initial guidance as I started in the Haring lab and for entertaining discussions and continual love and support. I would also like to thank Barbara Senger and Nolan Miles, for their assistance in becoming acquainted with the laboratory as I started my graduate career.

Thirdly, I would like to thank Trevor Baumgartner and Wendy Larson. You were the team that helped me to become a more knowledgeable scientist, a much better writer, and a decent human being. Thank you for always having my back. I would also like to thank Cristian Hernandez and Erin Richards whom I believe I learned just as much from as what I imparted to them. I would also like to thank the individuals that allowed me to gain mentorship experience: Samara Choudhury, Mary (Maggie) Lenertz, Olivia Stiller, Jenna Duttonhefner, Allison Christensen, and Anna Reinholz.

Finally, I would like to thank my family for all their love and support. Knowing that my mom and dad were proud of what I was trying to accomplish kept me dedicated to finishing. While words of encouragement from my sister kept me pressing on through the stressful times.

DEDICATION

For all those to come after, especially Trevor and Wendy. And for Stuart.

TABLE OF CONTENTS

ABSTRACT	iii
ACKNOWLEDGEMENTS	v
DEDICATION	vi
LIST OF TABLES	xiv
LIST OF FIGURES	xv
LIST OF ABBREVIATIONS.....	xix
LIST OF SYMBOLS	xxiii
LIST OF APPENDIX TABLES	xxiv
LIST OF APPENDIX FIGURES.....	xxv
CHAPTER ONE: INTRODUCTION.....	1
Replication Factor A	1
DNA Damage Response.....	2
Meiosis	6
RFA during the DDR and Meiosis	9
Description of Dissertation.....	11
CHAPTER TWO: CRISPR-Cas9.....	13
Introduction	13
Materials and Methods	17
Yeast strains and plasmids.....	17
Vegetative growth and sporulation of cells	21
Qualitative analysis of heteroallelic recombination and chromosome segregation by replica plating	22
Western blotting to detect Cas9 protein	22
Creation of <i>Saccharomyces cerevisiae</i> codon optimized <i>Cas9</i> , <i>ScCas9</i>	23

Results	26
Examination of BLS candidates	26
Creation and verification of actual <i>spo11Δ::Cas9-natMX</i> haploid strains.....	29
Sporulation efficiency of diploid strains on solid sporulation media.....	33
Heteroallelic recombination is only increased when Cas9 is targeted directly to a site that allows for recombinational repair.....	35
In the absence of Spo11, chromosome segregation is unaffected by Cas9 both in the absence and presence of any of the three different gRNAs utilized.....	41
Western blotting reveals Cas9 protein abundance did not increase during meiosis.....	49
Creation of a <i>Saccharomyces cerevisiae</i> codon optimized <i>Cas9</i> , <i>ScCas9</i>	50
Discussion	57
Inability of Cas9 to rescue a Spo11-deficient meiosis	57
Possibility of Cas9 off-target effects to replace Spo11	57
Future directions.....	59
Acknowledgements	59
CHAPTER THREE: DNA BINDING DOMAIN F PARTICIPATES IN DNA- DAMAGE SENSITIVE INTERACTIONS WITH CHECKPOINT PROTEINS.....	60
Introduction	61
Materials and Methods	65
Yeast strains and plasmids.....	65
Plasmid shuffle assay	68
Yeast two hybrid assay	68
Western blotting to investigate Rfa2 protein in a <i>rfa1-t11</i> mutant.....	70
DNA damage spot assay.....	72
Results	72
Plasmid shuffle assay	72

Yeast two-hybrid assay identifies potential protein-protein interactions of DNA-binding domain F (DBD-F)	74
Rfa2 phosphorylation is apparent in DBD-F mutant (<i>rfa1-t11</i>) cells.....	80
DNA damage sensitivity of checkpoint deficient mutants containing <i>rfa2</i> NT phospho-mimetic mutations	83
Discussion	85
Yeast DNA Binding Domain F does not allow for the human RPA complexes to substitute for yeast RFA in yeast cells	85
Yeast two-hybrid identifies novel potential protein interactions involving Rfa1 DBD-F	88
Rfa2 is phosphorylated even when Rfa1 DBD-F is mutated	89
Phospho-mimetic Rfa2 suggests that Rfa2 NT phosphorylation modifies the DNA damage response.....	92
Acknowledgements	96
CHAPTER FOUR: THE RFA2 NT IS REQUIRED FOR MEIOTIC PROGRESSION	97
Introduction	98
Materials and Methods	102
Yeast strains and plasmids.....	102
Vegetative growth and sporulation.....	107
Checkpoint adaptation assay	107
Western blotting for analysis of Rad53 protein and Rfa2 protein.....	108
DNA damage spot assay.....	110
Analysis of qualitative heteroallelic recombination and chromosome segregation by replica plating	110
Analysis of heteroallelic recombination frequency	111
DNA content analysis.....	112
Nuclear division analysis.....	112
Tetrad analysis by dissection and replica plating	113

Results	114
Confirmation of yeast haploid strains.....	114
Rfa2 NT mutants have a more pronounced effect in checkpoint adaptation measured in diploid cells	118
Rfa2 NT mutants recapitulate mitotic DNA damage sensitivities in meiotic yeast strains.....	122
Meiotic completion efficiency is mostly independent from the Rfa2 NT phospho-state.....	126
Proper progression through meiosis is dependent on the presence of the Rfa2 NT	130
Four different assessments reveal no obvious defects in homologous recombination.....	133
Rfa2 is modified during meiosis in SJH2-1 derivative strains	140
Mutants that do not allow for successful meiotic progression past MI appear mostly unaffected by <i>rfa2</i> extensive mutations.....	142
Initial evidence for Rad53 modification.....	147
Discussion	151
Acknowledgements	157
CHAPTER FIVE: RFA2 REGULATES MEC1 CHECKPOINT SIGNALING	158
Introduction	158
Materials and Methods	160
Yeast strains and plasmids.....	160
Checkpoint adaptation assay	163
SDS-PAGE and western blotting for Rfa2 and Rad53.....	164
Results	166
Generation of integrating <i>mec1-S1964</i> mutant plasmids.....	166
Rfa2 is phosphorylated during DNA damage by PHL and HO endonuclease in the <i>mec1-S1964</i> mutants.....	170
Rfa2 mutations change the adaptation phenotype of <i>mec1-S1964</i> mutants	173

The <i>rfa2</i> mutant effect on adaptation does not appear to be driven by Mec1-dependent phosphorylation of Rfa2 SQ sites	177
Discussion	182
Acknowledgements	185
CHAPTER 6: CONCLUDING DISCUSSION	186
RFA during the DNA Damage Response and Meiosis	187
RFA involvement in transcription	187
Appearance of phospho-Rfa2 correlated with time of Rad53 “deactivation”	188
Similar phenotypes of Rfa1-DBD-F (<i>rfa1-t11</i>) and Rfa2 (<i>rfa2-Dx</i>) mutations are likely caused by different, yet related mechanisms	188
Rfa2 phosphorylation may prevent Rad53 function during meiosis	190
RFA removal from DNA	191
Proposed Mechanism	192
Future Directions	194
REFERENCES	197
APPENDIX A. HAPLOID YEAST STRAINS	209
APPENDIX B. DIPLOID YEAST STRAINS	218
APPENDIX C. PLASMIDS	221
APPENDIX D. PRIMERS	225
APPENDIX E. IDT G-BLOCKS	230
APPENDIX F. RECIPES	236
Media	236
YPD (Yeast Peptone Dextrose)	236
YPD dissection plates	236
YP- (Yeast Peptone)	236
SD (- selective nutrient; Synthetic Dextrose)	237

SRG-His-Trp-Ura-Leu+X-gal (Synthetic Raffinose Galactose; For yeast two-hybrid)	237
5-FOA (5-Fluoroorotic Acid)	238
SPO (Sporulation) plate media	238
YPA (Yeast extract, Peptone, potassium Acetate; liquid)	238
SPO (liquid SPOrulation media) *Haring lab previously utilized recipe	239
CL-SPM (Cartagena-Lirola Sporulation Media, liquid) *(Cartagena-Lirola et al. 2006, Cartagena-Lirola et al. 2008)	239
ESPM (Extra potassium acetate SPorulation Media, liquid) *(Schindler et al. 2003)	239
SM (Schindler sporulation Media, liquid) *(Schindler et al. 2003)	239
LB (Luria-Bertani)	240
Western Blotting Reagents	240
Protein sample buffers	240
SDS-PAGE gel buffers	241
SDS electrophoresis buffers	241
Transfer buffer	242
Western blot wash buffer	242
APPENDIX G. SUPPLEMENTARY FIGURES	243
Agarose Gels	243
Verification of AWY mutant strains used in Chapter 3	243
Verification of AMA mutant strains used in Chapter 3 and generated as collaborate effort	246
DNA Damage Spot Assays	248
Integrated <i>rfa2</i> mutants (JKM179 vs. JKM139)	248
Integrated <i>rfa2</i> mutants vs. plasmid-based <i>rfa2</i> mutants (JKM179 vs NMM104)	248
Checkpoint protein deletions (<i>rad9Δ</i> , <i>rad17Δ</i> , <i>mec3Δ</i>) with <i>rfa2</i> phospho-mutants	251
Plasmid based <i>rfa2</i> mutants with S122A/D (NMM104)	251

Meiotic Rfa2 NT mutant strains	257
Investigation of <i>rfa2-S238/240A</i> strain sensitivity by Cristian Hernandez	257
APPENDIX H. MATING-TYPE SWITCHING ASSAY	264
Methods	264
Yeast strains and plasmids.....	264
Mating-type switching.....	264
Patch scoring and analysis.....	265
Results	265
Acknowledgements	267
APPENDIX I. CHAPTER 4 SUPPLEMENTARY TABLES	268
Data Referenced in Methods	268
Testing liquid sporulation media for RM96 derivative diploids	268
Liquid sporulation in SM is high for all RM96 derivative strains after 45 hours	269
Data Referenced in Results	270
Spore viability of Rfa2 N-terminal mutants from multiple genetic backgrounds.....	270
APPENDIX J. STATISTICAL ANALYSIS OF CHAPTER 5 DATA.....	271

LIST OF TABLES

<u>Table</u>	<u>Page</u>
2.1. Sporulation efficiency of <i>Cas9-natMX</i> diploids	28
2.2. Sporulation efficiency of <i>spo11Δ::Cas9-natMX</i> diploids with and without guide RNAs	34
2.3. Sporulation efficiency of <i>spo11Δ::Cas9-natMX</i> diploid strain cultures used for western blot analysis of Cas9 protein.....	49
3.1. Proteins that interact with DBD-F (N-terminus of RPA70) in <i>Homo sapiens</i>	64
3.2. Yeast two hybrid assay identified interactors of <i>Saccharomyces cerevisiae</i> Rfa1-DBD-F	76
3.3. Yeast two hybrid assay identified interactors of <i>Homo sapiens</i> RPA1 DBD-F	78
4.1. Diploid yeast strains.....	106
4.2. Sporulation efficiency of Rfa2 NT mutants.....	128
4.3. Gene conversion frequencies of Rfa2 NT mutants at a meiotic recombination hotspot	138
4.4. Gene conversion frequencies at other loci for <i>rfa2</i> NT mutants in the SJH2-1 background	139
4.5. Analysis of crossing over in the <i>CLY3-CDC14</i> interval for Rfa2 NT mutants	139
4.6. Sporulation efficiency of SJH2-1 derivatives used for western blotting	141
4.7. Sporulation efficiency of meiotic progression mutants used for western blotting	143
4.8. Sporulation efficiency of meiotic progression mutants with Rfa2 NT mutations	146
4.9. Sporulation efficiency of <i>dmc1Δ rfa2</i> NT double mutants after liquid sporulation in two different medias	147
5.1. Restriction enzyme information.....	162
5.2. Qualitative summary of <i>rfa2</i> mutant phenotypes.....	183

LIST OF FIGURES

<u>Figure</u>	<u>Page</u>
1.1. Subunits of the RFA complex.....	2
1.2. Recruitment of checkpoint proteins to a DSB	4
1.3. Meiotic process in <i>Saccharomyces cerevisiae</i>	6
1.4. Location and amino acid changes of <i>rfa2</i> extensive mutations	11
2.1. One-step gene replacement technique	18
2.2. Replacement of genomic <i>SPO11</i> with <i>Cas9-natMX</i> , and PCR verification locations for confirmation of <i>Cas9-natMX</i> insertion.....	19
2.3. Predicted plasmid map for pSP+ST-5	20
2.4. Confirmation of initial candidates containing <i>Cas9-natMX</i>	27
2.5. Verifying presence of <i>SPO11</i>	29
2.6. Candidates for <i>spo11Δ::kanMX</i>	31
2.7. Confirmation of pSP+ST-5 by diagnostic restriction digest.....	32
2.8. Verification of <i>spo11Δ::kanMXΔ::Cas9-natMX</i> candidates.....	33
2.9. Heteroallelic recombination during mitosis and meiosis.....	36
2.10. Qualitative heteroallelic recombination assay	38
2.11. Qualitative heteroallelic recombination assay of strains containing an X element gRNA.....	39
2.12. Qualitative heteroallelic recombination assay of strains containing a Y element gRNA.....	40
2.13. Qualitative heteroallelic recombination assay of strains containing a <i>LYS2</i> gRNA.....	42
2.14. Chromosome segregation during mitosis and meiosis.....	43
2.15. Qualitative chromosome segregation assay	45
2.16. Qualitative chromosome segregation assay of strains containing an X element gRNA.....	46
2.17. Qualitative chromosome segregation assay of strains containing a Y element gRNA.....	47

2.18. Qualitative chromosome segregation assay of strains containing a <i>LYS2</i> gRNA.....	48
2.19. Detection of Cas9 protein during meiosis.....	51
2.20. Digested pCRCT vector and amplified G-blocks for generation of <i>Saccharomyces cerevisiae</i> codon optimized <i>Cas9</i> (<i>ScCas9</i>).....	52
2.21. Diagnostic restriction digests of pCRT-ScCas9-1,5 candidates	53
2.22. Diagnostic restriction digest of potential pCRT-ScCas9 candidates that contain all 5 G-blocks for the complete <i>ScCas9</i> sequence.....	54
2.23. Diagnostic restriction digest of pCRT-ScCas9 candidates after mutagenesis to remove the introduced <i>BsaI</i> site.....	56
3.1. Schematic of Rfa1 protein	62
3.2. Confirmation of hybrid plasmid candidates.....	74
3.3. Rfa2 phosphorylation occurs in an <i>rfa1-t11</i> mutant	82
3.4. DNA damage spot assay of <i>rad9Δ</i> , <i>rad17Δ</i> , and <i>mec3Δ</i> mutants	84
3.5. Nuclear import of RFA	94
3.6. Once on ssDNA, DBD-F interacts with a variety of checkpoint proteins	94
3.7. RFA removal by replacement	95
4.1. One-step gene replacement technique with verification PCR product sizes	115
4.2. Example of <i>sae2Δ::hphNT</i> verification PCR.....	115
4.3. Example of <i>dmc1Δ::hphNT</i> and <i>ndt80Δ::natMX</i> verification PCR.....	116
4.4. Two-step gene replacement technique.....	117
4.5. Example of <i>rfa2</i> mutant verification.....	118
4.6. The effect <i>rfa2</i> NT mutations have on adaptation is more apparent in diploids.....	123
4.7. In trial with abnormally low adaption, the increase in adaptation in the <i>rfa2-Dx</i> diploid is more pronounced.....	124
4.8. Meiotic yeast strains with <i>rfa2</i> NT mutations recapitulate prior phenotypes	125
4.9. Reduction in 4-spore viable tetrads of Rfa2 phospho-mutant and NT deletion	129

4.10. Meiotic progression of Rfa2 N-terminal deletion mutant is consistent with sporulation.....	131
4.11. Qualitative assessment of heteroallelic recombination and chromosome segregation.....	134
4.12. No obvious heteroallelic recombination defect is observed	136
4.13. Analysis of Rfa2 protein in SJH2-1 derivative strains.....	141
4.14. Analysis of Rfa2 protein in meiotic progression mutants.....	144
4.15. Analysis of Rfa2 protein in a <i>dmc1Δ</i> mutant	145
4.16. Analysis of Rad53 protein in SJH2-1 derivative strains	149
4.17. Analysis of Rad53 protein in RM96 derivative strains.....	150
5.1. Confirmation of pAG416- <i>mec1</i> -aa1650-2290 candidates.....	167
5.2. Confirmation of pAG406- <i>mec1</i> -aa1650-2290 candidates.....	168
5.3. Confirmation of pAG406- <i>mec1</i> -aa1650-2290-S1964A candidates	168
5.4. Confirmation of pAG406- <i>mec1</i> -aa1650-2290-S1964E candidates.....	169
5.5. Confirmation of pAG406- <i>mec1</i> -aa1650-2290-S1964D candidates	169
5.6. Rfa2 is phosphorylated after phleomycin treatment	172
5.7. Rfa2 is phosphorylated after induction of HO endonuclease	172
5.8. Adaptation phenotype of <i>mec1-S1964</i> mutants is modified by <i>rfa2</i> mutations.....	174
5.9. Rad53 western blots for <i>mec1-S1964 rfa2 NT</i> double mutants	176
5.10. SQ motifs in Rfa2	177
5.11. Rfa2 phosphorylation is detected in cells with mutations that eliminate Mec1 phosphorylation target sites	178
5.12. Adaptation of <i>rfa2-S238/240</i> mutants.....	180
5.13. Mec1 target site mutations do not change adaptation proficiency.....	181
6.1. Model for interaction between RFA, Mec1, and Rad53 to stop the cell cycle	195
6.2. Model that promotes removal of RFA from ssDNA, limiting Mec1 activity.....	196

6.3. Model that prevents DBD-F from additional interactions with repair proteins once RFA is displaced 196

LIST OF ABBREVIATIONS

aa	amino acid(s)
abm	Applied Biological Materials Inc.
Amp	amperage
amp	ampicillin
A _x	Rfa2 N-terminal alanine extensive mutant
β-me	beta-mercaptoethanol
bp	base pair(s)
CPT	camptothecin
CRISPR	clustered, regularly interspaced, short palindromic repeats
crRNA	CRISPR RNA
D	dextrose
Da	dalton (molecular weight)
DAPI	4',6'-diamidino-2-phenylindole
DBD	DNA binding domain
DDR	DNA damage response
DNA	deoxyribonucleic acid
DSB	double-stranded break
dsDNA	double-stranded DNA
D _x	Rfa2 N-terminal aspartate extensive mutant
g	gram, gravity (context)
G ₁	growth or gap 1 phase
G ₂	growth or gap 2 phase
G ₂ M	between growth/gap 2 phase and mitosis

gal, Gal, or GALgalactose

gRNAguide RNA

H₂NTRfa2 *Homo sapiens* N-terminal mutant

HO.....heterothallic

HR.....homologous recombination

hrhour

HU.....hydroxyurea

hygrohygromycin B

id'didentified

k.....kilo

kan.....kanamycin

K_xR.....lysine to arginine extensive mutant

Lliter

mmili-

M.....molar (context)

M.....mitosis (context)

MI.....meiosis I

MIImeiosis II

MMR.....mismatch repair

MMSmethyl methane sulfonate

MWM.....molecular weight marker

N.....normal

NEB.....New England Biolabs

NHEJ.....non-homologous end joining

NTN-terminus or N-terminal

(Δ)N_xRfa2 NT deletion extensive mutant

OB.....oligonucleotide binding

ORF.....open reading frame

PCR.....polymerase chain reaction

Pphosphorylation domain

PHL.....phleomycin

raf, Raf, or RAFraffinose

RFA.....replication factor A

RICrecombination initiation complex

RNAribonucleic acid

RPA.....replication protein A

Ssynthesis phase (DNA replication) or Serine

SDsynthetic complete media with dextrose

SDSsodium dodecyl sulfate

SRG.....synthetic complete media with raffinose and galactose

ssDNA.....single-stranded DNA

tracrRNA.....transactivating CRISPR RNA

TBST.....Tris-buffered saline with Tween20 buffer

URS.....upstream regulatory sequence

W.....winged-helix domain

WTwild-type

X-gal5-bromo-4-chloro-3-indolyl- β -D-galactopyranoside

YPyeast extract, peptone media

YPA.....yeast extract, peptone, acetate media

YPD.....yeast extract, peptone, dextrose media

YPR.....yeast extract, peptone, raffinose media

YPRG.....yeast extract, peptone, raffinose, galactose media

LIST OF SYMBOLS

α	Alpha; used to designate an antibody or for mating type alpha.
β	Beta; used to describe location of functional groups of a chemical
Δ	Delta; used to describe gene deletions
μ	Micro, used to denote “micro” measurements
λ	Lambda, short-hand for microliters
$^{\circ}\text{C}$	Degree, used for temperatures (Celsius)
/	slash, used to denote “digestion with” when followed by an enzyme

LIST OF APPENDIX TABLES

<u>Table</u>	<u>Page</u>
H1. Mating type switching analysis.....	266
H2. Mating type switching analysis of mixed mating type patches	266
I1. Sporulation test of three different liquid sporulation medias	268
I2. Sporulation on solid spo vs. liquid SM media.....	269
I3. Spore viability of Rfa2 NT mutants in multiple genetic backgrounds	270
J1. Statistical analysis of mutant cellular arrest compared to wild-type arrest.....	271
J2. Statistical analysis of adaptation at 24 hours of all mutants compared to wild-type	272
J3. Statistical analysis of adaptation at 24 hours of all <i>mec1 rfa2</i> mutants compared to the <i>mec1</i> mutant containing wild-type <i>RFA2</i>	273
J4. Statistical analysis of adaptation at 48 hours of all mutants compared to wild-type	274
J5. Statistical analysis of adaptation at 48 hours of all <i>mec1 rfa2</i> mutants compared to the <i>mec1</i> mutant containing wild-type <i>RFA2</i>	275

LIST OF APPENDIX FIGURES

<u>Figure</u>	<u>Page</u>
G1. Verification of <i>rfa2</i> mutant status	244
G2. Verification of <i>geneΔ::selectable marker</i>	245
G3. Verification of AMA generated strains.....	247
G4. DNA damage assay for JKM179 vs. JKM139 mutants	249
G5. DNA damage assay for integrated vs. plasmid-based <i>rfa2</i> mutants	250
G6. Sensitivity of checkpoint protein mutants on concentrations of CPT	252
G7. Sensitivity of checkpoint protein mutants on concentrations of HU	253
G8. Sensitivity of checkpoint protein mutants on concentrations of MMS.....	254
G9. Sensitivity of checkpoint protein mutants on concentrations of PHL	255
G10. DNA damage assay for <i>rfa2</i> mutants.....	256
G11. Sensitivity of meiotic strain mutants on CPT- Set 1	258
G12. Sensitivity of meiotic strain mutants on CPT- Set 2.....	259
G13. Sensitivity of meiotic strain mutants on HU	260
G14. Sensitivity of meiotic strain mutants on MMS	261
G15. Sensitivity of meiotic strain mutants on PHL	262
G16. Investigation of <i>rfa2-S238/240A</i> DNA damage sensitivity	263

CHAPTER ONE: INTRODUCTION

Replication Factor A

Replication Factor A (RFA) is an essential, evolutionarily conserved, heterotrimeric, single-stranded DNA (ssDNA) binding complex required for DNA replication, repair, recombination, and cell cycle regulation (Brill and Stillman 1991, Wold 1997, Lee et al. 1998, Soustelle et al. 2002, Ghospurkar et al. 2015b). In *Saccharomyces cerevisiae*, or budding yeast, the RFA complex is made up of the subunits Rfa1, Rfa2, and Rfa3 (Brill and Stillman 1991), which is shown in Figure 1.1 labeled with the domains, amino acids (aa), and specific residues discussed throughout this dissertation. Rfa1 DBD-F appears to function primarily in protein-protein interactions rather than in binding ssDNA (Chen, Umezumi and Kolodner 1998, Umezumi et al. 1998, Soustelle et al. 2002, Zou and Elledge 2003, Zou, Liu and Elledge 2003, Seeber et al. 2016, Deshpande et al. 2017). Trimerization of the RFA complex is established by the interaction of the C-terminal regions of Rfa1 DBD-C, Rfa2 DBD-D, and Rfa3 DBD-E and is also suggested to have a role in transitioning RFA between the short and long ssDNA binding modes (Bochkareva et al. 2002). The short binding mode utilizes DBD-A and DBD-B to occlude 8-10 nucleotides, which is followed by sequential binding of DBD-C and DBD-D to occlude 23-30+ nucleotides for the long binding mode (Kim, Snyder and Wold 1992, Bochkarev et al. 1997, Bastin-Shanower and Brill 2001, Bochkareva et al. 2002, Wyka et al. 2003) RFA binds to ssDNA in a 5'→3' direction with no obvious sequence specificity, and the binding of RFA to ssDNA is facilitated by base-stacking interactions from specific aromatic residues positioned within the DBDs (Bochkarev et al. 1997, Bastin-Shanower and Brill 2001).

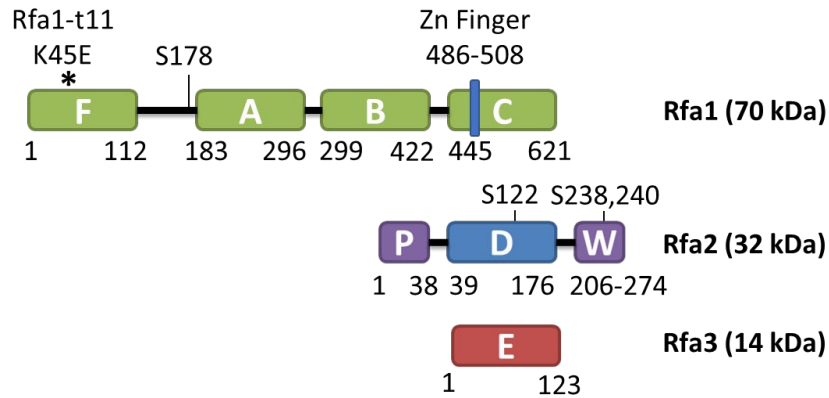


Figure 1.1. Subunits of the RFA complex

The RFA complex is made up of the subunits: Rfa1, Rfa2, and Rfa3 with the molecular weight for each denoted in kilo-Daltons (kDa). The DNA-binding domains (DBDs) are: F, A, B, C, D, and E. The putative phosphorylation domain (P) and putative winged-helix domain (W) of Rfa2 are depicted. Residue information was obtained via UniProt to label domains including the zinc (Zn) finger of Rfa1 (The UniProt 2018). Other specific residues denoted are: Rfa1 K45E mutation (*rfa1-t11*), Rfa1-S178 (Mec1 SQ target), Rfa2-S122 (Mec1 SQ target), and Rfa2-S238,240 (SQS motif, see Chapter 5).

DNA Damage Response

When the genome is subjected to DNA damage, proteins respond to the DNA lesions produced to facilitate DNA repair in order to preserve the genomic integrity and viability of the cell. Typically, the damage is recognized by a “sensor” protein that recruits in “effector” proteins to stop the cell-cycle and repair the damage (if damage can be repaired).

When processing a double-stranded break (DSB) for repair, typically the order of protein recruitment is thought to be in the order shown in Figure 1.2, which closely follows the model proposed by Lisby (Lisby et al. 2004). The Mre11-Rad50-Xrs2-Sae2 (MRXS) complex binds to the DSB and leads to the activation of the sensor kinase Tel1 (Lisby et al. 2004, Usui, Ogawa and Petrini 2001, Nakada, Matsumoto and Sugimoto 2003). MRXS is thought to promote initial end resection that accommodates nuclease binding to perform long range end resection (Lisby et al. 2004, Moreau, Morgan and Symington 2001, Moreau, Ferguson and Symington 1999, Lee et al. 1998). The nucleases responsible for end resection have been shown to be the Sgs1-Dna2

complex and Exo1, these nucleases function as two independent pathways for end resection (Zhu et al. 2008, Manfrini et al. 2010). Some studies have shown that the Sgs1-Dna2 nuclease complex is primarily used in mitotic cells while Exo1 is primarily used in meiotic cells (Zakharyevich et al. 2010, Keelagher et al. 2011, Mimitou, Yamada and Keeney 2017). The nucleases resect DNA in the 5'→3' direction, generating a 3' ssDNA tail for RFA to bind (Cejka et al. 2010, Mimitou et al. 2017, Zhu et al. 2008). The RFA-coated ssDNA is then detected by a second sensor kinase, Mec1 in complex with its binding partner Ddc2 (Zou and Elledge 2003). It has been demonstrated that Rfa1 DBD-F is the component of RFA that interacts with Ddc2 to recruit the Mec1-Ddc2 complex (Lisby et al. 2004, Deshpande et al. 2017, Cheng et al. 2018). Rfa1 DBD-F recruits or is inferred to recruit additional DNA Damage Response (DDR) proteins (*e.g.*, the checkpoint clamp loader: Rad24-Rfc2-5, the checkpoint clamp: Rad17-Ddc1-Mec3, and the effector kinase: Rad9-Rad53), because either a direct/indirect interaction with Rfa1 DBD-F has been shown or studies have demonstrated a requirement for DBD-F for proper localization of these checkpoint proteins [Note: Replication Protein A (RPA) is the human homolog, made up of the subunits: RPA1, RPA2, and RPA3 (Chen et al. 1998, Umezu et al. 1998, Soustelle et al. 2002, Zou and Elledge 2003, Zou et al. 2003, Seeber et al. 2016, Deshpande et al. 2017, Maréchal and Zou 2015, Majka, Niedziela-Majka and Burgers 2006b, Majka et al. 2006a)]. Only when the DDR proteins that interact with DBD-F (the Rad9 adaptor, checkpoint clamp, and checkpoint clamp loader) are all present, is Rad53 able to be phosphorylated by Mec1 (de la Torre-Ruiz, Green and Lownes 1998). Mec1 phosphorylation of Rad53 triggers Rad53 auto-phosphorylation, which leads to the full activation of Rad53 and cell cycle arrest (Sanchez et al. 1996, Lee et al. 1998, Kim et al. 1999, Pellicoli et al. 2001, Sweeney et al. 2005, Bonilla, Melo and Toczyski 2008).

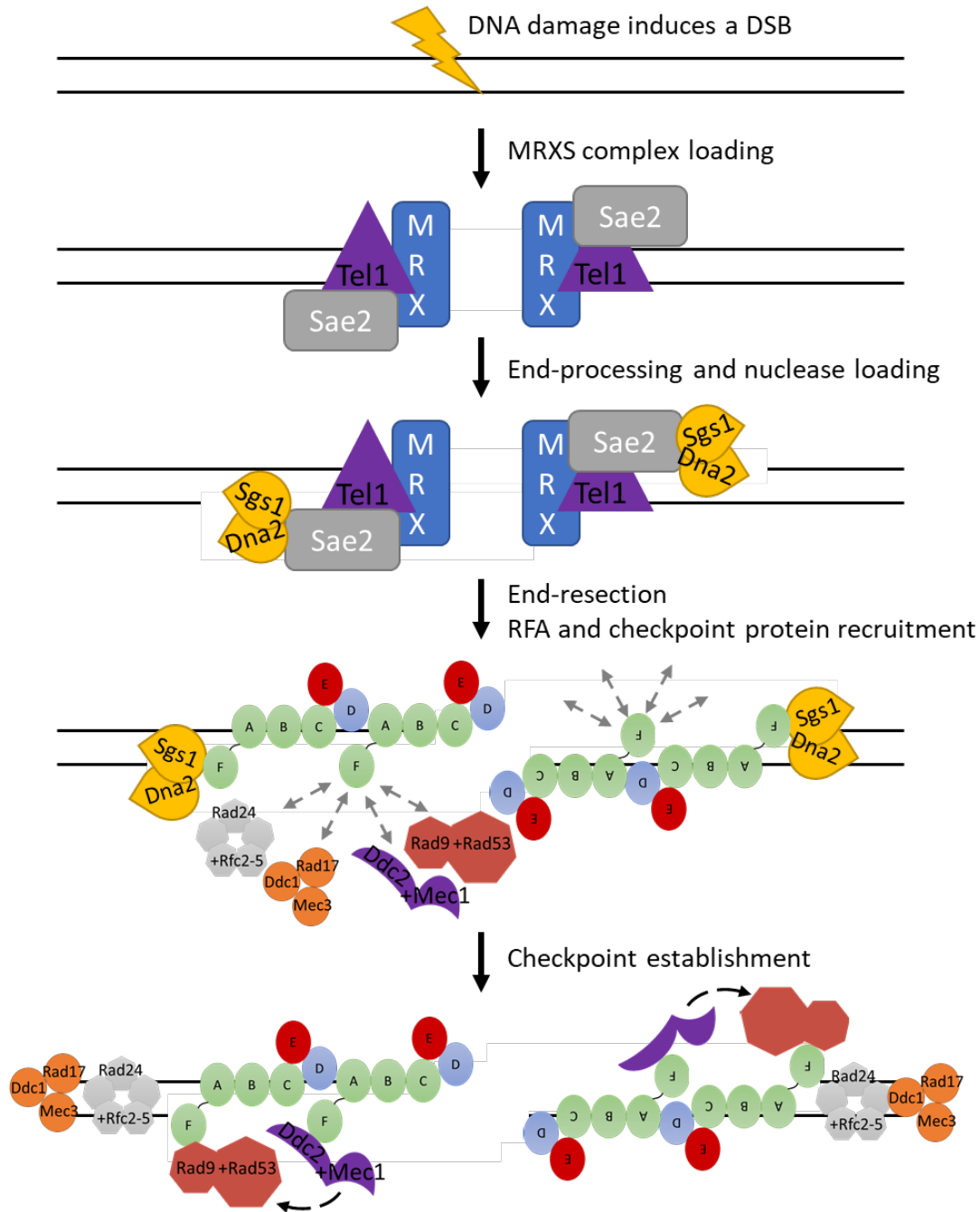


Figure 1.2. Recruitment of checkpoint proteins to a DSB

This model for checkpoint protein recruitment is based off the Lisby model (Lisby et al. 2004). Following the formation of a DSB, Tel1 and the Mre11-Rad50-Xrs2-Sae2 (MRXS) complex recognize the DSB. MRXS processes the ends of the DSB by short-range resection to allow for nucleases (Sgs1-Dna2, or Exo1) to be loaded. Nucleases perform long-range resection that allows for RFA to be loaded onto the 3' ssDNA tail (formed by resection). RFA recruits and loads checkpoint proteins (clamp loader: Rad24-Rfc2-5, clamp: Rad17-Ddc1-Mec3, sensor kinase: Ddc2-Mec1, effector kinase: Rad9-Rad53). Mec1 phosphorylates Rad53, which leads to checkpoint establishment.

Monitoring DNA damage and halting the cell cycle is only half of the DDR process. Cell cycle arrest must somehow be alleviated to allow for cell cycle progression (*i.e.*, cell growth). There are two identified ways to accomplish exit from a checkpoint: recovery and adaptation. Exit from a checkpoint via recovery occurs *after* the damage has been repaired, whereas exit from a checkpoint via adaptation occurs *before* the damage has been repaired (DNA damage persists) (Lee et al. 2000, Lee et al. 1998). Rad53 inactivation (dephosphorylation) has been demonstrated to be a commonality between both recovery and adaptation, while cells that do not exit a checkpoint maintain activated (phosphorylated) Rad53 (Lee et al. 2000, Vaze et al. 2002, Pellicioli et al. 2001, Lee et al. 1998, Lee et al. 2001, Lee et al. 2003). Degradation of either Rad53 or Mec1 (upstream of Rad53) also allows for cell cycle progression after arrest in adaptation-deficient mutants which further supports that inactivation of the checkpoint requires inhibiting Rad53's control on the cell cycle by either deactivating Rad53 or preventing additional Rad53 activation through inhibition of Mec1 activity (Pellicioli et al. 2001). The Ptc2 and Ptc3 phosphatases have been suggested to deactivate (dephosphorylate) Rad53 as evidence implies that the phosphatases both bind to Rad53 and are required for checkpoint inactivation/adaptation (Leroy et al. 2003, Guillemain et al. 2007).

Because the interaction between Mec1 and Rad53 is dependent on localization to the DSB by their interactions with other checkpoint proteins (de la Torre-Ruiz et al. 1998, Sweeney et al. 2005, Majka et al. 2006b, Bonilla et al. 2008, Navadgi-Patil and Burgers 2008, Deshpande et al. 2017), it has been suggested that Mec1 delocalization prevents continual Rad53 activation (Memisoglu et al. 2019). One way in which Mec1 might be delocalized from the DSB is when recombinational repair proteins replace RFA on ssDNA, since Mec1 localization is RFA dependent (Nakada et al. 2005, Deshpande et al. 2017). Interestingly, the localization of proteins

involved in recombinational repair (Rad52, Rad51, Rad55, Rad54) are all dependent on Rfa1 (Lisby et al. 2004). Ultimately, once the Rad51 filament is formed by replacing RFA on ssDNA, Mec1 will not be localized to the DSB and the cell undergoes homology search and strand invasion to repair the DSB by homologous recombination (Sung 1997, Lisby et al. 2004, Symington, Rothstein and Lisby 2014).

Meiosis

Meiosis is an essential process for sexually reproducing organisms in which a diploid cell goes through one round of DNA replication followed by two consecutive rounds of DNA division (Meiosis I, MI, and Meiosis II, MII) to produce haploid gametes (Figure 1.3). The first division is unique to meiosis, where homologous chromosomes are segregated (reductional division; MI). During this reductional division, the DNA is purposely broken by meiotic proteins, so that homologous chromosomes are tethered together through repair. This event ensures proper chromosome segregation in MI. (Roeder 1997, Honigberg and Purnapatre 2003) If chromosomes are not properly segregated in MI, aneuploidy can occur, which in humans can cause miscarriages or genetic diseases (Hassold and Hunt 2001).

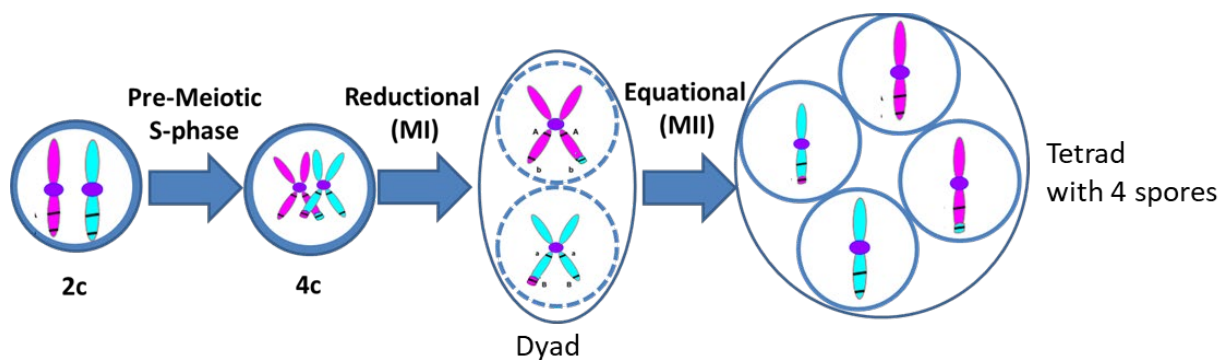


Figure 1.3. Meiotic process in *Saccharomyces cerevisiae*

Shown is the progression of a diploid (2C DNA content, C=chromatid(s)) through meiosis. The diploid cell undergoes pre-meiotic S-phase to replicate DNA (4C DNA content). This is followed by homolog pairing via HR repair that ensures proper chromosome segregation in the reductional (MI) division that forms the dyad cell. Finally, sister chromatids separate in the equational (MII) division to form the tetrad that contains 4 yeast spores.

In *Saccharomyces cerevisiae*, meiosis is tightly regulated and initiated by three key nutritional requirements: the absence of glucose, the presence of a nonfermentable carbon source, and nutrient starvation to arrest the cells in G₁ (Honigberg and Purnapatre 2003). Once these conditions are met, a transcriptional cascade is initiated by Ime1, a meiosis-specific transcription factor (Honigberg and Purnapatre 2003). Ime1 activates expression of Ime2, a CDK-like serine/threonine protein kinase that coordinates all meiotic processes (Mitchell, Driscoll and Smith 1990, Sia and Mitchell 1995, Foiani et al. 1996, Dirick et al. 1998, Bolte et al. 2002, Benjamin et al. 2003, Honigberg and Purnapatre 2003, Schindler and Winter 2006).

Initiated in part by Ime2, pre-meiotic DNA synthesis (replication) gives rise to the diploid cell that contains 2 chromatids per chromosome to have double the original DNA content (Dirick et al. 1998, Stuart and Wittenberg 1998, Benjamin et al. 2003). To divide homologous chromosomes (each containing two sister chromatids) apart from each other in the MI division, they must first be paired. Homologous chromosomes are aligned with each other by homologous (meiotic) recombination which is initiated by double stranded breaks (DSBs) catalyzed by Spo11 as part of the recombination initiation complex (Klapholz, Waddell and Esposito 1985, Keeney, Giroux and Kleckner 1997, Keeney 2008, Koehn et al. 2009). The recombination initiation complex (RIC) is made up of the following proteins: Spo11, Mei4, Rec102, Ski8/Rec103, Rec104, Rec114, Mer2/Rec107, Mre11, Rad50, Xrs2, and Sae2 (Mao-Draayer et al. 1996, Maleki et al. 2007, Murakami and Keeney 2008, Keeney 2008, Richardson, Horikoshi and Pandita 2004). Four proteins present in the RIC: Mre11, Rad50, Xrs2, and Sae2 are responsible for removal of Spo11 and resection of the Spo11-induced break (Richardson et al. 2004). This starts the HR repair process of the approximately 160 DSBs self-inflicted prior to the MI division in *Saccharomyces cerevisiae* (Pan et al. 2011).

Just like how DNA damage is monitored in mitosis, the pachytene checkpoint appears to monitor repair of meiotic DSBs. It has been demonstrated to be a “committal” point for meiotic completion because cells in stages prior to and including pachytene can return to a mitotic cell cycle with appropriate nutrient supplementation; whereas, cells past the pachytene checkpoint appear committed to meiotic completion (Xu, Weiner and Kleckner 1997, Xu et al. 1995, Ballew and Lacefield 2019). It appears there may be three connected components to the pachytene checkpoint, they are: (1) DSBs get repaired, (2) interhomolog bias is maintained, and (3) transcriptional activation of middle and late meiotic genes. It has been demonstrated that several mitotic checkpoint proteins (Mec1, Rad17, and Rad24) maintain arrest of the pachytene checkpoint (Lydall et al. 1996, Grushcow et al. 1999). The activation of the meiosis specific kinase Mek1 is DSB- and Mec1-dependent, seemingly replacing the checkpoint kinase role Rad53 has during mitosis (Hunter 2008, Carballo and Cha 2007, Carballo et al. 2008). However, there has been speculation on whether Mek1 is truly a checkpoint kinase that maintains arrest at the pachytene checkpoint to ensure interhomolog repair or rather just maintains arrests until breaks are repaired, since overexpression of Rad53 has rescued cells arrested at pachytene due to an interhomolog repair defect (in the presence of Mek1) (Usui and Kanehara 2013). Mek1 has been demonstrated to ensure interhomolog repair bias and some studies have even suggested that Mek1 may have some control over the amount of DSB formation (Niu et al. 2007, Niu et al. 2005, Xu et al. 1997, Wu, Ho and Burgess 2010). Interhomolog bias is also promoted by the meiosis-specific recombinase, Dmc1; however, it does not completely replace Rad51 as negative consequences (delayed recombinants, prolonged unrepaired DSBs, reduction in meiotic progression, decreased spore viability) are observed in the absence of Rad51 (Shinohara, Ogawa and Ogawa 1992, Shinohara et al. 1997, Shinohara et al. 2000, Cloud et al. 2012, Shinohara and

Shinohara 2013, Lee et al. 2017). Ndt80, a meiosis-specific transcription factor, is required for exit from the pachytene checkpoint since Ndt80 activates expression of middle and late meiotic genes (Xu et al. 1995, Chu et al. 1998). Both Ime2 and Mek1 have been demonstrated to control Ndt80 activity (Benjamin et al. 2003, Prugar et al. 2017, Chen et al. 2018, Pak and Segall 2002, Mitchell et al. 1990, Sia and Mitchell 1995).

While Rad53 does not seem to have an effector-kinase role in the pachytene checkpoint, Rad53 has been demonstrated recently to maintain meiotic commitment in the presence of mitosis-inducing signals (Lydall et al. 1996, Cartagena-Lirola et al. 2008, Ballew and Lacefield 2019). Investigating the role for Rad53 during meiosis has been limited, as thus far Rad53 seems able to be activated/phosphorylated in response to breaks made during MI only if it can be localized to the breaks, but Rad53 activation does not appear to have any ability to arrest cells prior to the MI division (Xu et al. 1997, Cartagena-Lirola et al. 2008). In fact, as mentioned above, if Rad53 is overexpressed in cells arrested prior to MI due to an interhomolog repair defect, it can alleviate the arrest (by promoting sister chromatid repair, whereby the resulting spores are inviable) (Usui and Kanehara 2013). It has additionally been shown that only if breaks persist past the MI division or if new breaks are introduced after MI, then Rad53 can arrest the cell cycle prior to the mitotic-like MII division (Cartagena-Lirola et al. 2008).

RFA during the DDR and Meiosis

RFA is phosphorylated by Mec1 on Rfa1-S178 and Rfa2-S122 in response to DNA damage during mitosis and in a cell-cycle dependent manner (Brush et al. 1996, Bartrand, Iyasu and Brush 2004, Bartrand et al. 2006, Brush and Kelly 2000, Kim and Brill 2003). The effects of the Rfa2 NT phospho-state have been studied previously in the Haring laboratory “extensive” mutation of *RFA2* in which all NT serine or threonine residues (from aa 3-34) have been mutated

to either aspartic acid to mimic phosphorylation (*rfa2-D_x*), alanine to have a non-phosphorylatable NT (*rfa2-A_x*), or the NT aa 3-37 have been removed (*rfa2-ΔN_x*; Figure 1.4) (Ghospurkar et al. 2015b, Ghospurkar 2015, Wilson 2018). It has been demonstrated that both *rfa2-D_x* and *rfa2-ΔN_x* mutations increase the DNA damage sensitivity of cells (Ghospurkar et al. 2015b, Wilson 2018). The increased sensitivity of these mutants is likely due to different reasons, since in addition to multiple different genetic interaction phenotypes, *rfa2-D_x* promotes checkpoint adaptation while *rfa2-ΔN_x* reduces checkpoint adaptation. Thus, cells containing *rfa2-D_x* may be exiting a checkpoint early leading to cells that are inviable because of unrepaired DNA, while cells containing *rfa2-ΔN_x* may have permanently arrested in response to the damage. These adaptation phenotypes are most clearly observed in adaptation-deficient mutants where *rfa2-D_x* rescues adaptation of all mutants tested and *rfa2-ΔN_x* has an additive effect with the adaptation-deficient mutation in which the double mutant's adaptation is further reduced. The *rfa2-A_x* mutant appears to be a hybrid of the phenotypes observed with the *rfa2-D_x* and *rfa2-ΔN_x* mutations. Interestingly, *rfa2-A_x* mutants are no more sensitive to DNA damage than wild-type strains and adapt at a similar frequency to that of wild-type cells. However, when the *rfa2-A_x* mutation is combined with an adaptation-deficient mutation, it often increases the DNA damage sensitivity and always increases the deficiency of adaptation-deficient mutants (at least for all cases tested). This suggests that alone *rfa2-A_x* may not cause any detrimental problems in a cell; however, if any other checkpoint deficiencies exist, *rfa2-A_x* will amplify the phenotype of the concurrent issues.

During meiosis, the Rfa2 NT is phosphorylated by Ime2 independently from DNA replication and programmed DSBs (Brush et al. 2001, Clifford et al. 2005, Clifford, Marinco and Brush 2004). Rfa2-S122 also gets phosphorylated during meiosis under the same conditions

Chapter 3 investigates the relationship between the putative protein interaction domain of RFA (Rfa1 DBD-F) and the Rfa2 NT by utilizing yeast two-hybrid to identify DNA damage sensitive protein interactions involving DBD-F, detecting Rfa2 phosphorylation in a DBD-F mutant, and observing effects on DNA damage sensitivity of cells when checkpoint-defective cells (because of a checkpoint protein gene deletion that has been suggested to associate with DBD-F) contain a phospho-mimetic form of Rfa2. Chapter 4 investigates the role of the Rfa2 NT during meiosis by utilizing meiotic assays to examine if the meiotic progression defects observed could be caused by a defect in any of RFA core functions: DNA replication, repair (specifically HR), or cell cycle regulation. Chapter 5 investigates how the Rfa2 NT may modify the checkpoint response of the DDR sensor kinase Mec1 by observing the effects that *rfa2* mutations have on Mec1 auto-phosphorylation recently implicated in controlling checkpoint adaptation by influencing Ddc2-Mec1 localization (*i.e.*, the amount of time Mec1 is able to “sense” the DNA damage).

The results of these studies detailed in the respective chapters support the hypothesis that the Rfa2 NT influences cell cycle regulation during both the mitotic and meiotic DDR, potentially by influencing the amount of time Mec1 is localized to the DNA damage that may be contingent on how quickly RFA is replaced on the ssDNA.

CHAPTER TWO: CRISPR-Cas9

Clustered Regularly Inter-Spaced Palindromic Repeats with Cas9 associated protein, CRISPR-Cas9, is a genome editing technique that can be thought of as a programmable DNA “scissors” in which CRISPR RNA (crRNA) guides the complex to a target DNA sequence. Off-target effects, that is cutting at sites other than the complementary target sequence, have been reported in *Arabidopsis thaliana* and in human cell studies. While off-target effects are undesirable for editing genomes, this study’s purpose attempted to capitalize on off-target effects to drive meiotic recombination. Double-Stranded Breaks (DSBs) required for meiotic recombination are catalyzed by the topoisomerase Spo11 during a normal meiosis. This study examined the possibility for using CRISPR-Cas9 as a replacement for Spo11. While the system used was unable to drive enough recombination to allow cells to proceed through meiosis, heteroallelic recombination (recombination that can occur during mitosis and meiosis) was increased when Cas9 was targeted to a heteroallelic locus. Examination of protein abundance via western blot showed that Cas9 was not increasing during meiosis, which is likely a contributing factor to the inability of Cas9 to drive enough meiotic recombination to rescue meiosis.

Introduction

CRISPR-Cas9 is a genome editing technique modified from its native function in the adaptative immune system of prokaryotes to be used in a wide variety of organisms (Peng, Lin and Li 2016, Sternberg and Doudna 2015, Oude Blenke et al. 2016, Jinek et al. 2012). The most commonly modified CRISPR-Cas9 system for use in molecular biology is the one from *Streptococcus pyogenes* (Oude Blenke et al. 2016, Sternberg and Doudna 2015). The two CRISPR-Cas9 systems used in this study are both based off the *Streptococcus pyogenes* mechanism. The difference in the systems lies with the structure of the components. In general,

for CRISPR-Cas9 to function as an RNA-guided endonuclease, the major parts needed to make the complex are the Cas9 endonuclease, the crRNA, and the transactivating CRISPR RNA (tracrRNA) (Jinek et al. 2012). These components can all be separately expressed from each other, allowing for tandem crRNAs that are processed by cleavage with RNase III so that each crRNA sequence is interacting with a tracrRNA to guide and activate Cas9 to the appropriate target site. Having the crRNA and tracrRNA expressed separately from each other is more similar to the native system and has been used for one-step multigene disruption in *Saccharomyces cerevisiae* (Bao et al. 2015). A variation in which crRNA and tracrRNA have been combined to be expressed together as a single “guide RNA” has been more commonly used in higher eukaryotes for gene editing (Oude Blenke et al. 2016, Peng et al. 2016).

While most of the time CRISPR- Cas9 is reported as an efficient genome editing tool, it has also been reported to cut at sites other than the target site, known as off-target effects. It has been suggested that use of the gRNA (instead of separate crRNA and tracrRNA) have reduced off-target effects, however off-target effects have still been reported to occur in *Arabidopsis thaliana* and in human cell studies (Fu et al. 2013, Peng et al. 2016, Cho et al. 2014, Zhang et al. 2018). These studies have also proposed methods to reduce the off-target effects, such as using a truncated gRNA. Guide RNAs are typically designed to hybridize to 20 nucleotides of the target DNA sequence, but using a gRNA with only 17-18 nucleotides has been shown to reduce off-target effects while still maintaining on-target efficiency (Fu et al. 2014). Another method that may reduce off-target effects is using separate complexes of CRISPR-Cas9 to cut the top and bottom strands of DNA. This could be achieved by using Cas9 nickases, in which one domain of Cas9 contains an aspartate to alanine substitution (D10A) to generate a single-stranded break at the target site instead of a double-stranded break (Cong et al. 2013). Thus, two Cas9 nickases can

be used in which one nickase + gRNA cuts the top strand and another nickase + gRNA cuts the bottom strand so that a double-stranded break is generated only if both gRNAs are on-target. Others have proposed simply limiting the amount of Cas9 and gRNA present, so logically less Cas9 equals less opportunity for off-target cutting.

Mathematical analysis suggests that for any one guide RNA (gRNA) designed for use on the human genome there are potentially 328 off-target sites (Zhou et al. 2017). As the human genome is approximately 250 times the size of the yeast genome, extrapolating the analysis to yeast would suggest that there is the potential for only 1 off-target site for any one guide RNA. While mathematical analysis would suggest that off-target effects in yeast are minimal, the analysis is based on data related to the propensity of off-target effects discovered mainly in human cell studies. Thus, without any biological studies performed to test off-target effects it cannot be determined that off-target effects would be so minimal in yeast.

While off target effects are undesirable for precise genome editing, this study aims to discover if off-target effects or potentially creating breaks on each chromosome could be beneficial when it comes to creating enough breaks to drive meiotic recombination to promote procedure through meiosis (Chapter 1).

During meiosis, recombination is essential for generating diversity and ensuring proper chromosome segregation during the first division. Meiotic recombination ensures proper chromosome segregation as homologous chromosomes will be tethered together as a result of repair of programmed DSBs. Thus, to allow for meiotic recombination to occur, the DNA must first be broken. Double-stranded breaks are catalyzed during meiosis by the conserved protein Spo11 which performs its function as part of the recombination initiation complex (RIC) (Keeney et al. 1997, Keeney 2008, Klapholz et al. 1985, Koehn et al. 2009). It has been

hypothesized that the RIC works together to regulate Spo11 activity such that breaks are made at the appropriate time and perhaps at the appropriate locations (Murakami and Keeney 2008). Many RIC proteins involved in processing the break for repair also function during mitotic recombination (Keeney 2008), so it may be possible to achieve similar levels of recombination without Spo11. Others have investigated this possibility by using site-specific endonucleases. Using site-specific endonucleases during meiosis has demonstrated similarities to the normal Spo11-induced meiotic recombination, such as: an increase in the number of recombinants, a higher percentage of crossover during meiosis than during mitosis, and longer lengths of resected DNA (Neale et al. 2002, Malkova et al. 2000). The endonucleases used were only targeted to one specific site, thus it is unknown whether induction of multiple breaks could produce enough recombination to allow for normal chromosome pairing.

To discover whether CRISPR-Cas9 off-target effects or targeting of multiple sites could substitute for Spo11 during meiosis, strains were generated to replace Spo11 with Cas9, so that Cas9 expression would be controlled by the Spo11 promoter to make Cas9 expression meiosis-specific. Under all of the experimental conditions of this study, Cas9 was unable to increase the sporulation rate of *SPO11* deletion (*spo11Δ*) strains. Cas9 was able to increase the number of recombinants when targeted to cut a heteroallelic locus but did not increase recombination of other sites that were measured. While Cas9 was designed to increase in protein abundance during meiosis (by use of the Spo11 promoter), western blotting reveals that Cas9 protein was not increasing throughout the meiotic time points analyzed. Thus, the Spo11-promoter driven Cas9 was unable to function efficiently as a meiosis-specific endonuclease to drive a proper meiosis in the absence of Spo11.

Materials and Methods

Yeast strains and plasmids

Yeast strains utilized in this project were K264-10D, RM26-26C, RM96, and derivatives of these strain backgrounds. Heterothallic (cells are unable to switch mating types so each haploid strain is exclusively one mating type, thus requires mating with a strain of the opposite mating type to reproduce) haploid strains (Appendix A) were engineered and crossed to generate the appropriate diploid strains (Appendix B).

The plasmid, pSP+ST-5 (B-1055, Appendix C) was constructed by undergraduate Barbara Senger by *in vivo* homologous recombination cloning. This plasmid contains the *SPO11* promoter (SP) and the *SPO11* terminator (ST) flanking the Cas9 coding region and nourseothricin resistance cassette (*natMX*) and was originally designed for use in one-step gene replacement (Figures 2.1, 2.2). Thus, the *Cas9-natMX* would replace the genomic *SPO11* and be expressed as *SPO11* would have been (with *SPO11* promoter and terminator sequences). In order to perform one-step gene replacement with *Cas9-natMX*, pSP+ST-5 was cut with *NsiI* (New England Biolabs, NEB) prior to lithium acetate yeast transformation to target *Cas9-natMX* homologous recombination at the *SPO11* locus in the yeast strains K264-10D and RM26-26C to remove *SPO11* and replace with *Cas9*, (*spo11Δ::Cas9-natMX*; Figure 2.2). This one-step gene replacement method was used by Barbara Senger to generate the initial *spo11Δ::Cas9-natMX* candidates. Analysis revealed that although the *Cas9-natMX* cassette was integrated into the genome, it was not integrated in a way that removed the *SPO11* gene. Thus, an alternative method was used to generate the desired strains.

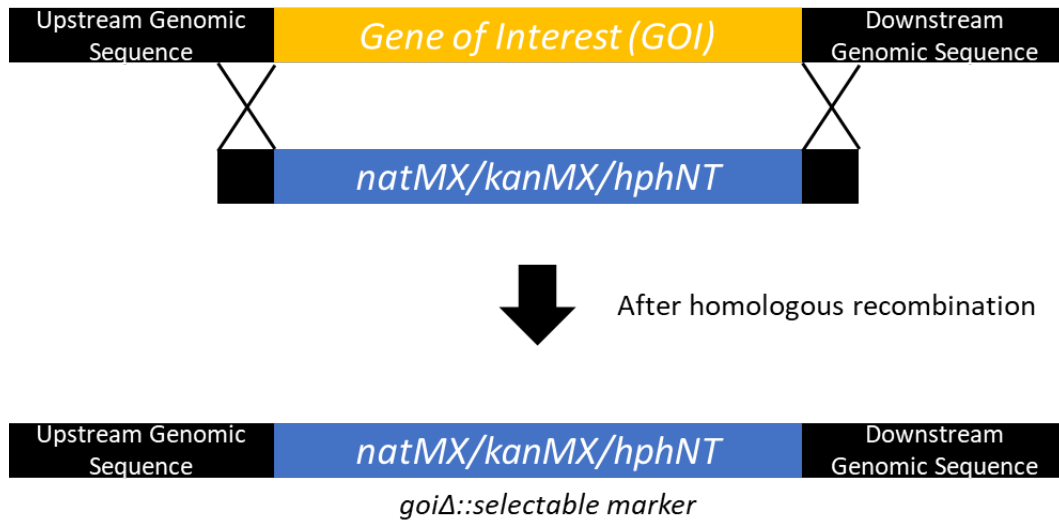


Figure 2.1. One-step gene replacement technique

A schematic representation of the one-step gene replacement technique. A selectable marker (resistance cassette) is amplified by PCR to contain homologous sequence upstream and downstream of GOI to be replaced through homologous recombination. Resistance cassettes that may be used throughout this dissertation: nourseothricin (*natMX*), geneticin or G418 sulfate (*kanMX*), or hygromycin B (*hphNT*). Once the gene has been deleted and replaced with a resistance cassette/selectable marker, this will be indicated by the naming convention of *goiΔ::selectable marker*.

To ensure that the *SPO11* gene was properly deleted and replaced with *Cas9-natMX*, haploid strains were generated by first deleting the *SPO11* gene via one-step gene replacement of *SPO11* with the geneticin (G418 sulfate) resistance cassette (*kanMX*). The *kanMX* cassette was amplified by polymerase chain reaction (PCR) from the plasmid pKKW1 using primers to add 40 nucleotides of homologous sequence immediately upstream and downstream of *SPO11* to generate a 1429 bp fragment that allows for homologous recombination at the *SPO11* locus (Appendices C and D; Figure 2.1).

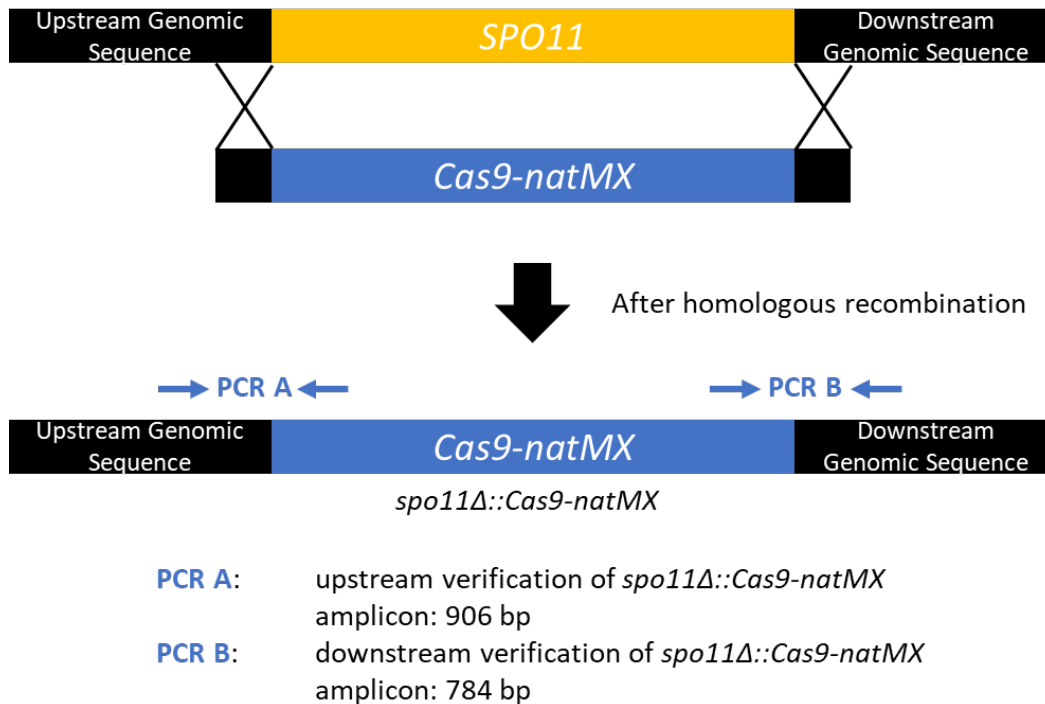


Figure 2.2. Replacement of genomic *SPO11* with *Cas9-natMX*, and PCR verification locations for confirmation of *Cas9-natMX* insertion

Amplicon sizes were calculated utilizing the freeware Serial Cloner. Note: both genomic *SPO11* and the *Cas9-natMX* cassette contain *Spo11* promoter and terminator sequences.

After confirming *spo11Δ::kanMX* candidates (by PCR, see paragraph below on candidate testing by PCR verification), the *kanMX* resistance cassette (at the genomic *SPO11* location) was replaced by one-step gene replacement with the *Cas9-natMX* cassette, cut out from pSP+ST-5. Prior to utilizing the *Cas9-natMX* cassette cut from pSP+ST-5, pSP+ST-5 was verified with diagnostic restriction digests using *BsoBI* (NEB) and *BsaHI* (NEB). A double digest with *NsiI* (NEB) and *AseI* (NEB) was performed on pSP+ST-5 that was used for lithium acetate yeast transformations. The *NsiI* (NEB) digest was done to cut out the *Cas9-natMX* cassette that would be utilized for gene replacement at the *SPO11* locus. The digest included *AseI* (NEB) to cut up leftover vector (containing CEN-ARS sequence) to reduce the possibility of obtaining transformants that grow on selective media due to the presence of intact plasmid (Figure 2.3).

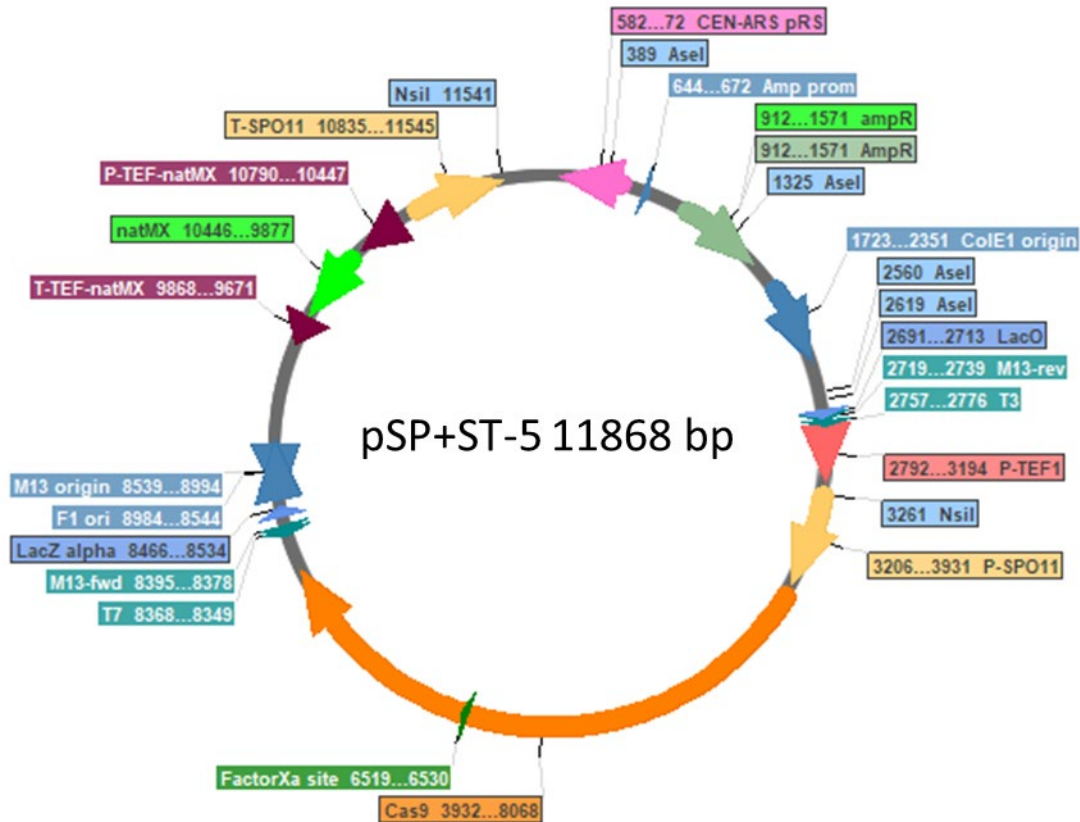


Figure 2.3. Predicted plasmid map for pSP+ST-5
Locations of *NsiI* and *AseI* restriction sites are shown.

All candidates were tested by isolating genomic DNA and performing upstream and downstream verification polymerase chain reaction (PCR). DNA was isolated from candidates and used in verification PCR. Verification of initial *Cas9-natMX* insertion candidates utilized the diagnostic primers (Appendix D): SPO11-UP-FOR, Cas9-NAT-UP-REV, Cas9-NAT-DOWN-FOR, SPO11-DOWN-REV to obtain a fragment for upstream verification (PCR A) and downstream verification (PCR B) (Figure 2.2). Verification of the presence/absence of genomic *SPO11* utilized the diagnostic primers SPO11-UP-FOR and SPO11-DOWN-REV (Appendix D). Verification of actual *spo11Δ::Cas9-natMX* haploids utilized primers further upstream/downstream than used for testing initial candidates: SPO11-UP-FOR-LONG, Cas9-NAT-UP-REV, Cas9-NAT-DOWN-FOR, SPO11-DOWN-REV-LONG (Appendix D).

Diploids were generated from crosses with initial and actual *spo11Δ::Cas9-natMX* haploids (Appendix B). RM96 derivative diploids were selected for on media lacking histidine (SD-His) because of genetic complementation of *his* gene mutations in the mated haploid strains.

RM96 derivative diploids were transformed by lithium acetate transformation to contain a plasmid that expresses a guide RNA for Cas9 utilization. The target DNA sequence for each guide RNA was incorporated into the same plasmid background, p426-SNR52p-gRNA.CAN1.Y-SUP4T. The three different guide RNA plasmids were generated by Brian Samuelson. Each gRNA plasmid type was transformed into strains separately, so that Cas9 would be targeted to break either the *LYS2* locus, X elements, or Y elements (X and Y elements are sub-telomeric regions of each chromosome). After transformation, RM96 derivative diploids containing a gRNA plasmid were selected for by growing on media lacking uracil (SD-Ura).

Vegetative growth and sporulation of cells

Mitotic growth utilized the rich media YPD (Appendix F). Diploids were sporulated on sporulation plate media (SPO) (2% potassium acetate, 0.039% COM supplement, pH 6.8; Appendix F) for 6 days at 30°C. Diploids containing a gRNA plasmid were sporulated similarly except that the SPO media lacked uracil. After sporulation, a sample taken from each sporulated patch was resuspended in sterile ddH₂O in order to observe cells on a hemocytometer under a light microscope (Olympus) at 40X magnification. Tetrads, dyads, and vegetative cells were counted (See Figure 1.3). Sporulation efficiency was calculated as the addition of tetrads and dyads observed divided by the total number of cells counted. Liquid sporulation of cells for protein collection and western blotting was performed as follows: Diploid cells grown in YPD to ~1.0 OD₆₀₀ in a 30°C shaker incubator was used to inoculate 50 mL YPA (1% potassium acetate, 2% peptone, 1% yeast extract; Appendix F). The YPA cultures were grown in a 30°C

shaker incubator overnight for 16 hours (hr). Cells were spun down, washed once in the liquid sporulation media commonly used by the Haring laboratory (H SPO; Appendix F) and then resuspended in 50mL H SPO. Equal volumes of cells were collected at timepoints indicated for western blotting. After 24 hours of liquid sporulation, the sporulation efficiency of each culture was calculated by observing the number of tetrads, dyads, and vegetative cells present on a hemocytometer using a light microscope.

Qualitative analysis of heteroallelic recombination and chromosome segregation by replica plating

RM96 strain background diploids were patched onto a master plate (YPD for strains without a gRNA and SD-Ura for strains with a gRNA) and replica plated to the following types of media for qualitative analysis of mitotic growth and meiotic spores (after diploid sporulation for 6 days at 30°C on SPO or SPO-Ura). Heteroallelic recombination at the *LEU1*, *LYS2*, and *TRP5* loci was assessed by colony growth on the respective SD-Leu, SD-Lys, and SD-Trp plates. As an indirect assessment of proper recombination, chromosome segregation of diploids was assessed both mitotically and meiotically by analyzing the diploid's heterozygous *CAN1^S* and *CYH2^S* alleles by replica plating to: SD+Can, SD+Cyh, SD+Can+Cyh. Mitotic diploids should be sensitive to both canavanine and cycloheximide whereas if chromosome segregation is occurring properly during meiosis, approximately half of spores should be able to grow on canavanine or cycloheximide. Replica plates were incubated for 4 days at 30°C. Pictures were taken.

Western blotting to detect Cas9 protein

Meiotic cell samples were collected by removing 6 mLs of cells from the H SPO culture at 0, 4, 5, 6, and 10 hours. Protein was extracted from meiotic cells samples with trichloroacetic

acid, precipitated by acetone washes, and resuspended in 1X Laemmli buffer containing 2.5% β -mercaptoethanol (β -me) (Cold Spring Harbor).

To detect Cas9 protein, 50 μ g of each protein sample was separated on a 6% resolving (37.5:1 mono:bis) with 4% stacking (29:1 mono:bis) SDS polyacrylamide gel by electrophoresis at 30 milli-Amperage (mAmp) constant current for 1.5 hours in 1X SDS buffer (Appendix F). After gel equilibration in transfer buffer (Appendix F), protein was transferred from the SDS PAGE gel to a nitrocellulose membrane at 0.4 Amp constant current for 1 hour in transfer buffer (Appendix F). Nitrocellulose membranes were ponceau stained (0.5% Ponceau S, 5% acetic acid) and de-stained (1% acetic acid) to check for even loading. Membranes were blocked for 2 hours with TBST buffer (Appendix F) + 3% nonfat dry skim milk powder. The membrane was incubated with HRP-conjugated Anti-CRISPR-Cas9 antibody (Abcam ab202580) at 1:5000 in TBST buffer + 3% skim milk powder at 4°C for 17.5 hours overnight on platform shaker. Western blots were washed five times with TBST buffer before developing. Western blots were developed using the PierceTM ECL 2 western blotting kit (Thermo Scientific) and imaged on the Storm 865 (GE Healthcare) imager provided by the NDSU Core Biology Facility.

Creation of *Saccharomyces cerevisiae* codon optimized Cas9, ScCas9

Saccharomyces cerevisiae codon optimized Cas9, ScCas9 was made by a two-step homologous recombination method to assemble five G-blocks into a vector backbone derivative of pCRCT (Bao et al. 2015) (Addgene, plasmid# 60621) (Appendix C). The vector backbone pCRCT was digested in 3.1 NEB buffer first with *BstEII* (NEB) at 60° C for 1 hour then second with *SwaI* (NEB) at 25° C for 1 hour to remove the *Streptococcus pyogenes* “improved” Cas9, iCas9, originally found in the vector (Bao et al. 2015). The five ScCas9 G-blocks, ScCas9-1 - ScCas9-5 (G-32 - G-36, Appendix E) were amplified by PCR with 50 ng of the G-block as the

starting template in each reaction with Q5 polymerase (NEB), 0.75mM added magnesium chloride, 0.4mM dNTPs, and 0.5μM primers. Primers used for g-block amplification were pCRT-ScCas9-F, ScCas9-2,4-R, ScCas9-2-F, ScCas9-2-R, ScCas9-3-F, ScCas9-3-R, ScCas9-4-F, ScCas9-4-R, pCRT-ScCas9-R-NEW, ScCas9-2,4-F (Appendix D).

A multi-step *in vivo* homologous recombination cloning method was used to assemble all the pieces, and the first step involved lithium acetate transformation of EGY194 with 5 μL of digested pCRCT and 15μL of each amplified G-block: ScCas9-1 and ScCas9-5 to allow for homologous recombination to create pCRT-ScCas9-1,5. Transformed yeast were selected for by plating to SD-Ura. A scrape of EGY194 transformed cells was taken and prepped for optimal plasmid recovery by following the yeast DNA isolation protocol without performing the RNaseA incubation. T1 *ccdB Escherichia coli* cells was transformed by electroporation with the obtained DNA and pCRT-ScCas9-1,5 was selected for on Luria-Bertani plates containing ampicillin (LB + amp). Isolated pCRT-ScCas9-1,5 candidate colonies were used to inoculate overnight bacterial cultures. Colony cracking was performed on 1 mL of cells, pelleted from culture. Cell pellets were resuspended in 50 μL of 1x lysis solution (also known as colony cracking buffer) (10mM Tris-HCl pH 8.0, 1mM EDTA pH 8.0, 15% sucrose, 2mg/mL lysozyme, 0.2mg/mL RNaseA, 0.1mg/mL BSA) and boiled at 100°C for 90 seconds. The tubes were then centrifuged to pellet debris. The supernatant was used to perform diagnostic restriction digestions using *SalI*-HF (NEB). The potential pCRT-ScCas9-1,5 candidate was mini-prepped and additional diagnostic restriction digestions were doing using *SalI*-HF, *BstEII*, *BglII*, *HincII*, and *XcmI* (NEB).

The second step of the *in vivo* homologous recombination cloning method involved lithium acetate transformation of EGY194 with 5 μL of pCRT-ScCas9-1,5/*SalI*-HF and 15μL of each amplified G-block: ScCas9-2, ScCas9-3, and ScCas9-4 to allow for homologous

recombination to create pCRT-ScCas9 selected for by plating to SD-Ura. The same steps were followed as before: taking a scrape of EGY194 transformed cells, isolating DNA for optimal plasmid recovery, electroporating T1 *ccdB Escherichia coli* cells with recovered DNA, and colony cracking cultures of candidates to use for diagnostic restriction digests with *BgIII* (NEB).

A candidate (pCRT-ScCas9#13) was sent for sequencing. Due to a frameshift mutation in the acquired pCRT-ScCas9#13 (B-1134, Appendix C), the plasmid was digested with *BstEII* (NEB) to allow for insertion of a new G-block ScCas9-1 by homologous recombination. The G-block ScCas9-1 was amplified by PCR with primers: pCRT-ScCas9-F and ScCas9-1-R (Appendix D). EGY194 were transformed by lithium acetate with 5 μ L pCRT-ScCas9#13/*BstEII* and 15 μ L amplified ScCas9-1. Similar steps were followed as before: taking a scrape of EGY194 transformed cells, isolating DNA for optimal plasmid recovery, electroporating T1 *ccdB Escherichia coli* cells with recovered DNA, and mini-prepping candidates to send for sequencing. Candidates had two mutations in the region of the G-block ScCas9-1. Site-directed mutagenesis was performed on the mutated pCRT-ScCas9 candidate by the BIOC474/674 2017 class utilizing the primers pCRT-ScCas9-Corrected (FS7)-*ScaI*-F and pCRT-ScCas9-Corrected(M161T)-*NdeI*-F.

The corrected pCRT-ScCas9 identified by RA from BIOC474/674 2017 was verified by sequencing and named pCRT-ScCas9.1 (B-1177, Appendix C). An unintentional *BsaI* site was introduced by the process of codon optimization. The extra *BsaI* site was removed by *in vitro* site-directed mutagenesis utilizing the primer REM-XTRA-*BsaI*-pCRT-ScCas9-F, the removal was necessary for the plasmid to be used for downstream golden-gate cloning to insert Cas9 target DNA (as originally designed for the vector backbone pCRCT). Two site-directed mutagenesis reactions were performed utilizing different polymerases, Q5 polymerase (NEB)

and Precision *Taq* (Applied Biological Materials Inc., abm) polymerase, thus candidates coming from the Q5 polymerase reaction include “Q” in their name and candidates coming from the Precision *Taq* reaction include “P” in their name. Candidates verified by diagnostic restriction digestion with *BsaI* (NEB) for loss of the extra *BsaI* site.

Results

Examination of BLS candidates

This project was originally started by Barbara Senger (BLS). Barbara had created the plasmid, pSP+ST-5 (B-1055), to use to replace genomic *SPO11* with *Cas9-natMX* and had obtained *spo11Δ::Cas9-natMX* candidates in the yeast strain backgrounds K264-10D and RM26-26C. Thus, I began this project with testing BLS’s candidates.

Verification of genomic integration of *Cas9-natMX* using PCR amplification (Figure 2.1), revealed several candidates for *Cas9-natMX* insertion (Figure 2.4). All candidates had an approximately 906 bp fragment produced from the upstream confirmation (PCR A) of *Cas9-natMX* insertion. PCR B was not as successful as PCR A, thus candidates from strain backgrounds were chosen based on amplification of the 784 bp fragment from the downstream confirmation (PCR B) of *Cas9-natMX* insertion.

After mating haploid candidates (denoted by * in Figure 2.4), diploids were selected for on SD-His. All possible combinations of the haploid candidates were crossed to obtain the diploid strains: AMA100-AMA108 (Appendix B). RM96, AMA100, AMA104, and AMA108 were sporulated on SPO for 5 days, then cells from patches were observed on a hemocytometer under a light microscope. The number of tetrads, dyads, vegetative, and total cells were recorded (Table 2.1). The calculated sporulation percentage was higher than wild-type for all diploids containing *Cas9-natMX*, which suggested that either 1) *Cas9-natMX* had been inserted into the

genome in such a way to allow PCR amplicons to confirm *Cas9-natMX* insertion, thus *SPO11* had not been deleted or 2) the presence of *Cas9-natMX* (without a gRNA to target Cas9 to a specific location(s)) was enough to cause sporulation.

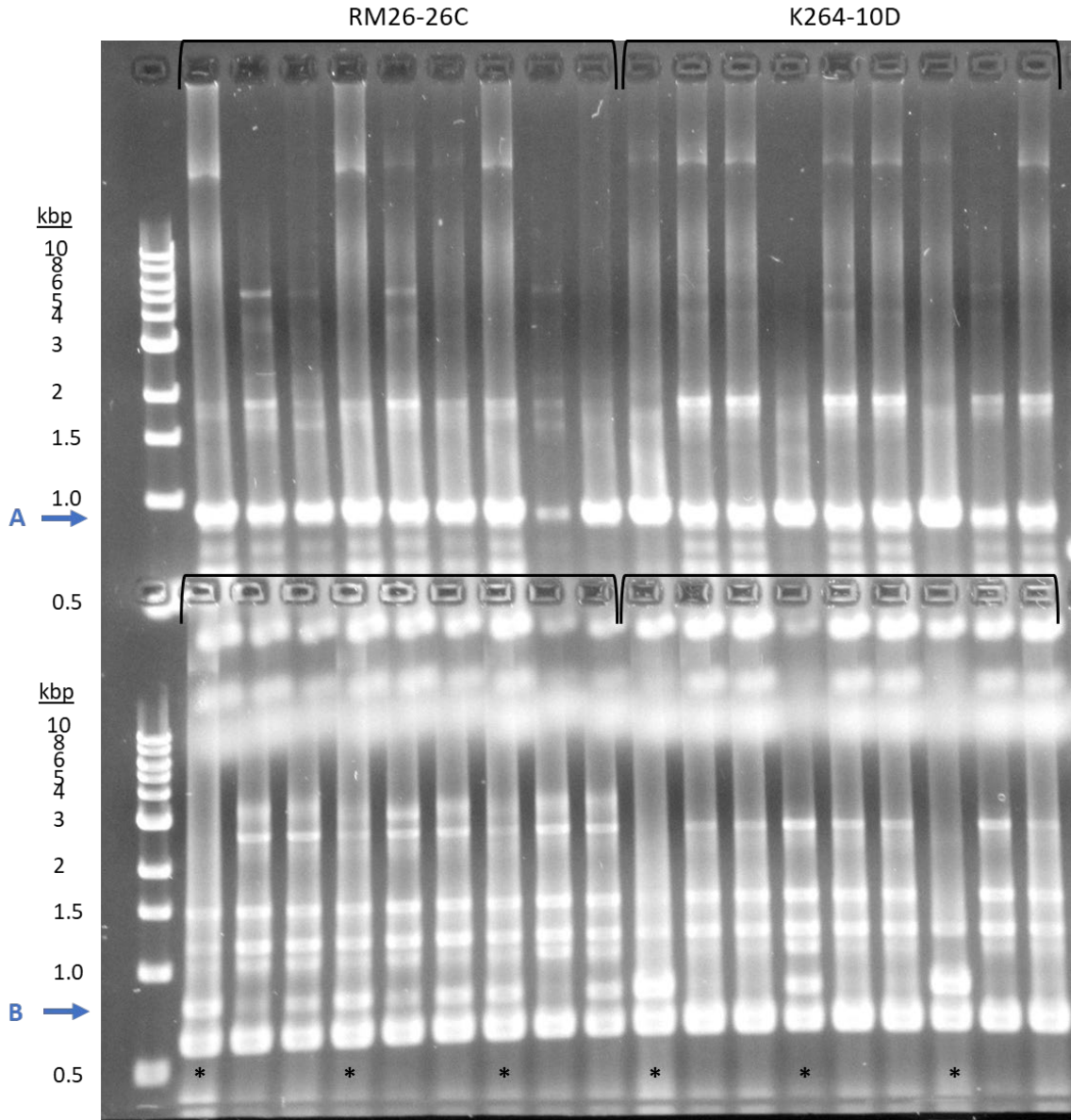


Figure 2.4. Confirmation of initial candidates containing *Cas9-natMX*

1.2% agarose gel, loaded in top lanes were PCR A samples from different candidates, with the lane directly below containing PCR B sample from the same candidate. Serial cloner predicts a *Cas9-natMX* insertion candidate should produce a 906 bp fragment upstream (A) and 784 bp fragment downstream (B). Nine candidates in each strain background (RM26-26C and K264-10D) were tested. *indicate which candidates were used to create diploids: RM26-26C candidates from left to right: 5.1, 6.1, 9.1; K264-10D candidates from left to right: 5.1, 6.1, 9.1.

Table 2.1. Sporulation efficiency of *Cas9-natMX* diploids

Strain	Relevant Genotype	Days ^a	Tetrads	Dyads	Vegetative Cells	Total Cells	% Sporulation
RM96	WT	5	67	11	394	472	16.5
AMA100	<i>Cas9-natMX/Cas9-natMX</i>	5	87	11	332	430	22.8
AMA104	<i>Cas9-natMX/Cas9-natMX</i>	5	122	16	268	406	34.0
AMA108	<i>Cas9-natMX/Cas9-natMX</i>	5	82	4	363	449	19.2

All strains listed are RM96 genetic background derivatives. RM96 is the wildtype (WT) control strain. ^a Number of days incubated at 30°C on solid sporulation media. Numbers reported are totals from analysis of two separate patches after sporulation. Percent sporulation was calculated by adding together the number of tetrads and dyads observed and dividing by the total number of cells analyzed.

As the first hypothesis was the simplest explanation for the observed phenomenon, I performed PCR with the outer *SPO11* primers (used prior in the separate upstream and downstream verification reactions) on wild-type (WT) strains, haploid candidates, and the three diploids in which sporulation efficiency had been measured (Figure 2.5). Utilizing the outer *SPO11* primers for PCR will produce a 1903 bp amplicon when *SPO11* is present. Three WT controls (both WT haploids and the WT diploid) were used as all would contain genomic *SPO11* and produce a 1903 bp fragment. The predicted 7609 bp amplicon produced if *spo11Δ::Cas9-natMX* occurred would have been unreliable to detect with PCR utilizing outer *SPO11* primers. Thus, the extension time chosen for PCR was for optimal amplification of the 1903 bp fragment to reduce the possibility for increased non-specific product amplification that could have occurred with longer extension times. An approximate 1903 bp amplicon was observed in all strains tested, indicating that genomic *SPO11* was still intact (Figure 2.5).

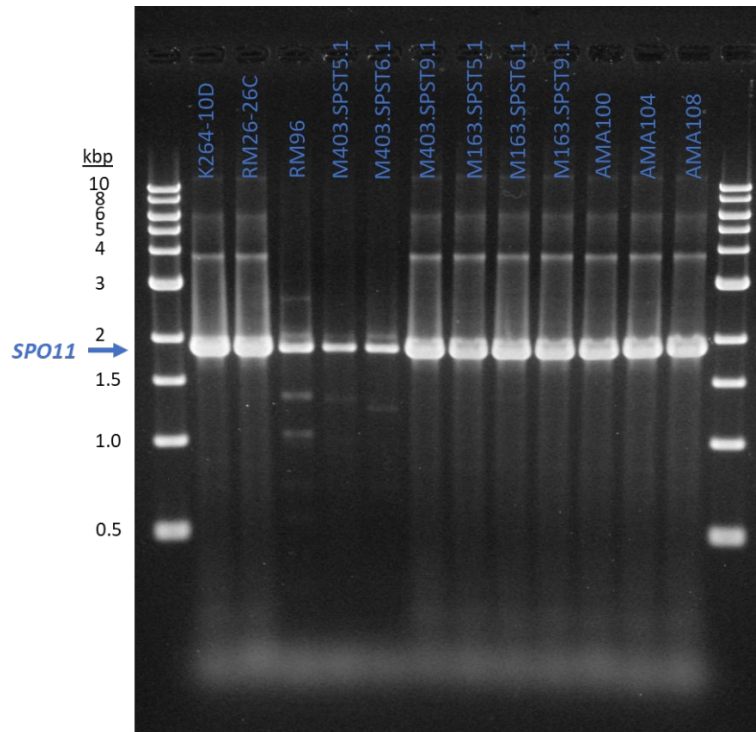


Figure 2.5. Verifying presence of *SPO11*

PCR samples produced from corresponding genomic DNA (labeled) with outer *SPO11* primers. Utilizing outer *SPO11* primers for PCR, Serial cloner predicts a 1903 bp fragment produced when genomic *SPO11* is present. Three wild-type (contain *SPO11*) controls were used: K264-10D (haploid), RM26-26C (haploid), and RM96 (diploid).

After testing BLS's original haploid strain candidates and 17 other candidates BLS had that were potential *spo11Δ::Cas9-natMX* candidates, it was discovered that genomic *SPO11* was present in all candidates (gels not shown). Thus, a new approach for creating *spo11Δ::Cas9-natMX* candidates was taken.

Creation and verification of actual *spo11Δ::Cas9-natMX* haploid strains

SPO11 was first deleted by one-step gene replacement with the *kanMX* cassette and then replaced with the *Cas9-natMX* cassette. In the first set of candidates tested, two *spo11Δ::kanMX* isolates in the RM26-26C strain background were identified (Figure 2.6 A). In the second set of candidates tested, two *spo11Δ::kanMX* isolates in the K264-10D strain background were identified (Figure 2.6 B). RM26-26C was used as the WT control for both sets of candidates.

After identifying correct candidates in set 1, one candidate was chosen to use as a positive control for identifying candidates in set 2. Positive candidates were renamed to reflect confirmed *spo11Δ*: M163S.4= M163spo11Δ.4, M163S.5= M163spo11Δ.5, M403.5= M403spo11Δ.5, M403.7= M403spo11Δ.7 (Appendix A).

Prior to digesting pSP+ST-5 for the purpose of using the *Cas9-natMX* cassette in one-step gene replacement, pSP+ST-5 was confirmed correct by diagnostic restriction digest (Figure 2.7). The precursor plasmid to pSP+ST-5 was pCas9-Nat-9, therefore pCas9-Nat-9 was used as a negative control. Additional plasmid isolates originally identified by BLS as containing SPO11 promoter and terminator sequences were also confirmed as correct (Figure 2.7).

Competent cells were made with the confirmed *spo11Δ::kanMX* isolates from each strain background, in order to replace the *kanMX* cassette (at the *SPO11* locus) with the *Cas9-natMX* cassette by one-step gene replacement. Candidates for *spo11Δ::kanMXΔ::Cas9-natMX* were tested by PCR utilizing the same internal *Cas9-natMX* primers as initially used but different external primers that were further upstream/downstream of the *SPO11* locus. Multiple correct candidates in both RM26-26C and K264-10D strain backgrounds were confirmed by PCR (Figure 2.8). The identified haploid candidates: M163spo11Δ::Cas9-natMX 1-2 (Figure 2.8A, B; RM26-26C background) and M403spo11Δ::Cas9-natMX 2-1 (Figure 2.8C; K264-10D background) were used in diploid creation (Appendix B).

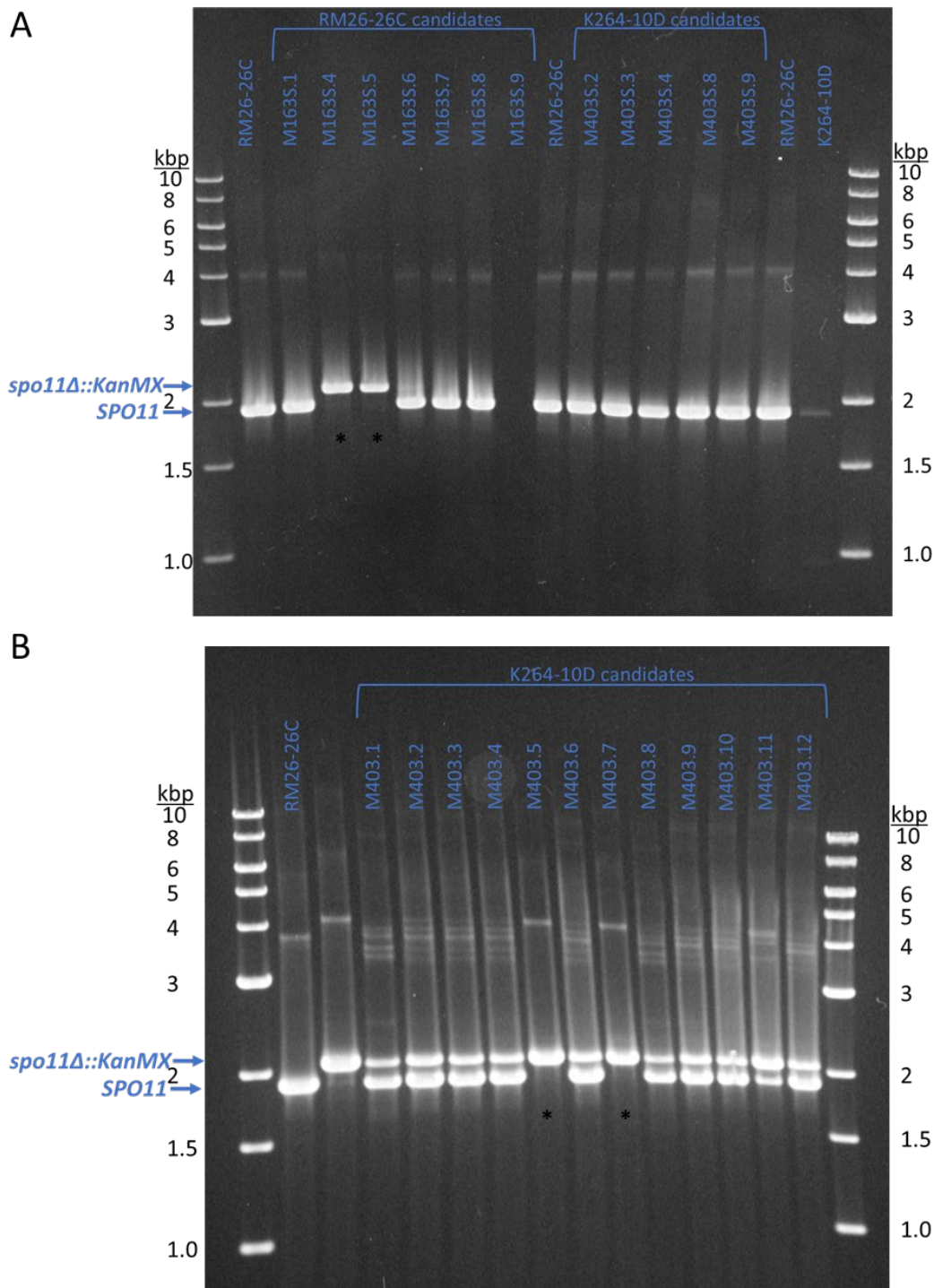


Figure 2.6. Candidates for *spo11Δ::kanMX*

(A) First set of candidates. (B) Second set of candidates. Both: PCR products produced from corresponding genomic DNA (labeled) with outer *SPO11* primers electrophoresed for ~3 hours on 1% agarose TAE gel. RM26-26C was used as the WT control. Predicted fragments: *SPO11*= 1903 bp, *spo11Δ::kanMX*= 2063 bp (insertion of the selectable marker makes this fragment longer). * indicates PCR product has confirmed *spo11Δ::kanMX* candidates.

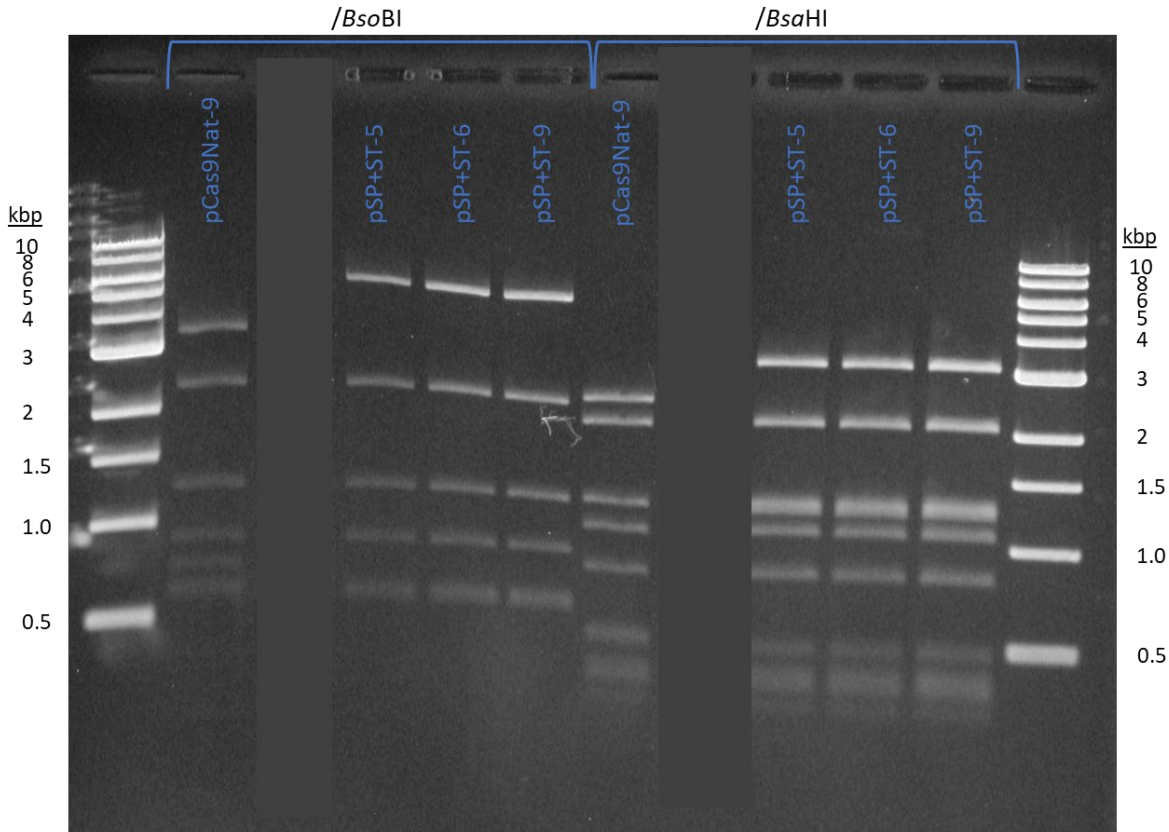


Figure 2.7. Confirmation of pSP+ST-5 by diagnostic restriction digest

Diagnostic restriction digests using *Bso*BI or *Bsa*HI was performed on pSP+ST-5 and two other potential *Cas9-natMX* plasmids with *SPO11* promoter and terminator sequences generated by BLS (pSP+ST-6 and pSP+ST-9). pCas9Nat-9 is shown as a control as it was the precursor plasmid BLS used to generate pSP+ST-5. Serial cloner predicted fragment sizes (bp):

pCas9Nat-9/*Bso*BI: 3975, 2316, 1253, 899, **745**, 631, 603, 25 **pSP+ST-5/*Bso*BI:** 6141, 2316, 1253, 899, 631, 603, 25 **pCas9Nat-9/*Bsa*HI:** 2406, 2072, 1259, 1227, 1066, 810, **503**, 474, 357, 273 **pSP+ST-5/*Bsa*HI:** 3116, 2072, 1259, 1227, 1066, 810, 474, 357, 273. Bolded sizes are different fragment sizes observed between the plasmids.

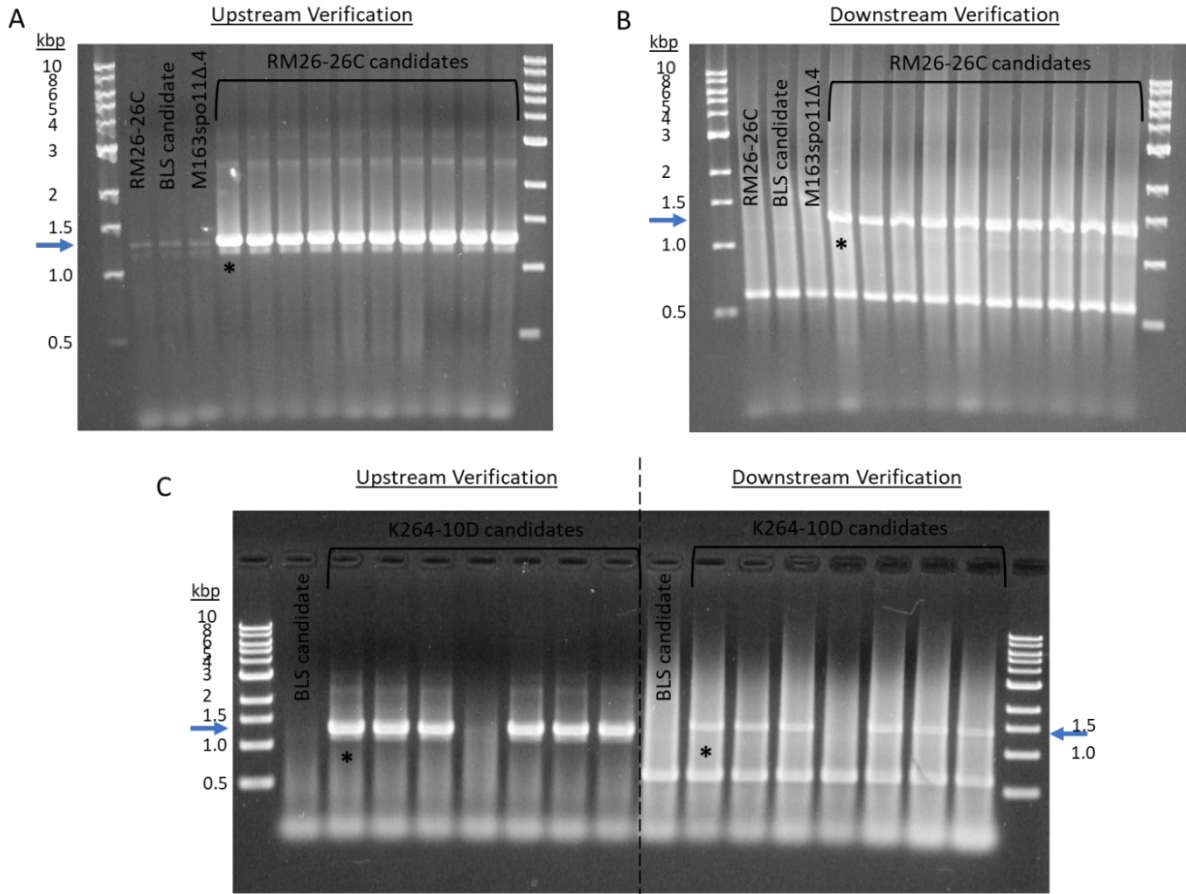


Figure 2.8. Verification of *spo11Δ::kanMXΔ::Cas9-natMX* candidates

Separate upstream and downstream PCR reactions were performed to verify insertion of *Cas9-natMX*. Verification for RM26-26C background *spo11Δ::kanMXΔ::Cas9-natMX* candidates are shown in (A) upstream and (B) downstream verification gel images and verification for K264-10D background *spo11Δ::kanMXΔ::Cas9-natMX* candidates is shown in (C). Negative controls that are shown in these images are: RM26-26C (WT), a BLS candidate (*SPO11* present and *Cas9-natMX* inserted), and M163spo11Δ.4 (*spo11Δ*, no *Cas9-natMX* inserted). Arrows indicate the approximate location of the predicted upstream fragment (1274 bp) and downstream fragment (1382 bp) that will only be produced upon successful *Cas9-natMX* insertion. *indicates the confirmed haploids (RM26-26C background: M163spo11Δ::Cas9-natMX 1-2; K264-10D background: M403spo11Δ::Cas9-natMX 2-1) used to create diploids.

Sporulation efficiency of diploid strains on solid sporulation media

Diploid strains created from correctly integrated haploids were AMA109-AMA114 (RM96 strain background). RM96, AMA109-AMA114, and the strains: AMA109, AMA112-AMA114 containing each of the three different gRNAs were sporulated on SPO for 6 days, then cells from patches were observed via light microscopy. The number of tetrads, dyads, vegetative,

and total cells were recorded (Table 2.2). The calculated sporulation percentage was 27.1% for the wild-type RM96 strain (Table 2.2). Derivative diploids containing only one wild-type copy of *SPO11* (heterozygous) sporulated at a similar frequency (26.9% and 31.1%) to the wild-type RM96 strain (Table 2.2). and all homozygous *spo11Δ* RM96 derivative diploids had reduced sporulation rates (9%, 6.6%, 8.3%) similar to the homozygous *spo11Δ* (AMA109) control strain at 6.7% (Table 2.2). The sporulation rates of all homozygous *spo11Δ* RM96 derivative diploids remained low with the addition of gRNAs (Table 2.2).

Table 2.2. Sporulation efficiency of *spo11Δ::Cas9-natMX* diploids with and without guide RNAs

Strain	Relevant Genotype	guide RNA	Tetrads	Dyads	Vegetative Cells	Total Cells	% Sporulation
RM96	WT	N/A	105	10	310	425	27.1
AMA109	<i>spo11Δ/ spo11Δ</i>	N/A	11	18	402	431	6.7
AMA110	<i>SPO11/ spo11Δ</i>	N/A	102	10	305	417	26.9
AMA111	<i>spo11Δ/ SPO11</i>	N/A	116	16	292	424	31.1
AMA112	<i>spo11Δ/ spo11Δ:: Cas9-natMX</i>	N/A	19	17	363	399	9.0
AMA113	<i>spo11Δ :: Cas9-natMX/ spo11Δ</i>	N/A	13	15	395	423	6.6
AMA114	<i>spo11Δ :: Cas9-natMX/ spo11Δ :: Cas9-natMX</i>	N/A	20	21	455	496	8.3
AMA109	<i>spo11Δ/ spo11Δ</i>	Y element	9	1	417	427	2.3
AMA112	<i>spo11Δ/ spo11Δ:: Cas9-natMX</i>	Y element	12	3	494	509	2.9
AMA113	<i>spo11Δ :: Cas9-natMX/ spo11Δ</i>	Y element	9	5	453	467	3.0
AMA114	<i>spo11Δ :: Cas9-natMX/ spo11Δ :: Cas9-natMX</i>	Y element	13	10	468	491	4.7
AMA109	<i>spo11Δ/ spo11Δ</i>	X element	10	2	402	414	2.9

Table 2.2. Sporulation efficiency of *spo11Δ::Cas9-natMX* diploids with and without guide RNAs (continued)

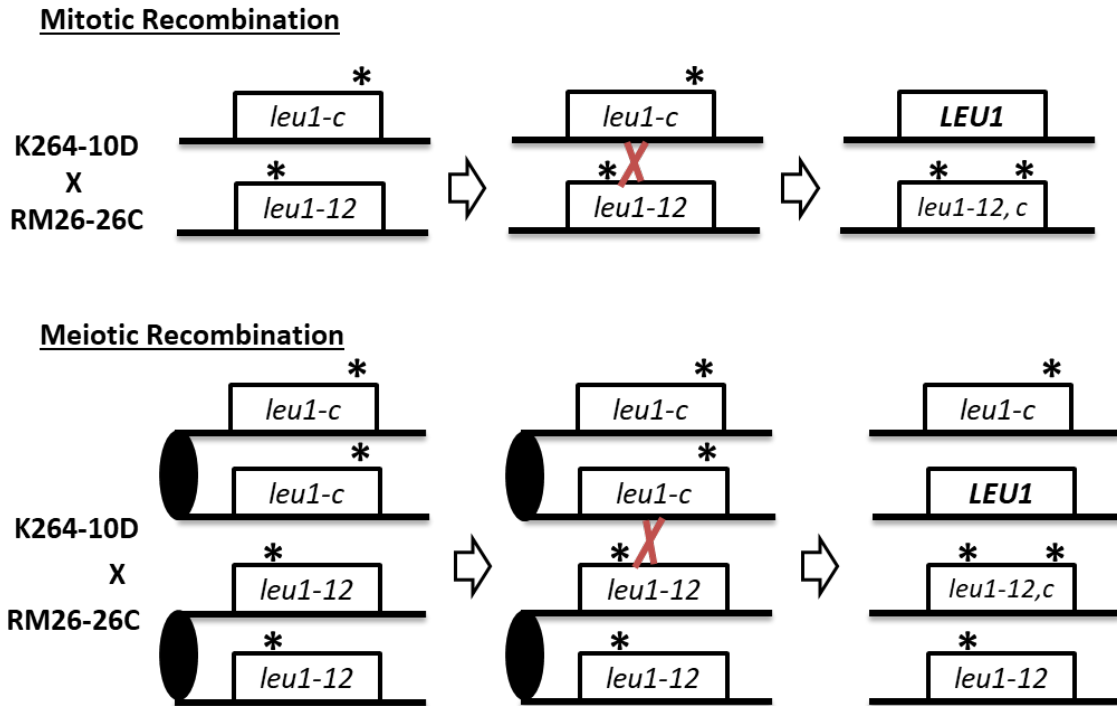
Strain	Relevant Genotype	guide RNA	Tetrads	Dyads	Vegetative Cells	Total Cells	% Sporulation
AMA112	<i>spo11Δ/ spo11Δ:: Cas9-natMX</i>	X element	7	3	452	462	2.2
AMA113	<i>spo11Δ :: Cas9-natMX/ spo11Δ</i>	X element	2	6	449	457	1.8
AMA114	<i>spo11Δ :: Cas9-natMX/ spo11Δ :: Cas9-natMX</i>	X element	8	5	444	457	2.8
AMA109	<i>spo11Δ/ spo11Δ</i>	<i>LYS2</i>	6	13	429	448	4.2
AMA112	<i>spo11Δ/ spo11Δ:: Cas9-natMX</i>	<i>LYS2</i>	8	8	406	422	3.8
AMA113	<i>spo11Δ :: Cas9-natMX/ spo11Δ</i>	<i>LYS2</i>	6	4	397	407	2.5
AMA114	<i>spo11Δ :: Cas9-natMX/ spo11Δ :: Cas9-natMX</i>	<i>LYS2</i>	12	7	468	487	3.9

All strains listed are RM96 genetic background derivatives. All strains were analyzed after incubation for 6 days at 30°C on solid sporulation media. For strains without a guide RNA, the numbers reported are totals from analysis of two separate patches. For strains with a guide RNA, the numbers reported are totals from analysis of the two guide RNAs targeting the same locus/loci but on opposite DNA strands. Statistical analysis (t-test: two-sample assuming unequal variances) was performed with Microsoft Excel software: strains containing one or more copies of *SPO11* did not sporulate with any statistically significant ($P < 0.05$) difference from the wild-type strain, all homozygous *spo11Δ* strains (with gRNA, *Cas9-natMX*, or *Cas9-natMX* + gRNA) did not sporulate with any statistically significant ($P < 0.05$) difference from the homozygous *spo11Δ* strain without a guide RNA, sporulation percentages of the wild-type strain and the homozygous *spo11Δ* strain without a guide RNA were statistically significant differences ($P < 0.05$).

Heteroallelic recombination is only increased when Cas9 is targeted directly to a site that allows for recombinational repair.

Heteroallelic recombination at the *LEU1*, *LYS2*, and *TRP5* loci was assessed by colony growth after replica plating to the respective SD-Leu, SD-Lys, and SD-Trp plates. As the diploid strains contain heteroalleles for all three loci (*LEU1*, *LYS2*, and *TRP5*), a recombination event

can occur between the mutations of the heteroalleles that results in a chromatid now containing the wild-type allele, as shown for the *LEU1* locus (Figure 2.9). After multiple mitotic divisions, a colony will be observed on media lacking leucine.



21

Figure 2.9. Heteroallelic recombination during mitosis and meiosis

This heteroallelic recombination example depicts the alleles for the *LEU1* locus in the RM96 (K264-10D X RM26-26C) diploid strain background. Mitotic heteroallelic recombination is only depicting chromatids involved directly in recombination. In both mitotic and meiotic recombination, if a recombination event occurs between two different heteroalleles, it is possible to obtain a wild-type allele and a mutant allele containing both mutations. Depicted for meiotic recombination is all chromatids present after pre-meiotic DNA synthesis in order to show the resulting spore genotypes from the recombination event depicted.

Qualitative analysis of heteroallelic recombination of RM96 derivative diploids was performed prior to introduction of a gRNA to investigate whether Cas9 off-target effects could increase the number of recombinant colonies, especially during meiosis in the absence of Spo11. All homozygous *spo11Δ* strains whether heterozygous or homozygous for *Cas9*, had either a similar number of recombinants or less recombinants when qualitatively compared to wild-type

(*SPO11*) cells during mitotic growth and when qualitatively compared to the homozygous *spo11Δ* diploid after growth of meiotic products (Figure 2.10). Interestingly, the heterozygous *spo11Δ* strains produced a similar number of meiotic recombinants as the wild-type strain, indicating that only one copy of *SPO11* is needed to obtain wild-type levels of meiotic recombination (Figure 2.10).

Strains containing Cas9 without a gRNA did not increase the number of heteroallelic recombinants. Next, gRNAs were introduced to target either X elements, Y elements, or the *LYS2* locus. Two gRNAs, targeting either X elements or Y elements, were designed to target the telomeric regions of the chromosome ends (Wellinger and Zakian 2012). Thus, the X element and Y element gRNAs would give Cas9 the ability to make breaks on multiple chromosomes. When strains containing both *Cas9* (AMA113; heterozygous and AMA114; homozygous) and an X element or Y element gRNA were qualitatively compared to strains lacking a gRNA (RM96, AMA109, AMA113, and AMA114) or the *spo11Δ* control strain (lacking *Cas9* but containing a gRNA) there was no apparent increase in the number of recombinant colonies (Figures 2.11 and 2.12).

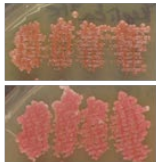
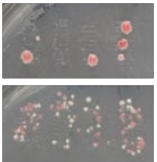
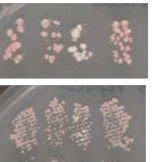
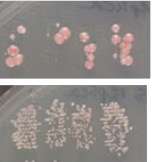
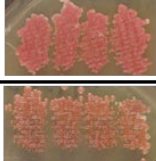
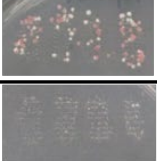
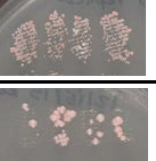
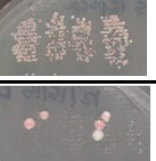
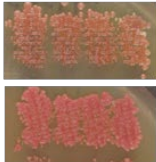


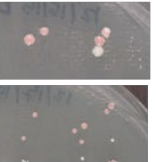
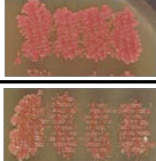
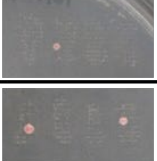
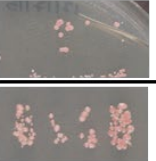
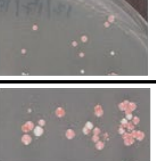

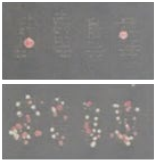
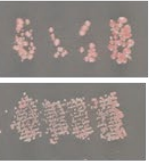
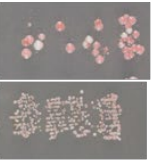
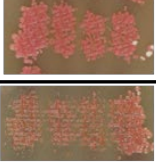
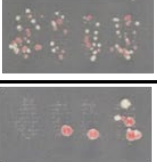
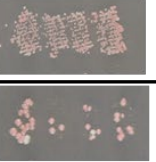
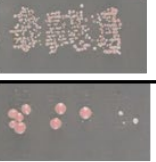
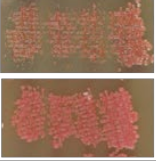
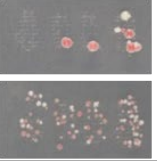
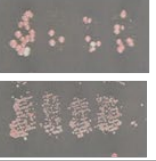
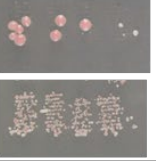
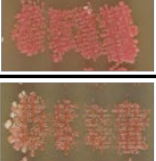
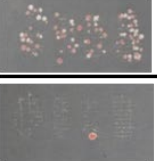
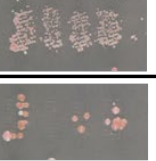
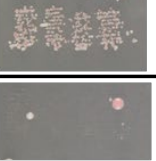
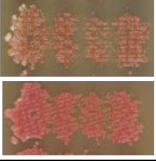
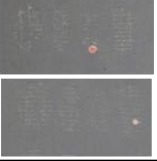
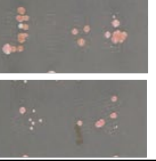
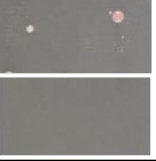
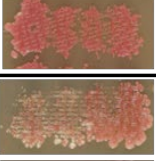
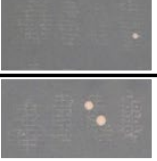
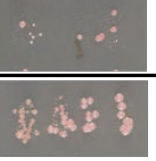
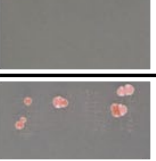
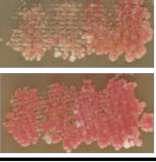
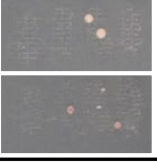

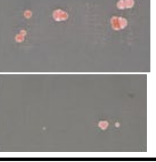
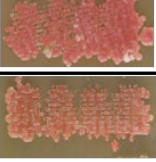
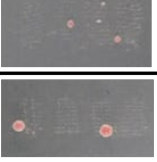
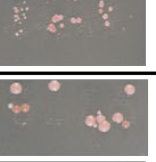
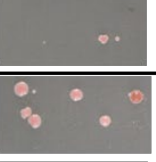
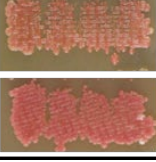
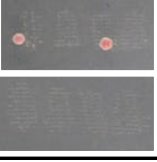
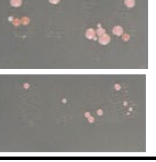
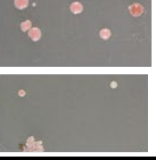

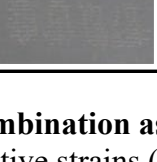


Relevant Genotype	YPD	SD-Lys	SD-Leu	SD-Trp	
WT					mitotic
					meiotic
<i>spo11Δ/ spo11Δ</i>					
					
<i>SPO11/ spo11Δ</i>					
					
<i>spo11Δ/ SPO11</i>					
					
<i>spo11Δ/ spo11Δ:: CAS9-NatMX</i>					
					
<i>spo11Δ:: CAS9-NatMX/ spo11Δ</i>					
					
<i>spo11Δ:: CAS9-NatMX/ spo11Δ:: CAS9-NatMX</i>					
					

Figure 2.10. Qualitative heteroallelic recombination assay

The relevant genotype for each RM96 derivative strains (AMA109, AMA113, AMA114) is denoted. Growth was analyzed on rich media (YPD), media lacking lysine (SD-Lys), media lacking leucine (SD-Leu), and media lacking tryptophan (SD-Trp). All growth was analyzed after 4 days at 30°C for both mitotic patches (top) and patches that had previously been sporulated (meiotic, bottom). One set of patches (out of two sets performed) for each strain is shown to represent the mitotic and meiotic growth observed. There were no observable differences between the two sets. None of these strains contained a gRNA.




















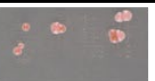


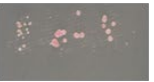









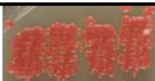



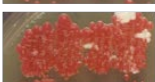


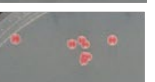
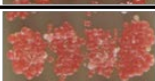


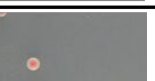

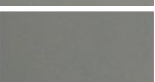


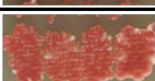


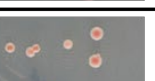



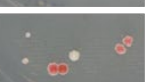
Relevant Genotype	YPD	SD-Lys	SD-Leu	SD-Trp	
WT					mitotic
					meiotic
<i>spo11Δ/ spo11Δ</i>					
					
<i>spo11Δ:: CAS9-NatMX/ spo11Δ</i>					
					
<i>spo11Δ:: CAS9-NatMX/ spo11Δ:: CAS9-NatMX</i>					
					
<i>spo11Δ/ spo11Δ</i> + X element gRNA					
					
<i>spo11Δ:: CAS9-NatMX/ spo11Δ</i> + X element gRNA					
					
<i>spo11Δ:: CAS9-NatMX/ spo11Δ:: CAS9-NatMX</i> + X element gRNA					
					

Figure 2.11. Qualitative heteroallelic recombination assay of strains containing an X element gRNA

The relevant genotype for each RM96 derivative strains (AMA109, AMA113, AMA114) is denoted. Growth was analyzed on rich media (YPD), media lacking lysine (SD-Lys), media lacking leucine (SD-Leu), and media lacking tryptophan (SD-Trp). All growth was analyzed after 4 days at 30°C for both mitotic patches (top) and patches that had previously been sporulated (meiotic, bottom). One set of patches (out of two sets performed) for each strain is shown to represent the mitotic and meiotic growth observed. There were no observable differences between the two sets.

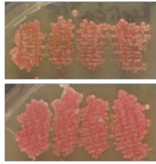
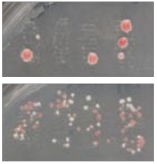
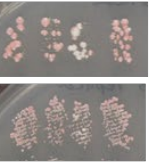

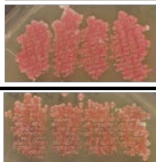
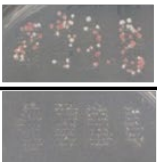
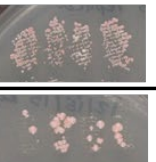
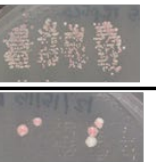
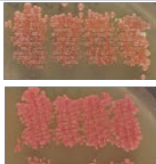

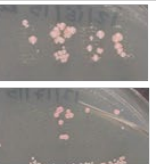

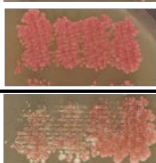
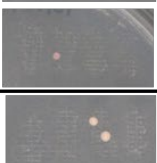
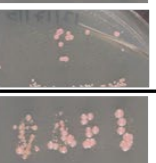
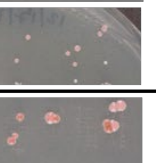
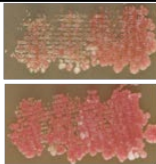
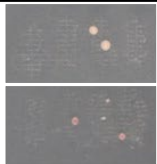
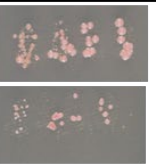
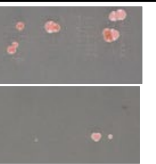
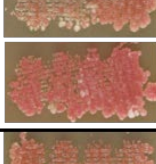

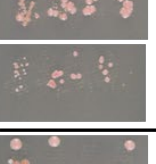
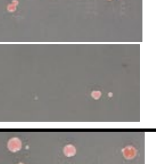
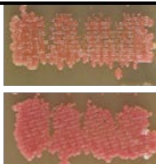

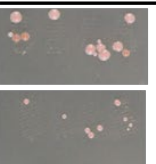
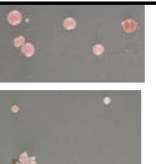
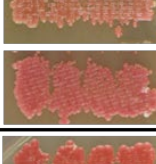
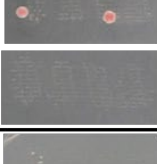
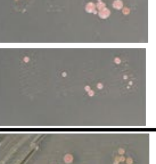
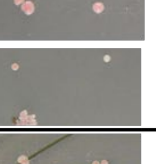
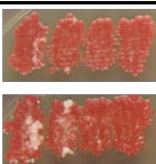
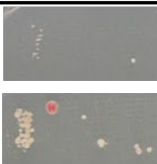
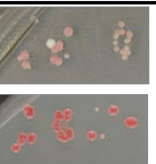
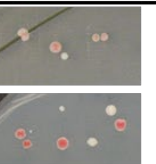
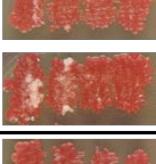
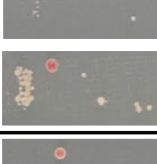
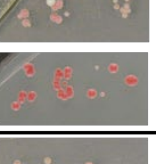
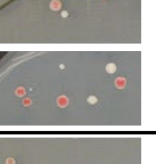
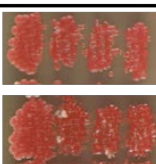
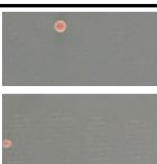
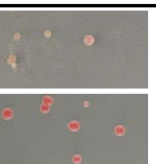
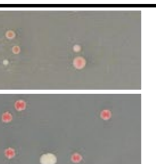
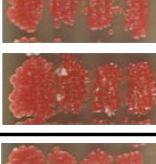
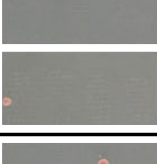
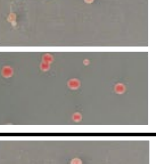
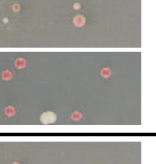
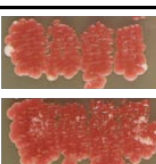
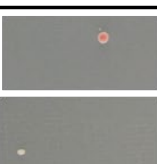
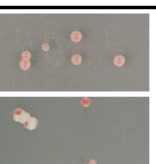
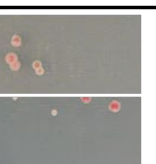
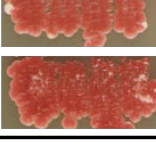

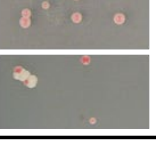
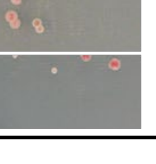
Relevant Genotype	YPD	SD-Lys	SD-Leu	SD-Trp	
WT					mitotic
					meiotic
<i>spo11Δ/ spo11Δ</i>					
					
<i>spo11Δ:: CAS9-NatMX/ spo11Δ</i>					
					
<i>spo11Δ:: CAS9-NatMX/ spo11Δ:: CAS9-NatMX</i>					
					
<i>spo11Δ/ spo11Δ</i> + Y element gRNA					
					
<i>spo11Δ:: CAS9-NatMX/ spo11Δ</i> + Y element gRNA					
					
<i>spo11Δ:: CAS9-NatMX/ spo11Δ:: CAS9-NatMX</i> + Y element gRNA					
					

Figure 2.12. Qualitative heteroallelic recombination assay of strains containing a Y element gRNA

The relevant genotype for each RM96 derivative strains (AMA109, AMA113, AMA114) is denoted. Growth was analyzed on rich media (YPD), media lacking lysine (SD-Lys), media lacking leucine (SD-Leu), and media lacking tryptophan (SD-Trp). All growth was analyzed after 4 days at 30°C for both mitotic patches (top) and patches that had previously been sporulated (meiotic, bottom). One set of patches (out of two sets performed) for each strain is shown to represent the mitotic and meiotic growth observed. There were no observable differences between the two sets.

The only gRNA that appeared to create an observable change in the number of recombinants was the *LYS2* gRNA (Figure 2.13). Strains containing *Cas9* (AMA113; heterozygous and AMA114; homozygous) and the *LYS2* gRNA showed an observable increase in the number of *LYS2* recombinants when compared to all other conditions, including wild-type, under both mitotic and meiotic conditions (Figure 2.13). There was no observable increase in the number of *LEU1* or *TRP5* recombinants when comparing strains containing both *Cas9* and the *LYS2* gRNA to strains lacking a gRNA (RM96, AMA109, AMA113, and AMA114) or the *spo11Δ* control strain (lacking *Cas9* but containing a gRNA) (Figure 2.13). These data suggest that *Cas9* is indeed functioning to make a break at the site that allows for heteroallelic recombinational repair. The data also suggest that *Cas9* protein may be present in similar amounts during both mitosis and meiosis (expression may not be meiotically-controlled), and that under these conditions if there are any off-target effects, they are unable to increase heteroallelic recombination (and likely unable to increase cell viability).

In the absence of Spo11, chromosome segregation is unaffected by Cas9 both in the absence and presence of any of the three different gRNAs utilized

Chromosome segregation was assessed by analyzing the heterozygous *CAN1* and *CYH2* alleles for colony growth on the respective SD+Can plates, SD+Cyh plates, and SD+Can+Cyh plates. Mutant alleles of *can1* and *cyh2* are recessive and confer resistance to canavanine and cycloheximide, respectively. Therefore, mitotic diploids containing one copy of each *CAN1^S* and *CYH2^S* should be sensitive to both canavanine and cycloheximide. If chromosome segregation is occurring properly during meiosis, approximately half of spores should be able to grow on either canavanine or cycloheximide as there is a 50% chance for spores to inherit the resistant (mutant) allele for each gene, an example is shown for *CAN1* locus (Figure 2.14).

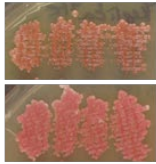
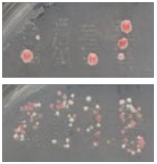
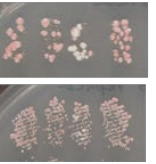
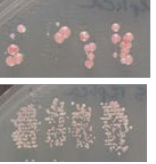
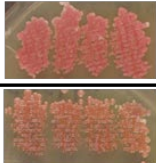
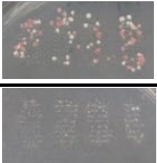
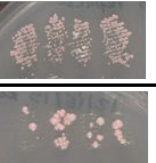
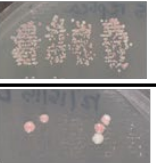
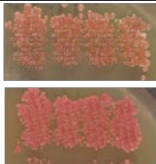



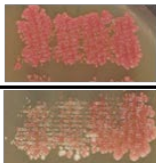
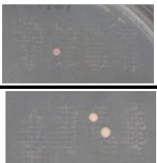
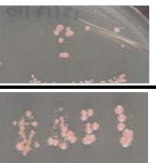
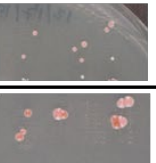
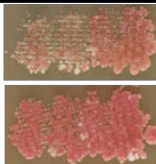
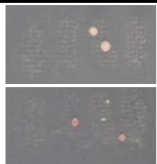

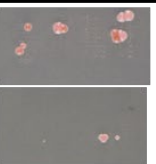
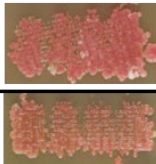
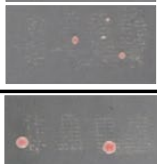
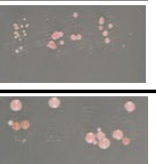
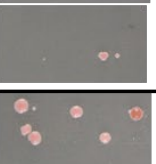
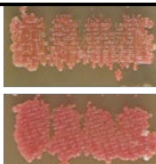
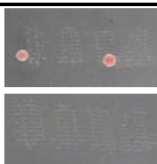
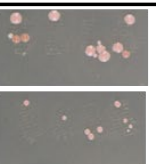
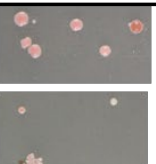
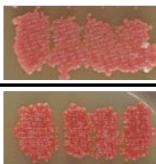
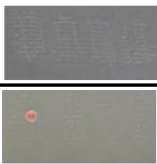
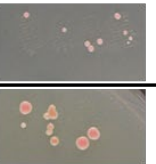
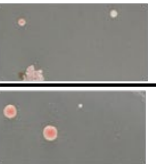
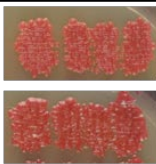
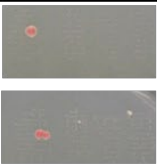
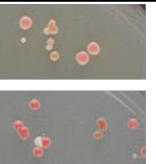
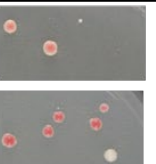
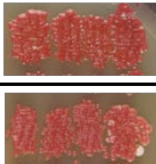
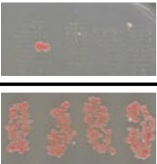
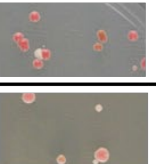
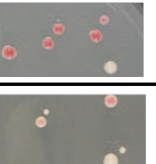
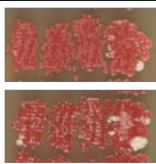
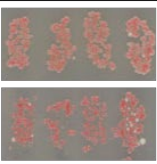
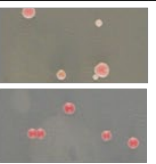
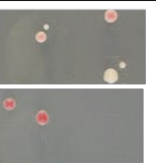
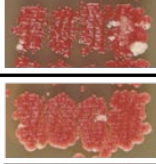
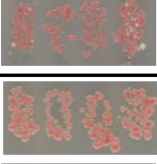
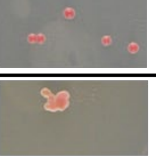
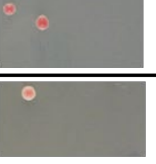
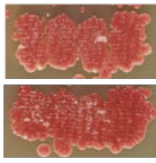
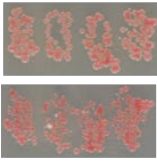
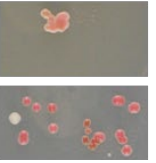
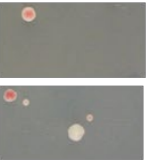
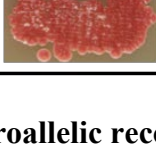
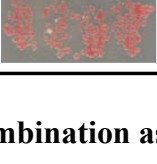


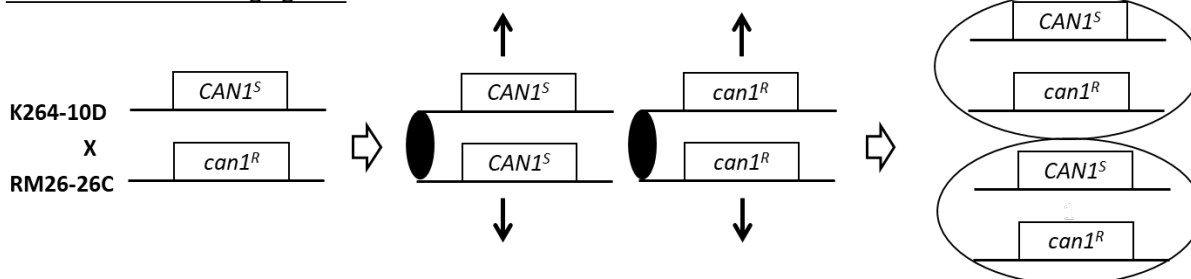
Relevant Genotype	YPD	SD-Lys	SD-Leu	SD-Trp	
WT					mitotic
					meiotic
<i>spo11Δ/ spo11Δ</i>					
					
<i>spo11Δ:: CAS9-NatMX/ spo11Δ</i>					
					
<i>spo11Δ:: CAS9-NatMX/ spo11Δ:: CAS9-NatMX</i>					
					
<i>spo11Δ/ spo11Δ</i> + <i>LYS2</i> gRNA					
					
<i>spo11Δ:: CAS9-NatMX/ spo11Δ</i> + <i>LYS2</i> gRNA					
					
<i>spo11Δ:: CAS9-NatMX/ spo11Δ:: CAS9-NatMX</i> + <i>LYS2</i> gRNA					
					

Figure 2.13. Qualitative heteroallelic recombination assay of strains containing a *LYS2* gRNA

The relevant genotype for each RM96 derivative strains (AMA109, AMA113, AMA114) is denoted. Growth was analyzed on rich media (YPD), media lacking lysine (SD-Lys), media lacking leucine (SD-Leu), and media lacking tryptophan (SD-Trp). All growth was analyzed after 4 days at 30°C for both mitotic patches (top) and patches that had previously been sporulated (meiotic, bottom). One set of patches (out of two sets performed) for each strain is shown to represent the mitotic and meiotic growth observed. There were no observable differences between the two sets.

Mitotic Chromosome Segregation



Meiotic Chromosome Segregation

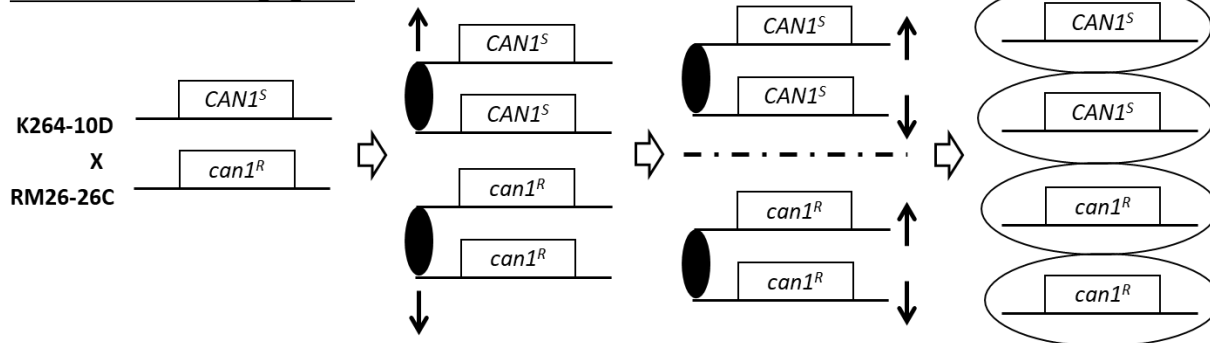


Figure 2.14. Chromosome segregation during mitosis and meiosis

This chromosome segregation example depicts the alleles for the *CAN1* locus in the RM96 (K264-10D X RM26-26C) diploid strain background. Mitotic chromosome segregation yields a genetic duplicate (daughter) of the original. In this case, original and daughter are both canavanine sensitive due to the presence of one copy of *CAN1^S*. Meiotic chromosome segregation yields spores with half the DNA content of the original. In this case, without any gene conversion events, two spores will be sensitive to canavanine (contain *CAN1^S*) while two spores will be resistant to canavanine (contain *can1^R*).

Qualitative analysis of chromosome segregation of RM96 derivative diploids was also performed prior to introduction of a gRNA. Due to genotype the wild-type (RM96) strain would only have colonies (growth) during mitosis if gene conversion occurs. Thus, colony growth on all mitotic plates containing canavanine and cycloheximide should be minimal (limited by the frequency of mitotic gene conversion). After meiosis however, the wild-type (RM96) strain should have a noticeable increase in growth on media containing canavanine and cycloheximide due to chromosome segregation. However, experimental analysis of the wild-type strain (RM96) only showed the expected growth on media containing cycloheximide (Figure 2.15). When analyzing mitotic and meiotic product growth on media containing canavanine, the wild-type

RM96 strain had unexpectedly high mitotic growth (Figure 2.15). Surprisingly, meiotic product growth on media containing canavanine was noticeably decreased in all homozygous *spo11Δ* strains when compared to the wild-type (RM96) and heterozygous *SPO11* strains (Figure 2.15). This suggests that although mitotic growth of all strains on media containing canavanine was much greater than expected, a significant portion of meiotic product growth is still dependent on proper chromosome segregation promoted by Spo11 that is necessary for viability.

The homozygous *spo11Δ* strain (AMA109), a heterozygous *Cas9* strain (AMA113), and the homozygous *Cas9* strain (AMA114) containing a gRNA showed a slight increase in meiotic product growth when compared to the same strains without a gRNA, consistent between each different gRNA (Figures 2.16, 2.17, 2.18). Because meiotic product growth of the *spo11Δ* control (+ gRNA) strain was increased when compared to the same strain without a gRNA (Figures 2.16, 2.17, 2.18), this makes it unlikely that the gRNA addition to the *Cas9*-containing strains caused the increase in meiotic product growth. The slight increase in meiotic product growth observed could be attributed to replica plating strains containing a gRNA at a different time than the strains without a gRNA. Therefore, it appears *Cas9* with a gRNA was unable to promote proper chromosome segregation.

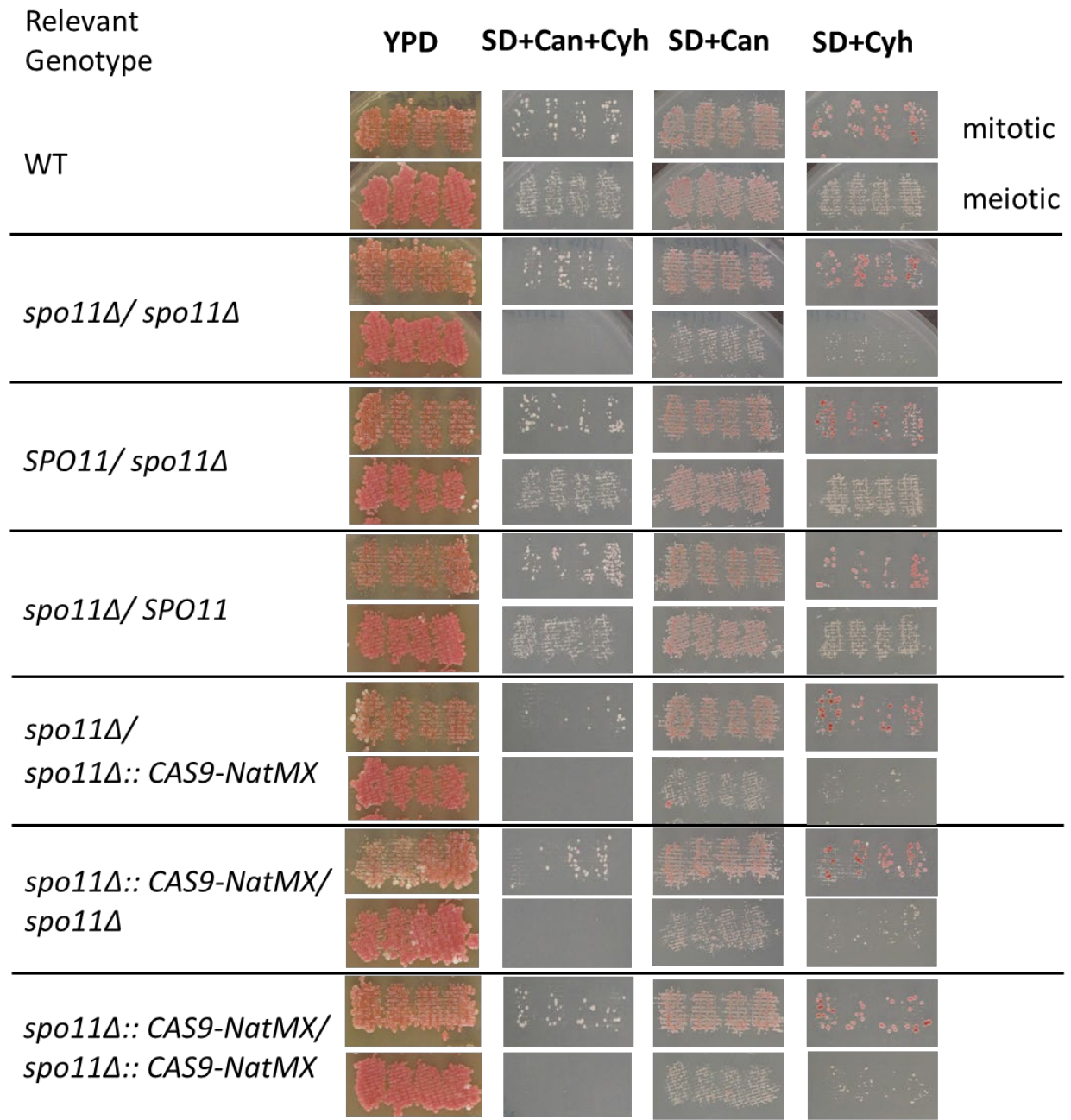


Figure 2.15. Qualitative chromosome segregation assay

The relevant genotype for each RM96 derivative strains (AMA109, AMA113, AMA114) is denoted. Growth of patches was assessed on rich media (YPD), media containing either canavanine (SD+Can) or cycloheximide (SD+Cyh) or both canavanine and cycloheximide (SD+Can+Cyh). All growth was analyzed after 4 days at 30°C for both mitotic patches (top) and patches that had previously been sporulated (meiotic, bottom). One set of patches (out of two sets performed) for each strain is shown to represent the mitotic and meiotic growth observed. There were no observable differences between the two sets. None of these strains contained a gRNA.

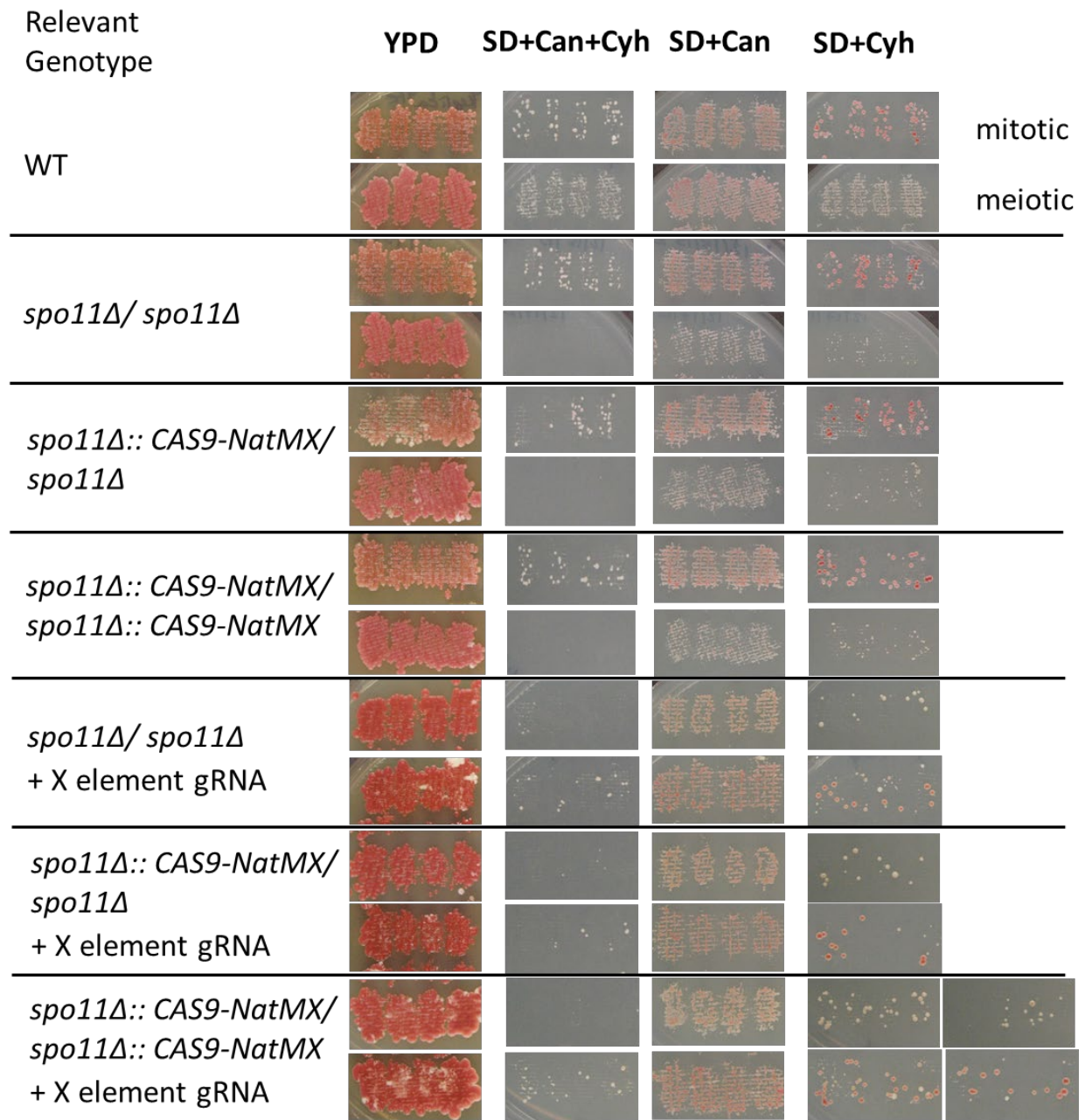


Figure 2.16. Qualitative chromosome segregation assay of strains containing an X element gRNA

The relevant genotype for each RM96 derivative strains (AMA109, AMA113, AMA114) is denoted. Growth of patches was assessed on rich media (YPD), media containing either canavanine (SD+Can) or cycloheximide (SD+Cyh) or both canavanine and cycloheximide (SD+Can+Cyh). All growth was analyzed after 4 days at 30°C for both mitotic patches (top) and patches that had previously been sporulated (meiotic, bottom). Due to the difference in microcolony amount between the two sets, both sets of patches are shown for the homozygous *spo11Δ::Cas9-natMX* (AMA114) + X element gRNA on SD+Cyh media.

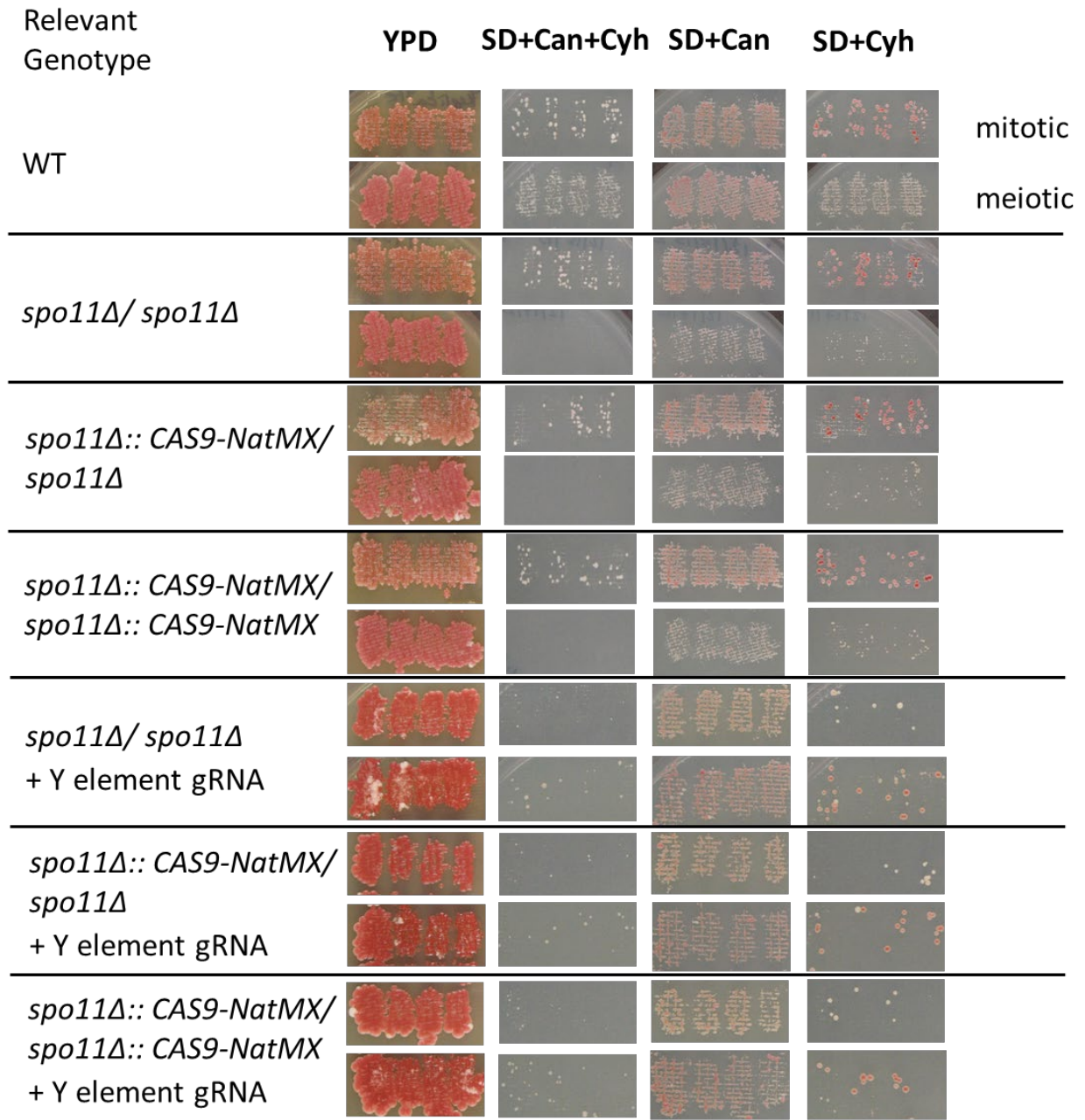


Figure 2.17. Qualitative chromosome segregation assay of strains containing a Y element gRNA

The relevant genotype for each RM96 derivative strains (AMA109, AMA113, AMA114) is denoted. Growth of patches was assessed on rich media (YPD), media containing either canavanine (SD+Can) or cycloheximide (SD+Cyh) or both canavanine and cycloheximide (SD+Can+Cyh). All growth was analyzed after 4 days at 30°C for both mitotic patches (top) and patches that had previously been sporulated (meiotic, bottom). There were no observable differences between the two sets of patches for Y element gRNAs.

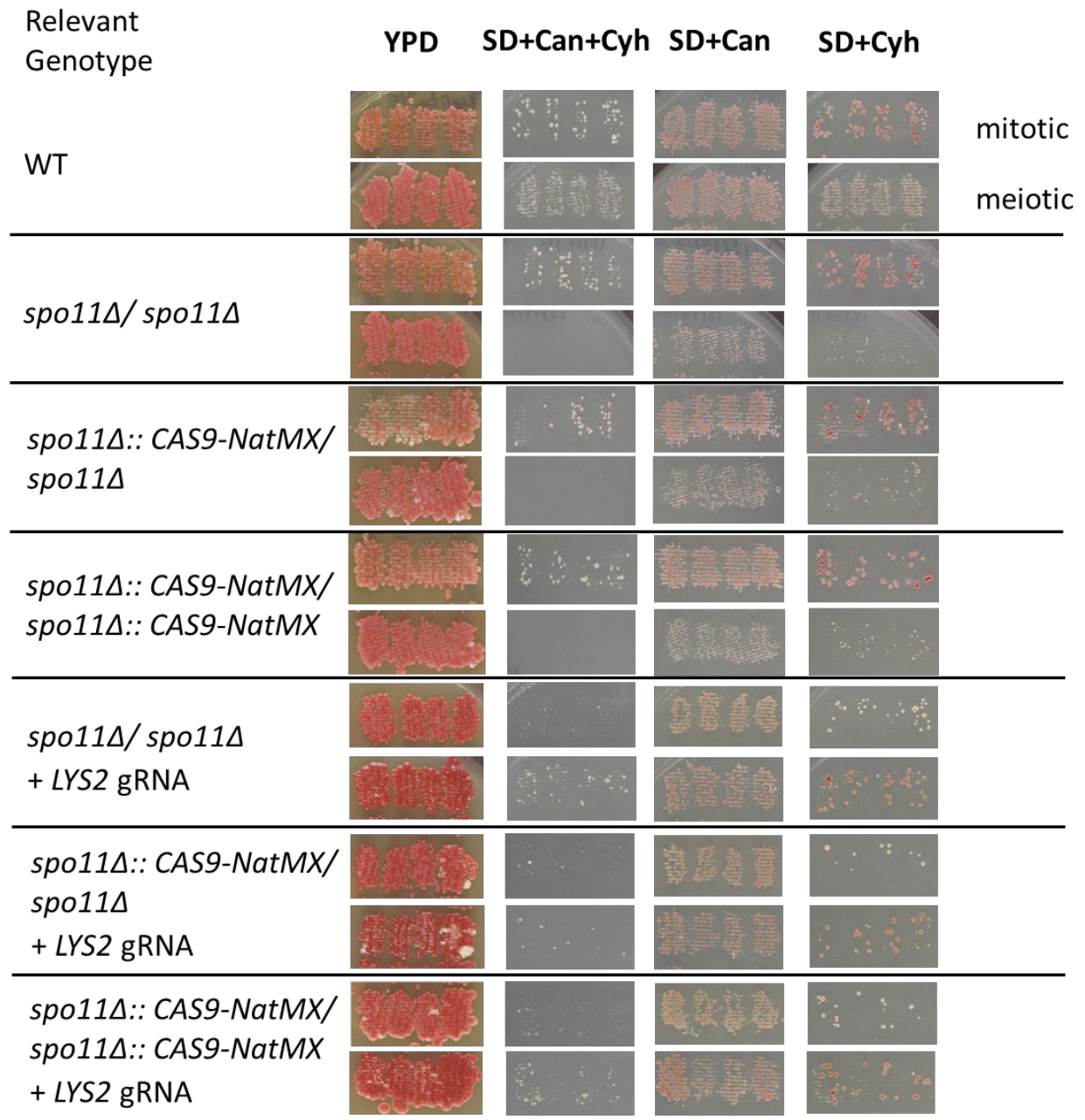


Figure 2.18. Qualitative chromosome segregation assay of strains containing a *LYS2* gRNA

The relevant genotype for each RM96 derivative strains (AMA109, AMA113, AMA114) is denoted. Growth of patches was assessed on rich media (YPD), media containing either canavanine (SD+Can) or cycloheximide (SD+Cyh) or both canavanine and cycloheximide (SD+Can+Cyh). All strains were analyzed for mitotic chromosome segregation after 4 days of incubation at 30°C (top). All growth was analyzed after 4 days at 30°C for both mitotic patches (top) and patches that had previously been sporulated (meiotic, bottom). There were no observable differences between the two sets of patches for *LYS2* gRNAs.

Western blotting reveals Cas9 protein abundance did not increase during meiosis

As mentioned above, analysis of heteroallelic recombination at the *LYS2* locus indicated that Cas9 protein is not only expressed at some level during mitosis, but also may not be increasing in abundance during meiosis. Therefore, samples were taken from *Cas9*-containing strains at different time points during liquid sporulation to use for protein analysis by western blotting. After 24 hours of liquid sporulation, cultures were observed under a microscope to count the number of tetrads, dyads, and vegetative cells present to calculate the sporulation efficiency. The wild-type RM96 strain sporulated at 52.4%, the homozygous *spo11Δ* strain sporulated at 20.1%, and all homozygous *spo11Δ* strains containing *Cas9* sporulated at similar frequencies (11.5-11.8%) and less than homozygous *spo11Δ* strain without *Cas9* (Table 2.3).

Table 2.3. Sporulation efficiency of *spo11Δ::Cas9-natMX* diploid strain cultures used for western blot analysis of Cas9 protein

Strain	Relevant Genotype	Tetrads	Dyads	Vegetative Cells	Total Cells	% Sporulation
RM96	WT	107	3	100	210	52.4
AMA109	<i>spo11Δ/</i> <i>spo11Δ</i>	33	11	175	219	20.1
AMA112	<i>spo11Δ/</i> <i>spo11Δ::</i> <i>Cas9-natMX</i>	22	6	212	240	11.7
AMA113	<i>spo11Δ ::</i> <i>Cas9-natMX/</i> <i>spo11Δ</i>	22	5	202	229	11.8
AMA114	<i>spo11Δ ::</i> <i>Cas9-natMX/</i> <i>spo11Δ ::</i> <i>Cas9-natMX</i>	21	5	201	227	11.5

All strains listed are RM96 genetic background derivatives. All strains were analyzed after 24 hours of sporulation in H SPO at 30°C in shaker incubator.

Two western blots were done utilizing protein samples of the homozygous *spo11Δ* strain (AMA109), a heterozygous *Cas9* strain (AMA113), and the homozygous *Cas9* strain (AMA114). Examination of the timing of Cas9 protein expression (Figure 2.19A, Timing) shows that the Cas9 antibody specifically detected Cas9 protein as two migratory species; no species were detected in the homozygous *spo11Δ* strain (AMA109). It is unclear why two species are specifically detected by the Cas9 antibody; the top species could be a post-translationally-modified Cas9 or the bottom species could be a degradation product. Examination of the dosage of Cas9 protein expression was performed to compare the amount of Cas9 protein present in the heterozygous *Cas9* strain versus the homozygous *Cas9* strain; the heterozygous strain appears to have less Cas9 protein present at zero and four hours, at five and six hours the heterozygous strain is indistinguishable from the homozygous strain (Figure 2.19B, Dosage). However, protein loaded from the homozygous *Cas9* strain in both the timing and dosage western blots came from the same sample, so it is unlikely that any appearance of differing amounts of Cas9 can be attributed to an actual difference in the amount of protein (Figure 2.19). It is clear that Cas9 is expressed at 0 hours (mitosis) and that its expression does not appear to increase much (if at all) during meiosis.

Creation of a *Saccharomyces cerevisiae* codon optimized *Cas9*, *ScCas9*

The *Saccharomyces cerevisiae* codon optimized *Cas9*, *ScCas9*, was created by a multi-step *in vivo* homologous recombination cloning method that allowed for the assembly of the five *ScCas9* G-blocks into the vector backbone of pCRCT (Bao et al. 2015). The vector backbone pCRCT was digested with *BstEII* and *SwaI* to create two pieces: (1) 3583 bp of iCas9 (the original non-yeast *Cas9*) and (2) 7255 bp of vector with cut ends available for use in homologous

recombination (Figure 2.20A). The amplified G-blocks were all approximately 1000 bp (Figure 2.20B).

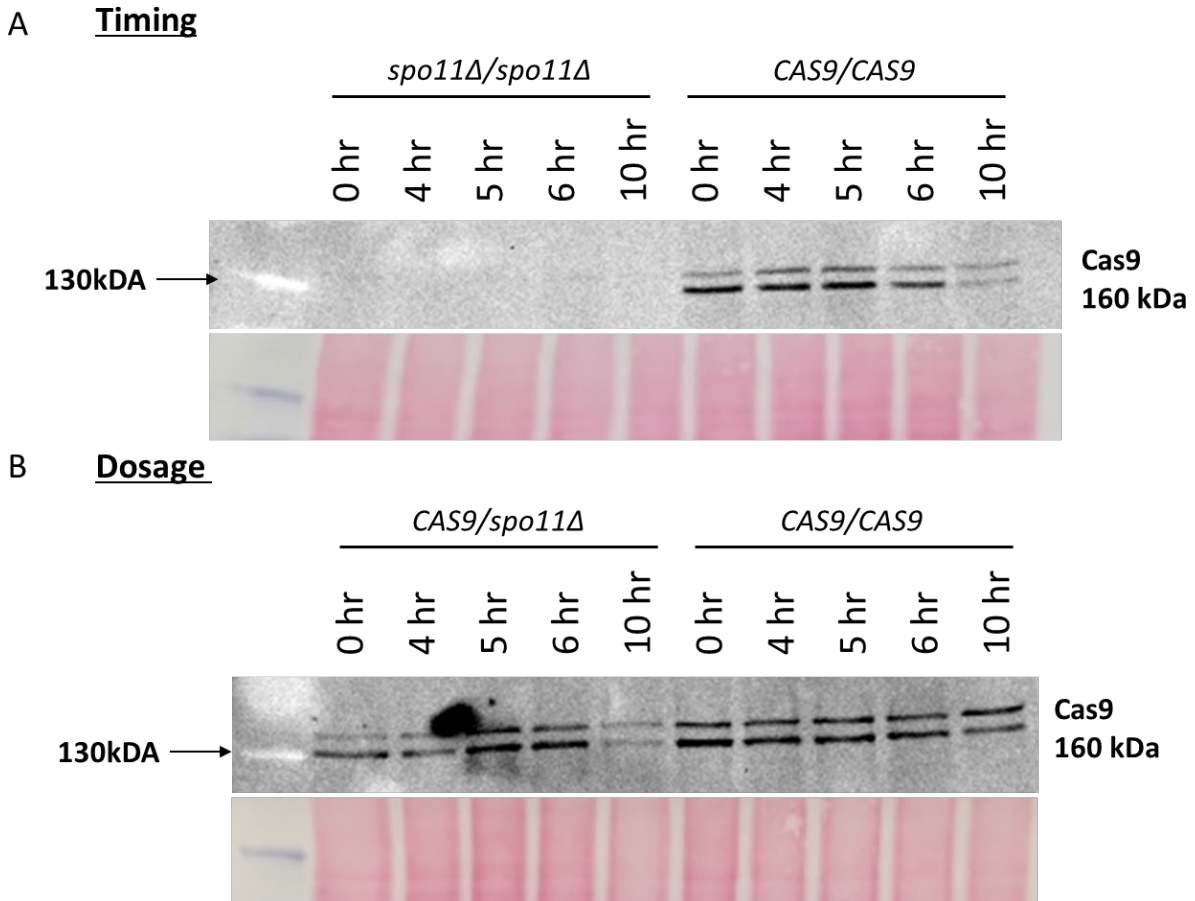


Figure 2.19. Detection of Cas9 protein during meiosis

Cas9 protein observed via western blot in RM96 derivatives during meiosis at the indicated timepoints (in hours, hr). The 130 kDa molecular weight band is shown. A 6% resolving (37.5:1 mono:bis) with 4% stacking (29:1 mono:bis) SDS polyacrylamide gel was used to separate 50 μg of total protein from each sample. Anti-CRISPR Cas9 antibody (1:5000 Abcam ab202580) was used to detect the Cas9 protein. Ponceau staining was performed to check for even loading and shown below each blot. (A) Timing blot shows Cas9 protein is detected in homozygous *spo11Δ::Cas9* strain (AMA114, *CAS9/CAS9*) and not in the homozygous *spo11Δ* strain (AMA109). (B) Dosage blot shows Cas9 protein is detected in heterozygous (AMA113) and homozygous (AMA114) Cas9 diploids. Note: It is unclear whether the two species observed represent either a Cas9 + post-translationally modified Cas9 (top species) or a Cas9 + degradation product (bottom species). Both species are specifically recognized by the Cas9 antibody, as no species are observed in the *spo11Δ* strain (AMA109).

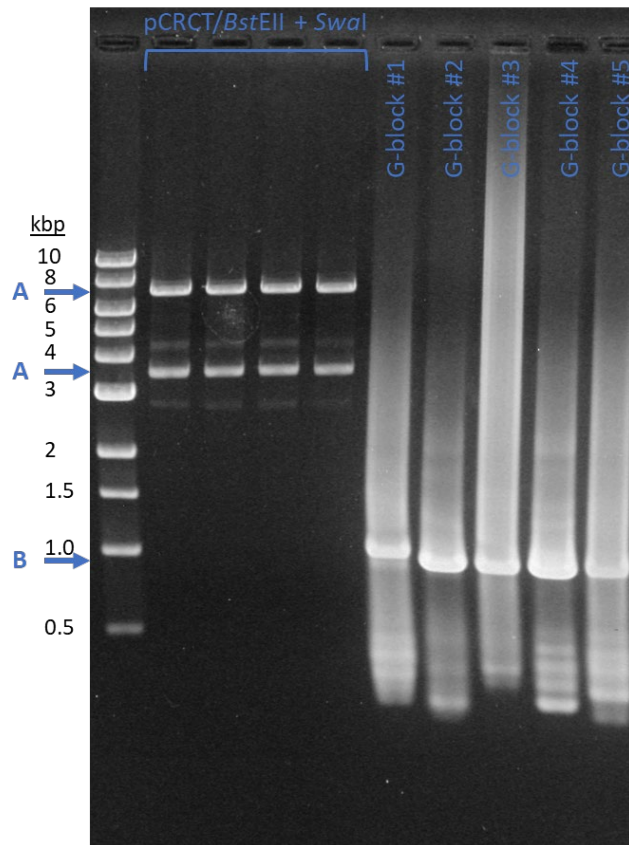


Figure 2.20. Digested pCRCT vector and amplified G-blocks for generation of *Saccharomyces cerevisiae* codon optimized *Cas9* (*ScCas9*)

Analysis of vector and G-blocks prepared for use in HR cloning on 1% agarose TAE gel. Fragment sizes of DNA ladder are labeled. Denoted by arrows labeled “A” are Serial cloner predicted fragment sizes (bp): pCRCT/*BstEII* + *Swal*: 7255, 3583. Denoted by arrows labeled “B” are the amplified G-blocks approximately 1000 bp.

The first step of the *in vivo* cloning method generated pCRT-*ScCas9*-1,5. Correct candidate plasmids should be linearized when digested with *SalI*, creating an approximately 8600 bp fragment (Figure 2.21A). The candidate identified in Figure 2.21A as pCRT-*ScCas9*-1,5 was more thoroughly analyzed by performing multiple diagnostic restriction digests and compared to digests of the pCRCT control (Figure 2.21B). Fragments sizes observed for pCRT-*ScCas9*-1,5 digests appear to be representative of predicted fragment sizes (Figure 2.21B).

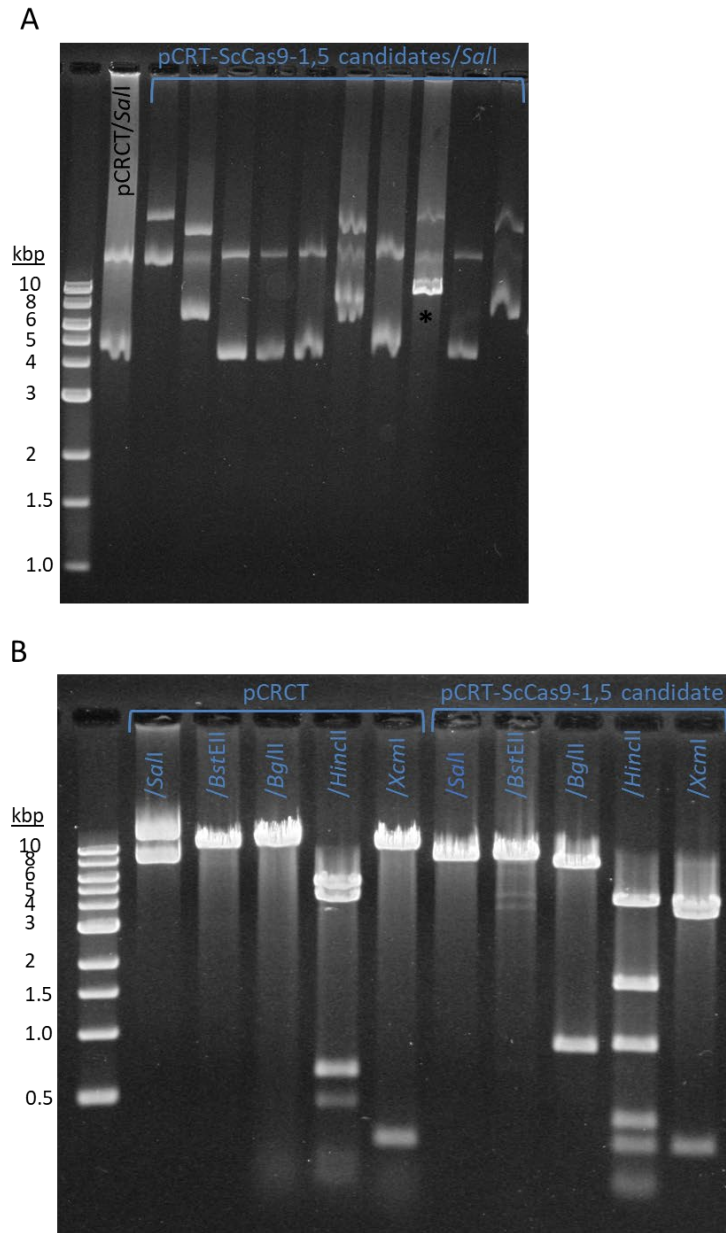


Figure 2.21. Diagnostic restriction digests of pCRT-ScCas9-1,5 candidates

(A) Colony cracked candidates digested with *SalI*. pCRCT digested with *SalI* is uncut, shown as a control. pCRT-ScCas9-1,5 is linearized by *SalI*, producing one fragment approximately 8600 bp. *indicates the candidate identified as pCRT-ScCas9-1,5. Note: gel box had connectivity issues during electrophoresis (B) Thorough analysis of candidate identified in (A). Serial cloner predicted fragment sizes (bp), in order shown on gel: pCRCT/*SalI*: uncut pCRCT/*BstEII*: linearized 10805 pCRCT/*BglIII*: linearized 10805 pCRCT/*HincII*: 5459, 4486, 711, 136, 13 pCRCT/*XcmI*: 10504, 300 pCRT-ScCas9-1,5/*SalI*: linearized 8619 pCRT-ScCas9-1,5/*BstEII*: linearized 8619 pCRT-ScCas9-1,5/*BglIII*: 7672, 947 pCRT-ScCas9-1,5/*HincII*: 4486, 1746, 971, 423, 306, 136, 114, 106, 93, 90, 75, 60, 13 pCRT-ScCas9-1,5/*XcmI*: ~4400, ~3800, ~300.

For the second step of the *in vivo* cloning method, pCRT-ScCas9-1,5/*Sa*II provided the available ends to allow for the G-blocks: ScCas9-2, ScCas9-3, and ScCas9-4 to be incorporated into the vector through HR repair. The pCRT-ScCas9 candidates were digested with *Bgl*II. Four out of the 20 candidates were identified as pCRT-ScCas9 based on the fragments observed from the restriction digest (Figure 2.22). pCRT-ScCas9#13 was sent for sequencing and was determined to have a frameshift mutation within the first 1 kbp of *ScCas9* (the region corresponding to the G-block ScCas9-1). pCRT-ScCas9#13 was digested with *Bst*EII to allow for HR repair with a new G-block ScCas9-1. Candidates were sent for sequencing. 2 mutations were present in the first 1 kbp (region corresponding to the G-block ScCas9-1) of pCRT-ScCas9. The BIOC 474/674 2017 class performed site-directed mutagenesis on the pCRT-ScCas9 candidate to obtain the correct pCRT-ScCas9 identified by RA, named: pCRT-ScCas9.1.

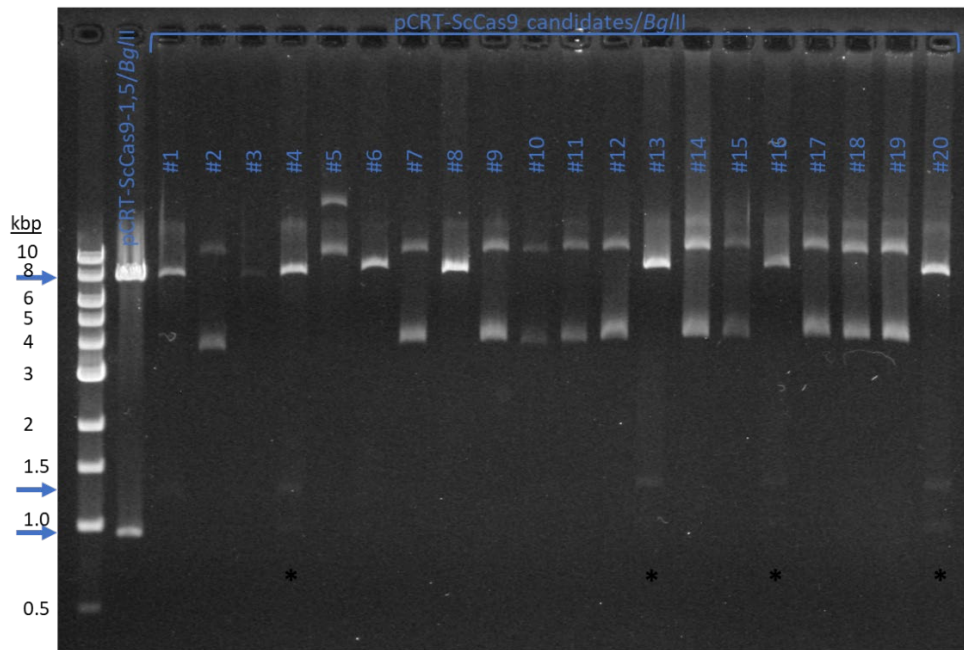


Figure 2.22. Diagnostic restriction digest of potential pCRT-ScCas9 candidates that contain all 5 G-blocks for the complete *ScCas9* sequence

Diagnostic restriction digest on colony cracked candidates. The fragment sizes of the DNA ladder are labeled. Arrows point out the approximate location for the pCRT-ScCas9 predicted fragments. Predicted fragment sizes (bp): pCRT-ScCas9-1,5/*Bgl*II: 7672, 947 pCRT-ScCas9/*Bgl*II: 7640, 1250, 947, 936. *indicates candidates identified as pCRT-ScCas9.

The plasmid pCRT-ScCas9.1 had an additional *BsaI* site introduced through Cas9 codon optimization that would make the vector unable to be used for downstream applications utilizing golden gate cloning. The additional *BsaI* site was removed by *in vitro* site-directed mutagenesis, and candidates were tested by a diagnostic restriction digest with *BsaI*. Two different polymerases were used for site-directed mutagenesis; thus, candidates were named with either a “Q” for Q5 polymerase or a “P” for Precision Taq polymerase. Five candidates were identified as pCRT-ScCas9 (Figure 2.23). This plasmid has been used extensively by the BIOC 474/674 class to practice multiple recombinant DNA techniques and provides a useful tool for generating future yeast mutants (especially multi-mutants) in the Haring laboratory.

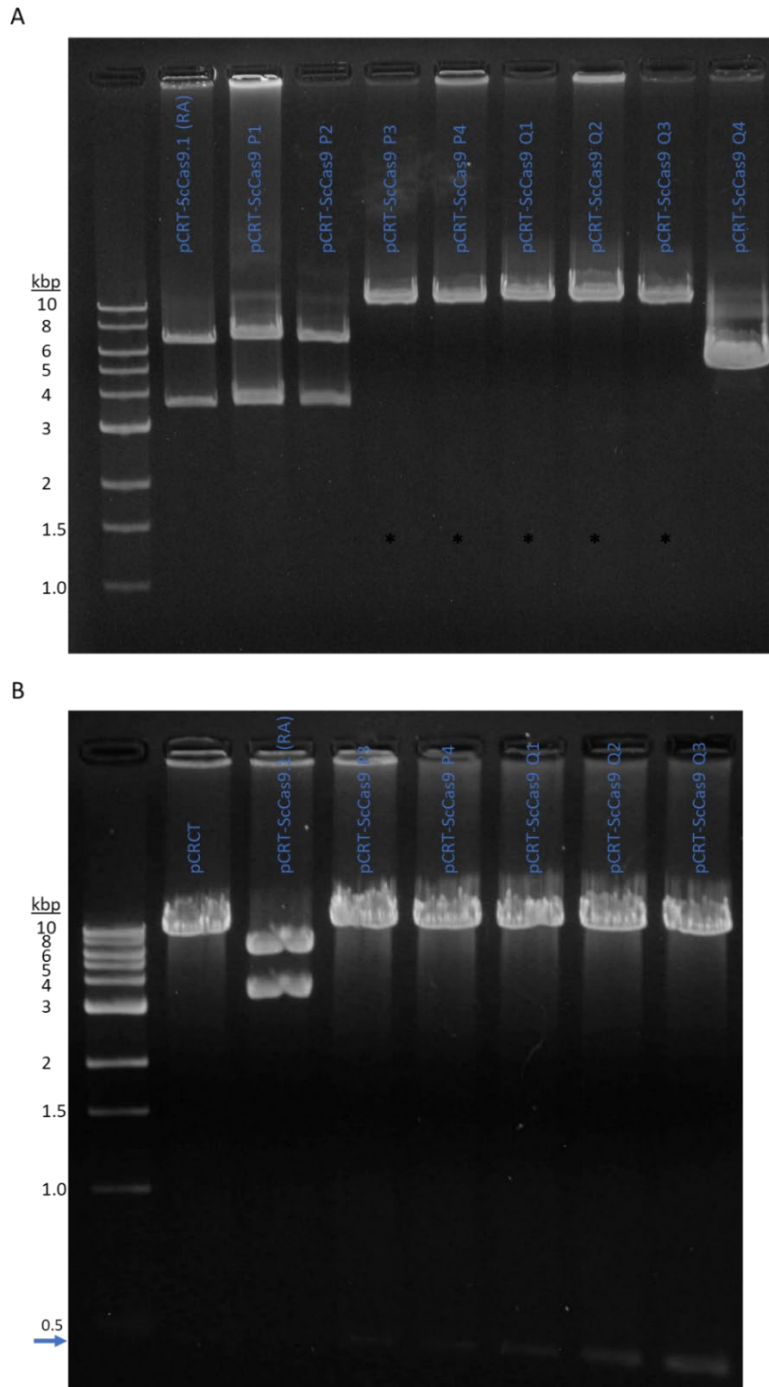


Figure 2.23. Diagnostic restriction digest of pCRT-ScCas9 candidates after mutagenesis to remove the introduced *BsaI* site

Candidates obtained from site-directed mutagenesis of pCRT-ScCas9.1 (RA). Fragment sizes of DNA ladder are denoted. (A) All candidates obtained digested with *BsaI*. pCRT-ScCas9/*BsaI* should product 2 fragments (bp): 10326, 447. The 447 bp fragment is not observed in (A).

*denotes the plasmids identified as pCRT-ScCas9 (B) Plasmids identified as pCRT-ScCas9 in (A) were re-digested with 1 μ g DNA. A faint band is observed under the 500 bp ladder band (See arrow). pCRCT was also digested as a control.

Discussion

Inability of Cas9 to rescue a Spo11-deficient meiosis

The sporulation rates of all *spo11Δ::Cas9* diploids both with and without a guide RNA were all very similar to the homozygous *spo11Δ* diploids (Table 2.2). This suggests that Cas9 was unable to promote sporulation through an increase in meiotic recombination to the level that would allow for proper chromosome segregation in the first division. This is also supported by the qualitative analyses of heteroallelic recombination and chromosome segregation, since recombination was not increased at the heteroallelic loci investigated and proper chromosome segregation was not increased since the amount of growth observed could not be attributed to an increased ability to properly divide chromosomes (Figures 2.11- 2.18). The similar increase of *LYS2* recombinants observed in the homozygous *spo11Δ::Cas9 + LYS2* gRNA diploid cells in both mitotic and meiotic patches indicated that Cas9 may not be functioning under a meiotically control program (Figure 2.13). If increased recombination due to the presence of Cas9 + gRNA occurred specifically during meiosis, the typical 100-1000 fold increase in meiotic recombinants over mitotic recombinants should have been observed if Cas9 were able to rescue the Spo11-deficient meiosis.

Possibility of Cas9 off-target effects to replace Spo11

While the experimental results of this study do not support the idea that Spo11 can be replaced by Cas9, it may still be possible to replace Spo11 with Cas9 to generate a “like-normal” meiosis. The biggest issue with the results mentioned above that suggest an inability of Cas9 to replace Spo11 could all be attributed to the fact that Cas9 protein abundance was low at the initial meiotic time point and did not increase at subsequent timepoints (Figure 2.19). As was mentioned in the introduction, having breaks occur at the right time and place during meiosis is

important for proper chromosome pairing to promote proper division. Not only do breaks need to occur at the appropriate time, but Cas9 protein abundance also needs to be high to increase the possibility for Cas9 off-target effects to produce enough breaks to tether all 16 yeast chromosomes together through HR repair prior to the first division. Using the codon optimized Cas9, *ScCas9*, in future studies may be one way to increase protein abundance, additionally other ways to control Cas9 expression may also have to be explored as using the *SPO11* promoter appeared to allow for similar amounts of Cas9 expression during both mitosis and meiosis.

Apart from increasing Cas9 protein as a means to increase off-target effects, additional system modifications could be made such as increasing the length of the complementary target sequence in the gRNAs used or instead of using gRNAs, express crRNAs separately from the tracrRNA to provide additional target sequences available for interaction with Cas9. In this study Cas9 was targeted with the same gRNA to every chromosome with the X element and Y element gRNAs. The X element and Y element gRNAs targeted Cas9 to the telomeric regions (or ends) of every chromosome. Telomeric regions are normally heterochromatic as they are protected by bound proteins, and those regions may have been inaccessible by Cas9 (Wellinger and Zakian 2012). Additionally, it has been shown that the rate of non-disjunction is increased when recombination occurs at the ends of chromosomes (Ross, Maxfield and Dawson 1996). This may be explained by the need for additional meiotic proteins to associate with telomeres (chromosome ends) to promote chromosome dynamics during meiosis (Niwa, Shimanuki and Miki 2000, Chu et al. 2017, Conrad, Dominguez and Dresser 1997). Thus, targeting X and Y element regions may not be the best way to ensure breaks are made on multiple chromosomes when the goal is to promote recombination that will influence proper chromosome segregation.

Future directions

Determining if the codon optimized *ScCas9* leads to an increase in the amount of Cas9 protein under an inducible promoter during mitosis should be the first step in determining if Cas9 protein abundance may be able to be controlled during meiosis. Rather than relying on off-target effects to promote enough recombination to rescue meiosis, I would start with targeting multiple locations on each chromosome in non-centromeric and non-telomeric regions in order to initially determine if it is possible for breaks made by Cas9 to replace Spo11-induced breaks during the meiotic process. Cas9 activity would have to be controlled to occur with approximately the same timing as Spo11 activity which could be achieved by using an inducible Cas9 and monitoring break formation by Southern blotting or qPCR.

Acknowledgements

Barbara Senger generated the integrating plasmid, pSP+ST-5 (B-1055). Brian Samuelson generated the guide RNA plasmids. Nolan Miles mini-prepped some of the pCRT-ScCas9 candidates that were tested. Wendy Larson inoculated some overnight cultures for downstream testing. The 2017 BIOC474/674 class, especially RA, for recovering the desired plasmid.

CHAPTER THREE: DNA BINDING DOMAIN F PARTICIPATES IN DNA-DAMAGE SENSITIVE INTERACTIONS WITH CHECKPOINT PROTEINS

The Rfa1 protein is made up of four DNA binding domains (DBDs). The focus of this study is on DNA binding domain F (DBD-F), which is located at the Rfa1 NT and appears to function predominantly in facilitating protein-protein interactions rather than in binding ssDNA. Many proteins involved in the DNA damage checkpoint (See Chapter 1, Figure 1.2) and repair have been shown to interact with both human and yeast DBD-F domains. This study utilizes domain-swapping with plasmid shuffle, yeast two-hybrid assays, western blotting, and DNA damage spot assays to investigate DBD-F function.

The yeast two-hybrid interactions identified were sensitive to DNA damage, suggesting that these interactions are abrogated during the DNA damage response and that DBD-F may have a higher affinity for other binding partners when subjected to genotoxic agents. Due to similarities between the DBD-F (*rfa1-t11*) mutant and the phospho-mimetic Rfa2 (*rfa2-D_x*) mutant in DNA damage checkpoints, modification of Rfa2 in the *rfa1-t11* mutant was investigated. In the *rfa1-t11* mutant, Rfa2 appears to be phosphorylated similarly to wild-type. This led to further investigation of the effect of the phospho-state of Rfa2 on deficient DNA damage checkpoints. DNA damage sensitivity was investigated with Rfa2 extensive phospho-mutants (*rfa2-A_x*, *rfa2-D_x*) in three checkpoint protein gene deletion (*checkpointΔ*) strain backgrounds of which all proteins removed by gene deletion have been suggested to interact with DBD-F. The phospho-mimetic Rfa2 (*rfa2-D_x*) increases the DNA damage sensitivity making all *checkpointΔ rfa2-D_x* double mutants as sensitive to all DNA damaging agents tested (CPT, HU, MMS, PHL) as the single *rfa2-D_x* mutant. Because the *rfa2-D_x* mutation increases DNA damage sensitivity of cells regardless of checkpoint defects, this suggests that Rfa2 NT phosphorylation

may have a greater impact than these checkpoint proteins on the modification of the DDR and that if Rfa2 NT phosphorylation occurs early it may modify the response before any deleterious effects of the *checkpointΔ* can come to fruition.

Introduction

The Rfa1 protein is made up of four DNA binding domains (DBDs): A, B, C, and F (Figure 3.1). DBD-A and DBD-B have the highest affinity for binding ssDNA (Arunkumar et al. 2003, Fan and Pavletich 2012). DBD-C plays an important role in interacting with Rfa2 and Rfa3 in forming the trimerization core for RFA complex formation that has been suggested to facilitate the transition between the short DNA binding mode (with DBD-A and DBD-B) to the long DNA binding mode (with DBDs A-D) (Bochkareva et al. 2002, Kim et al. 1992, Bochkarev et al. 1997, Bastin-Shanower and Brill 2001, Wyka et al. 2003). DBD-C also contains a zinc finger region (The UniProt 2018). The remaining DBD, DBD-F, located at the Rfa1 NT appears to function predominantly in protein-protein interactions, because cells containing the commonly used DBD-F mutation, *rfa1-t11*(K45E, charge reversal) have eliminated or reduced protein-protein interactions. Additionally, a *Homo sapiens* RPA mutant with a NT deletion has been shown to bind ssDNA as well as wild-type (Gomes and Wold 1996). In the linker region between DBD-F and DBD-A is serine 178 (S178) which is part of an SQ motif that is phosphorylated by the Mec1 sensor kinase in a cell-cycle and DNA damage dependent manner (Brush et al. 1996, Brush and Kelly 2000, Bartrand et al. 2004).

A few *in vivo* studies have shown Mec1 recruitment under DNA damage is reduced in *rfa1-t11* mutant cells (Zou and Elledge 2003, Seeber et al. 2016, Deshpande et al. 2017). This is supported by structural analysis that shows the mutant DBD-F (*rfa1-t11*) is still able to interact with Mec1 but with less affinity than wild-type Rfa1 (Deshpande et al. 2017). Besides Mec1,

recruitment of additional repair factors in *rfa1-t11* mutant strains is reduced, many of these repair factors are also required for Mec1 activation (Chen et al. 1998, Umezue et al. 1998, Soustelle et al. 2002, Zou et al. 2003, Majka et al. 2006a, Majka et al. 2006b, Seeber et al. 2016, Deshpande et al. 2017). Cells containing the *rfa1-t11* mutation show a slight reduction in the ability to recruit Ddc1 (of the checkpoint clamp complex: Ddc1-Mec3-Rad17) to an HO endonuclease-induced DNA-break (Zou et al. 2003). Recruitment of the checkpoint clamp depends on the clamp loader (Rad24-Rfc2-5), which has been shown with the homologous human proteins to bind ssDNA at a higher affinity when RPA is present (Zou et al. 2003, Majka et al. 2006a). Furthermore, DBD-F interaction with Rad24 (clamp loader component) has been characterized in yeast (Piya et al. 2015). Sgs1 and Dna2 have also been identified previously as interactors of Rfa1 (Piya et al. 2015). Together, Sgs1, Dna2, and RFA have been extensively shown to be required for DNA resection *in vitro* and *in vivo*, likely comprising the minimal required associated proteins capable of resection (Cejka et al. 2010, Zhu et al. 2008, Cannavo, Cejka and Kowalczykowski 2013, Chen, Lisby and Symington 2013, Ngo et al. 2014).

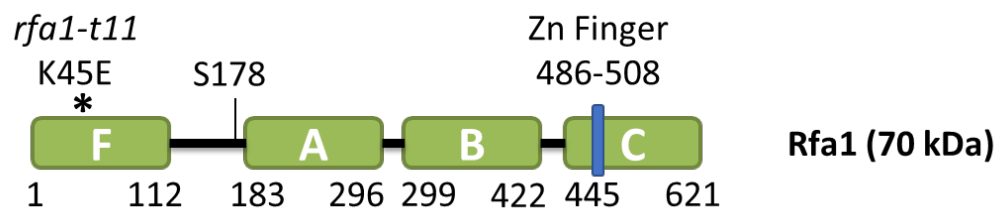


Figure 3.1. Schematic of Rfa1 protein

Shown are the DNA-binding domains (DBDs) of Rfa1: F (N-terminal), A, B, and C. Uniprot was used to obtain amino acid/residue information for designating each specific region (denoted below region) and the Zinc (Zn) Finger region (denoted above DBD-C) (Seeber et al. 2016, The UniProt 2018). Denoted is the location of S178, which becomes phosphorylated by the Mec1 kinase in response to DNA damage (Brush and Kelly 2000). Also denoted is the location of the *rfa1-t11* mutation.

In *H. sapiens*, several factors involved in the DNA damage response have been demonstrated to interact with DBD-F (RPA70/RPA1 NT) (Maréchal and Zou 2015). Of these,

many homologous proteins in *S. cerevisiae* have been demonstrated to interact directly with Rfa1 or inferred to interact with DBD-F through investigation of interactions with the *rfa1-t11* mutation (Table 3.1, *Ibid*). This suggests that many protein-protein interactions involving DBD-F are conserved from yeast to humans. It is unclear how many of these protein-protein interactions are species-specific. In a prior Haring laboratory publication, it was shown that the human RPA complex could not support viability in yeast (Ghospurkar et al. 2015a). In this study it was hypothesized that the protein-protein interactions of DBD-F may be species-specific, thus a *Sc*DBD-F (*S. cerevisiae* DBD-F)-RPA hybrid complex might support viability in yeast.

However, this study found that although DBD-F interacts with many proteins that could be species-specific interactions, DBD-F may not facilitate all species-specific interactions of RFA because the RPA hybrids containing *Sc*DBD-F still did not support viability in yeast. This study further investigated the protein-protein interactions of DBD-F through yeast two-hybrid assays to identify interactors of both yeast and human DBD-F domains. The interactions identified were sensitive to DNA damage, suggesting that these interactions are abrogated during the DNA damage response and that DBD-F may have a higher affinity for other binding partners when subjected to genotoxic agents. Previous analysis of RFA mutants has revealed similar phenotypes between the DBD-F (*rfa1-t11*) mutant and the phospho-mimetic Rfa2 (*rfa2-D_x*) mutant in which both initiate the G2/M checkpoint, promote checkpoint adaptation, and are synthetically lethal in conjunction with an Mre11 gene deletion (*mre11Δ*) (Lee et al. 1998, Ghospurkar et al. 2015b) Due to these similarities, modification of Rfa2 in the *rfa1-t11* mutant was investigated. In the *rfa1-t11* mutant, Rfa2 appears to be phosphorylated similarly to wild-type under the DNA damage conditions in which Rfa2 phosphorylation is detected. This led to further investigation of the effect of the phospho-state of Rfa2 on deficient DNA damage

checkpoints utilizing gene deletions of which the checkpoint proteins have been suggested to interact with DBD-F. The double mutants containing *rfa2-D_x* appear as sensitive to DNA damage as the single *rfa2-D_x* mutant, which suggests that Rfa2 NT phosphorylation may modify the DNA damage response indiscriminately from checkpoint defects.

Table 3.1. Proteins that interact with DBD-F (N-terminus of RPA70) in *Homo sapiens*

<i>H. sapiens</i> protein(s) ^a	Reference ^b	<i>S. cerevisiae</i> homolog (% identical)	Demonstrated interaction in <i>S. cerevisiae</i> ?	Notes
ATR, ATRIP	(Zou and Elledge 2003)	Mec1 (42%), Ddc2 (36%)	Yes	Defective recruitment by <i>rfa1-t11</i> mutant. Structural data.
BID	(Liu et al. 2011)	None		BID regulates apoptosis in multicellular organisms
MRE11, RAD50, NBS1	(Shiotani et al. 2013, Robison et al. 2004, Oakley et al. 2009, Xu et al. 2008)	Mre11 (43%), Rad50 (52%), Xrs2/Mek1* (36%)	Yes	Xrs2 is the functional homolog of NBS1, as it forms a complex (MRX) with Mre11 and Rad50 in yeast. *Mek1 is homologous by sequence search, no demonstrated interaction with Rfa1.
PRP19, BCAS2	(Maréchal et al. 2014, Wan and Huang 2014)	Prp19 (40%), None	No	-
p53 (TP53)	(Bochkareva et al. 2005, Li and Botchan 1993)	None	-	-
53BP1 (TP53BP1)	(Yoo et al. 2005)	Rad9	Yes	Rad9 is the functional homolog of 53BP1
RAD17	(Zou et al. 2003, Majka et al. 2006a, Ellison and Stillman 2003)	Rad24 (28%)	Yes	-

^aProteins listed together for those acting together in a complex. ^bUtilized (Maréchal and Zou 2015) as a source to obtain RPA70 N interactor references. Homologous proteins in *S. cerevisiae* identified by obtaining *H. sapiens* protein sequences from Uniprot to search via ProteinPathTracker (Mier, Pérez-Pulido and Andrade-Navarro 2018), linked BLAST information provided percentage of identical sequence. Demonstrated interaction in *S. cerevisiae* determined by referencing the BioGrid database.

Materials and Methods

Yeast strains and plasmids

Yeast strains and plasmids used in this section are listed in Appendix A and Appendix C, respectively. EGY48 was utilized for *in-vivo* homologous recombination (HR) cloning and in the yeast two-hybrid assay. RMY122-A was used for plasmid shuffle assays. RMY122-A has chromosomal deletions of *RFA1* and *RFA2*. Since deletions of RFA subunits are lethal, RMY122-A contains the supplementary plasmid (pJM132, *URA3* selectable marker) expressing *RFA1* and *RFA2* from their native promoters. pJM132-RPA2-RPA3-RPA1-kanMX (canonical human RPA complex; cRPA) and pJM132-Rpa4-RPA3-RPA1-kanMX (alternative human RPA complex; aRPA) are plasmids containing all *Homo sapiens* RPA subunits and the *kanMX* selectable marker; these plasmids were created by Padmaja Ghospurkar.

The following was done to replace DNA binding domain F (DBD-F) of the *Homo sapiens* RPA complexes with the *Saccharomyces cerevisiae* DBD-F. Approximately 500 ng of both cRPA and aRPA plasmids were digested with *MfeI* (Cutsmart buffer, 37 °C, 1.5 hours). EGY48 was transformed with cut vector (cRPA or aRPA plasmids; ~500ng) for *in vivo* HR cloning with 10 µL of the following g-blocks (Appendix E): rpa1-rfa1-DBD-F-Linker (*ScDBD-F+L*) or rpa1-rfa1-DBD-F (*ScDBD-F*); these transformation reactions were set up with separate aliquots of EGY48 to yield 4 total experimental reactions. A scrape of transformed EGY48 colonies was taken and prepped for optimal plasmid recovery by following the yeast DNA isolation protocol without performing the RNaseA incubation. The obtained DNA was then used to transform T1 *ccdB Escherichia coli* cells by electroporation and bacterial transformants containing the potential plasmids: cRPA + *ScDBD-F*, cRPA + *ScDBD-F+L*, aRPA + *ScDBD-F*, and aRPA + *ScDBD-F+L* were selected for on Luria-Bertani plates containing kanamycin (LB +

kan; Appendix F). Isolated candidate colonies were used to inoculate overnight bacterial cultures. Colony cracking was performed on 1 mL of cells, pelleted from culture. Cell pellets were resuspended in 50 μ L of 1x lysis solution (also known as colony cracking buffer) (10mM Tris-HCl pH 8.0, 1mM EDTA pH 8.0, 15% sucrose, 2mg/mL lysozyme, 0.2mg/mL RNaseA, 0.1mg/mL BSA) and boiled at 100°C for 90 seconds, then centrifuged to pellet debris. The supernatant was used to perform diagnostic restriction digestions using *SspI* (NEB) and *EcoRV*(NEB). The *SspI* digest was performed to check the integrity of the vector and the *EcoRV* digest was performed to confirm candidates containing the proper DBD-F/DBD-F+L replacement (pAMA41-44; Appendix C).

JKM139, JKM179, NMM104, and their derivative yeast strains were used for spot assays (as part of a collaboration with some figures shown as part of this chapter and others as part of Appendix G: Supplementary Figures A1-A4, A6). AWY strains are JKM139 and JKM179 derivatives provided by Andre Walther (Cedar Crest College). The provided AWY strains were genotyped by replica plating, PCR, and sequencing. The presence of selectable markers were confirmed by replica plating to determine growth for the following: *rad9 Δ ::kanMX*, *rad17 Δ ::LEU2*, *mec3 Δ ::TRP1*, and *rad52 Δ ::TRP1*. The extensive *rfa2* alanine/aspartate mutations (*rfa2-A_x*, *rfa2-D_x*) were confirmed by PCR (utilizing the primers RFA2-UP-FOR and RFA2-DOWN-REV) and sequencing utilizing the primer RFA2-UP-FOR by Eton Biosciences (Appendix D: Primers; Appendix G: Supplemental Figures G1). PCR was performed to confirm gene deletions by insertion of the selectable marker (*gene Δ ::selectable marker*), for the following: *rad52 Δ ::TRP1*, *tof1 Δ ::hphNT*, *rad9 Δ ::kanMX*, *rad17 Δ ::LEU2*, *mec3 Δ ::TRP1* with appropriate primers (Appendix D: Primers; Appendix G: Supplemental Figures G2). As the directionality of each selectable marker (insertion) was unknown, four separate reactions were

prepared so that regardless of direction, the insertion could be confirmed by PCR product produced from the upstream and downstream PCR (2/4 reactions per direction of the insertion). Additionally, PCR product can only be produced (in 2/4 reactions) if the insertion has correctly integrated. *Note: Verification and experiments performed with these strains were part of a collaborate effort between Stuart Haring, Andre Walther, Timothy Wilson, Trevor Baumgartner, and myself. Verification PCR agarose gels are shown in Figures G1-G2 (Appendix G).

Correct *rad17Δ::LEU2* and *rad52Δ::TRP1* mutants (AMA135 – AMA140) were made by *in vivo* HR cloning. The selectable marker was PCR amplified from verified *rad17Δ::LEU2* and *rad52Δ::TRP1* strains using the primers: RAD52-F, RAD52-R, RAD17-F, RAD17-R, respectively. Competent confirmed JKM179 derivatives containing the desired *rfa2* mutation were transformed with the PCR products by lithium acetate transformation and desired deletions were selected for on appropriate media (SD-Leu or SD-Trp). These AMA mutants were PCR confirmed utilizing the same primers as above AWY mutants (Appendix D: Primers; Appendix G: Supplemental Figures G3). *Note: Verification and experiments performed with these strains were part of a collaborate effort between Stuart Haring, Andre Walther, Timothy Wilson, Trevor Baumgartner, and myself. Verification PCR agarose gels are shown in Figure G3 (Appendix G).

Wendy Larson provided WAL105 and WAL106 strains. She utilized NMM101, a JKM179 derivative containing a chromosomal deletion of *RFA1* and the supplementary plasmid pJM132, to generate WAL105 and WAL106 by plasmid shuffle. WAL105 contains pRS315-*RFA1* (*LEU2* selectable marker) and WAL106 contains pRS315-*rfa1-t11* (*LEU2* selectable marker).

Plasmid shuffle assay

The RMY122-A yeast strain (containing pJM132, *URA3* selectable marker) was transformed by lithium acetate transformation with the created hybrid plasmids (pAMA41-44): cRPA + *ScDBD-F*, cRPA + *ScDBD-F+L*, aRPA + *ScDBD-F*, and aRPA + *ScDBD-F+L* and transformants containing the hybrid plasmids were selected for on YPD+G418. A master plate was picked with colonies obtained to YPD + G418 to maintain selection for the hybrid plasmids. The master plate was replica plated to SD-Ura, 5-FOA (SD complete media containing 5-fluoroorotic acid; 5-FOA; Appendix F), and YPD. 5-FOA is used as a negative/counter selection for *URA3*, selecting for cells that have “shuffled-out” the original pJM132 plasmid.

Yeast two hybrid assay

EGY48 (from the Origene DupLEX-A Yeast Two-Hybrid System, DKT100) was used as the strain to identify protein-protein interactions. EGY48 contains a *LEU2* reporter gene regulated by six *lexA* operator sequences. Bait plasmids used were derivatives of pEG202K (*HIS3* and *kan^r* selectable markers). Bait plasmids used in this study contained the *lexA* DBD fused to either *Homo sapiens* RPA1 DBD-F (pEG202K-LexA-RPA1-F) or *Saccharomyces cerevisiae* Rfa1 DBD-F (pEG202K-LexA-Rfa1-F) (Appendix C). An additional reporter plasmid, pSH18-34K containing *URA3* and *kan^r* selectable markers and *lacZ* regulated by eight *lexA* operator sequences (Appendix C) was used. EGY48 was transformed by lithium acetate transformation to contain one of the bait plasmids and the additional reporter plasmid; the plasmids were selected for by growth on SD-His-Ura. The collection of EGY48 cells containing the Rfa1 DBD-F bait plasmid was named “EGY48 Y”. The collection of EGY48 cells containing the RPA1 DBD-F bait plasmid was named “EGY48 H”. EGY48 Y cells were transformed with the *Saccharomyces cerevisiae* DupLEX-A Yeast Two-Hybrid Genomic DNA Library (Origene,

prey plasmids are all pJG4-5 derivatives), while EGY48 H cells were transformed with the MCF7 cDNA library from Origene (DLH117; prey plasmids are all pJG4-5 derivatives). EGY48 Y cells and EGY48 H cells containing prey plasmids were selected for on SD-His-Trp-Ura. The transformants were collected and stored at -80 °C in 25% glycerol. Utilizing the determined transformation efficiency and the average cell titer (determined by counting colony forming units from plated dilutions), cells were spread to obtain isolated colonies on synthetic media containing raffinose (R) and galactose (G), SRG -His-Trp-Ura-Leu + X-gal (5-bromo-4-chloro-3-indolyl- β -D-galactopyranoside), SRG -HTUL + X-gal, was used to initially identify colonies with interaction potential. With this system if an interaction occurs between the bait plasmid (containing DBD-F) and a prey plasmid (from the library), the colony will be a leucine prototroph and will be blue on media containing X-gal (depending on interaction strength). From these plates identifying an initial interaction, 720 isolated colonies were picked for each experimental condition (Yeast vs. Human) and maintained on SD-His-Trp-Ura master plates. To further test the initially identified interactors, master plates were replica plated to SRG plates with the following combinations: -HTUL, -HTUL + CPT (camptothecin), -HTUL + PHL (phleomycin), -HTUL + MMS (methyl methanesulfonate), -HTU + X-gal, -HTU +X-gal +PHL. Colonies that were leucine prototrophs and were sensitive to a DNA damaging agent (CPT, MMS, PHL) were further investigated to identify the prey plasmid. The chosen colonies were grown in liquid SD-Trp media so that only the prey plasmid to be isolated was still under selective pressure. DNA was obtained from the cultures using the optimal plasmid recovery protocol (following the yeast DNA isolation protocol without performing the RNaseA incubation). There were 61 DNA preps for yeast prey plasmids and 31 DNA preps for human prey plasmids. Heat-shock was used to transform *Escherichia coli* T1 ccDB cells with the DNA

preps. T1 ccDB cells had been prepared for heat shock by growing cells to exponential phase, cooling on ice for 10 minutes, pelleting cells at 1500x gravity(g) for 15 minutes at 4°C, resuspending cells in 100mM ice cold calcium chloride, incubating on ice for 25 minutes, pelleting cells at 1500xg for 15 minutes at 4°C, then lastly resuspending in 100mM ice cold calcium chloride (CaCl₂) + 15% glycerol. Heat shock transformation of 50 µL T1 CaCl₂ competent cells was performed using 1 µL of each DNA, incubating for 30 minutes on ice, then incubating at 42°C 1 minute (heat-shock), incubating on ice for 5 minutes, incubating in 1 mL LB for 1 hour at 37°C (recovery), and plating the entire reaction (centrifuged down to plate 200 µL) on LB + amp. One colony per transformation was grown overnight in liquid LB + amp and mini-prepped. Each mini-prepped DNA was digested with *Bsa*HI (NEB) to avoid sequencing empty prey vectors. Prey vectors were sequenced by Eton Biosciences using the primer pJG4-5-UP-Sequence (Appendix D). Obtained DNA sequences were searched via the NCBI nucleotide BLAST (Basic Local Alignment Search Tool) to identify the sequence. For all identified interactors except those noted, (Table 3.1 and 3.2) the nucleotide sequence was analyzed in Serial Cloner to verify that the nucleotide sequence present in the vector was in-frame; the translated amino acid sequence was searched via the NCBI protein BLAST to confirm results of the NCBI nucleotide BLAST.

Western blotting to investigate Rfa2 protein in a *rfa1-t11* mutant

JKM179 derivatives containing *RFAl* (WAL105) and *rfa1-t11* (WAL106) were grown overnight in YPD at 30°C in shaker incubator to an OD₆₀₀ of 0.9-1.0. Cell cultures were then subjected to the following DNA damaging agents: 0.06% MMS, 10ug/mL CPT, and 10ug/mL PHL. Cell samples were collected at 10 OD equivalents at 0 hours (prior to adding damaging agent), and at the following time points after addition of damaging agent: 4, 12, 16, and 24 hours.

Protein was extracted from samples with trichloroacetic acid, precipitated by acetone washes, and resuspended in 1X Laemmli buffer (Cold Spring Harbor).

To detect Rfa2 protein, 10 μ g protein in 1X Laemmli buffer + 4% β -Me was separated on 15% (29:1) SDS-polyacrylamide gel by electrophoresis at 10 mAmp/gel for 15 min, then 20 mAmp/gel for 2 hrs 55 min in 1X SDS buffer (Appendix F). After gel equilibration in transfer buffer, this was followed by transfer to a nitrocellulose membrane at 0.04 Amp constant current for 16 hours overnight in transfer buffer (Appendix F). Membranes were Ponceau S stained (0.5% Ponceau S, 5% acetic acid) and destained (1% acetic acid) to check for even loading. Membranes were blocked for 2 hrs with TBST buffer + 5 mM sodium fluoride + 1% bovine serum albumin (Appendix F). Primary anti-Rfa2 antibody was provided by Steven Brill and used at 1:40000 in TBST buffer + 5mM sodium fluoride + 0.5% nonfat dry skim milk powder + 0.5% bovine serum albumin at 4°C for 18.5 hrs overnight on a platform shaker. Western blots were washed 4 times using 1X TBST + 5mM sodium fluoride (Appendix F) with a total wash time of approximately 1 hour. Secondary goat-anti-rabbit IgG-HRP antibody (Bethyl A120101P) was used at 1:40000 in TBST buffer + 5mM sodium fluoride + 0.2% nonfat dry skim milk powder and incubated for 2 hrs at room temperature. Western blots were washed again 4 times using 1X TBST + 5mM sodium fluoride (Appendix F) with a total wash time of approximately 1 hour.

Western blots were developed using the SuperSignal™ West Pico Plus Chemiluminescent substrate kit (Thermo Scientific). Images were obtained with the Wilkinson laboratory myECL™ (Thermo Scientific) imager and myImageAnalysis™ software (Thermo Scientific).

DNA damage spot assay

All strains used for DNA damage spot assays appearing in this chapter were JKM179 derivatives (AWY092, AWY096, AWY019, AWY033, AWY035, AWY040, AWY45, AWY114, AWY200, AWY201, AMA135) and wild-type JKM179. JKM179 and derivative strains were grown in YPD at 30°C in shaker incubator overnight. Cell cultures were diluted and a cellometer (Nexcelom) was used to determine the cell concentration. Cell cultures were initially diluted to 1×10^7 cells/mL which was then used for five 10-fold serial dilutions, using sterile water as the diluent. The initial dilution and the serial dilutions were spotted using 5 μ L of each dilution onto YPD and YPD plate media containing the following damaging agents: 0.2-25.0 μ g/mL camptothecin (CPT), 40-320 mM hydroxyurea (HU), 0.0075-0.06% methyl methane sulfonate (MMS), and 0.2-25.0 μ g/mL phleomycin (PHL). The best representative concentration was used to create the figure for the spot assay. The entire range of concentrations and images of all replicates can be found in Appendix G: Figures G6-G9.

Results

Plasmid shuffle assay

RPA complexes that exist in *Homo sapiens* are canonical RPA (cRPA; RPA1, RPA2, and RPA3) and alternative RPA (aRPA; RPA1, RPA4, RPA3). In *Homo sapiens* aRPA does not support DNA replication (Mason et al. 2009, Haring, Humphreys and Wold 2010). It has been shown that expression of the human RPA complexes can occur in yeast, however the entire complex cannot support yeast viability in the absence of *Saccharomyces cerevisiae* RFA, nor can subunits of these two species interact (Ghospurkar et al. 2015a). Since the subunits of the RPA complexes interact through OB folds of DBD-C, DBD-D, and DBD-E (Bochkareva et al. 2002), forming the complex may be species-specific (i.e., only *Homo sapiens* OB folds can interact

properly with other human OB folds to form the complex). Additionally, RPA1 and specifically DBD-F of RPA1 have been reported to interact with several replication and repair factors. These protein-protein interactions may also be species-specific, which may explain why the human RPA complexes do not support viability in yeast. In order to test if a *Homo sapiens* RPA complex could support viability with a *Saccharomyces cerevisiae* DBD-F domain, hybrid plasmids were created through *in vivo* HR cloning to replace the *Homo sapiens* DNA binding domain F (DBD-F) and DBD-F with linker region (DBD-F+L) of RPA complexes (cRPA and aRPA) with the *Saccharomyces cerevisiae* DBD-F or DBD-F+L. Hybrid candidates were confirmed by linearization of the plasmid with *EcoRV* digestion (Figure 3.2). RMY122-A yeast cells (containing chromosomal deletions of *RFA1* and *RFA2*, and the pJM132 supplementary plasmid expressing *RFA1* and *RFA2* with a *URA3* selectable marker) were transformed with the hybrid plasmids. Selective pressure was maintained for the hybrid plasmids on the patch master plate which was replica plated to SD-Ura, 5-FOA, and YPD plates. Cells retaining pJM132 will grow on SD-Ura. 5-FOA is used as a negative selection for *URA3*, which means that for cells to grow on 5-FOA they had to lose pJM132 and retain the hybrid plasmid. No growth on 5-FOA plates was observed, indicating that no hybrid plasmid supported cell growth in the absence of pJM132 (data not shown).

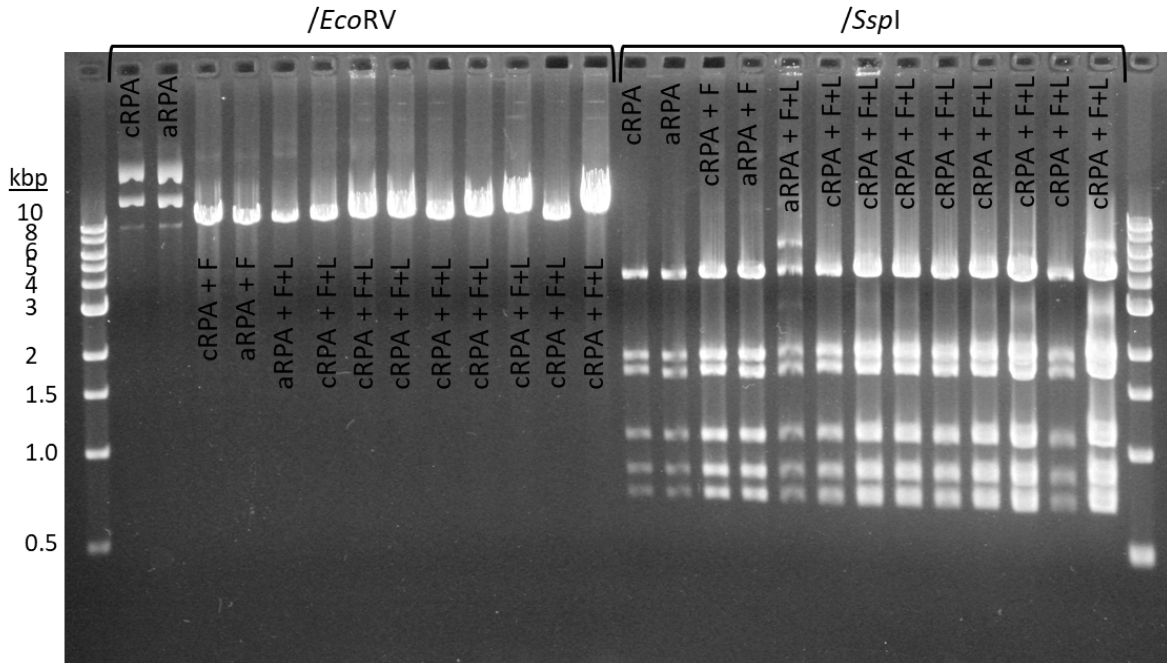


Figure 3.2. Confirmation of hybrid plasmid candidates

1.2% agarose TAE gel, electrophoresed at 150V. DNA ladder fragment sizes are labeled. Plasmids: cRPA and aRPA were digested as controls and are uncut by *EcoRI* (three native plasmid species are observed: supercoiled, nicked circular, and linearized). Hybrid plasmids: cRPA or aRPA containing the ScDBD-F (labeled F) or ScDBD-F+L (labeled F+L) are linearized by *EcoRI*. Plasmids digested with *SspI* are similar to cRPA and aRPA controls as this digest was done to confirm plasmid integrity.

Yeast two-hybrid assay identifies potential protein-protein interactions of DNA-binding domain F (DBD-F)

Yeast two-hybrid assays allow for the identification of protein-protein interactions *in vivo*. Two genetic screens were done with this method to identify potential protein-protein interactors of DBD-F from both *Saccharomyces cerevisiae* (yeast) RFA and *Homo sapiens* (human) RPA, using a yeast genomic library and a human cDNA library, respectively. By only using DBD-F the identified interactions between DBD-F and the interactor occur outside of the context of the RFA/RPA complex (i.e., identified interactions do not require complex formation or ssDNA binding). With 720 initially identified colonies demonstrating a protein-protein interaction (activation of the reporter by growth on media lacking leucine) for each of the yeast

and human DBD-F yeast two-hybrid screens, the interactors that were chosen for identification were narrowed to the interactions that were sensitive to DNA damaging agents.

The three most abundantly identified interactors (hits) of the yeast Rfa1-DBD-F (bait) were Rad24, Sgs1, and Dna2 (Table 3.2). These three proteins have been rather well characterized regarding their interaction with DBD-F (Bae et al. 2003, Hegnauer et al. 2012, Piya et al. 2015). In fact, Rad24 interaction with DBD-F was characterized previously in the Haring laboratory. It was identified that Rfa1 DBD-F interacts with the Rad24 C-terminal region and that this interaction is sensitive to MMS (Piya et al. 2015). The yeast two-hybrid results of this study not only recapitulate MMS sensitivity, but also show the interaction is sensitive to CPT and PHL (Table 3.2). Sgs1 and Dna2 were also shown previously to have MMS-sensitive protein interactions with Rfa1 (Piya et al. 2015), this study suggests that DBD-F may be the Rfa1 region interacting with Sgs1 and Dna2 that is abrogated under MMS treatment (Table 3.2).

Nine out of the thirteen proteins identified as interactors of yeast DBD-F were novel interactors (Table 3.2). One candidate of particular interest is Snt309 which associates with the Prp19 complex. Prp19 is an ubiquitin ligase which comprises the major part of the Prp19 complex demonstrated to be important in spliceosome activation (Chan et al. 2003). In *Homo sapiens*, DBD-F has been shown to interact with proteins of the PRP19 complex (Maréchal et al. 2014, Wan and Huang 2014) (Table 3.1), thus the Rfa1-DBD-F interaction with Snt309, which associates with the Prp19 complex, suggests that interactions involving the Prp19 complex may be conserved across species.

Table 3.2. Yeast two hybrid assay identified interactors of *Saccharomyces cerevisiae* Rfa1-DBD-F

Gene	ORF	Times Id'd	Colony color (blue/white)	Colony damage sensitivities	Description of gene
<i>RAD24</i>	YER173W	7	blue/white	MMS, CPT, PHL	Checkpoint protein; involved in the activation of the DNA damage and meiotic pachytene checkpoints; subunit of a clamp loader that loads Rad17p-Mec3p-Ddc1p onto DNA
<i>SGS1</i>	YMR190C	4	blue	MMS	RecQ family nucleolar DNA helicase; role in genome integrity maintenance, chromosome synapsis, meiotic joint molecule/crossover formation; forms nuclear foci upon DNA replication stress
<i>DNA2</i>	YHR164C	4	blue	MMS	Tripartite DNA replication factor; single-stranded DNA-dependent ATPase, ATP-dependent nuclease, helicase; involved in DNA repair/processing of meiotic DNA double strand breaks; forms nuclear foci upon DNA replication stress
<i>RPN3*</i>	YER021W	2	blue	MMS	Essential non-ATPase regulatory subunit of the 26S proteasome lid; similar to the p58 subunit of the human 26S proteasome; temperature-sensitive alleles cause metaphase arrest, suggesting a role for the proteasome in cell cycle control
<i>AIM33*</i>	YML087C	1	blue	MMS	Protein of unknown function, highly conserved across species
<i>AFG2*</i>	YLR397C	1	blue	MMS	ATPase of the CDC48/PAS1/SEC18 (AAA) family; essential for pre-60S maturation and release of several pre-ribosome maturation factors
<i>HSL1*</i>	YKL101W	1	white	MMS	Nim1p-related protein kinase; septin-binding kinase that localizes to the bud neck septin ring and regulates the morphogenesis checkpoint

Table 3.2. Yeast two hybrid assay identified interactors of *Saccharomyces cerevisiae* Rfa1-DBD-F (continued)

Gene	ORF	Times Id'd	Colony color (blue/white)	Colony damage sensitivities	Description of gene
<i>SNT309*</i>	YPR101W	1	blue	MMS	Member of the NineTeen Complex (NTC); this complex contains Prp19p and stabilizes U6 snRNA in catalytic forms of the spliceosome containing U2, U5, and U6 snRNAs; interacts physically and genetically with Prp19p
<i>SUB1</i>	YMR039C	1	blue	MMS, PHL	Transcriptional regulator; facilitates elongation through factors that modify RNAP II; role in the hyperosmotic stress response through polymerase recruitment at RNAP II and RNAP III genes; negatively regulates sporulation; protein abundance increases in response to DNA replication stress
<i>SAK1*</i>	YER129W	1	blue	MMS, PHL	Upstream serine/threonine kinase for the SNF1 complex; plays a role in pseudo-hyphal growth
<i>PHM7*</i>	YOL084W	1	white	MMS	Protein of unknown function; expression is regulated by phosphate levels; green fluorescent protein (GFP)-fusion protein localizes to the cell periphery and vacuole; protein abundance increases in response to DNA replication stress
<i>PAC2*</i>	YER007W	1	white	MMS	Microtubule effector required for tubulin heterodimer formation; binds alpha tubulin, required for normal microtubule function
<i>TBS1*</i>	YBR150C	1	blue	MMS	Protein of unknown function; the authentic, non-tagged protein is detected in highly purified mitochondria in high-throughput studies

ORF= Open Reading Frame, systematic name for gene in yeast. Id'd= identified. Description of gene from the yeast genome database. * indicates novel interactors.

Of the thirteen identified interactors of the *Homo sapiens* DBD-F, twelve were novel interactions (Table 3.3). Many interactors identified are known transcriptional factors or contain a zinc-finger domain. Studies performed in both yeast and humans have suggested that RFA/RPA may have a role in transcriptional regulation, especially during the DDR (Singh and Samson 1995, Schramke et al. 2001, Kaustov et al. 2006, Ljungman 2007). The interaction between TP53 and DBD-F has been previously characterized in human studies (Li and Botchan 1993, Bochkareva et al. 2005). Identifying this interaction in the context of the yeast cell lends credibility to using a yeast two-hybrid assay to identify potential interactions between human proteins that could be investigated further in human cell studies to confirm an interaction. Thus, the transcription factors identified to interact with RPA1 DBD-F would be good candidates to confirm an interaction and further investigate the possibility of a transcriptional role for RPA in human cells.

Table 3.3. Yeast two hybrid assay identified interactors of *Homo sapiens* RPA1 DBD-F

Gene	ORF	Times Id'd	Colony color (blue/white)	Colony damage sensitivities	Description of gene
BSDC1*	1p35.1	6	blue	MMS	BSD domain containing 1
FIZ1 ^{a*}	19q13.42	4	blue	MMS	(flt3-interacting zinc finger protein 1) This gene encodes zinc finger protein, which interacts with a receptor tyrosine kinase involved in the regulation of hematopoietic and lymphoid cells. This gene product also interacts with a transcription factor that regulates the expression of rod-specific genes in retina.
DNMT3B*	20q11.21	3	blue	MMS	This gene encodes a DNA methyltransferase which is thought to function in de novo methylation, rather than maintenance methylation. The protein localizes primarily to the nucleus and its expression is developmentally regulated.

Table 3.3. Yeast two hybrid assay identified interactors of Homo sapiens RPA1 DBD-F (continued)

Gene	ORF	Times Id'd	Colony color (blue/white)	Colony damage sensitivities	Description of gene
GSN ^{a*}	9q33.2	3	blue	MMS	The protein encoded by this gene binds to the "plus" ends of actin monomers and filaments to prevent monomer exchange. The encoded calcium-regulated protein functions in both assembly and disassembly of actin filaments. Also known as ADF and AGEL.
SCYL1 ^{a*}	11q13.1	2	blue	MMS	This gene encodes a transcriptional regulator belonging to the SCY1-like family of kinase-like proteins. The protein has a divergent N-terminal kinase domain that is thought to be catalytically inactive and can bind specific DNA sequences through its C-terminal domain. It activates transcription of the telomerase reverse transcriptase and DNA polymerase beta genes.
TP53 ^a	17p13.1	2	blue	MMS	This gene encodes a tumor suppressor protein containing transcriptional activation, DNA binding, and oligomerization domains. The encoded protein responds to diverse cellular stresses to regulate expression of target genes, thereby inducing cell cycle arrest, apoptosis, senescence, DNA repair, or changes in metabolism.
ZFAND2B ^{a*}	2q35	2	white	MMS	This gene encodes a protein containing AN1-type zinc-fingers and ubiquitin-interacting motifs. The encoded protein likely associates with the proteasome to stimulate the degradation of toxic or misfolded proteins.
EIF3J [*]	15q21.1	1	white	MMS	This gene encodes a core subunit of the eukaryotic initiation factor 3 complex, which participates in the initiation of translation by aiding in the recruitment of protein and mRNA components to the 40S ribosome.

Table 3.3. Yeast two hybrid assay identified interactors of Homo sapiens RPA1 DBD-F (continued)

Gene	ORF	Times Id'd	Colony color (blue/white)	Colony damage sensitivities	Description of gene
FAM50A ^{a*}	Xq28	1	blue	MMS	This gene belongs to the FAM50 family. The encoded protein is highly conserved in length and sequence across different species. It is a basic protein containing a nuclear localization signal and may function as a DNA-binding protein or a transcriptional factor.
HTATIPZ ^{a*}	11p15.1	1	white	MMS	HIV-1 Tat interactive protein 2
PKM ^{a*}	15q23	1	white	MMS	This gene encodes a protein involved in glycolysis. The encoded protein is a pyruvate kinase that catalyzes the transfer of a phosphoryl group from phosphoenolpyruvate to ADP, generating ATP and pyruvate. This protein has been shown to interact with thyroid hormone and may mediate cellular metabolic effects induced by thyroid hormones. This protein has been found to bind Opa protein, a bacterial outer membrane protein involved in gonococcal adherence to and invasion of human cells, suggesting a role of this protein in bacterial pathogenesis.
TRERF1 ^{a*}	6p21.1	1	blue	MMS	This gene encodes a zinc-finger transcriptional regulating protein which interacts with CBP/p300 to regulate the human gene CYP11A1. Alternative splicing results in multiple transcript variants encoding different isoforms.
U2AF1L5 ^{a*}	21p12	1	white	MMS	U2 small nuclear RNA auxiliary factor 1 like 5, mRNA splicing

^a Interactors were not verified by analysis of the protein sequence. ORF= Open Reading Frame. Id'd= identified. Description of gene from National Center for Biotechnology Information (NCBI) Gene database. *indicates novel protein interactors

Rfa2 phosphorylation is apparent in DBD-F mutant (*rfa1-t11*) cells

Cells containing the Rfa1 DBD-F charge-reversal (*rfa1-t11*) mutation have been shown to have reduced interactions with a variety of repair proteins, which likely contributes to the

increased DNA damage sensitivity of *rfa1-t11* mutants (Chen et al. 1998, Umezu et al. 1998, Soustelle et al. 2002, Zou et al. 2003, Zou and Elledge 2003, Majka et al. 2006a, Majka et al. 2006b, Piya et al. 2015, Seeber et al. 2016, Deshpande et al. 2017). Rfa2 is phosphorylated in response to DNA damage in wild-type yeast cells and this phosphorylation is especially evident at later timepoints after induction of an irreparable break (Wilson 2018). Both the *rfa1-t11* mutation and the phospho-mimetic Rfa2 mutation (*rfa2-D_x*) have been demonstrated to promote cell cycle progression (checkpoint adaptation) in the presence of irreparable DNA damage (Lee et al. 1998, Pelliccioli et al. 2001, Ghospurkar et al. 2015b, Wilson 2018). Because DBD-F interacts with a wide variety of repair factors and in human cells DBD-F interacts with ATR (Mec1 homolog) that phosphorylates RPA2, it was hypothesized that DBD-F may interact with the kinase that is phosphorylating Rfa2 (Wilson 2018, Maréchal and Zou 2015, Zou and Elledge 2003). Evidence suggests that the Rfa2 NT is not directly phosphorylated by Mec1, however Mec1 may be required for complete hyperphosphorylation of Rfa2 since Mec1 phosphorylates Rfa2-S122 (Wilson, Richards unpublished data) (Wilson 2018, Brush et al. 1996, Brush et al. 2001, Bartrand et al. 2004, Bartrand et al. 2006). Interestingly, the phosphorylation of Rfa2 is very similar between wild-type and *rfa1-t11* mutant cells (Figure 3.3). Rfa2 phosphorylation does appear to happen a bit earlier in *rfa1-t11* mutant cells than in wild-type cells when damaged with MMS and CPT (comparing the 4 hour timepoints of *RFA1* and *rfa1-t11*); however, when comparing all timepoints after PHL damage, Rfa2 phosphorylation in the *rfa1-t11* strain appears to be slightly reduced. Because interactions with repair factors are reduced in cells containing the *rfa1-t11* mutation, these cells might have intrinsic DNA damage incurred from replication or other cellular stresses that resulted in earlier Rfa2 phosphorylation. Overall, the differences in Rfa2 phosphorylation between wild-type cells and *rfa1-t11* mutant cells are subtle which

suggests that Rfa2 phosphorylation still occurs when Rfa1 DBD-F is mutated. This also suggests that any interaction with the unknown kinase responsible for delayed Rfa2 phosphorylation is not significantly altered by the *rfa1-t11* mutation. These results, utilizing strains independently-generated by Wendy Larson via plasmid shuffle to have a wild-type control containing pRS315-*RFA1* rather than pJM132, corroborate data published in a prior dissertation (Wilson 2018).

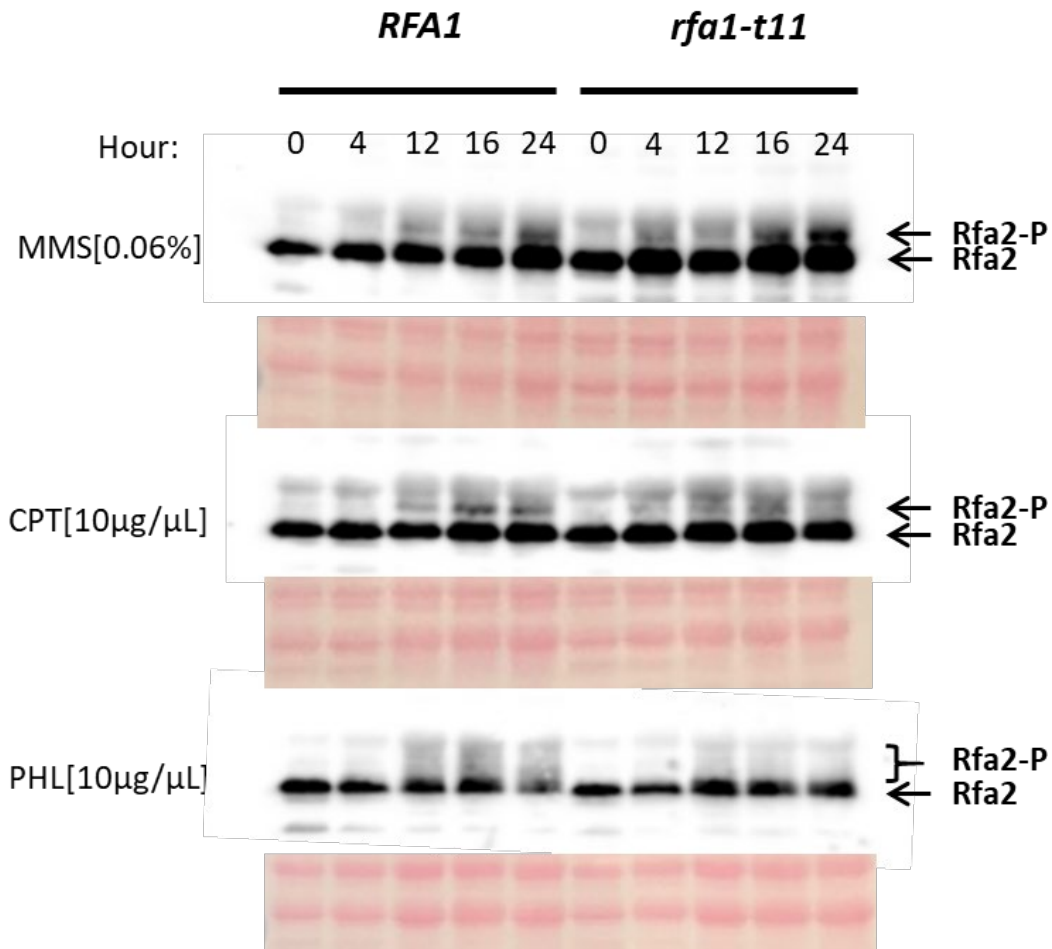


Figure 3.3. Rfa2 phosphorylation occurs in an *rfa1-t11* mutant

Rfa2 protein detected via western blot. Protein was TCA extracted from samples taken at 10 OD equivalents from JKM179 derivatives containing *RFA1* (WAL105; left) and *rfa1-t11* (WAL106; right) at the time points indicated (in hours) after addition of the DNA damaging agents: MMS, CPT, and PHL. The western blotting procedure is detailed in the materials and methods section. Ponceau S staining (shown below each western blot) was done to check for even loading and transfer. The Rfa2 species indicated are unmodified Rfa2 and phosphorylated Rfa2 (Rfa2-P).

DNA damage sensitivity of checkpoint deficient mutants containing *rfa2* NT phosphomimetic mutations

Synthetic genetic interactions often provide insight into whether proteins could be part of the same pathway (epistatic interactions, where the phenotype of the double mutant mimics the phenotype of one of the single mutants) or different pathways (synergistic interactions, where the phenotype of the double mutant appears to be combined phenotypes of both single mutants). The *rfa1-t11* mutation has been implicated in the reduction of many protein-protein interactions necessary for maintaining a checkpoint, it is unclear whether these reduced protein-protein interactions are directly driving checkpoint adaptation or whether the observed Rfa2 phosphorylation (Figure 3.3) is driving checkpoint adaptation in *rfa1-t11* mutant cells. To better observe what effect Rfa2 phosphorylation may have on a defective DNA damage checkpoint, three different checkpoint protein gene deletion (*checkpointΔ*) strains were used to investigate the role of Rfa2 phosphorylation by sensitivity to different genotoxic agents. Checkpoint protein gene deletions (*checkpointΔ*) used were Rad17 (*rad17Δ*), Mec3 (*mec3Δ*), and Rad9 (*rad9Δ*); which have all been suggested to interact with DBD-F through studies demonstrating reduced localization with DBD-F (*Ibid*). The DNA damage sensitivity of cells containing each *checkpointΔ* was investigated in conjunction with *rfa2* NT extensive mutations (*rfa2-D_x*, phosphomimetic; *rfa2-A_x*, non-phosphorylatable) by a DNA damage spot assay, in which dilutions of each strain were spotted onto various concentrations of genotoxic agents (Figure 3.4, Appendix G: G6-G9).

Each genotoxic agent utilized produces a different type of damaged DNA structure. Camptothecin (CPT) is a topoisomerase inhibitor leading to the creation of double-stranded breaks that may produce topoisomerase-associated broken ends. Hydroxyurea (HU) depletes

nucleotide pools, which during DNA replication can lead to long stretches of ssDNA and replication fork collapse. Methylmethane sulfonate (MMS) is an alkylating agent which promotes use of the base excision repair pathway, which temporarily produces broken DNA during repair (Krokan and Bjørås 2013). Phleomycin (PHL) intercalates into DNA which creates double-stranded breaks with ends free of associated protein at the time of the break. While each genotoxic agent may influence which proteins initially recognize the DNA damage, at some point ssDNA will be generated and will be bound by RFA. Multiple genotoxic agents were used in order to observe if there would be a change to DNA damage sensitivity only under certain types of damage or if the change was global.

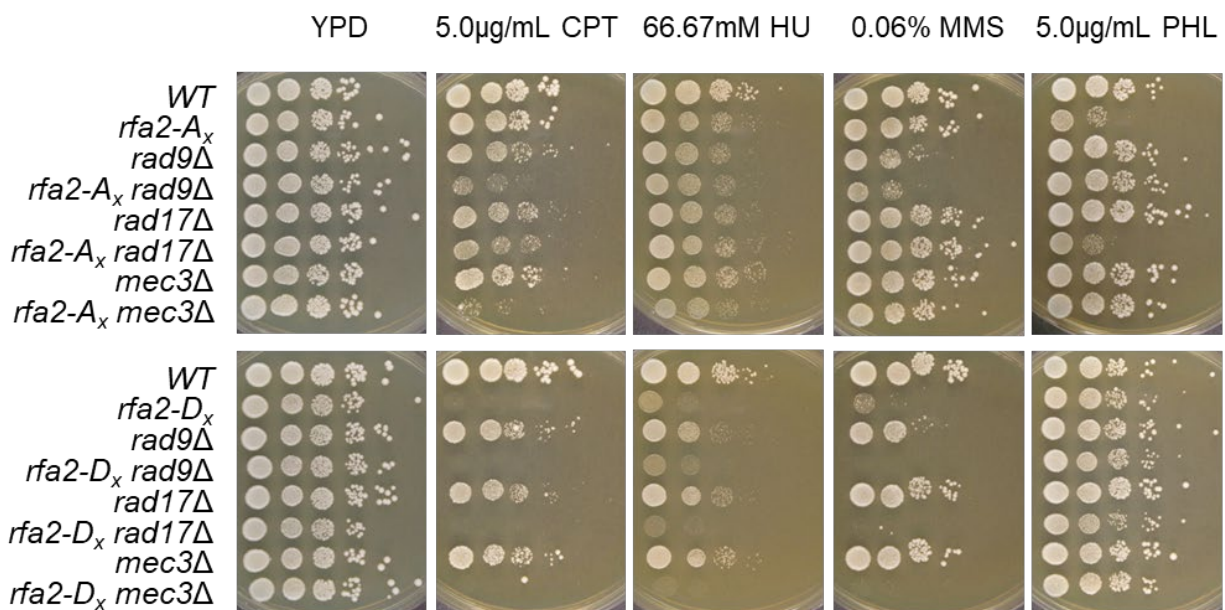


Figure 3.4. DNA damage spot assay of *rad9Δ*, *rad17Δ*, and *mec3Δ* mutants

Cells from each strain (labeled) were spotted in decreasing concentrations from left to right onto YPD plates or YPD plates containing genotoxic agents (CPT, HU, MMS, PHL at the labeled concentrations). Each spot contained 5 µL from the initial dilution of 1×10^7 cells/mL or from the five additional 1:10 serial dilutions. The best representative images were chosen for this figure. Additional images and concentrations located in Appendix G: Supplementary Figures G6-G9.

The non-phosphorylatable Rfa2 mutant, *rfa2-A_x*, appeared to have a synergistic effect (additive sensitivity) with *rad9Δ* on CPT and MMS only, and with *mec3Δ* on CPT and HU only

(Figure 3.4). On PHL, *rfa2-A_x* appears epistatic to *rad17Δ* (Figure 3.4). In contrast, *rfa2-D_x* appears that it may be epistatic to all three gene deletions on CPT, HU, MMS, and, although less apparent, PHL (Figure 3.4; Appendix G: A6-A9). Because the sensitivities are not definitively synergistic nor epistatic, it cannot yet be determined where Rfa2 phosphorylation fits into the checkpoint pathway in relation to Rad17, Mec3, and Rad9. However, *rfa2-D_x* clearly increases the DNA damage sensitivity of all *checkpointΔ* strains used here, which suggests that Rfa2 phosphorylation may alter modification of the DDR more significantly than these checkpoint proteins and may even modify the DDR early (i.e., before any additional negative effects of the *checkpointΔ* can be observed). This might also suggest that Rfa2 phosphorylation is driving the checkpoint adaptation phenotype of *rfa1-t11* mutant cells.

Discussion

Yeast DNA Binding Domain F does not allow for the human RPA complexes to substitute for yeast RFA in yeast cells

As previously published and tested here with modification, human RPA complexes are unable to substitute for yeast RFA. This inability to substitute may be due to a variety of factors. First, although RNA and protein of human RPA subunits were detectable in yeast (Ghospurkar et al. 2015a), it is unknown whether the human RPA subunits are properly folded to support genomic integrity functions in yeast. However, it has been shown that the human RPA subunits expressed in yeast can interact with each other as evidenced through yeast two-hybrid analysis (Ghospurkar et al. 2015a), which suggests that in yeast the structure of the human subunits is at least maintained well enough to facilitate their interaction with each other. Second, although the human RPA subunit proteins are detectable in yeast, as was shown by yeast two-hybrid for all subunits and by western blotting for RPA1 and RPA2 (Ghospurkar et al. 2015a), it was not

examined whether these subunits properly localize to the nucleus, as required, to carry out the essential functions in genomic maintenance. Finally, although single-stranded binding proteins are conserved, the protein-protein interactions they participate in may not be conserved between orthologs (homologous proteins in different species). One study analyzing results of large-scale protein-protein interaction data sets found that predicting interactions between homologous proteins is more reliable for homologous proteins existing in the same species rather than across species, because even when orthologs shared a high percentage of sequence identity (>70%) the highest accuracy for assuming protein-protein interactions among the data sets analyzed was only approximately 10% (Mika and Rost 2006). While the aforementioned study assessed whether a protein-protein interaction in one species could be used to accurately predict the interaction of homologous proteins in a separate species, it would be reasonable to hypothesize that substituting an ortholog (or heterospecific homolog like an RFA-RPA hybrid) may be unlikely to support the same interactions. Since RPA/RFA complexes both interact with numerous repair and cell-cycle regulatory factors, many opportunities exist for insufficient homology transfer of protein-protein interactions needed to support cell viability.

The inability to infer homology transfer of protein-protein interactions between species may also extend to support the second point made about the potential for RPA to be unable to localize to the nucleus. Recently, Rtt105 was demonstrated to be a chaperone of RFA nuclear import and RFA loading onto ssDNA both *in vitro* by using DNA curtains and *in vivo* by measuring the amount of RFA at origins of replication during nucleotide depletion (Li et al. 2018). Interestingly, it was found that cells lacking Rtt105 (*rtt105Δ*) are still viable contrary to the phenotype reported by the yeast genome database and the reported chaperone role for Rtt105 (Li et al. 2018), suggesting that Rtt105 isn't the sole chaperone for RFA. Prior to this recent

finding, Kap95, an essential nuclear import protein belonging to the Karyopherin β family, was demonstrated to be important for efficient RFA nuclear import as temperature sensitive mutants reduced the amount of nuclear RFA (Belanger et al. 2011). Thus, two protein-protein interactions are known to facilitate RFA import into the nucleus (Figure 3.5). Neither of these studies characterized which region of RFA was being bound by the chaperones, thus no conclusion can be drawn to suggest if any RFA-RPA hybrid should be able to localize to the nucleus. However, it has been suggested that the C-termini of RFA DBD-C, DBD-D, and DBD-E facilitate nuclear import (Belanger et al. 2011). Similar regions of RPA were demonstrated to form the trimerization core in human cells (Bochkareva et al. 2002); thus, the necessity for these domains could simply be for complex formation rather than the trimerization core directly facilitating nuclear import. Furthermore, additional research performed in the Haring laboratory by Trevor Baumgartner tested multiple combinations of RPA-RFA subunit hybrid complexes in which all hybrids contained the RFA trimerization core and no hybrid complex supported viability in yeast. Thus, the inability for RPA complexes to support viability in yeast does not appear to be solely due to the absence of the yeast trimerization core.

I hypothesize that the major issue with substituting RPA subunits to create RPA-RFA hybrid complexes is because of species-specific protein-protein interactions. This hypothesis could be further examined by using a yeast two-hybrid assay to test proteins known to interact with a specific region of RFA as bait with the RPA and RFA subunits as the prey; RPA and RFA subunits are suggested here to be used as the prey, since subunits other than RPA1/Rfa1 autoactivate the reporter gene when used as bait. With this experimental set-up, the RFA subunits would serve as controls that should be able to grow when the bait plasmid is tested in conjunction with the subunit with which it is known to interact, whereas RFA/RPA subunits that

have not been shown to interact may exhibit variability in growth and interaction. If the homologous RPA subunit does not show a similar ability to interact with the bait proteins tested, this is supportive of the hypothesis that RPA/RFA cellular functions are dependent on species-specific protein-protein interactions. The specific region(s) of RFA that interact with Rtt105 and Kap95 (the chaperones of RFA nuclear import) have not been characterized. Identifying which specific subunit of RFA is responsible for interacting with these chaperones and whether human RPA is capable of interaction with the yeast proteins Rtt105 and Kap95 would indicate whether nuclear import of RPA subunits is possible through the same mechanism as RFA nuclear import in yeast.

Yeast two-hybrid identifies novel potential protein interactions involving Rfa1 DBD-F

Identifying protein-protein interactions that are sensitive to DNA damage provides insight into how protein interactions can change under genotoxic conditions. In this study, the yeast two-hybrid screens identified both known and novel protein interactions involving DBD-F in which the interaction between the two proteins was abrogated under DNA-damage-induced cellular stress (Table 3.2 “yeast interactors”, Table 3.3 “human interactors”). Known interactors identified with yeast DBD-F were Rad24, Sgs1, and Dna2 (Figure 3.6). Of the interactors identified with human DBD-F, TP53 was the only interactor previously known. Both screens identified interactors that were proteins involved in transcription.

Out of all the interactors identified, the most intriguing find was discovering that Snt309 interacts with Rfa1-DBD-F (yeast). Identifying Snt309, a protein known to associate in complex with the ubiquitin ligase Prp19, as an interactor of DBD-F (yeast) suggests that interactions involving Prp19-associated proteins may be conserved from yeast to humans. In *Homo sapiens* DBD-F was shown to be required to interact with Prp19 *in vitro*, while *in vivo* RPA only appears

to interact with Prp19 in a damage-dependent manner; therefore, this protein seems unlikely to be identified in the yeast two-hybrid assay as a DNA damage-sensitive interactor (Maréchal et al. 2014). In yeast, phenotypic observations of DNA damage sensitivities of Prp19-complex mutants have been made (Pungartnik et al. 2002), which suggest a role for Prp19 proteins in the DNA damage response.

Thus far, the role of PRP19 in the DNA damage response has been very minimally studied. In *Homo sapiens*, PRP19 has been demonstrated to be necessary for DNA-damage-dependent ubiquitylation and phosphorylation of RPA2 (Maréchal et al. 2014), which implies a role for the ubiquitin ligase in the DNA damage response. This is interesting as currently unpublished data generated by Wendy Larson demonstrates that cells containing a mutant form of Rfa2 (*rfa2-K_xR*) which is unable to be ubiquitylated appear to have more DNA-damage-induced Rfa2 phosphorylation than wild-type cells. If a direct interaction between Prp19 and Rfa1 DBD-F can be established in *Saccharomyces cerevisiae*, considering data from both prior studies, this information would suggest that Rfa2 phosphorylation may be dependent on Prp19-dependent ubiquitylation of other proteins and that the extent of Rfa2 phosphorylation may be controlled by direct Prp19 ubiquitylation of Rfa2.

Rfa2 is phosphorylated even when Rfa1 DBD-F is mutated

DBD-F has been reported to interact with several factors necessary for repairing damaged DNA and arresting the cell cycle (Figure 3.6), however it does not appear to be necessary for Rfa2 phosphorylation in response to DNA damage because Rfa2 phosphorylation in cells containing a DBD-F mutation (*rfa1-t11*) is nearly indistinguishable from wild-type under three different inducers of DNA damage (Figure 3.3).

Research published regarding phosphorylated Rfa2 in *Saccharomyces cerevisiae* is very minimal. In *Homo sapiens*, research on RPA2 NT phosphorylation has shown that specific residues are phosphorylated by different kinases under stressed and unstressed conditions. Minimal research has focused on the cellular consequences of RPA2 phosphorylation, such as attenuated or enhanced protein interactions with either RPA2 or the RPA complex as a direct result of RPA2 phosphorylation.

In *Saccharomyces cerevisiae*, the Mec1 kinase has been demonstrated to phosphorylate both Rfa1-S178 and Rfa2-S122 following DNA damage (Brush and Kelly 2000, Brush et al. 1996); however, these events do not play a detectable role in the DNA damage response (Ghospurkar et al. 2015b, Mallory et al. 2003). During meiosis, when occurrence of DNA damage is programmed, there is at least one major site (S27) of the Rfa2 NT that becomes phosphorylated by a meiosis-specific kinase prior to DNA damage (Clifford et al. 2005). Domain swapping of the Rfa2 NT in yeast with the human RPA2 NT (*rfa2-H2NT*; yeast Rfa2 with human NT) allows for NT phosphorylation of the hybrid to be easily detected at early time points after DNA damage (Ghospurkar et al. 2015a, Wilson 2018). In comparison, phosphorylation of the native yeast Rfa2 NT is delayed, yet still dependent on mitotic DNA damage (Wilson 2018). There are no SQ/TQ motifs (Mec1 target sites) in the Rfa2 NT and delayed Rfa2 NT phosphorylation is independent from the phospho-state of Rfa2-S122, an early Mec1 target (Wilson 2018). Late hyper-phosphorylation of Rfa2 is reduced in a *mec1Δ* mutant (Wilson unpublished work); it is unclear whether Rfa2 NT phosphorylation is affected or if the observed reduction is due to the absence of Rfa2-S122 phosphorylation. It does seem unlikely that Rfa2 NT phosphorylation is directly dependent on Mec1, especially considering the time difference between the early Rfa2-S122 phosphorylation and late Rfa2 NT phosphorylation. The

appearance of hyper-phosphorylated Rfa2 is correlated with the de-phosphorylation or reappearance of the unmodified/inactive form of the checkpoint kinase Rad53 (Wilson 2018). Given that both yeast Rfa2 and human RPA2 are phosphorylated in response to DNA damage, the data suggest there may be a conserved role for Rfa2/RPA2 NT phosphorylation in the DNA damage response.

Due to the similar characteristics between *rfa2-D_x* and the *rfa1-t11* mutant strains: both single mutants can initiate the G₂/M checkpoint, promote checkpoint adaptation, and are synthetically lethal with *mre11Δ* (Lee et al. 1998, Ghospurkar et al. 2015b), it would be reasonable to hypothesize that the *rfa2-D_x* mutation also reduces interaction with repair factors that maintain cell cycle arrest. It has been proposed through *in vitro* experimentation with phospho-mimetic human RPA2 that phosphorylation may prevent DBD-F from interacting with DNA and facilitating dsDNA unwinding (Binz et al. 2003). Thus, a negatively charged Rfa2 NT interacting with DBD-F could also potentially stop DBD-F from interacting with other proteins. Further studies are required to determine DBD-F's affinity for checkpoint proteins and phosphorylated RFA2. This study shows initially promising data with yeast two-hybrid assays demonstrating that DBD-F has protein interactions that are weaker under genotoxic stress when Rfa2/RPA2 would be negatively-charged (phosphorylated). This leads one to speculate that the *in vivo* interactions identified by yeast two-hybrid assays in this study (such as: Rad24, Dna2, Sgs1) may have been sensitive to DNA damaging agents because DBD-F was preferentially interacting with phospho-RFA2/RPA2 over the identified prey vector.

DBD-F interactions that are not sensitive to DNA damaging agents could suggest that DBD-F has a higher affinity for those proteins over the speculated phospho-Rfa2/RPA2-NT interaction, which would leave Rfa2/RPA2 free for interaction. Thus, an additional mechanism

may have to exist to prevent DBD-F from engaging in protein interactions that are not sensitive to DNA damaging agents. This mechanism could involve removal of RFA with Rad51 and Rad52 to switch repair mechanisms from “DNA synthesis” to “homologous recombination”. The possibility for RFA to be involved in a repair mechanism switch was demonstrated in *Homo sapiens* with RPA2 isolated from DNA damage induced cells (phosphorylated RPA2) that was preferentially bound by the recombinases Rad51 and Rad52 in immunoprecipitation assays (Wu et al. 2005). Conversely, *rfa1-t11* protein has been demonstrated to be more slowly displaced from ssDNA by Rad51 *in vitro* using proteins produced with recombinant DNA (i.e., non-phosphorylated Rfa2/RPA2) (Kantake et al. 2003). Thus, phosphorylated Rfa2 may promote recruitment of Rad51/Rad52, which are then loaded onto ssDNA by DBD-F facilitation leading to RFA removal from ssDNA (Figure 3.7). After RFA removal, phospho-Rfa2 may prevent DBD-F from additional interactions with repair proteins. This proposed mechanism is consistent with the reported reduction in recombination of the *rfa1-t11* mutant (Umezu et al. 1998, Soustelle et al. 2002), and additionally observed during a study to determine the frequency of mating type switching performed by Mary (Maggie) Lenertz (Appendix H).

Phospho-mimetic Rfa2 suggests that Rfa2 NT phosphorylation modifies the DNA damage response

Three checkpoint protein gene deletions (*rad17Δ*, *mec3Δ*, and *rad9Δ*) were used in conjunction with Rfa2 phospho-mutants to investigate the role of Rfa2 phosphorylation during a defective checkpoint. The interactions of these checkpoint proteins with DBD-F have been inferred because a direct interaction with DBD-F has not yet been shown in yeast. Rad17 and Mec3 comprise 2/3 components of the Ddc1-Mec3-Rad17 sliding checkpoint clamp. Rfa1-DBD-F has been demonstrated to be necessary for efficient loading of the sliding clamp to 5' DNA

junctions (Majka et al. 2006a), and necessary for efficient loading of the clamp at double-stranded breaks as shown with the *rfa1-t11* mutation by a slight reduction in Ddc1 at an HO break (Zou et al. 2003). Localization of the clamp is dependent on the clamp loader but not Rad9 (Melo, Cohen and Toczyski 2001). Rad9 is the adaptor needed for activation of the checkpoint effector kinase Rad53 that stops the progression of the cell cycle (de la Torre-Ruiz et al. 1998). In human cells the functional homolog of Rad9, 53BP1, interacts with RPA1 and RPA2; this interaction is CPT sensitive (Yoo et al. 2005). Interestingly, 53BP1 appears to be required for RPA2 hyperphosphorylation 1 hour after CPT treatment, with the interaction between 53BP1 and RPA2 becoming severely reduced 2 hours after CPT treatment (i.e., after RPA2 hyperphosphorylation) (Yoo et al. 2005). This implies that the Rad9 adaptor may be required for Rfa2 phosphorylation, and after Rfa2 phosphorylation, Rad9 may no longer be able to interact with Rfa2. Rad9 exists in a branch of the DNA damage response that is separate from the clamp and clamp loader, with eventual convergence, since both pathways are required for the activation of Rad53 (de la Torre-Ruiz et al. 1998) Considering that the synthetic genetic data leans towards supporting that the *rfa2-D_x* mutation is epistatic to the three gene deletions (clamp: Rad17, Mec3; Rad9) tested (Figure 3.4), Rfa2 phosphorylation might modify both DNA damage response pathways that converge to activate Rad53.

In summary, RFA may be the convergent point to coordinate repair mechanisms. Protein-protein interactions involving RFA are likely species-specific interactions due to the inability of RFA-RPA hybrid complexes to support viability. Many opportunities exist for the essential RFA interactions to be species-specific, such as those interactions necessary for RFA nuclear import and the functions of nuclear RFA (i.e., replication, repair, cell cycle; Figures 3.5, 3.6). Once RFA is removed from the DNA, DBD-F may prevent RFA from DNA re-association by having a

decreased affinity for DNA and potentially by preventing the other DBDs from interacting with DNA when DBD-F binds to phosphorylated Rfa2 (Figure 3.7).

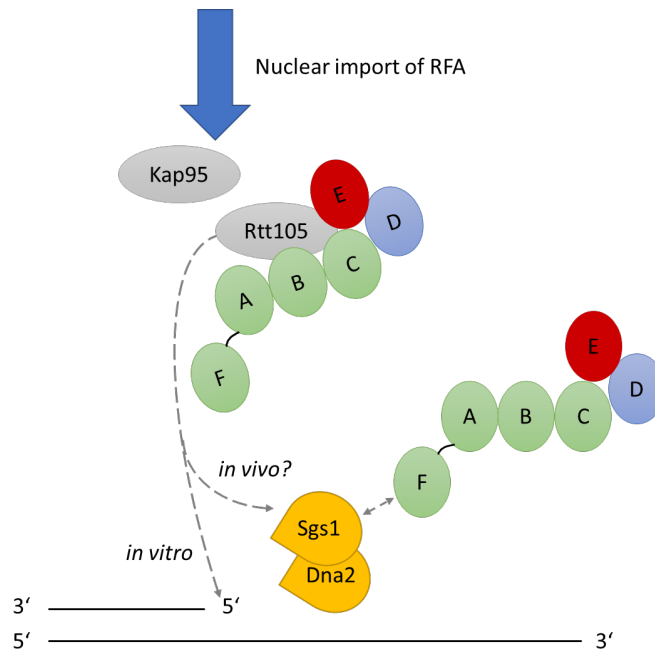


Figure 3.5. Nuclear import of RFA

RFA is imported into the nucleus by Kap95 (β -importin) and chaperone Rtt105. *In vitro* Rtt105 was shown to increase efficiency of RFA loading onto ssDNA. *In vivo*, perhaps Sgs1/Dna2 facilitates loading onto ssDNA through interaction with DBD-F, since Sgs1-Dna2 have also been demonstrated to increase the efficiency of RFA loading onto ssDNA.

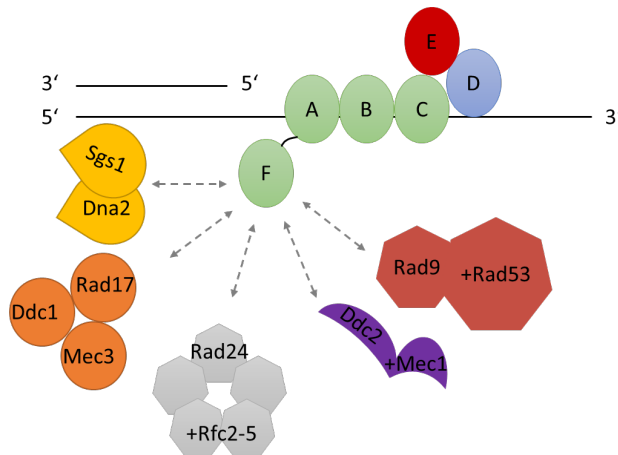


Figure 3.6. Once on ssDNA, DBD-F interacts with a variety of checkpoint proteins

DBD-F coordinates repair by interacting with a variety of checkpoint proteins such as the helicase-nuclease pair (Sgs1-Dna2), the clamp loader (Rad24-Rfc2-5), the sliding clamp (Rad17-Ddc1-Mec3), the Ddc2-Mec1 binding partner and sensor kinase, and the Rad9 adaptor for the effector kinase Rad53.

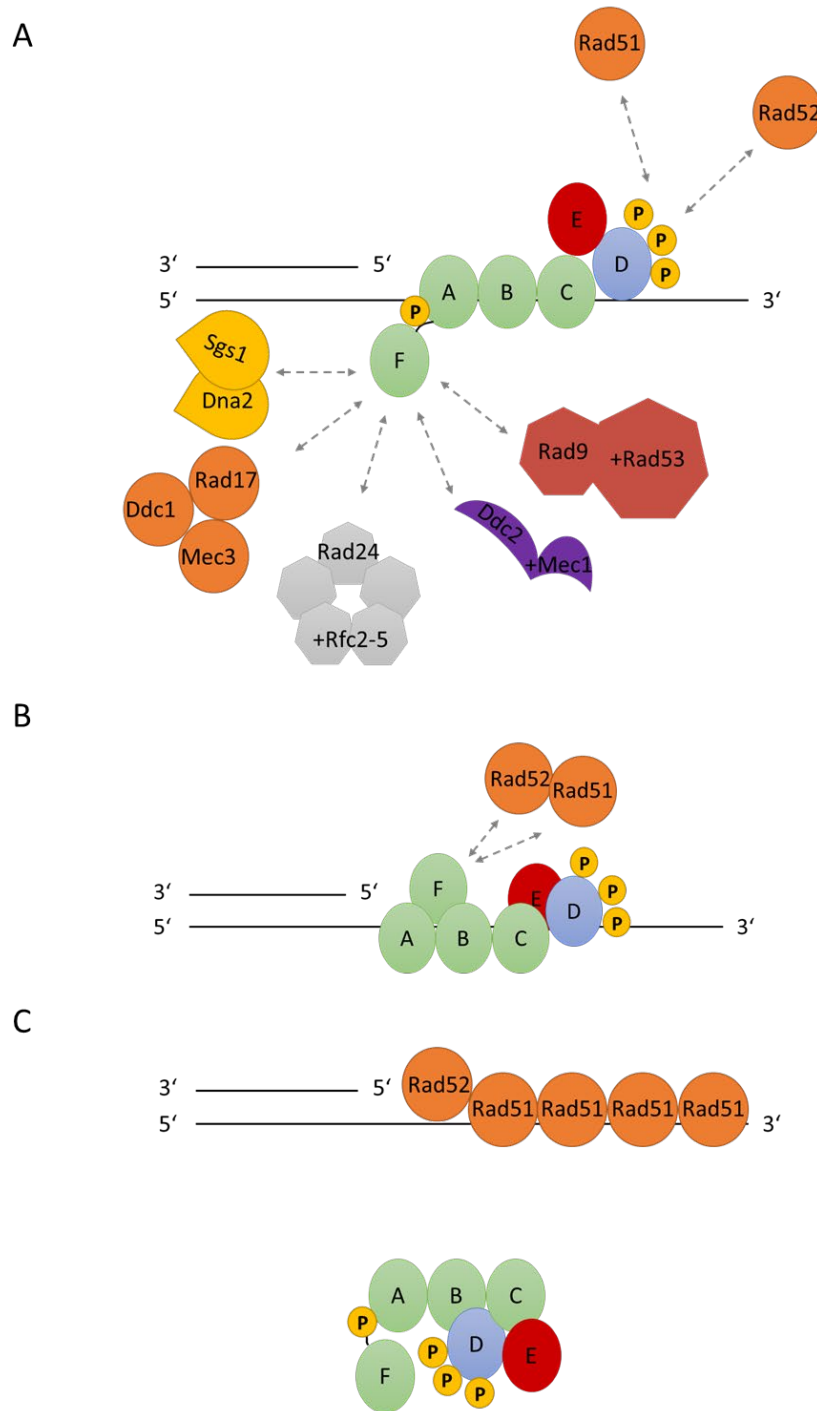


Figure 3.7. RFA removal by replacement

(A) After phosphorylation of the Rfa2 NT, Rad51 and Rad52 are recruited. (B) RFA is removed when Rad51 loading onto the ssDNA is facilitated by DBD-F, either directly or through interaction with additional proteins (such as Rad52). (C) When Rad51 and Rad52 replace RFA on ssDNA, DBD-F binds the negatively charged Rfa2 NT, which prevents further interactions with ssDNA or other checkpoint proteins.

Acknowledgements

Padmaja Ghospurkar for creating the *Homo sapiens* cRPA and aRPA plasmids. (Alexis Larson and Jason Balster for creating the plasmids used in the yeast 2-hybrid screens. John Wilkinson and Wilkinson lab: Sierra Giebel and Sujata Birua for allowing and assisting with use of the myECL™ (Thermo Scientific) imager and myImageAnalysis™ software (Thermo Scientific).

CHAPTER FOUR: THE RFA2 NT IS REQUIRED FOR MEIOTIC PROGRESSION

Meiosis is an essential process to generate haploid gametes by one round of DNA replication and two rounds of DNA division. Many meiotic proteins are conserved in eukaryotes; thus, the budding yeast *Saccharomyces cerevisiae* provides a model system for the induction and study of meiosis. In yeast, meiosis is controlled by a transcriptional cascade orchestrated by the meiosis-specific kinase, Ime2. One of the early targets of Ime2 is the Rfa2 N-terminus (NT), one of the three subunits of the Replication Factor A (RFA) complex. RFA or RPA (Replication Protein A) is an evolutionarily conserved, heterotrimeric, single-stranded DNA (ssDNA)-binding protein required for DNA replication, repair, recombination, and cell-cycle regulation. We generated Rfa2 NT mutants to investigate the role the Rfa2 NT may have during meiosis.

Our data suggest the Rfa2 NT is playing a significant role in cells proceeding through meiosis, as our mutant missing the Rfa2 NT (*rfa2-ΔN_x*) displays reduced sporulation efficiency with fewer tetrads and more dyads (severely decreased tetrad:dyad ratio). Tetrads that are formed also have a severe reduction in spore viability. The requirement for the Rfa2 NT for proper meiotic divisions is independent from roles in DNA replication and homologous recombination. Phosphorylation of the domain may be dispensable during an otherwise normal meiosis as our mutant that cannot be phosphorylated (*rfa2-A_x*) is not distinctly different from wild-type (WT) cells. However, a phospho-mimetic mutant (*rfa2-D_x*) shows reduced viability. Examination of our mutants in both mitosis and meiosis suggests that the Rfa2 NT could have a cell-cycle regulatory role that affects the mitotic-like divisions, mitosis and meiosis II.

Introduction

During the cell cycle if broken DNA is detected, mechanisms exist to stop the cell cycle and allow for repair. One sensor of broken DNA is Replication Protein A (RPA)/Replication Factor A (RFA) which is an evolutionarily conserved, heterotrimeric, single-stranded DNA (ssDNA)-binding protein required for DNA replication, repair, recombination, and cell-cycle regulation (Wold 1997, Lee et al. 1998, Soustelle et al. 2002, Ghospurkar et al. 2015b). The RFA complex in *Saccharomyces cerevisiae* is made up of Rfa1, Rfa2, and Rfa3. Rfa1-S178 and Rfa2-S122 have both been shown to be phosphorylated by the checkpoint sensor-kinase Mec1 in response to DNA damage during mitosis (Brush and Kelly 2000, Brush et al. 1996, Kim and Brill 2003, Bartrand et al. 2004, Bartrand et al. 2006).

The effects of hyperphosphorylated Rfa2 have been studied in mitosis by utilizing extensive mutants, in which all of the NT serine and threonine residues have been mutated to either aspartic acids (*rfa2-D_x*) to mimic phosphorylation or to alanines (*rfa2-A_x*) to prevent phosphorylation and mimic the non-phosphorylated state (Ghospurkar et al. 2015b). The study showed that the NT phosphorylation domain of Rfa2 contributes to DNA damage sensitivity and checkpoint adaptation (Ghospurkar et al. 2015b). Checkpoint adaptation is the ability of a cell to proceed through the cell cycle with unrepaired DNA after arresting at the G₂/M checkpoint (Lee et al. 1998, Lee et al. 2000, Galgoczy and Toczyski 2001, Pelliccioli et al. 2001). The phospho-mimetic Rfa2 extensive mutant (*rfa2-D_x*) has increased DNA damage sensitivity and causes checkpoint adaptation to occur in the adaptation-deficient *yku70Δ* mutant (Ghospurkar et al. 2015b). Its ability to rescue checkpoint adaptation is not due to an inability to establish the checkpoint, as initially the mitotic checkpoint effector kinase Rad53 is phosphorylated to an extent indistinguishable from wild-type cells (Ghospurkar et al. 2015b, Pelliccioli et al. 2001).

However, *rfa2-D_x* appears to drive deactivation of the checkpoint (especially apparent in adaptation-deficient strains) by the reduction of activated Rad53 and restores checkpoint adaptation in adaptation-deficient strains, while adaptation-deficient strains containing *rfa2-A_x* or *rfa2-ΔN_x* have persistent Rad53 phosphorylation and remain adaptation-deficient (Ghospurkar et al. 2015b, Pelliccioli et al. 2001, Wilson 2018).

Rfa2 also becomes hyperphosphorylated during meiosis (Brush et al. 2001, Clifford et al. 2005). Meiosis is an essential process for sexually reproducing organisms in which a diploid cell goes through a single round of DNA replication followed by two consecutive rounds of DNA division to produce haploid gametes. One division is unique to meiosis, where homologous chromosomes are segregated (reductional division; MI). During this reductional division, the DNA is purposely broken by meiotic proteins to tether together homologous chromosomes through repair. This event ensures proper chromosome segregation in MI and is facilitated by many meiosis-specific proteins such as: Spo11, Dmc1, Mek1, and Ndt80, as well as some proteins that are part of mitotic repair processes as well: such as Mre11, Rad50, Xrs2, Sae2, Mec1, Rad17, and Rad24.

The DNA breaks during meiosis are catalyzed by Spo11 as part of the recombination initiation protein complex (Klapholz et al. 1985, Keeney 2008, Koehn et al. 2009, Keeney et al. 1997). Mre11, Rad50, Xrs2, and Sae2 are additional proteins that are part of the recombination initial complex that are responsible for removal of Spo11 and resection of the Spo11-induced break, which ultimately starts the process of repair (Lengsfeld et al. 2007). In the absence of Spo11, *spo11Δ* cells have been shown to have a four-fold reduction in tetrad formation from wild-type, severe reduction in viability, and no detectable 100-1000 fold increase in recombination typically observed when comparing meiotic to mitotic cells (Klapholz et al.

1985). In the absence of *Sae2*, *sae2Δ* cells rarely form a tetrad, as the majority of cells end up arresting prior to MI with an accumulation of DSBs (Prinz, Amon and Klein 1997, Lengsfeld et al. 2007).

Some proteins required for repair occurring during mitosis are also required for meiotic repair, such as: Mec1 (checkpoint kinase), Rad17 (clamp component), and Rad24 (clamp loader component); however, there are others such as Rad9 (adaptor for Rad53, the checkpoint effector kinase) and Rad53 that are not required (Lydall et al. 1996, Sweeney et al. 2005, Cartagena-Lirola et al. 2008, Shinohara et al. 2003, Shinohara and Shinohara 2013, Grushcow et al. 1999). Rad9 is seemingly dispensable because in MI its function is replaced by Hop1, adaptor for the meiosis-specific effector kinase, Mek1 (Carballo et al. 2008, Hunter 2008). Hop1-Mek1 seem to replace the Rad9-Rad53 pair during MI, because Hop1-Mek1 are part of a homolog bias mechanism to promote interhomolog repair rather than sister chromatid repair, which is promoted by Rad9-Rad53 in mitosis and the mitotic-like MII division (Niu et al. 2005, Niu et al. 2007, Usui and Kanehara 2013, Cartagena-Lirola et al. 2008). Homolog bias in MI is also promoted by the meiosis-specific recombinase, Dmc1. Dmc1 is tolerant of mismatched base-pairs making it preferential for recombinational repair through homologous chromosomes over the mitotic recombinase, Rad51 which is not as tolerant to mismatches (Lee et al. 2017). While Dmc1 is essential for meiotic recombination utilizing homologous chromosomes that may have sequence variability, Rad51 is still needed to assist Dmc1 with repair (Shinohara et al. 2000, Cloud et al. 2012). In the absence of Dmc1, cells arrest prior to the MI division (Bishop et al. 1992).

The role of Mek1 during MI is similar to the role that Rad53 plays during mitosis and MII, in that Mek1 inhibits progression through MI until all breaks are being repaired. When

Mek1 becomes activated in MI by the presence of double-stranded breaks, it inhibits progress through MI (specifically pachytene) by phosphorylating Ndt80 (Chen et al. 2018, Prugar et al. 2017). Ndt80 is the major transcriptional activator of middle and late meiotic genes (Chu et al. 1998). Ndt80 promotes exit from the pachytene checkpoint when no longer inhibited by Mek1 and when Ndt80's activity is promoted by Ime2's transcriptional activation and phosphorylation (Chen et al. 2018, Benjamin et al. 2003). In the absence of Ndt80, cells do not sporulate and remain arrested at the pachytene checkpoint of MI (Xu et al. 1995).

Phosphorylation of Rfa2 also occurs during meiosis, but in two sequential events (Brush et al. 2001). The second event during meiosis is similar to the mitotic damage response, in which Rfa2-S122 phosphorylation is dependent on both programmed double-stranded breaks and Mec1 (Brush et al. 2001, Bartrand et al. 2006). The first event occurs independently from DNA replication (Brush et al. 2001) and is dependent on Ime2 (Clifford et al. 2004, Clifford et al. 2005). Ime2 is the Cyclin-Dependent-Kinase (CDK)-like meiosis-specific kinase, that activates transcription of many meiotic genes (Sia and Mitchell 1995, Foiani et al. 1996, Benjamin et al. 2003, Honigberg and Purnapatre 2003, Schindler and Winter 2006). The majority of phosphorylation in the primary event occurs on Rfa2-S27, although mass spectrometry analysis revealed a total of three phospho-sites on Rfa2 aa 2-35 (Clifford et al. 2005). It is still unclear what purpose Ime2 phosphorylation of Rfa2 serves during meiosis.

This study utilizes *rfa2* NT extensive mutant strains to further study the role the Rfa2 NT has during meiosis. The *rfa2-A_x* mutant which has an NT that cannot be phosphorylated proceeds through meiosis like wildtype, similar to what was found when Rfa2-S27 was mutated to alanine (Clifford et al. 2005). The phospho-mimetic *rfa2-D_x* mutant also proceeds similarly to wildtype but consistently produces less 4 spore viable tetrads. The NT deletion mutant, *rfa2-ΔN_x*, also has

reduced spore viability, which is more severe than the *rfa2-D_x* mutant. It appears that cells containing *rfa2-ΔN_x* have an overall decreased ability to proceed through meiosis, observed commonly by a reduction in sporulation that leads to decreased tetrad: dyad ratios in all instances examined. The sporulation deficiencies of *rfa2-ΔN_x* strains do not appear to be caused by defects in replication or recombination per the assays performed. The effect these *rfa2* mutants have on the mitotic cell-cycle is observed through both physiological and biochemical analysis (observing Rad53 modification) of checkpoint adaptation with diploid strains that corroborate results utilizing haploid strains in prior studies (Ghospurkar et al. 2015b, Wilson 2018). The mitotic results suggest that the defects observed may be due to a cell cycle regulatory role of the Rfa2 NT that affects Rad53 activity most likely during the mitotic-like MII; however, due to recent evidence of a different role for Rad53 during MI this cannot yet be ruled out (Ballew and Lacefield 2019). Double mutants were also made to study if the *rfa2* mutations had any effect on meiotic progression in the absence of proteins with key roles in MI, as introduced above: Spo11, Sae2, Dmc1, and Ndt80. With the preliminary results obtained in this study, it does not appear that the *rfa2* mutations rescue meiotic progression of these mutants. Since the mutants affect the MI division and there is no observable change with the *rfa2* mutations, these results further support the idea that the Rfa2 NT specifically affects Rad53 activity during MII.

Materials and Methods

Yeast strains and plasmids

Yeast strains utilized are listed in Appendix A and Appendix B, diploid crosses are also listed in Table 4.1. Strains used for adaptation are JKM179 and JKM139 derivatives, original strains kindly provided by Jim Haber (Lee et al. 1998).

All plasmids utilized are listed in Appendix C. M2034 α was generated by Brian Samuelson by transformation of p_{GAL}-HO into RM96-15A-390, inducing expression of HO endonuclease to promote mating type switching and verified by replica plating to assess mating type.

The integrating vectors used to create the *RFA2* extensive mutant strains were generated by Timothy Wilson by *in vivo* HR cloning by the procedure as follows (Wilson 2018). The respective pRS315-derivative plasmid was digested with *PvuII* to remove the *rfa2* NT extensive mutant cassette from the vector. Then, *in vivo* cloning was utilized to clone the *rfa2* NT mutant cassette into a pRS316 vector, and transformants were selected for on SD-Ura. Following yeast genomic DNA isolation for plasmid recovery, DH10B *E. coli* cells were transformed with the isolated DNA via electroporation, and plasmids were selected for on LB+Amp. Bacterial transformants were analyzed via colony cracking and restriction digestion to verify each pRS316-*rfa2* NT extensive mutant. Site directed mutagenesis was used to remove the *CEN6/ARS4* centromeric and autonomously replicating sequence, using the primer Remove-ARSH4-CEN6 (Appendix D).

RFA2 mutants were created using two-step gene replacement in the following haploid strains (and isogenic derivatives of these): JKM139, JKM179, K264-10D, RM26-26C, RM96-15A-0C1, RM182-55C-C1 (Appendix A). The pRS306 vectors generated above were digested with *SnaBI*, transformed into yeast, and yeast containing the integration were selected for on SD-Ura (pop-ins). To stimulate pop-out of the wildtype *RFA2* copy with the *URA3* gene, cells were grown in YPD at 30°C (24°C for temperature sensitive strains) overnight and then spread on SD media supplemented with complete amino acids and 0.6-1.0 mg/mL 5-FOA (SD+Com+5-FOA). The *rfa2* mutants were verified by PCR using the primers: RFA2-UP-FOR and RFA2-

DOWN-REV and sequencing utilizing the primer RFA2-UP-FOR by Eton Biosciences (Appendix D). AWY strains were provided by Andre Walther (Ghospurkar et al. 2015b). TMW strains were generated and verified by Timothy Wilson. CMK strains were generated by Courtney Karnopp.

The following gene deletions/insertions: *dmc1Δ::hphNT*, *spo11Δ::kanMX*, *ndt80Δ::natMX* were generated by one-step gene replacement to generate single gene deletion strains followed by the two-step gene replacement above to generate double mutant strains (containing gene deletion + *rfa2* mutation). The single mutation *sae2Δ::hphNT* haploid strains were also generated by the following one-step gene replacement method. To generate the gene deletions by one-step gene replacement, first the following resistance cassettes: hygromycin B (*hphNT*), glutathione sulfate (*kanMX*), or nourseothricin (*natMX*) from the respective plasmids: pFA6-hphNT1, pKKW1, pCas9Nat-9 (Appendix C) with appropriate primers (Appendix D) were amplified so that the ends of the amplicon contained sequence homologous to the upstream and downstream sequences of the gene to be deleted. The amplicons were transformed into haploid strains: K264-10D and RM26-26C by lithium acetate transformation. Deletion strains were selected for by plating to YPD media containing the corresponding selective agent. Strains were verified by PCR using primers (Appendix D) further upstream and downstream from the desired gene knockout for *dmc1Δ::hphNT*, *spo11Δ::kanMX*, *ndt80Δ::natMX*. The *sae2Δ::hphNT* haploid strains were verified by PCR to confirm insertion by performing an upstream verification reaction and a downstream verification reaction.

For double mutant strains containing a *sae2Δ::hphNT* and a *rfa2* mutation, strains were generated by a crossing and dissecting method as strains with a *sae2Δ* cannot perform mitotic HR repair necessary for integrating the *rfa2* NT mutation. Additionally, it took 3 separate

transformation attempts to obtain the single *sae2Δ::hphNT* in the two desired strain backgrounds and no correct *sae2Δ::hphNT* strains were identified by PCR following one-step gene replacement in *rfa2* mutant haploids. Therefore, the method of crossing was the best course of action to guarantee generation of the desired double mutants. Haploids AMA154 (K264-10D derivative) and AMA152 (RM26-26C derivative) were crossed with the respective isogenic haploid of the opposite mating type (K264-10D- α and RM26-26C-A) to generate a diploid that was sporulated, dissected, and replica plated to obtain AMA210 (isogenic to K264-10D- α except *sae2Δ::hphNT*) and AMA213 (isogenic to RM26-26C-A except *sae2Δ::hphNT*). AMA210 and AMA213 were then crossed with the isogenic K264-10D and RM26-26C derivative *rfa2* mutant strains to generate a diploid that was sporulated, dissected, then genotyped by replica plating and PCR of the *RFA2* locus to obtain double mutants of both mating types in both haploid strain backgrounds.

Haploids were crossed to create the diploid strains (Table 4.1; Appendix B). JSJ1 derivative diploids were determined to be diploid by their ability to sporulate and inability to mate with B9Ba/ α determined by replica plating to SD-Ura media. RM96 derivative diploids were selected for on SD-His because of genetic complementation of *his* gene mutations in the crossed haploid strains. SJH2-1 derivative diploids were selected for by replica plating mated patches to SD-Leu and then struck out for isolated colonies on SD-Lys, because only the diploid will be able to grow on both types of media. Allelism testers were generated by dissecting SJH2-390T and replica plating to determine spore alleles.

Table 4.1. Diploid yeast strains

Strain	Cross	Relevant Genotype
JSJ1 ^a	JKM139 x JKM179	WT, <i>RFA2/RFA2</i>
AMA293	AWY194 x AWY092	Isogenic to JSJ1, except <i>rfa2-A_x/rfa2-A_x</i>
AMA295	AWY016 x AWY096	Isogenic to JSJ1, except <i>rfa2-D_x/rfa2-D_x</i>
AMA297	AMA147 x AWY097	Isogenic to JSJ1, except <i>rfa2-ΔN_x/rfa2-ΔN_x</i>
RM96	K264-10D x RM26/26C	WT, <i>RFA2/RFA2</i>
AMA118	TMW307 x TMW302	Isogenic to RM96, except <i>rfa2-A_x/rfa2-A_x</i>
AMA206	AMA122 x AMA141	Isogenic to RM96, except <i>rfa2-D_x/rfa2-D_x</i>
AMA120	TMW309 x TMW304	Isogenic to RM96, except <i>rfa2-ΔN_x/rfa2-ΔN_x</i>
AMA172	AMA145 x AMA149	Isogenic to RM96, except <i>spo11Δ::kanMX</i>
AMA299	AMA202 x AMA233	Isogenic to AMA172, except <i>rfa2-A_x/rfa2-A_x</i>
AMA300	AMA243 x AMA222	Isogenic to AMA172, except <i>rfa2-D_x/rfa2-D_x</i>
AMA301	AMA205 x AMA242	Isogenic to AMA172, except <i>rfa2-ΔN_x/rfa2-ΔN_x</i>
AMA176	AMA154 x AMA152	Isogenic to RM96, except <i>sae2Δ::hphNT</i>
AMA302	AMA227 x AMA231	Isogenic to AMA176, except <i>rfa2-A_x/rfa2-A_x</i>
AMA303	AMA228 x AMA237	Isogenic to AMA176, except <i>rfa2-D_x/rfa2-D_x</i>
AMA304	AMA229 x AMA224	Isogenic to AMA176, except <i>rfa2-ΔN_x/rfa2-ΔN_x</i>
AMA180	AMA161 x AMA168	Isogenic to RM96, except <i>dmc1Δ::hphNT</i>
AMA244	AMA193 x AMA188	Isogenic to AMA180, except <i>rfa2-A_x/rfa2-A_x</i>
AMA245	AMA240 x AMA190	Isogenic to AMA180, except <i>rfa2-D_x/rfa2-D_x</i>
AMA246	AMA217 x AMA216	Isogenic to AMA180, except <i>rfa2-ΔN_x/rfa2-ΔN_x</i>
AMA184	AMA167 x AMA165	Isogenic to RM96, except <i>ndt80Δ::natMX</i>
AMA247	AMA196 x AMA218	Isogenic to AMA184, except <i>rfa2-A_x/rfa2-A_x</i>
AMA248	AMA199 x AMA192	Isogenic to AMA184, except <i>rfa2-D_x/rfa2-D_x</i>
AMA249	AMA201 x AMA220	Isogenic to AMA184, except <i>rfa2-ΔN_x/rfa2-ΔN_x</i>
SJH2-390T ^b	B9B-A x M2034α	<i>HIS2/his2-390 ura1/URA1</i>
SJH2-1	RM96-15A-0C1 x RM182-55C-C1	WT, <i>his2-390, Δc/his2-Δc RFA2/RFA2</i>
AMA129	CMK001 x AMA126	Isogenic to SJH2-1, except <i>rfa2-A_x/rfa2-A_x</i>
AMA131	CMK003 x AMA124	Isogenic to SJH2-1, except <i>rfa2-D_x/rfa2-D_x</i>
AMA116	CMK005 x CMK011	Isogenic to SJH2-1, except <i>rfa2-ΔN_x/rfa2-ΔN_x</i>

^a This cross was originally made in (Sollier et al. 2004). ^b This cross dissected to generate the haploid strains to use as *his2* allelism testers.

Vegetative growth and sporulation

Temperature sensitive RM182-55C-C1 derivatives and spores dissected from RM182-55C-C1 derivative crosses were grown at 24°C. All other strains were grown and/or sporulated at 30°C. Mitotic growth utilized rich media, YPD (Appendix F). Sporulation on plates utilized SPO media (Appendix F). Cells were sporulated for 3, 4, or 7 days. Sporulation efficiency was calculated as the addition of tetrads and dyads observed divided by the total number of cells. To determine spore viability, cells from SPO plates were suspended in either ddH₂O or 1M sorbitol and subjected to zymolyase treatment, followed by tetrad dissection on YPD. The ratio of viable: inviable spores for each tetrad was recorded. Spore viability was calculated by the number of viable spores divided by the total number of spores. Liquid sporulation was performed as follows: diploids grown in YPD to oversaturation were used to inoculate YPA (Appendix F) at 1.0 OD₆₀₀ and grown overnight (16-20 hours). Cells were spun down, washed once in liquid sporulation media, CL-SPM (0.3% potassium acetate, 0.02% raffinose; Appendix F; Cartagena-Lirola *et al.* 2008.), then resuspended in liquid sporulation media. Cells were collected at timepoints indicated for various meiotic assays (western blotting, DNA content analysis, and nuclear division analysis) described below.

Checkpoint adaptation assay

The yeast strains, JKM179 and JKM139, were designed to make an irreparable break at the *MAT* locus when HO endonuclease expression is induced by galactose. These strains and derivatives of these strains provide for a way to study G₂/M checkpoint exit by adaptation as described previously (Lee et al. 1998). JKM139 derivatives and JSJ1 derivatives (JKM139 x JKM179) were grown at least 14 hours overnight in liquid YP+Raf (1% yeast extract, 2% peptone, 2% raffinose; Appendix F) to reach 0.6-1.0 OD₆₀₀ before inducing expression of HO by

adding galactose [2%]. 8 hours after galactose induction, 0.025 OD₆₀₀ equivalents of cells were sonicated and plated to YP+Raf+Gal plates (1% yeast extract, 2% peptone, 2% raffinose, 2% galactose, 2% agar; Appendix F). After spreading, cells were counted to determine the percentage of cells arrested at the G₂/M checkpoint, appearing as two joined cells (a large-budded cell) by microscopic examination. Cells were counted again at 24 hours and 48 hours after galactose induction to determine the percentage of adapting cells, which appear as any cell cluster with 3 or more cells per cluster. Cells were collected from liquid YP+Raf+Gal cultures at the timepoints indicated for western blotting.

Western blotting for analysis of Rad53 protein and Rfa2 protein

Cell samples collected at 10 OD₆₀₀ equivalents from liquid sporulation and liquid checkpoint adaptation time courses for use in western blotting were extracted with trichloroacetic acid, precipitated by acetone washes, and resuspended in 1X Laemmli buffer (Cold Spring Harbor).

To detect Rad53 protein, protein was separated on 6% resolving (37.5:1 mono:bis) with 4% stacking (37.5:1) SDS-polyacrylamide gel by electrophoresis in 1X SDS buffer and transferred to a nitrocellulose membrane at 0.04 Amp constant current for 16 hours overnight in transfer buffer (Appendix F). Membranes were Ponceau stained (0.5% Ponceau S, 5% acetic acid) and de-stained (1% acetic acid) to check for even loading. Membranes were blocked for 2 hrs with TBST buffer + 5 mM sodium fluoride + 1% bovine serum albumin (Appendix F). Primary anti-Rad53 antibody (Abcam ab104232) was used at 1:6000 in TBST buffer + 5mM sodium fluoride + 0.5% nonfat dry skim milk powder + 0.5% bovine serum albumin at 4°C for approximately 16 hrs overnight on a platform shaker. Secondary goat-anti-rabbit IgG-HRP

antibody (Bethyl A120-101P) was used at 1:40000 in TBST buffer + 5mM sodium fluoride + 0.2% nonfat dry skim milk powder and incubated for 2 hrs at room temperature.

To detect Rfa2 protein, protein was separated on a 15% (29:1) resolving, 4% (37.5:1) stacking SDS-polyacrylamide gel by electrophoresis in 1X SDS buffer (Appendix F) and transferred to a nitrocellulose membrane at 0.04 Amp constant current for 16 hours overnight in transfer buffer (Appendix F). Membranes were Ponceau stained (0.5% Ponceau S, 5% acetic acid) and de-stained (1% acetic acid) to check for even loading. Membranes were blocked for 2 hrs with TBST buffer + 5 mM sodium fluoride + 1% bovine serum albumin (Appendix F). Primary anti-Rfa2 antibody was provided by Steven Brill and used at 1:40000 in TBST buffer + 5mM sodium fluoride + 0.5% nonfat dry skim milk powder + 0.5% bovine serum albumin at 4°C for approximately 16 hrs overnight on a platform shaker. Secondary goat-anti-rabbit IgG-HRP antibody (Bethyl A120-101P) was used at 1:40000 in TBST buffer + 5mM sodium fluoride + 0.2% nonfat dry skim milk powder and incubated for 2 hrs at room temperature.

1X TBST + 5mM sodium fluoride was used for all washes (Appendix F). Western blots were developed using the PierceTM ECL 2 western blotting kit (Thermo Scientific) or the SuperSignalTM West Pico Plus Chemiluminescent substrate kit (Thermo Scientific). Images were obtained by either: the NDSU Core Facility image systems: Storm 865 (GE Healthcare) or iBright FL1500 (Invitrogen), or the Wilkinson laboratory myECLTM (Thermo Scientific) imager and myImageAnalysisTM software (Thermo Scientific)..

Specific details for each western blot are provided in the figure legend of the results section.

DNA damage spot assay

Haploids derived from K264-10D, RM26-26C, RM96-15A-0C1, and RM182-55C-C1 and isogenic derivations from diploids SJH2-1 and RM96 were grown overnight to oversaturation in liquid YPD at 30°C or 24°C for temperature sensitive strains. Cells were initially diluted to 1.0 OD₆₀₀ (approximately 1.0 X 10⁷ cells/mL) and five 1:10 serial dilutions were made. 5 µL of each dilution was spotted on YPD plate media or YPD plate media containing genotoxic agents at various concentrations with the highest concentration of cells on the left (1.0 OD₆₀₀) and lowest concentration on the right (1.0 X 10⁻⁵ OD₆₀₀). Plates were incubated for 2 days at 30°C for plates containing non-temperature sensitive strains and 24°C for plates containing temperature sensitive strains; pictures were taken.

Analysis of qualitative heteroallelic recombination and chromosome segregation by replica plating

RM96 derivative diploids were patched onto a master plate and replica plated to the following types of media to visually assess heteroallelic recombination both mitotically and meiotically (after diploid sporulation on SPO): SD-His, SD-Leu, SD-Lys, and SD-Trp. SD-His is a diploid control. Heteroallelic recombination at the *LEU1*, *LYS2*, and *TRP5* loci were assessed by colony growth on the respective SD-Leu, SD-Lys, and SD-Trp plates.

Chromosome segregation of diploids was performed initially to indirectly measure proper recombination of both mitotic and meiotic cells by analyzing the diploid's heterozygous *CAN1*^S and *CYH2*^S alleles by replica plating to: SD+Can, SD+Cyh, SD+Can+Cyh. Mitotic diploids should be sensitive to both canavanine and cycloheximide whereas if chromosome segregation is occurring properly during meiosis, approximately half of spores

should be able to grow on canavanine or cycloheximide. Replica plates were incubated for 4 days at 30°C. Images were captured via digital camera.

Analysis of heteroallelic recombination frequency

For mitotic determination of heteroallelic recombination frequency, RM96 derivative diploids were grown overnight in YPD to saturation. Cells were diluted 1:10 in 1X PBS before counting via a cellometer (Nexcelom). Serial dilutions were made for spreading cells to determine the actual number of cells plated (SD+Com), and to determine number of recombinants at the *LEU1* and *TRP5* loci (SD-Leu and SD-Trp).

After testing liquid spo medias (Appendix I: Table I1), SM media (2% potassium acetate, 10 µg/mL adenine, 5 µg/mL histidine, 30 µg/mL leucine, 7.5 µg/mL lysine, 10 µg/mL tryptophan, 5 µg/mL uracil; Appendix F; (Schindler et al. 2003) was chosen for sporulating RM96 derivative diploids for determining the meiotic heteroallelic recombination frequency.

For meiotic heteroallelic recombination, RM96 derivatives were grown to saturation in YPD to use for inoculating YPA at 1.0 OD₆₀₀ equivalents and grown for 20 hours before washing and resuspending in the liquid sporulation media, SM. RM96 derivatives were grown in SM for 45 hours before diluting cultures 1:10 in 1X PBS and counting via a cellometer (Nexcelom) for meiotic plate spreads. Cells were also counted by light microscopy to determine the sporulation percentage of these strains, which is usually higher than the sporulation of these strains on solid SPO media (Appendix I: Table I2). Similar to how mitotic cells were plated, serial dilutions for meiotic cells were made and spread to SD+Com, SD-Leu, and SD-Trp. For both mitotic and meiotic heteroallelic recombination the number of colonies on SD-Leu and SD-Trp plates were counted and divided by the number of colonies plated (from SD+Com

plates) to use to determine the average heteroallelic recombination frequency at the *LEU1* and *TRP5* loci. Average overall frequency was calculated by combining data from both loci.

DNA content analysis

For analysis of DNA content, 1.0 OD₆₀₀ of SJH2-1 derivative cells were collected at timepoints indicated from sporulating cells and fixed with 70% methanol. Cells were stored at 4°C until ready for staining. Cells were pelleted and resuspended in 1X PBS and incubated 1 hour at room temperature. Cells were treated with RNaseA (0.25 mg/mL) for 4 hours at 37°C, followed by Proteinase K (0.25 mg/mL) treatment for 16 hours overnight at 50°C. Cells were stained with 5 µM SYTOX green (Invitrogen) and incubated for 2 hours at room temperature in the dark. Stained cells were sonicated and then analyzed by flow cytometry using a BD Accuri C6 system provided by the NDSU Core Facility. 200,000 ungated events were recorded. DNA content histograms were generated using FlowJo software.

Nuclear division analysis

For analysis of meiotic nuclear divisions, 900 µL of each SJH2-1 derivative was collected at timepoints indicated from sporulating cells and fixed with formaldehyde [3.7%]. When ready for staining, cells were washed twice in 1X PBS, incubated in 70% ethanol for 1 hour, washed in 1X PBS, sonicated, and stained with 4',6'-diamidino-2-phenylindole (DAPI) at 0.05 µg/mL. DAPI-stained cells were placed on a microscope slide and sealed using a coverslip and clear nail polish. Pictures were taken using a fluorescent microscope provided by the NDSU Core Facility. At least 500 cells were analyzed for nuclear divisions at each timepoint for each mutant. Analysis was repeated on a second, separate time course collection. Averages and standard deviation between the two experiments was calculated.

Tetrad analysis by dissection and replica plating

SJH2-1 derivative diploids were sporulated for 3-4 days at 24°C, due to temperature sensitive mutations. Asci were dissected on YPD and isolated spores incubated at 24°C. Tetrads with 4 viable spores were patched onto a YPD master plate. Master plates were replica plated to SD-Leu, SD-Lys, SD-Trp, SD-Arg+Can, YP+glycerol, SD-Ura, SD-His. Patch growth was recorded. To test for recombination at the *HIS2* recombination hotspot, haploid master plates were mated with allelism testers on YPD, replica plated to select for diploids on SD-Ura, then new master plates were picked to SD-Ura. Diploids (allelism tester crossed with haploids from dissection) were sporulated for 3 days on sporulation media lacking uracil and were replica plated to SD-His. This allows the original haploids from SJH2-1 dissection that contained only *his2-ΔC* to have meiotic recombination occur with the *his2-390* of the allelism tester, which may generate *HIS2* allowing for microcolony growth when replica plated to SD-His media. Tetrads exhibiting gene conversions for more than two markers outside of the *HIS2* locus were considered false and were discounted. To test for crossing over in the *CLY3-CDC14* interval of chromosome VI, the *cdc14^{ts}* and *cly3^{ts}* temperature sensitive markers were used to score growth of dissected spore YPD master plates at 37 °C. Tetrads exhibiting gene conversion (more than 2 spores grow at 37 °C) in the *CLY3-CDC14* interval were excluded. The ratio of spores that grew to spores that didn't grow for each tetrad type are: parental ditypes= 2:2, tetratypes= 1:3, and non-parental ditypes= 0:4. Genetic distances were determined using the Perkins equation: $cM = 100 * (TT + 6NPD) / (2 (PD + TT + NPD))$ where PD= parental ditype, TT= tetratype, NPD= non-parental ditype. Standard errors of genetic distance were calculated using Stahl's Online Tools (<http://elizabethhousworth.com/StahlLabOnlineTools/compare2.php>).

Results

Confirmation of yeast haploid strains

Shown is the one-step gene replacement technique used to generate *sae2Δ::hphNT*, *dmc1Δ::hphNT*, *spo11Δ::kanMX*, and *ndt80Δ::natMX* (Figure 4.1). The predicted product sizes generated by PCR used to confirm the gene deletions are listed (Figure 4.1). An example for results of the verification PCR performed for *sae2Δ::hphNT* candidates shows no PCR products are obtained when the wild-type *SAE2* gene is present while candidates that have the predicted fragment sizes confirm that *hphNT* is correctly integrated (Figure 4.2). An example for results of the verification PCR performed for *dmc1Δ::hphNT* and *ndt80Δ::natMX* shows confirmed candidates have the predicted fragment sizes corresponding to the deletion::insertion and do not show the predicted fragment size generated by the wild-type gene presence (Figure 4.3). For an example of *spo11Δ::kanMX* candidate confirmation, see Chapter 2.

The two-step gene replacement technique used to generate the *rfa2* mutants is shown in Figure 4.4. An example for the verification PCR results for *rfa2* mutants generated by two-step gene replacement shows the predicted fragment sizes (Figure 4.5). The Rfa2 phospho-mutations (*rfa2-A_x* and *rfa2-D_x*) generate smaller PCR fragments than the wild-type strain due to using the *RFA2* cDNA sequence rather than the genomic sequence for generating the mutated forms of *rfa2* (intron is absent in the mutant version; Figure 4.5) (Ghospurkar et al. 2015b). Pop-in controls are amplified to show PCR products of both the wild-type *RFA2* and the mutant *rfa2* genes, when cells are plated to SD-Ura media to select for cells that have completed the first step of the two-step gene replacement method (Figure 4.4, 4.5).

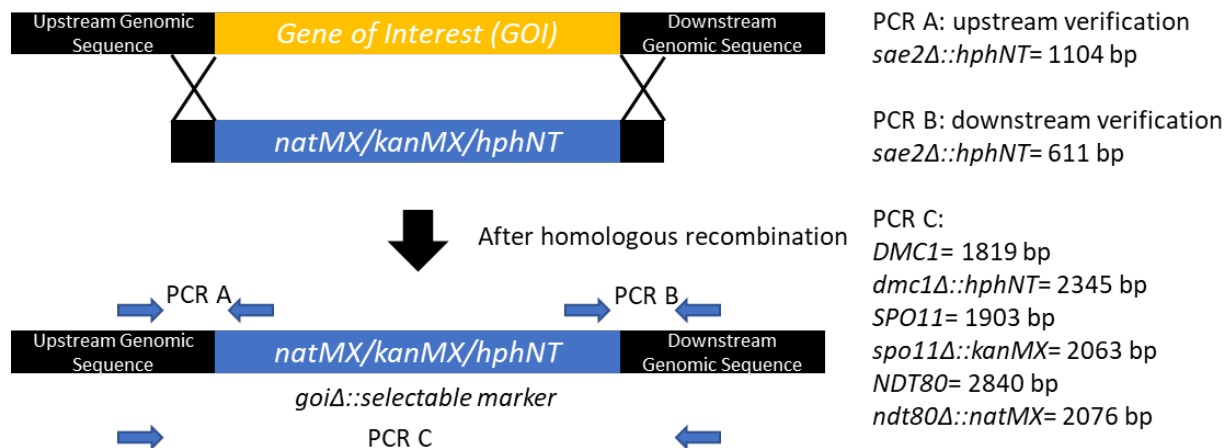


Figure 4.1. One-step gene replacement technique with verification PCR product sizes
A schematic representation of the one-step gene replacement technique. A selectable marker (resistance cassette) is amplified by PCR to contain homologous sequence upstream and downstream of the *GOI* (gene of interest) to be replaced through homologous recombination. Predicted product sizes are listed for gene deletions performed in this chapter, predicted product sizes were obtained using the freeware Serial Cloner. Note: PCR A and B will not produce a product if wild-type *SAE2* is present.

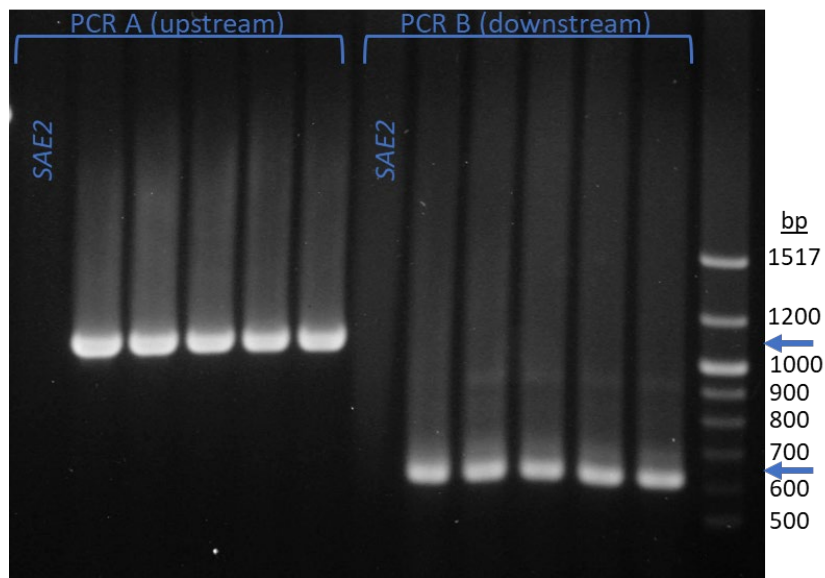
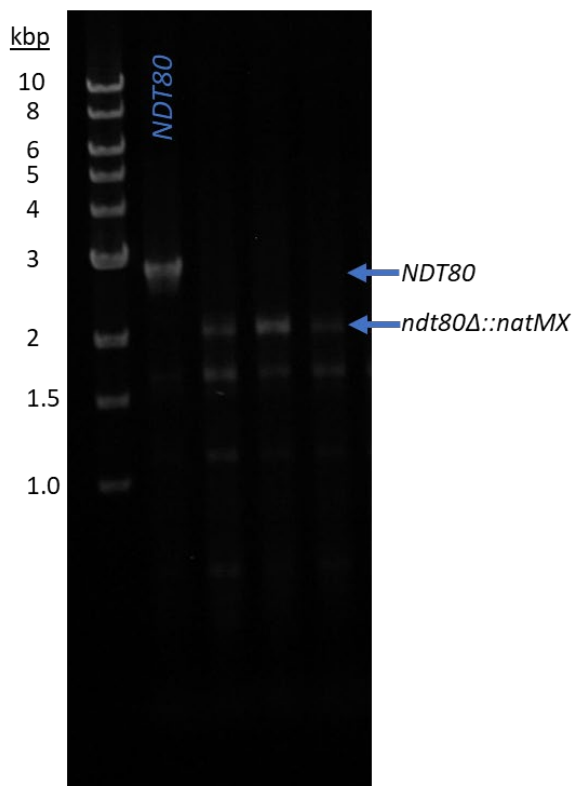


Figure 4.2. Example of *sae2Δ::hphNT* verification PCR
Shown is an example of how *sae2Δ::hphNT* candidates were confirmed by the PCR product sizes given in Figure 4.1 for PCR A (upstream) and PCR B (downstream) verification (indicated by arrows). A wild-type strain (*SAE2*) was used as a control to show no PCR product is formed in the absence of the correctly integrated *hphNT* insertion. The DNA ladder fragment sizes are labeled.

A



B

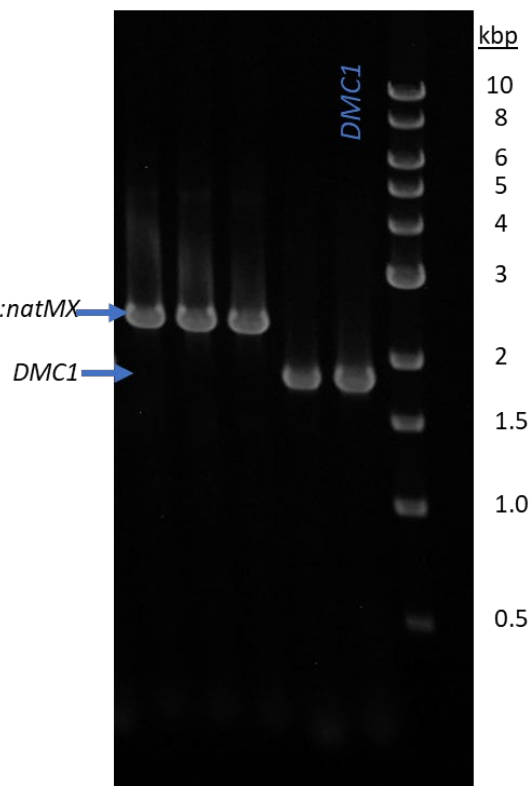


Figure 4.3. Example of *dmc1Δ::hphNT* and *ndt80Δ::natMX* verification PCR

Shown is an example of how *dmc1Δ::hphNT* and *ndt80Δ::natMX* candidates were confirmed by the PCR product sizes given in Figure 4.1 for PCR C (predicted sizes indicated by arrows). A wild-type strain (*NDT80*, *DMC1*) was used as a negative control.

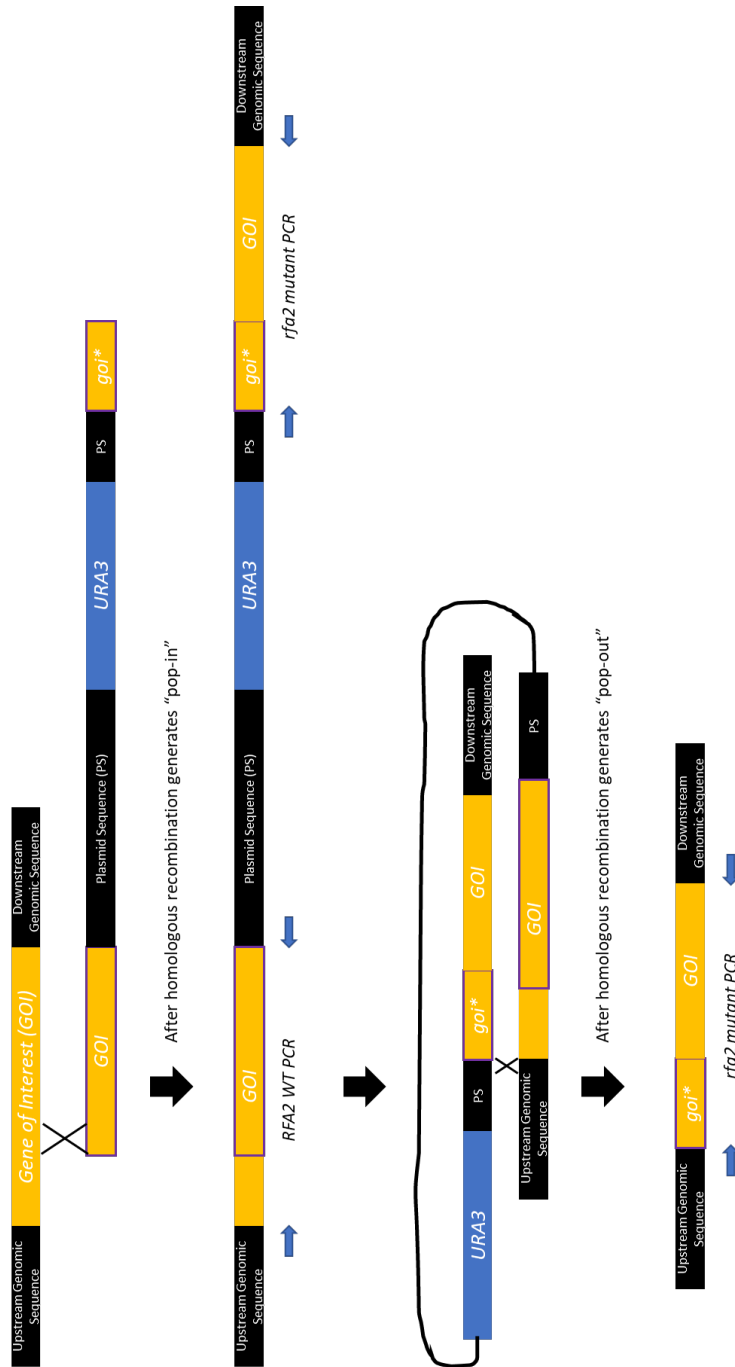


Figure 4.4. Two-step gene replacement technique

A schematic representation of the two-step gene replacement technique. The integrating pRS306-*rfa2* mutant vectors were linearized with *Sna*BI to promote the first homologous recombination (HR) event. After the first HR event integrates the linearized plasmid into the genome, the “pop-in” will generate two fragments when outer *RFA2* locus primers are used. (Note: Plasmid Sequence (PS) also contains upstream and downstream genomic sequence) After a second HR event occurs on the opposite side of the first event (as drawn), the mutation is integrated into the genome and the “pop-out” generated is the *URA3* gene, the wild-type *RFA2* sequence, and the PS. See legend for Figure 4.5 for predicted product sizes.

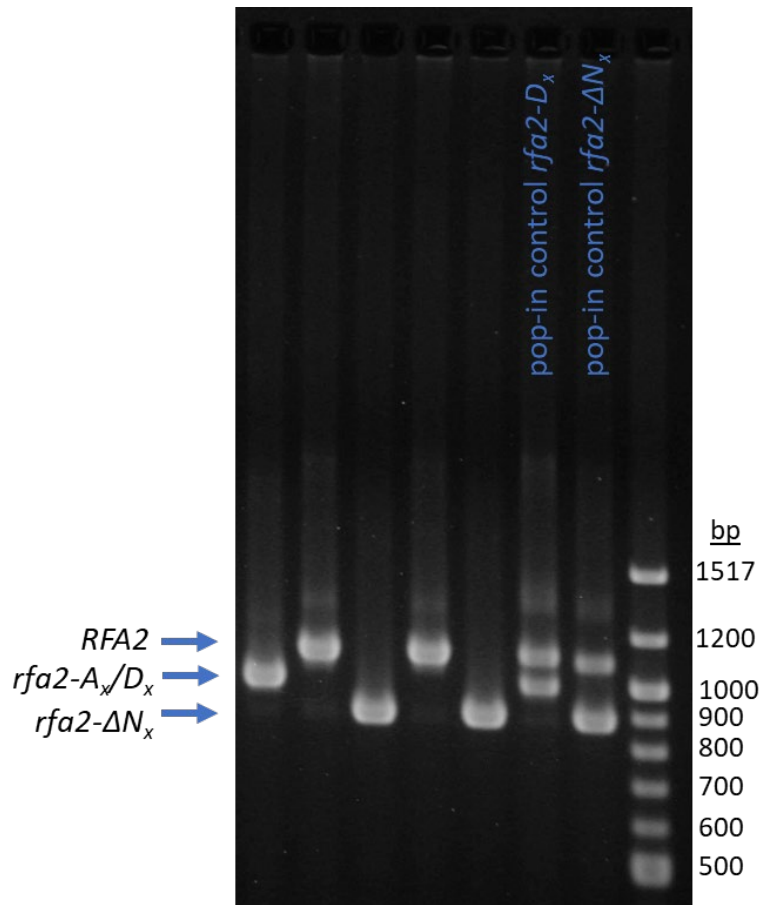


Figure 4.5. Example of *rfa2* mutant verification

DNA fragments separated on a 1.5% agarose TAE gel. DNA ladder fragment sizes are labeled. Indicated by arrows are the approximate sizes of the PCR products produced. Predicted fragment sizes generated using Serial Cloner: *RFA2* = 1106 bp, *rfa2-A_x/D_x* = 998 bp, *rfa2-ΔN_x* = 884 bp. Controls used were pop-in candidates for *rfa2-D_x* and *rfa2-ΔN_x*. Pop-ins contain both wild-type *RFA2* and the *rfa2* mutation alleles, observed by the presence of two fragments on the gel, see Figure 4.4.

Rfa2 NT mutants have a more pronounced effect in checkpoint adaptation measured in diploid cells

Checkpoint adaptation is a mechanism suggested to be used by cells in order to survive in the presence of unrepaired DNA damage (Galgoczy and Toczyski 2001). To study checkpoint adaptation, first the checkpoint must be established. In JKM179 and JKM139 derivative strains this occurs by galactose induction of a non-repairable double-stranded DNA break, causing cells to halt the cell cycle and arrest at G₂/M (Lee et al. 1998). In yeast, establishment of the G₂/M

checkpoint is observable by cell morphology (the presence of a large, budded cell; cells at the G₂/M checkpoint appear as a connected pair under the microscope) and by activation of the checkpoint kinase Rad53 by phosphorylation (Lee et al. 1998, Pelliccioli et al. 2001). Exiting the checkpoint leads to the formation of cell clusters (3 or more cells) and a reduction in Rad53 phosphorylation (Lee et al. 1998, Pelliccioli et al. 2001). Checkpoint adaptation has occurred when cells exit the checkpoint with persistent DNA damage.

The Rfa2 N-terminal (NT) extensive mutant strains were generated to change the serine and threonine residues (from aa 3-34) to either: aspartic acids to mimic Rfa2 phosphorylation (*rfa2-D_x*), alanines to have a non-phosphorylatable N-terminus (*rfa2-A_x*), or the residues were removed in the NT deletion of aa 3-37 (*rfa2-ΔN_x*). The Rfa2 NT mutations have been investigated in previous checkpoint adaptation studies. Previously, when plasmid-based *rfa2* mutations were studied in a haploid JKM179 derivative strain, *rfa2-D_x* was shown to increase adaptation while *rfa2-A_x* was shown to decrease adaptation in which the increase/decrease was more apparent in an adaptation-deficient strain background (Ghospurkar et al. 2015b). Additionally, the JKM179 derivative strain containing the plasmid based Rfa2 NT deletion, *rfa2-ΔN_x*, also leads to a decrease in adaptation that is further reduced from that observed of *rfa2-A_x* mutants, again the *rfa2-ΔN_x* strain adaptation-deficiency is enhanced in an adaptation-deficient strain background (Wilson 2018).

Increasing the amount of HO cut sites has been shown to reduce the ability of haploid wild-type cells to adapt, as a haploid with two different irreparable cut sites (one at the *MAT* locus and the other at *URA3*) leads to an accumulation of cells in G₂/M upon induction of HO endonuclease, whereas one site allows for adaptation (Lee et al. 1998). Because of DNA replication, each cut site technically generates two chromatids with a break. Thus, a haploid with

two sites for cleavage would generate 4 broken chromatids; this is the same number of broken chromatids that would be generated in a diploid cell homozygous for one cut site. The JKM139 and JKM179 derivative mutants that contained integrated *rfa2* mutations were crossed to generate homozygous diploids, JSJ1 derivatives (Sollier et al. 2004). The JKM139 derivatives with integrated *rfa2* mutations were used as the haploid comparison. This study is the first to measure checkpoint adaptation in diploid cells. All strains arrested at the G₂/M checkpoint, evident by the high percentages (greater than 80%) of cells arrested with a large bud (or 2 cell cluster) at 8 hours (Figure 4.6A). The wildtype diploid had a lower percentage of clusters with 3 or more cells present at both 24 and 48 hours, 75% and 77% compared to the wildtype haploid at 88% and 89%, respectively (Figure 4.6A). These results suggest that the overall ability of a diploid to adapt is reduced. A similar reduction in adaptation was observed when comparing the *rfa2-A_x* and *rfa2-ΔN_x* diploids to their haploid counterparts. This is consistent with the idea that more irreparable breaks make it harder for the cells to exit the G₂/M checkpoint (Lee et al. 1998). Interestingly, *rfa2-D_x* had a more pronounced effect on adaptation of a diploid, as the percentage of clusters with 3 or more cells present in the diploid was 83% at both 24 and 48 hours, while the JKM139 haploid was 79% at 24 hours and 81% at 48 hours (Figure 4.6A). An additional experimental replicate was excluded from Figure 4.6A, due to the overall severe reduction in adaptation. In the excluded replicate the wild-type diploid adapted at 30% and 37% (Figure 4.7) compared to the consistent replicates' average of 75% and 77% for analyses at 24 and 48 hours, respectively (Figure 4.6A). However, this excluded experiment had adaptation trends of *rfa2* mutants consistent with trends in Figure 4.6A (i.e. *rfa2-A_x* percent adaption is similar to wild-type and *rfa2-ΔN_x* showed the greatest decrease), and the ability of *rfa2-D_x* to increase adaptation

was more pronounced, which is similar to the increased adaptation observed in adaptation-deficient strains containing the *rfa2-D_x* mutation (Ghospurkar et al. 2015b, Wilson 2018).

When the G₂/M checkpoint is established in strains containing the Rfa2 NT extensive mutations, the G₂/M checkpoint kinase Rad53 is activated, observed by the presence of phosphorylated Rad53 (Ghospurkar et al. 2015b). Maximum Rad53 phosphorylation is normally observed around 8 hours (Ghospurkar et al. 2015b), in well-resolved blots it appears as though *rfa2-D_x* mutants never reach maximum Rad53 phosphorylation (Wilson 2018). This has also been observed in other strains containing the *rfa2-D_x* mutation by Trevor Baumgartner and Wendy Larson (unpublished work). Consistent with these observations is the Rad53 phosphorylation observed in the JSJ1 derivative diploids and JKM139 derivative haploids at 8 hours (Figure 4.6B; the non-phosphorylated Rad53 species is shown in the zero hour timepoint). The biochemical observation of reduced Rad53 phosphorylation at 8 hours in *rfa2-D_x* mutants correlates with the physiological observation of a reduced percentage of arrested cells of *rfa2-D_x* mutants when compared to other strains at 8 hours (Figure 4.6). In haploids, an observable reduction of phosphorylated Rad53 normally occurs by ~16-18 hours in wild-type and *rfa2-D_x* mutants, whereas *rfa2-A_x* and *rfa2-ΔN_x* maintain Rad53 phosphorylation (Ghospurkar et al. 2015b, Wilson 2018). The timing of reduced Rad53 phosphorylation is especially evident in adaptation-deficient strains (Ghospurkar et al. 2015b, Wilson 2018). In this study, phosphorylation of Rad53 is barely detectable in *rfa2-D_x* mutants by 24 hours, while wild-type and the non-phosphorylatable *rfa2* mutants (*rfa2-A_x*, *rfa2-ΔN_x*) still display some level of Rad53 phosphorylation (Figure 4.6B). The most Rad53 phosphorylation is observed in the diploid *rfa2-A_x* and *rfa2-ΔN_x* mutants which is consistent with the diploid mutants' reduced adaptation percentages (Figure 4.6).

Rfa2 NT mutants recapitulate mitotic DNA damage sensitivities in meiotic yeast strains

As it appears that the phospho-state of the Rfa2 NT alters the mitotic cell cycle when DNA damage persists, we wanted to investigate if it could have a similar role in the meiotic cell cycle. During meiosis, DNA damage is programmed to occur prior to the MI division, yet Rad53 does not get detectably activated in response to Spo11-induced DNA damage (Cartagena-Lirola et al. 2008). During early meiosis (prior to MI), Rfa2 is phosphorylated by the meiosis-specific kinase, Ime2, with the majority of Rfa2 phosphorylation occurring on Rfa2-S27 (Clifford et al. 2005). Considering these published observations led to the hypothesis that the mechanism promoting adaptation might also be occurring during meiosis to keep Rad53 inactive (i.e., allow for meiotic progression). While the JSJ1 genetic background was necessary to study adaptation of diploid cells, this strain is not typically used for meiotic studies, as to my knowledge, there is only one known publication that has utilized the JSJ1 strain to study meiosis (Sollier et al. 2004). Thus, in addition to the JSJ1 derivative diploids, *rfa2* NT extensive mutants were generated by the two-step gene replacement method in four haploid yeast strains that have been used in prior meiotic studies.

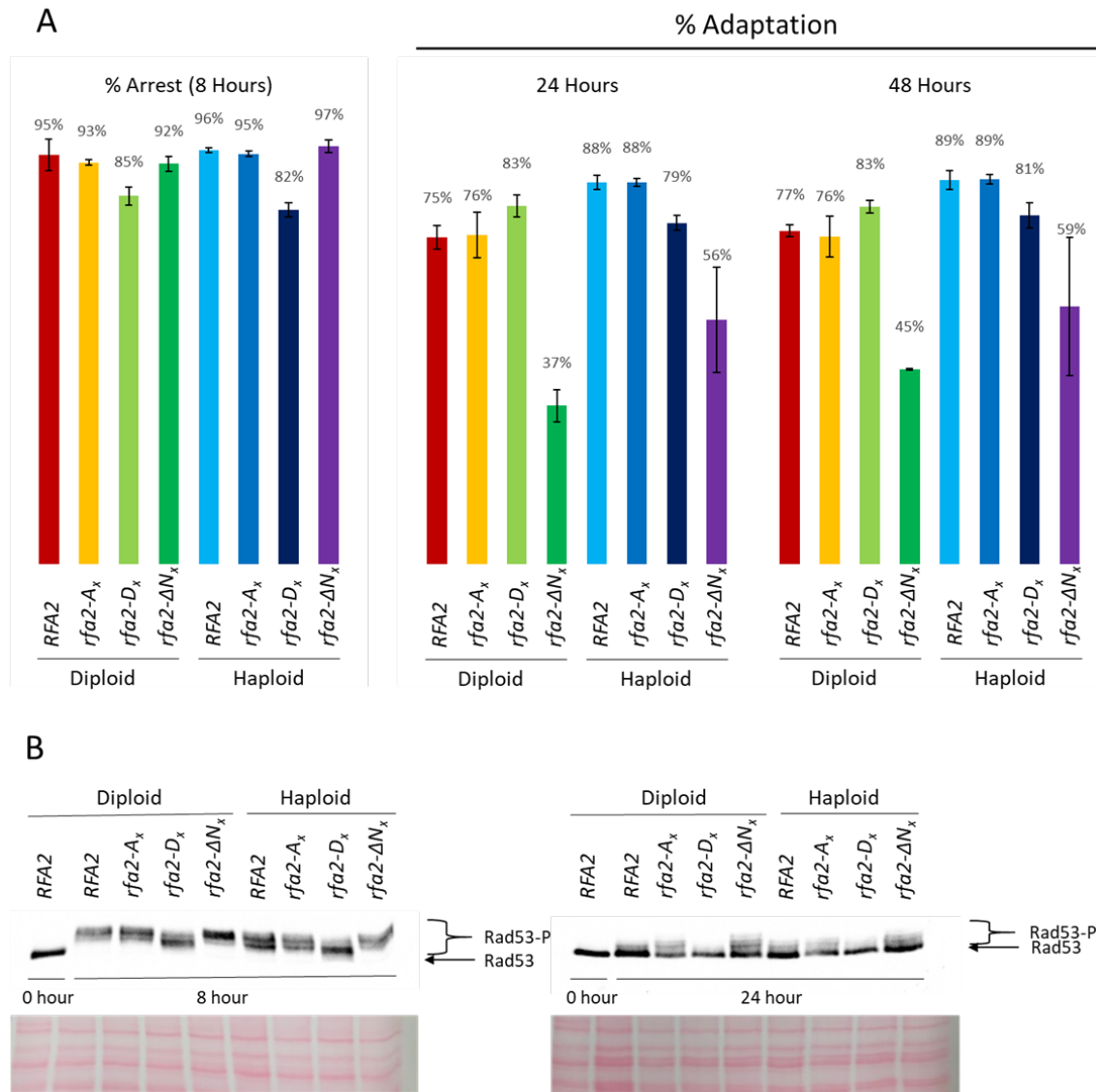


Figure 4.6. The effect *rfa2* NT mutations have on adaptation is more apparent in diploids
 Cell cycle arrest and adaptation was analyzed in diploids (JSJ1 background) and haploids (JKM139 background). (A) Microscopic examination of cell cycle arrest (8 hours post-break induction) and adaptation at 24 and 48 hours. “% Arrest” is the percentage of cells observed arrested as a large-budded cell (two cell cluster). “% Adaptation” is the percentage of cells observed as clusters of 3 or more cells at 24 and 48 hours. Percentages reported are averages from 3 separate experiments, error bars indicate the standard deviation. (B) Western blot analysis of Rad53. Species indicated are unmodified Rad53 (arrow) and phosphorylated Rad53 species (Rad53-P; bracket). Rad53 at zero hours is unmodified. Rad53 detected at 8 hours (left) are Rad53 species observed during arrest and Rad53 detected at 24 hours (right) are Rad53 species observed during adaptation. Ponceau staining was performed to check for even loading and is shown below each blot. Methods specific to these blots: 40µg total protein in 1X Laemmli buffer + 4% β-Me was loaded in each lane. Blots were developed with the SuperSignal™ West Pico Plus Chemiluminescent substrate kit (ThermoScientific) and imaged on the NDSU Core Facility iBright (Invitrogen).

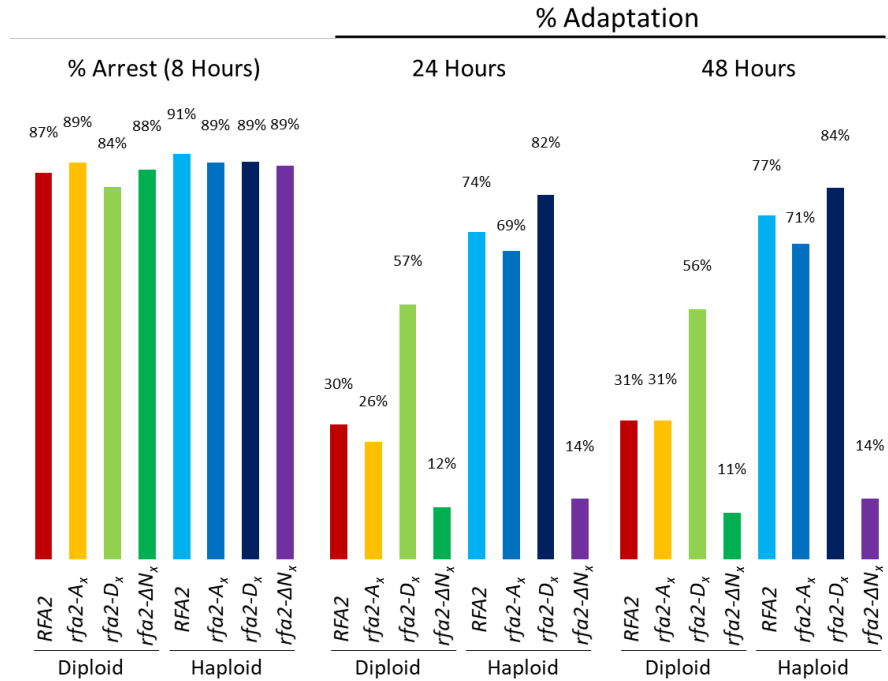


Figure 4.7. In trial with abnormally low adaption, the increase in adaptation in the *rfa2-D_x* diploid is more pronounced

Microscopic examination of cell cycle arrest (8 hours post-induction) and adaptation at 24 and 48 hours. “% Arrest” is the percentage of cells observed arrested as a large-budded cell (two cell cluster). “% Adaptation” is the percentage of cells observed as clusters of 3 or more cells at 24 and 48 hours.

The meiotic *Rfa2* NT extensive mutant haploids (backgrounds: K264-10D, RM26-26D, RM182-55-C1, and RM96-15A-0C1) recapitulate published DNA damage sensitivity phenotypes (Figure 4.8), where *rfa2-D_x* and *rfa2-ΔN_x* mutants are more sensitive to DNA damaging agents observed by a reduction in growth than the *RFA2* wild-type and *rfa2-A_x* mutants (Ghospurkar et al. 2015b). To view the entire range of DNA damaging agents’ concentrations used and replicates performed see Appendix G (Figures G11-G15). Diploids were more resistant to DNA damage observed by increased growth from the haploid counterparts when comparing growth on plates containing the same concentration of DNA damaging agents; diploids are likely more resistant because diploids have double the amount of DNA available to use as a template for repair (Figure 4.8C, Figures G11-G15).

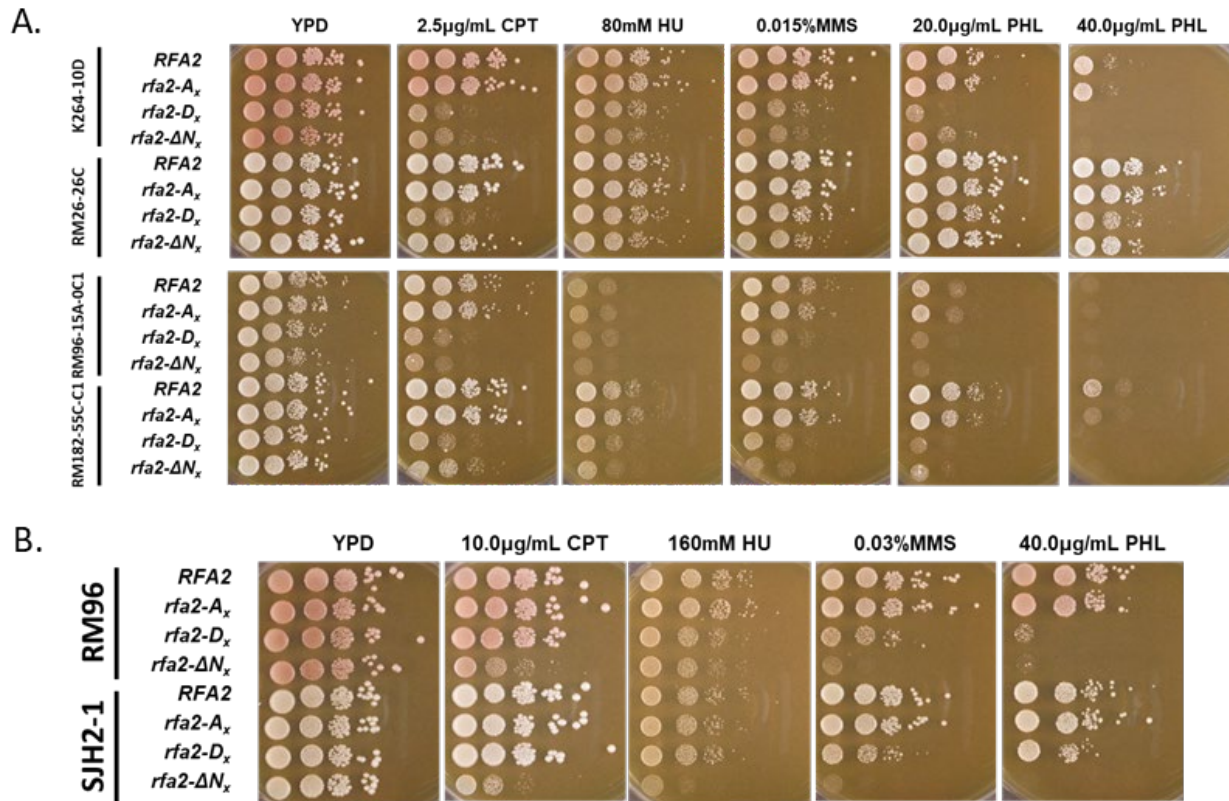


Figure 4.8. Meiotic yeast strains with *rfa2* NT mutations recapitulate prior phenotypes 5 µL of cells from either the initial dilution at 1×10^7 cells/mL (1 OD₆₀₀) or five 1:10 serial dilutions were spotted in decreasing concentration from left to right on YPD media or YPD media containing genotoxic agents (CPT, HU, MMS, PHL, at the labeled concentrations). Plates were incubated for 2 days at 30°C or 24°C if plates contained temperature sensitive strains before imaging growth. (A) DNA damage assay of haploid *rfa2* NT mutants (B) DNA damage assay of diploid *rfa2* NT mutants. (C, next page) Comparison of haploid sensitivity to diploid resistivity on the same concentrations of DNA damaging agents. Additional images are in Appendix G (Figures G11-G15).

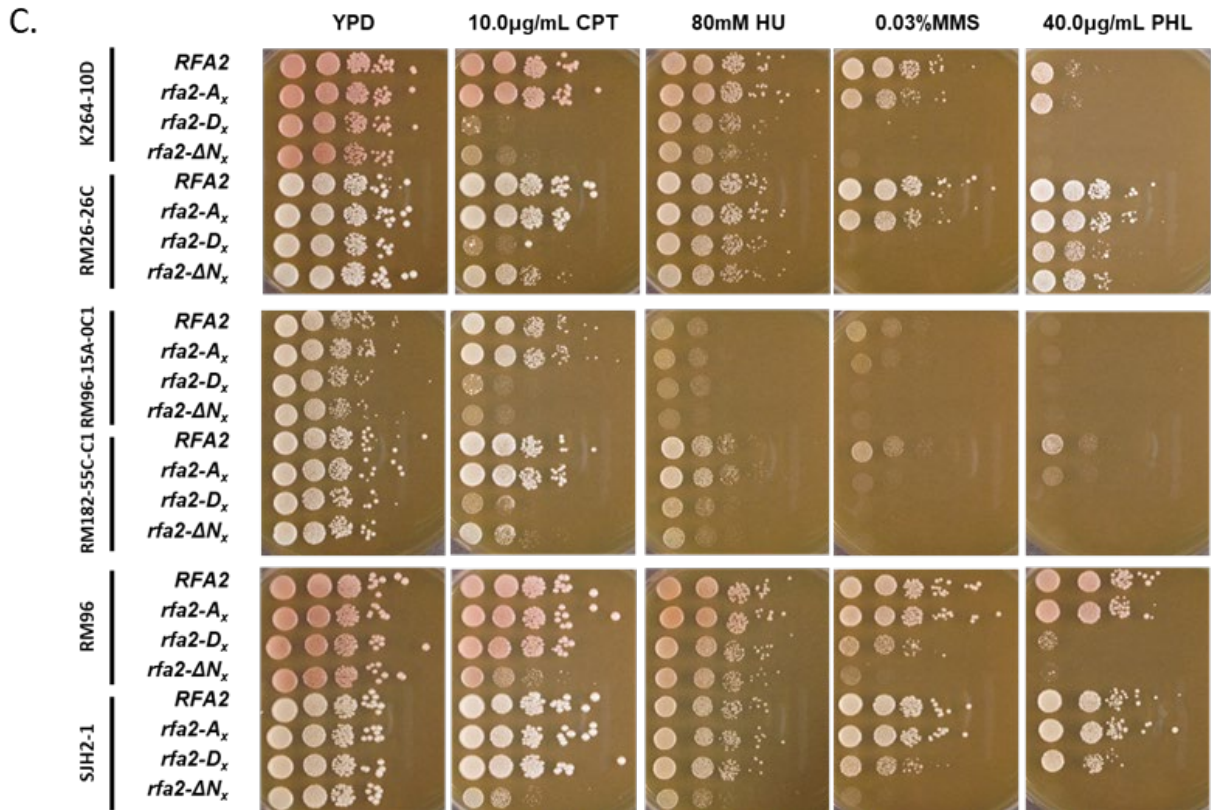


Figure 4.8. Meiotic yeast strains with *rfa2* NT mutations recapitulate prior phenotypes (continued)

5 µL of cells from either the initial dilution at 1×10^7 cells/mL (1 OD₆₀₀) or five 1:10 serial dilutions were spotted in decreasing concentration from left to right on YPD media or YPD media containing genotoxic agents (CPT, HU, MMS, PHL, at the labeled concentrations). Plates were incubated for 2 days at 30°C or 24°C if plates contained temperature sensitive strains before imaging growth. (A, previous page) DNA damage assay of haploid *rfa2* NT mutants (B, previous page) DNA damage assay of diploid *rfa2* NT mutants. (C) Comparison of haploid sensitivity to diploid resistivity on the same concentrations of DNA damaging agents. Additional images are in Appendix G (Figures G11-G15).

Meiotic completion efficiency is mostly independent from the Rfa2 NT phospho-state

First sporulation efficiency and spore viability were measured to test if a constitutively phosphorylated Rfa2 could cause faster progression through the meiotic cell cycle. Since faster progression might cause some induced DNA damage to go unrepaired, a reduction in sporulation and in spore viability might be observed. Diploids were sporulated on SPO plates and cells were counted to determine the number of tetrads, dyads, and vegetative cells. The percentage of

sporulated cells was determined by adding the number of tetrads and dyads counted together and dividing by the total number of cells counted. After sporulation on plate media, tetrads were dissected to determine spore viability. No decrease in sporulation was observed with the two phospho-mutants, as the *rfa2-A_x* and *rfa2-D_x* mutants sporulated at a similar frequency (within 5% difference) to wildtype in three different strain backgrounds (Table 4.2). Viability for strains of the SJH2-1 genetic background was lower than all other backgrounds (81.4% for wild-type, Appendix I: Table I3), this can be attributed to cell resuspension with sterile water rather than 1M sorbitol prior to zymolyase incubation and dissection (Figure 4.9). While no discrepancy in sporulation efficiency exists when comparing each of the three *rfa2-D_x* mutant strains to the respective wild-type strain, there did appear to be a slight reduction in the overall spore viability in all strains (Appendix I: Table I3). A consistent pattern was produced in all three strains when graphing strain viability based on tetrad type viability ratios. The *rfa2-D_x* mutant strains produced fewer tetrads in which all four spores were viable by an approximate reduction of 10-30% (Figure 4.9).

Table 4.2. Sporulation efficiency of Rfa2 NT mutants

Strain	Relevant		# Cells	%	%	%	Tetrad:
Background	Genotype	Days ^a	Examined	Sporulation	Tetrads ^b	Dyads ^b	Dyad
JSJ1	<i>RFA2</i>	4	451	34.4	30.4	4.0	7.6
	<i>rfa2-Ax</i>		450	37.6	31.8	5.8	5.5
	<i>rfa2-Dx</i>		450	33.3	30.4	2.9	10.5
	<i>rfa2-ΔN_x</i>		446	18.4	13.2	5.2	2.5
RM96	<i>RFA2</i>	4	704	39.3	37.4	2.0	18.7
	<i>rfa2-Ax</i>		767	35.5	33.2	2.2	15.1
	<i>rfa2-Dx</i>		679	34.3	31.1	3.2	9.7
	<i>rfa2-ΔN_x</i>		727	35.2	22.3	12.9	1.7
RM96	<i>RFA2</i>	7	729	52.7	47.5	5.2	9.1
	<i>rfa2-Ax</i>		762	53.9	47.2	6.7	7.0
	<i>rfa2-Dx</i>		727	51.4	46.1	5.4	8.5
	<i>rfa2-ΔN_x</i>		702	42.2	27.5	14.7	1.8
SJH2-1	<i>RFA2</i>	4	407	70.0	65.1	4.9	13.3
	<i>rfa2-Ax</i>		404	65.6	62.4	3.2	19.5
	<i>rfa2-Dx</i>		406	71.7	65.3	6.4	10.2
	<i>rfa2-ΔN_x</i>		410	34.4	16.3	18.0	0.9

^a Number of days incubated at 30°C on solid sporulation media. ^b Percent sporulation is categorized into the % Tetrads and % Dyads observed. Percent sporulation was calculated by adding the number of tetrad and dyads observed and dividing by the total number of cells examined. The numbers reported here are totals from the addition of analysis of two or more sporulated patches of cells. Utilizing the numbers obtained from the separate patches, the average % sporulation of cells containing wild-type *RFA2* and *rfa2-ΔN_x* were analyzed for statistical significance in Microsoft Excel by t-test (assuming unequal variances). The t-test resulted in the following P-values(one-tail) = 0.058904 (JSJ1), 0.153354 (RM96, 4 days), 0.03048 (RM96, 7 days), 0.041207 (SJH2-1), when P < 0.05 is needed to be statistically significant.

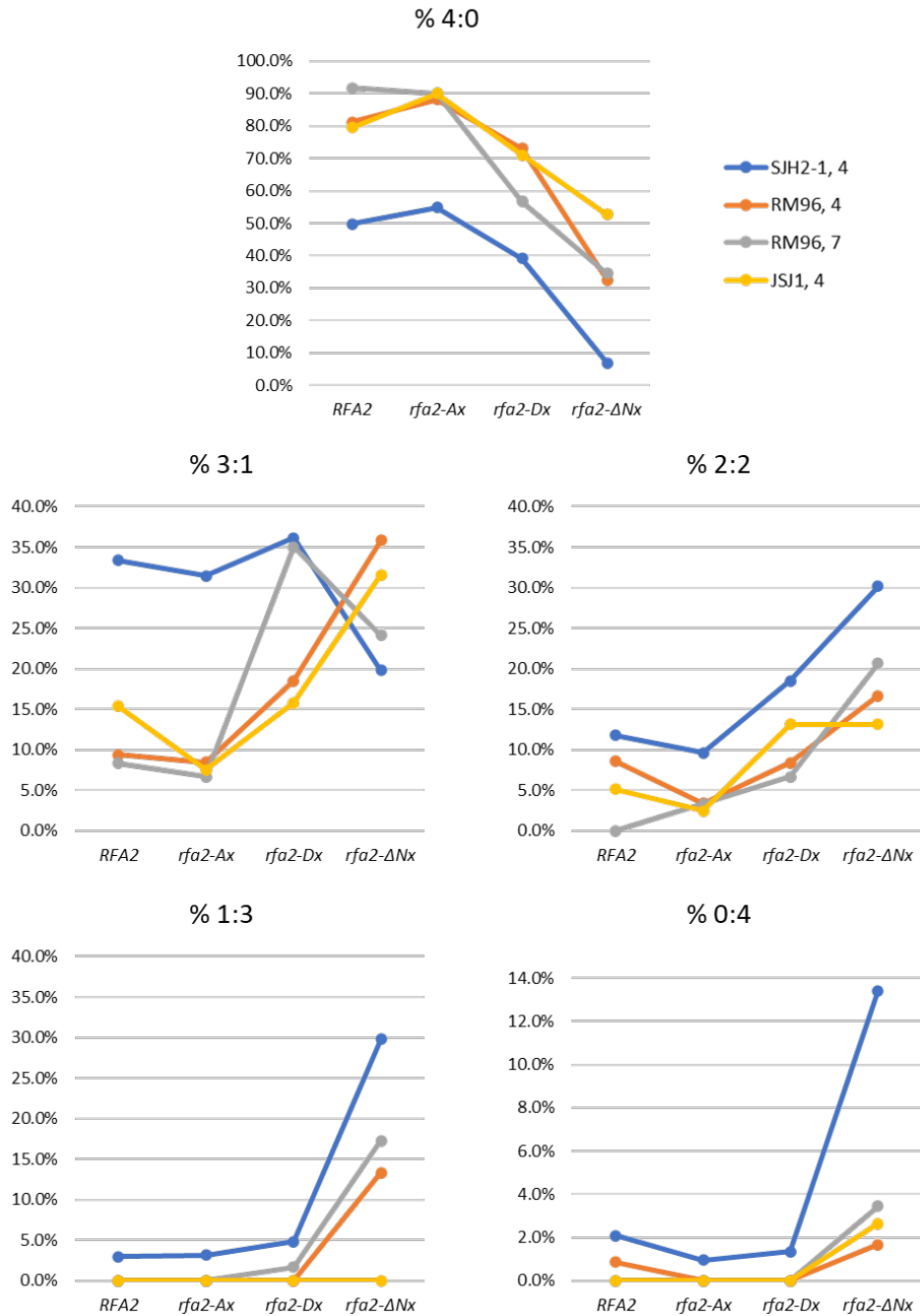


Figure 4.9. Reduction in 4-spore viable tetrads of Rfa2 phospho-mutant and NT deletion
 Spore viability of 3 different diploid strains graphed according to each viable:inviable spores ratio for each tetrad. *RFA2* mutant diploid strains were sporulated on SPO plates for 4 or 7 days, depicted by different colored lines for the “strain, days sporulated”. Tetrads had been resuspended in ddH₂O (SJH2-1 derivatives) or 1M Sorbitol (RM96 and JSJ1 derivatives), incubated with zymolyase, and dissected on YPD. Each viable:inviable spores ratio is shown on a separate graph as the percentage of that type out of all tetrads dissected. The total number of tetrads dissected for each strain/condition and the overall spore viability percentage can be found in Appendix I, Table I3.

Proper progression through meiosis is dependent on the presence of the Rfa2 NT

While the efficiency of meiotic completion appears to be mostly unaffected by the phospho-state of the Rfa2 NT it is affected by the absence of the Rfa2 NT. The largest reduction in sporulation efficiency is observed with the JSJ1 background *rfa2-ΔN_x* mutant (18.4%, wild-type = 34.4%) and the SJH2-1 background *rfa2-ΔN_x* mutant (34.4%, wild-type = 70.0%; Table 4.2). In the RM96 background, the *rfa2-ΔN_x* mutant has a more observable reduction in sporulation efficiency after 7 days (42.2%, wild-type = 52.7%; Table 4.2). As sporulation efficiency is calculated by dividing the sum of tetrads and dyads by the total number of cells counted, a defect in completing both divisions may not be as apparent when analyzing percent sporulation. Instead, the amount of tetrads and dyads present should be considered to assess sporulation completion by comparing the tetrad:dyad ratios (Table 4.2). In all strain backgrounds the amount of dyads was increased in *rfa2-ΔN_x* mutants, which severely reduced the tetrad:dyad ratio (Table 4.2). This was an indication that the Rfa2 NT is needed for efficient completion of meiosis in these strain backgrounds. Additionally, spore viability was reduced in *rfa2-ΔN_x* mutants in all strain backgrounds, and examination of tetrad viability ratios showed the most severe reduction in four-spore viable tetrads (Appendix I: Table I3, Figure 4.9)

To determine if the reduction in spore viability in the *rfa2-D_x* and *rfa2-ΔN_x* mutants could be caused by differences in meiotic progression, SJH2-1 derivatives were examined for the ability to perform pre-meiotic DNA synthesis by DNA content analysis (flow cytometry) and the ability to proceed through meiotic divisions by nuclear division analysis (DAPI staining nuclei). There were no obvious differences in the timing or the amount of completion of pre-meiotic DNA synthesis among all SJH2-1 derivatives (Figure 4.10A; representative figure). In all SJH2-1 derivatives, a population of cells that failed to initiate pre-meiotic DNA synthesis was

observed in every timepoint in both replicates, this may be explained by the overall low sporulation rate (Figure 4.10A, average % sporulation).

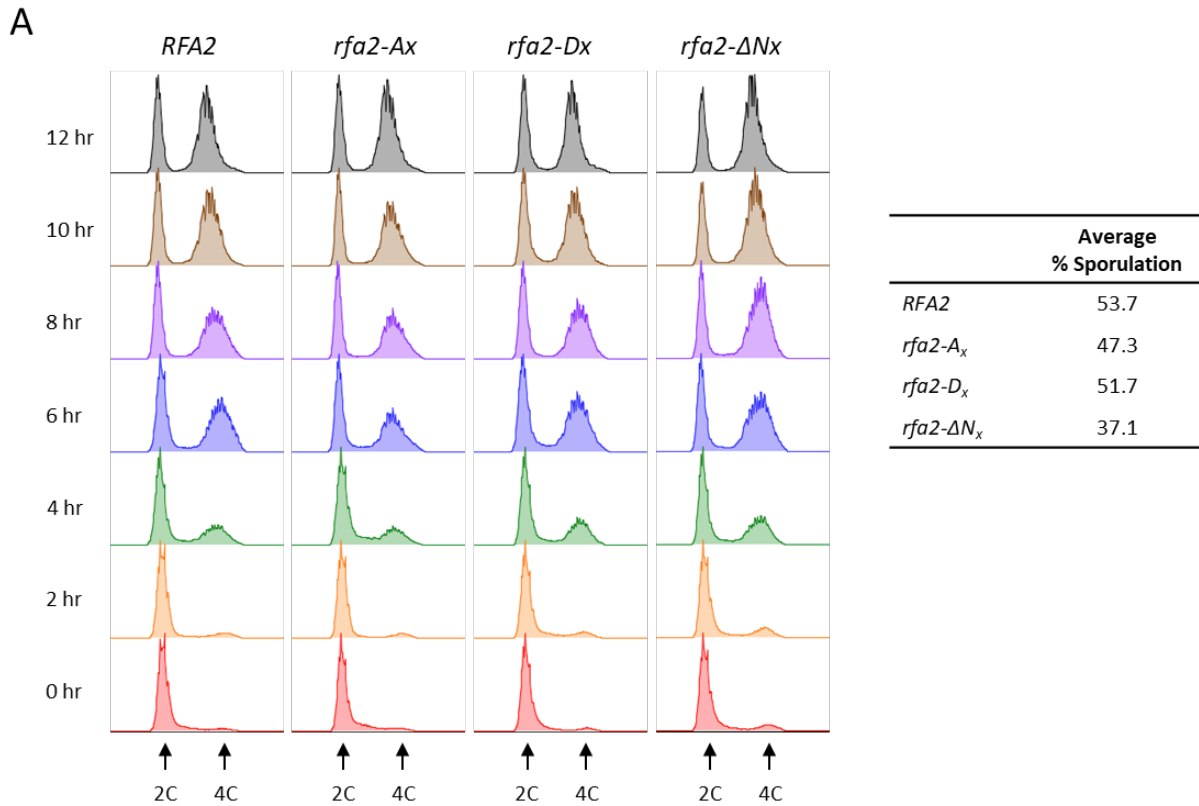


Figure 4.10. Meiotic progression of Rfa2 N-terminal deletion mutant is consistent with sporulation

(A) Representative DNA content analysis of the two trials performed of sporulating SJH2-1 derivative strains analyzed at the timepoints indicated. Prior to meiotic DNA replication, a 2C DNA content is observed, while after a 4C DNA content is observed. Microscopic examination of cell cultures at 24 hours from which the cells analyzed in (A) and (B) were collected allowed for determination of the average percent (%) sporulation of cells at 24 hours, shown with (A). (B, next page) Nuclear division analysis of sporulating SJH2-1 derivative strains. DAPI stained nuclei from each strain (labeled by different colors) were analyzed at the timepoints indicated. Cells with 2 nuclei had completed MI and cells with >2 nuclei had completed MII. Graphed percentages are averages based on two separate analyses. Shown on left is the percentage of cells in each strain that completed both MI and MII divisions (%MI + %MII) Shown on right is the comparison of cells for each strain completing either one (%MI; open circles) or both divisions (%MII; filled squares) at the 24-hour timepoint with standard deviation. Standard deviation for *rfa2-ΔN_x* %MII at 24 hours is +/- 0.1%.

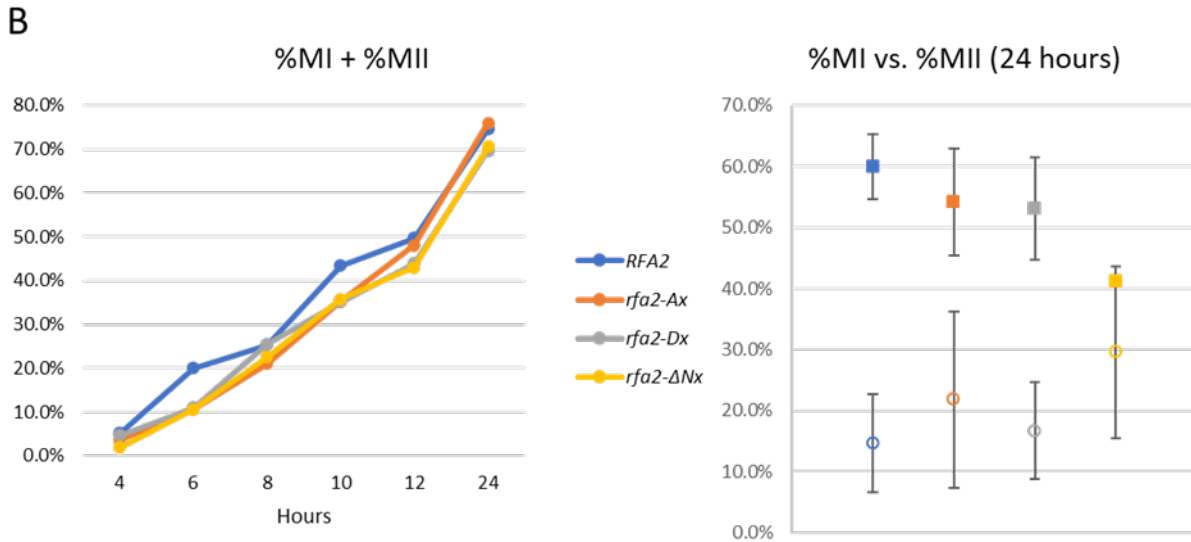


Figure 4.10. Meiotic progression of Rfa2 N-terminal deletion mutant is consistent with sporulation (continued)

(A, previous page) Representative DNA content analysis of the two trials performed of sporulating SJH2-1 derivative strains analyzed at the timepoints indicated. Prior to meiotic DNA replication, a 2C DNA content is observed, while after a 4C DNA content is observed.

Microscopic examination of cell cultures at 24 hours from which the cells analyzed in (A) and (B) were collected allowed for determination of the average percent (%) sporulation of cells at 24 hours, shown with (A, previous page). (B) Nuclear division analysis of sporulating SJH2-1 derivative strains. DAPI stained nuclei from each strain (labeled by different colors) were analyzed at the timepoints indicated. Cells with 2 nuclei had completed MI and cells with >2 nuclei had completed MII. Graphed percentages are averages based on two separate analyses. Shown on left is the percentage of cells in each strain that completed both MI and MII divisions (%MI + %MII) Shown on right is the comparison of cells for each strain completing either one (%MI; open circles) or both divisions (%MII; filled squares) at the 24-hour timepoint with standard deviation. Standard deviation for *rfa2-ΔNx* %MII at 24 hours is +/- 0.1%.

Nuclear division analysis, by DAPI staining, was performed to determine if there was an obvious difference in meiotic divisions. Nuclei were counted and graphed for at least 500 cells at each timepoint as indicated (Figure 4.10B). Nuclear division analysis indicated that all mutants were able to initiate meiosis at the same frequency as wildtype, since similar percentages of cells entered the meiotic program which was determined by adding the percentages of cells that had completed either one (%MI) or both divisions (%MII) together (Figure 4.10B “%MI + %MII”). Analyzing each division separately shows that the SJH2-1 *rfa2-ΔNx* mutant has an increase in the

percentage of MI cells (open circle) and a decrease in percentage of MII cells (closed square; Figure 4.10B “%MI vs. %MII”). The standard deviation for the average %MII of the *rfa2-ΔN_x* mutant is +/- 0.1% which suggests that the *rfa2-ΔN_x* mutant average %MII is significantly different from all other data points shown except for %MI of the *rfa2-ΔN_x* mutant (Figure 4.10B “%MI vs. %MII”). The decreased ability of the *rfa2-ΔN_x* mutant to complete both nuclear divisions is consistent with the reported sporulation percentage and the tetrad:dyad ratio (Figure 4.10B “%MI vs. %MII” and Table 4.2).

Four different assessments reveal no obvious defects in homologous recombination

Homologous recombination was initially assessed by a qualitative heteroallelic recombination assay using RM96 derivative diploids (See Chapter 2, Figure 2.9). Replica plating showed no obvious differences in either mitotic recombination or meiotic recombination at the *LEU1*, *LYS2*, and *TRP5* loci in *rfa2* NT mutant diploids (Figure 4.11A). Less recombinants were observed from sporulated *rfa2-ΔN_x* mutant patches (Figure 4.11A). This suggests that recombination might be affected; however, the reduction in microcolony growth due to recombination may also be attributed to an overall reduction in growth (result of low sporulation efficiency and low spore viability) that is not due to a HR defect. The SD-His plates are shown as a control, confirming mutants are diploids.

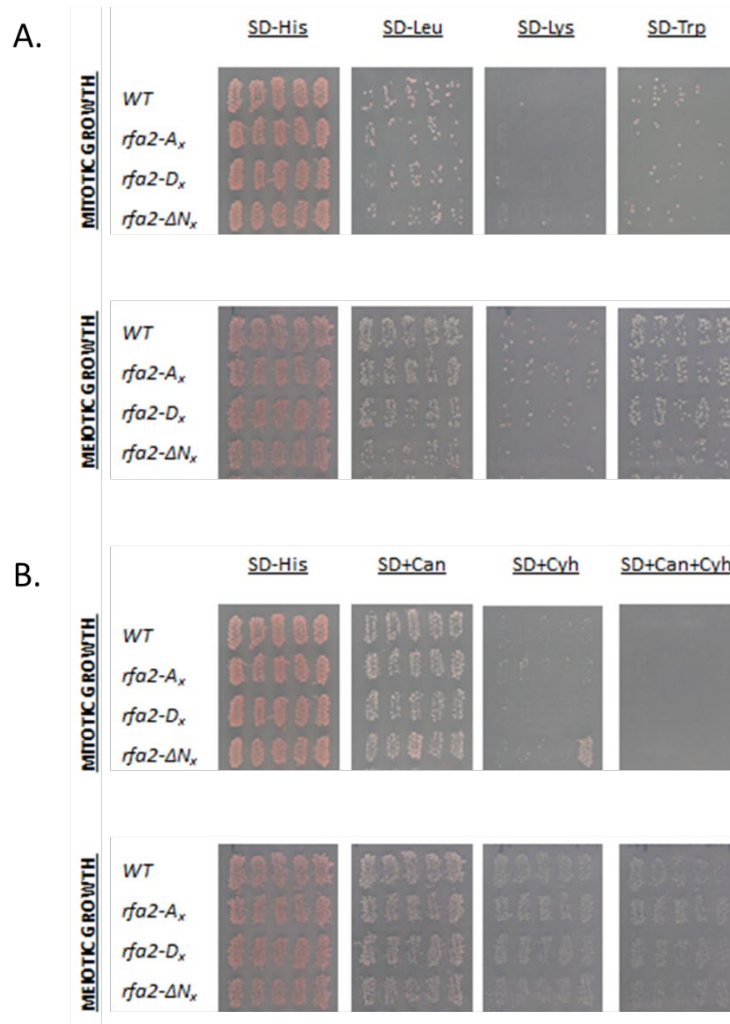


Figure 4.11. Qualitative assessment of heteroallelic recombination and chromosome segregation

RM96 derivative diploids were replica plated to indicated media after mitotic growth or meiotic sporulation. Each patch originated from an independent colony of the strain. Diploid status is confirmed by growth on SD-His. (A) Microcolony growth on drop-out media (SD-Leu, SD-Lys, and SD-Trp plates) indicates that heteroallelic recombination at the *LEU1*, *LYS2*, and *TRP5* loci (respectively) generated the wild-type copy of the gene allowing for growth to occur. (B) Chromosome segregation of *CAN1^S/can1^R* and *CYH2^S/cyh2^R* alleles is visually assessed by growth on media containing canavanine (Can) and/or cycloheximide (Cyh). Mitotic growth should be minimal as diploids contain both alleles, making the diploid sensitive to both agents (unless a gene conversion event occurs). After sporulation, growth (“meiotic growth”) should be observed only with haploids containing the resistant allele.

Chromosome segregation was assessed in the RM96 derivative diploids using replica plating to assess segregation of the heterozygous *CAN1^S* and *CYH2^S* alleles (See Chapter 2, Figure 2.14). These alleles prevent growth on media containing canavanine and cycloheximide,

respectively. The recessive *can1^R* and *cyh2^R* mutant alleles confer resistance to these cytotoxic agents. In theory, diploids should be unable to grow in the presence of canavanine and cycloheximide, whereas after proper chromosome segregation occurs during meiosis approximately half of the spores should contain the resistant mutant alleles to allow for growth. However, mitotic gene conversion may allow diploids to grow, as was likely the case for all strains showing minimal mitotic growth on SD+Can (Figure 4.11B). Increased growth is observed in all strains after meiosis, which is most apparent when viewing plates containing cycloheximide, this is indicative of proper chromosome segregation occurring in all strains that were able to produce viable spores (Figure 4.11B). Assessment of proper chromosome segregation is an indirect measure of homologous recombination during meiosis since proper chromosome segregation is dependent on HR pairing the chromosomes. The results of this assay suggest that HR may not be affected as there are no obvious growth differences due to an inability to properly segregate chromosomes after HR.

Homologous recombination was then quantitatively measured by determining the heteroallelic recombination frequency of RM96 derivative diploids. The heteroallelic recombination frequency was measured by plating serial dilutions to determine actual number of cells plated and to determine the number of recombinants at *LEU1* and *TRP5* loci, see Materials and Methods. When observing recombination frequencies at *LEU1* and *TRP5* loci independently, the *rfa2-D_x* mutant appears to have a recombination frequency that is reduced from wild-type only at the *LEU1* locus during both mitosis and meiosis (Figure 4.12, top left; mitosis and top right; meiosis) and an increase in frequency at the *TRP1* locus only during meiosis (Figure 4.12, top right). The *rfa2-ΔN_x* mutant also had a reduction from wild-type in the heteroallelic recombination frequency at the *LEU1* locus but only during meiosis (Figure 4.12 top right) and

an increase in frequency at the *TRP5* locus during both mitosis and meiosis (Figure 4.12, top graphs). However, the average recombination frequencies (combining data for both loci together) in both mitosis and meiosis for all mutants were not significantly different from wild-type (Figure 4.12, bottom). The recombination frequencies (gene conversion measurement) of these two loci are low (Lax and Fogel 1978, Malone et al. 1994), which may make it difficult to determine if any mutations are influencing recombination. It can be said that these *rfa2* mutations are not influencing recombination to the extent of a recombination deficiency, since the reduction in recombination frequency of deficient mutants is typically 10-100-fold, which is not observed.

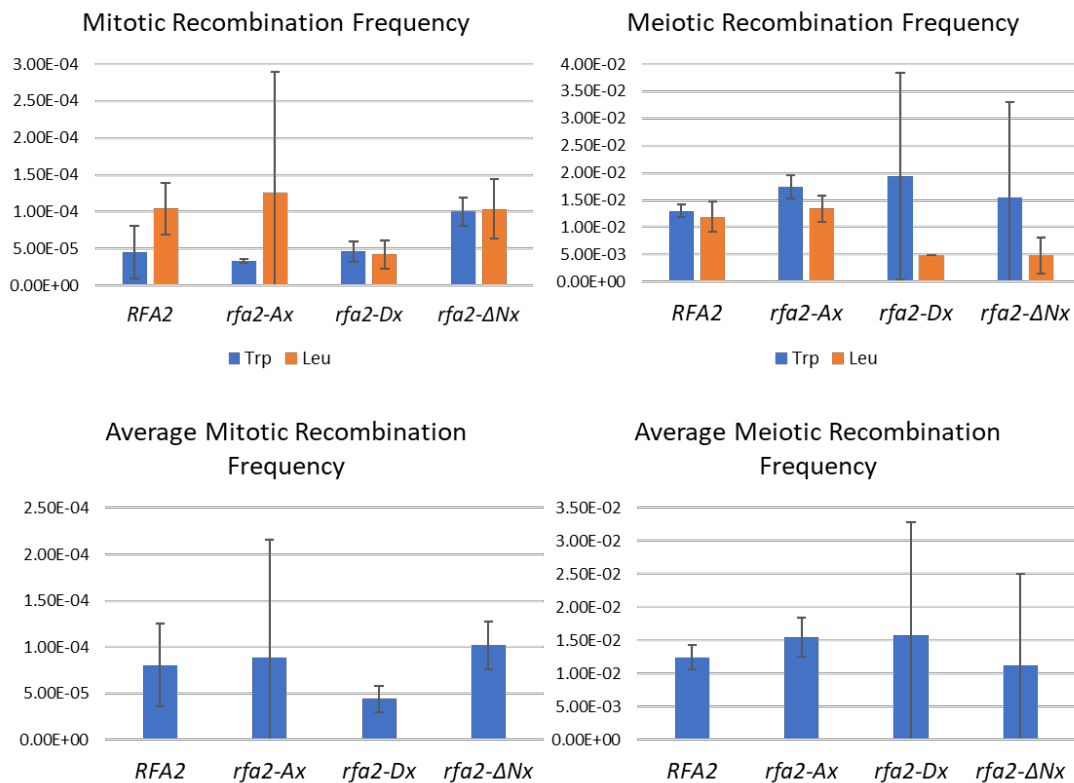


Figure 4.12. No obvious heteroallelic recombination defect is observed

Heteroallelic recombination frequency of the *LEU1* (Leu) and *TRP5* (Trp) loci in RM96 derivatives determined by quantitation. The recombination frequency is shown for mitotic cells (left) and meiotic cells (right) of the *LEU1* (top graphs, orange) and *TRP5* (top graphs, blue) loci or the average recombination rate (bottom graphs) determined by combining Leu and Trp data. There were at least two replicates used to determine the recombination frequency at each locus.

A more precise quantitative recombination measurement by tetrad analysis was performed to specifically measure gene conversion at the *HIS2* hotspot and crossing over in the *CLY3-HIS2-CDC14* interval in SJH2-1 derivative diploids, see Materials and Methods. SJH2-1 has a high frequency of recombination at the genetically engineered *HIS2* locus, reported as 29.2% for gene conversion (Haring et al. 2003). We report gene conversion at the *HIS2* locus for wildtype SJH2-1 at 30%, for the *rfa2-A_x* mutant at 29.7%, for the *rfa2-D_x* mutant at 25.9%, for the *rfa2-ΔN_x* mutant at 30% (Table 4.3). Gene conversion percentages for other loci (*CAN1*, *TRP1*, *LYS2*, and *LEU2*) with low recombination frequencies are relatively similar among the strains (Table 4.4). While gene conversion at the *HIS2* locus was slightly reduced in the *rfa2-D_x* mutant (Table 4.3), genetic distance of the *CLY3-HIS2-CDC14* interval was slightly increased (7.5 cM) compared to the wildtype SJH2-1 (5.3 cM) and the *rfa2-A_x* mutant (5.4 cM), note that the increase in genetic distance might not be statistically significant due to overlapping standard error (Table 4.5). A slight reduction in *HIS2* gene conversion is observed in the *rfa2-D_x* mutant, while the genetic distance of the *CLY3-HIS2-CDC14* interval has slightly increased, taken together these data might suggest that the overall amount of crossovers has remained the same with perhaps only a change in the location. A slight increase in genetic distance has been reported using a different *rfa2* mutant (*rfa2-S122D*) only in one (*HIS4-MAT*) out of three intervals tested (Bartrand et al. 2006), thus rather than the Rfa2 NT or Rfa2-S122 specifically influencing crossovers, the change might instead be attributed to a negatively-charged Rfa2. More testing would be required to determine if a negatively charged Rfa2 has a global effect on crossover frequency, since the data generated thus far is unclear. An even larger increase in genetic distance of the *CLY3-HIS2-CDC14* interval was observed for the *rfa2-ΔN_x* mutant (10.0 cM) which was outside of the standard error calculated for the wild-type strain (Table 4.5).

Interestingly, gene conversion for the *rfa2-ΔN_x* mutant at the *HIS2* locus was the same as wild-type (Table 4.3). These data might suggest that the viability of the tetrads formed from the *rfa2-ΔN_x* mutant with all four spores viable might be attributed to an increase in crossovers.

Table 4.3. Gene conversion frequencies of Rfa2 NT mutants at a meiotic recombination hotspot

Relevant Genotype ^a	Gene Conversion of <i>his2-390</i>				Total # GC	Total # Tetrads	% GC
	3+:1-	1+:3-	4+:0-	0+:4-			
<i>RFA2</i>	36	51	2	0	89	297	30.0
<i>rfa2-Ax</i>	49	36	2	1	88	296	29.7
<i>rfa2-Dx</i>	44	29	1	3	77	297	25.9
<i>rfa2-ΔN_x</i>	12	8	1	0	21	70	30.0

^a Genotype for all SJH2-1 genetic background strains was *his2-390, Δc/his2-Δc*. Allelism testers were used to measure gene conversion (GC) for the *his2-390* allele by spore growth on SD-His, categorized by the number of spores that grew: spores did not grow (spores+: spores-). The total number of 4-spore viable tetrads analyzed is reported. Percent (%) GC was calculated with the number of tetrads displaying gene conversion and the total number of tetrads analyzed.

Table 4.4. Gene conversion frequencies at other loci for *rfa2* NT mutants in the SJH2-1 background

Relevant Genotype ^a	Locus	Gene Conversion at Locus				# GC	Tetrads	% GC
		3+:1-	1+:3-	4+:0-	0+:4-			
<i>RFA2</i>	<i>CAN1</i>	3	8	0	0	11	297	3.7
<i>rfa2-A_x</i>		5	5	0	0	10	296	3.4
<i>rfa2-D_x</i>		5	10	0	0	15	297	5.1
<i>rfa2-ΔN_x</i>		3	0	0	0	3	70	4.3
<i>RFA2</i>	<i>TRP1</i>	1	0	0	0	1	297	0.3
<i>rfa2-A_x</i>		4	0	0	0	4	296	1.4
<i>rfa2-D_x</i>		1	1	0	0	2	297	0.7
<i>rfa2-ΔN_x</i>		0	0	0	0	0	70	0
<i>RFA2</i>	<i>LYS2</i>	2	2	0	1	5	297	1.7
<i>rfa2-A_x</i>		2	1	0	1	4	296	1.4
<i>rfa2-D_x</i>		4	0	0	0	4	297	1.3
<i>rfa2-ΔN_x</i>		1	0	0	0	1	70	1.4
<i>RFA2</i>	<i>LEU2</i>	4	8	1	0	13	297	4.4
<i>rfa2-A_x</i>		8	8	0	0	16	296	5.4
<i>rfa2-D_x</i>		5	3	0	0	8	297	2.7
<i>rfa2-ΔN_x</i>		0	1	0	0	1	70	1.4

^a Genotype for all SJH2-1 genetic background strains was *CAN1^S/can1^R*, *trp1-1/TRP1*, *LYS2/lys2-1*, *leu2-1/LEU2*. Percent gene conversion is calculated by adding the number of tetrads segregating in a nonmendelian fashion divided by the total number of tetrads multiplied by 100.

Table 4.5. Analysis of crossing over in the *CLY3-CDC14* interval for *Rfa2* NT mutants

Relevant Genotype	Genetic Distance (cM)	Tetrad Type ^a			Total # Tetrads
		PD	TT	NPD	
<i>RFA2</i>	5.34 +/- 0.91	259	31	0	290
<i>rfa2-A_x</i>	5.38 +/- 1.32	262	25	1	288
<i>rfa2-D_x</i>	7.47 +/- 1.42	250	37	1	288
<i>rfa2-ΔN_x</i>	10.0 +/- 2.39	56	14	0	70

Genotype for all SJH2-1 genetic background strains used to measure crossing over was *CLY3/cly3^{ts}*, *his2-390*, *Δc/his2-Δc*, *CDC14/cdc14-1^{ts}*. ^a PD = parental ditype; TT = tetratype; NPD = nonparental ditype. Genetic distance (cM) was calculated using the Perkins Equation through use of Stahl's online tools to also obtain standard error (see Methods for web address).

All homologous recombination assays performed in this study are inherently biased as they all required viable spores. Tetrad analysis, in particular, can only be performed on 4-spore viable tetrads, which are difficult to obtain in strains with reduced sporulation and reduced spore viability like the *rfa2-ΔN_x* mutant (Note: number of tetrads examined in Table 4.3). Additionally, viability is a reflection of adequate homologous recombination, as enough homologous recombination would have had to have occurred to properly segregate homologous chromosomes during MI. If enough homologous recombination had not occurred to properly segregate homologous chromosomes during the first division, this could result in inviable spore(s).

Overall, the Rfa2 NT does not have any obvious consequences on a cell's ability to perform homologous recombination in cells *that have produced 4-spore viable tetrads*. Unless the *rfa2* mutations affect meiosis-specific HR proteins or the defect cannot be observed in viable tetrads, it seems unlikely that HR is the culprit for reduced viability as a mating-type switching assay performed for another study shows that *rfa2* mutants are not HR defective (Appendix H).

Rfa2 is modified during meiosis in SJH2-1 derivative strains

Samples of liquid sporulating SJH2-1 derivative *rfa2* mutants were also collected for western blotting analysis of Rfa2 protein. The liquid sporulation efficiency of samples used in western blotting is shown in Table 4.6. Rfa2 is phosphorylated during meiosis in the SJH2-1 strain (Figure 4.13), similarly to published data (Brush et al. 2001), that shows a primary and secondary phosphorylation event. In the SJH2-1 strain, the primary event appears during cell incubation in pre-sporulation media (YPA), while the exact timing of the secondary event (Rfa2-PP) is difficult to discern in these blots as a haze above the primary phosphorylation (Rfa2-P) is visible in samples from 6-14 hours (Figure 4.13). In the *rfa2* mutants, the primary phosphorylation event will not be observed due to the mutations preventing Ime2 from

phosphorylating the N-terminus (Clifford et al. 2005, Clifford et al. 2004). However, the 8 hour samples from the *rfa2* mutants are shown as the secondary phosphorylation event demonstrated to occur on S122 (Brush et al. 2001) would still be able to be observed; thus the haze observed above the detected Rfa2 mutant protein species is likely S122 phosphorylation.

Table 4.6. Sporulation efficiency of SJH2-1 derivatives used for western blotting

Relevant Genotype	% Tetrads	% Dyads	Total Cells	% Sporulation	Tetrad:Dyad
WT	55.3	0	237	55.3	NA
<i>rfa2-A_x</i>	43.7	0.9	229	44.5	50
<i>rfa2-D_x</i>	45.7	0.4	245	46.1	112
<i>rfa2-ΔN_x</i>	18.2	4.6	325	22.8	3.9

All strains listed are SJH2-1 genetic background derivatives. All strains were analyzed after 26 hours of sporulation in CL SPM at 30°C in shaker incubator.

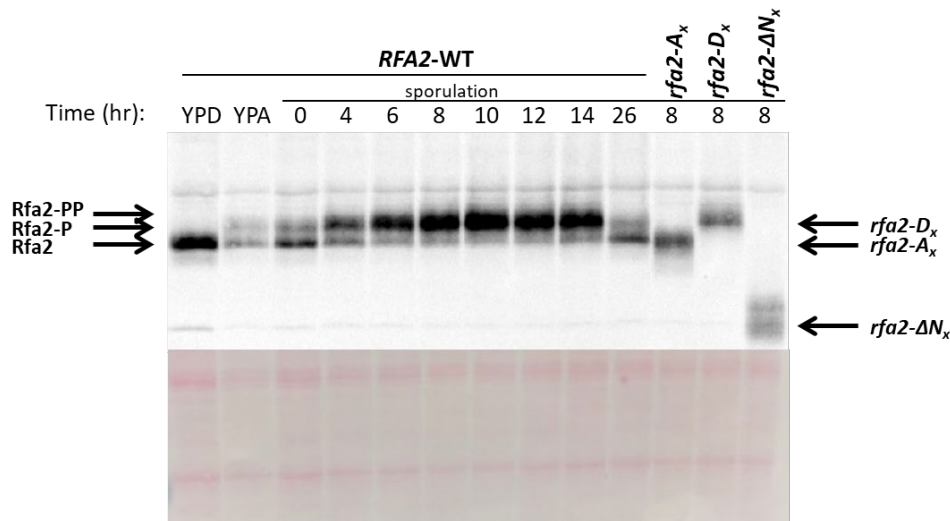


Figure 4.13. Analysis of Rfa2 protein in SJH2-1 derivative strains

Rfa2 protein observed via western blot from samples taken from rich media (YPD), pre-sporulation media (YPA), or at specified intervals (in hours, hr) during sporulation. Arrows on left point out the species of wild-type Rfa2 observed; unmodified (Rfa2), Rfa2 after primary phosphorylation (Rfa2-P), and Rfa2 after secondary phosphorylation (Rfa2-PP). Arrows on right point out the location of the Rfa2 mutant forms (from *rfa2-A_x*, *rfa2-D_x*, and *rfa2-ΔN_x*). Ponceau staining was performed to check for even loading and is shown below the blot. Methods specific for this blot: For each lane, 10 μg protein in 1X Laemmli buffer (no β-Me added) was loaded for SDS-PAGE. Western blot was developed with the Pierce™ ECL 2 Western blotting substrate kit (Thermo Scientific) and imaged with the Storm 865 (GE Healthcare) imager.

Mutants that do not allow for successful meiotic progression past MI appear mostly unaffected by *rfa2* extensive mutations

Several meiotic progression mutants exist that affect the cell's ability to successfully proceed past the first meiotic division. These mutants: *spo11Δ*, *sae2Δ*, *dmc1Δ*, and *ndt80Δ*, are well-characterized and are commonly used to study mutations affecting the first division (especially meiotic recombination). Spo11 makes the programmed DSBs but remains covalently attached until removed by Sae2-dependent processing of the break. (Keeney et al. 1997, Keeney 2008, Cartagena-Lirola et al. 2006, Clerici et al. 2005) Therefore, a *spo11Δ* mutant does not produce DSBs, this leads to a decrease in sporulation and a decrease in viability. A *sae2Δ* mutant allows for the DSBs to be made but prevents their processing as Spo11 will remain attached to the DSB end, which ultimately prevents sporulation (Lengsfeld et al. 2007, Prinz et al. 1997). Dmc1 is the meiosis-specific recombinase that allows for DSBs to be repaired via homologous chromosomes rather than through sister-chromatids (mediated by Rad51 recombinase). Due to the presence of Rad51 when Dmc1 is absent, DSBs may instead be repaired via Rad51, however sporulation is severely reduced, as is viability, both to almost zero (Lydall et al. 1996). Ndt80 is the regulator of the pachytene checkpoint, without Ndt80, cells cannot progress through MI, which means *ndt80Δ* cells do not sporulate even though DSBs have been made (Xu et al. 1995).

These mutations: *spo11Δ*, *sae2Δ*, *dmc1Δ*, and *ndt80Δ*, were generated in the RM96 genetic background. These mutants were sporulated in liquid sporulation media to collect samples for western blotting analysis of Rfa2 protein. After the last sample was collected at 26 hours, the sporulation efficiency of the RM96 derivative strains was determined from cells counted via light microscopy. The wild-type RM96 strain sporulated at 59.8%, the *spo11Δ* strain

sporulated at 22.1%, the *dmc1Δ* strain sporulated at 4.9%, while *sae2Δ* and *ndt80Δ* strains did not sporulate (Table 4.7).

Table 4.7. Sporulation efficiency of meiotic progression mutants used for western blotting

Relevant Genotype	% Tetrads	% Dyads	Total Cells	% Sporulation	Tetrad:Dyad
WT	49.8	10.0	271	59.8	5
<i>spo11Δ</i>	14.7	7.4	231	22.1	2
<i>sae2Δ</i>	0	0	200	0	0
<i>dmc1Δ</i>	1.0	3.9	203	4.9	0.25
<i>ndt80Δ</i>	0	0	200	0	0

All strains listed are RM96 genetic background derivatives. All strains were analyzed after 26 hours of sporulation in CL SPM at 30°C in shaker incubator.

Rfa2 protein has been analyzed in a *spo11Δ* strain and a *dmc1Δ* strain in a publication (Brush et al. 2001). The Rfa2 primary phosphorylation event observed had been determined to be dependent only on the Ime2 kinase (Clifford et al. 2004) and is otherwise independent from DNA replication, DSB formation, and DSB repair (Brush et al. 2001). The secondary Rfa2 phosphorylation event observed was determined to be Rfa2-S122 phosphorylation which is dependent on Mec1 and DSB formation by Spo11 (Brush et al. 2001).

Overall, the results of analyzing Rfa2 protein in this study's strains support these previous conclusions (Figures 4.14, 4.15). Rfa2 phosphorylation during meiosis had not yet been shown in *sae2Δ* and *ndt80Δ* strains. However, Rfa2 phosphorylation had been shown in a *rad50S* strain which is like a *sae2Δ* strain as both mutations prevent removal of Spo11. Observance of Rfa2 phosphorylation in the *ndt80Δ* strain is supportive of previous conclusions and further demonstrates that the phosphorylation events are Ndt80-independent.

Note that the Rfa2 protein observed for the wild-type (WT) strain in both figures was from the same set of samples collected from the meiosis time course, as the transfer for the initial

western blot using the *dmc1Δ* strain samples was set-up improperly. The secondary phosphorylation event is observed at 10-hours in the second run of the wild-type samples but is not observed in the first run even though the protein used is from the exact same samples (Figures 4.14, 4.15). The difficulty in resolving the secondary Rfa2 phosphorylation event is not isolated to this study as the variability in appearance of the secondary event is observed in published work (Brush et al. 2001, Clifford et al. 2004, Clifford et al. 2005).

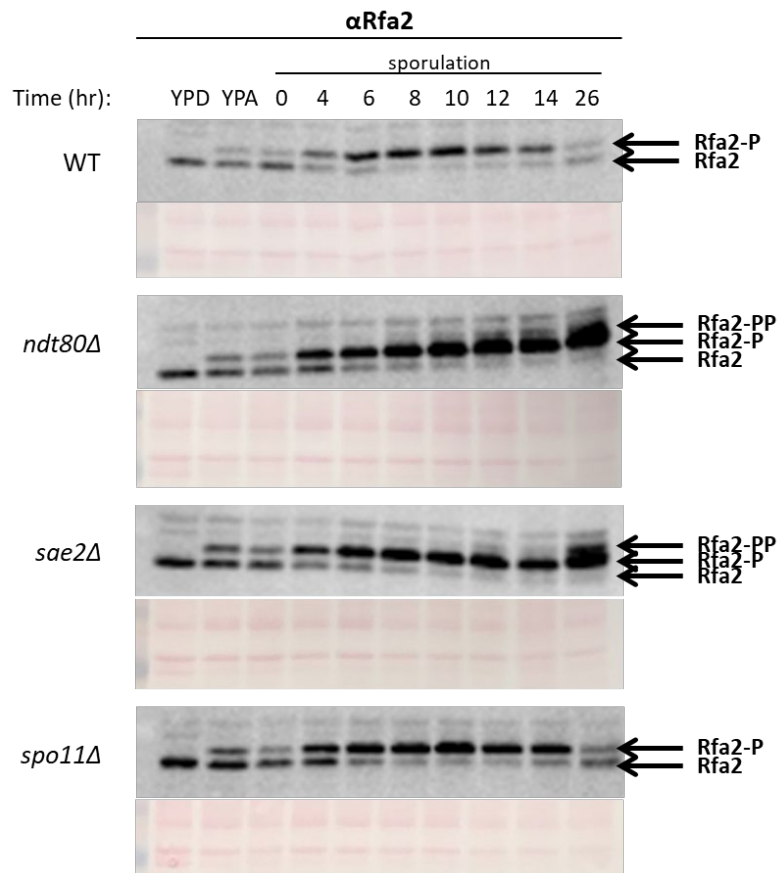


Figure 4.14. Analysis of Rfa2 protein in meiotic progression mutants

Rfa2 protein observed via western blot of RM96 derivative strains from samples taken from rich media (YPD), pre-sporulation media (YPA), or at specified intervals (in hours, hr) during sporulation. Arrows on right point out the species of wild-type Rfa2 observed; unmodified (Rfa2), Rfa2 after primary phosphorylation (Rfa2-P), and Rfa2 after secondary phosphorylation (Rfa2-PP). Ponceau staining was done to check for even loading and shown below each western blot. Methods specific for these blots: For each lane, 5 μ g protein in 1X Laemmli buffer with 4% β -Me added was loaded for SDS-PAGE. Western blots were developed with PierceTM ECL 2 Western blotting substrate kit (Thermo Scientific) and imaged with the Storm 865 (GE Healthcare) imager.

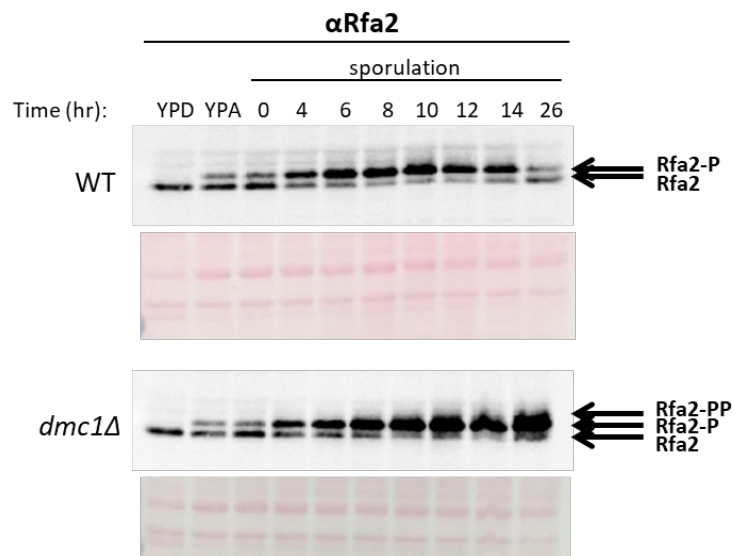


Figure 4.15. Analysis of Rfa2 protein in a *dmc1Δ* mutant

Rfa2 protein observed via western blot of RM96 derivative strains from samples taken from rich media (YPD), pre-sporulation media (YPA), or at specified intervals (in hours, hr) during sporulation. Arrows on right point out the species of wild-type Rfa2 observed; unmodified (Rfa2), Rfa2 after primary phosphorylation (Rfa2-P), and Rfa2 after secondary phosphorylation (Rfa2-PP). Ponceau staining was done to check for even loading and shown below each western blot. Methods specific for these blots: For each lane, 5 μ g protein resuspended in 1X Laemmli buffer with 4% β -Me added was loaded for SDS-PAGE. Western blots were developed with PierceTM ECL 2 Western blotting substrate kit (Thermo Scientific) and imaged with the Storm 865 (GE Healthcare) imager.

Since *rfa2* mutations have been demonstrated to affect cell cycle progression in this study (and from other studies especially in adaptation-deficient strain backgrounds), it was investigated whether they could affect cell cycle progression in meiotic progression mutants. Double mutants were generated and sporulated on solid SPO media in order to analyze sporulation efficiency. No substantial differences in the percentage of sporulated cells are observed when comparing the single meiotic progression mutants to the double mutants (Table 4.8). The *spo11Δ rfa2-ΔN_x* strain did sporulate slightly higher than the *spo11Δ* strain, however due to the overall low sporulation of the RM96 strain and the *spo11Δ* strain this warrants further study in a higher sporulating strain to determine if this is a reproducible phenotype.

Table 4.8. Sporulation efficiency of meiotic progression mutants with Rfa2 NT mutations

Relevant Genotype	% Tetrads	% Dyads	Total Cells	% Sporulation	Tetrad: Dyad
WT	45.2	3.3	630	48.6	13.6
<i>spo11Δ</i>	10.4	3.3	422	13.7	3.1
<i>spo11Δ rfa2-A_x</i>	8.4	5.2	407	13.5	1.6
<i>spo11Δ rfa2-D_x</i>	9.8	3.0	428	12.9	3.2
<i>spo11Δ rfa2-ΔN_x</i>	11.9	4.5	421	16.4	2.6
<i>sae2Δ</i>	0	0	200	0	NA
<i>sae2Δ rfa2-A_x</i>	0	0	200	0	NA
<i>sae2Δ rfa2-D_x</i>	0	0	213	0	NA
<i>sae2Δ rfa2-ΔN_x</i>	0	0	213	0	NA
<i>dmc1Δ</i>	0.5	0.4	1077	0.8	1.3
<i>dmc1Δ rfa2-A_x</i>	0.1	0.3	1033	0.4	0.3
<i>dmc1Δ rfa2-D_x</i>	0	0.1	1049	0.1	0
<i>dmc1Δ rfa2-ΔN_x</i>	0.1	0.1	1061	0.2	1.0
<i>ndt80Δ</i>	0	0	1037	0	NA
<i>ndt80Δ rfa2-A_x</i>	0	0	1033	0	NA
<i>ndt80Δ rfa2-D_x</i>	0	0	1038	0	NA
<i>ndt80Δ rfa2-ΔN_x</i>	0	0	1050	0	NA

All strains listed are RM96 genetic background derivatives. All strains were analyzed after 4 days of sporulation on SPO at 30°C.

Interestingly, higher sporulation was also observed in a *dmc1Δ rfa2-ΔN_x* strain when compared to the *dmc1Δ* strain during liquid sporulation in CL SPM media (Table 4.9). However, low sporulation percentages are obtained for all strains containing a *dmc1Δ* when SM media is used for liquid sporulation (Table 4.9). Additionally, the variability of the data collected from both types of media contributes to averages that were within the standard deviation calculated for each mutant. This is another case that would warrant further study in a higher sporulating strain. In conclusion, the *rfa2* mutations did not have an obvious effect on cell cycle progression of MI meiotic progression mutants.

Table 4.9. Sporulation efficiency of *dmc1Δ rfa2* NT double mutants after liquid sporulation in two different medias

Relevant Genotype	Media	% Tetrads	% Dyads	Total Cells	% Sporulation	Tetrad: Dyad
WT	CL SPM	52.0	5.3	225	57.3	9.8
<i>dmc1Δ</i>	CL SPM	2.2	4.9	225	7.1	0.5
<i>dmc1Δ rfa2-A_x</i>	CL SPM	4.5	3.2	220	7.7	1.4
<i>dmc1Δ rfa2-D_x</i>	CL SPM	0	2.0	204	2.0	0
<i>dmc1Δ rfa2-ΔN_x</i>	CL SPM	5.2	6.0	248	11.3	0.9
WT	SM	61.0	0	218	61.0	133
<i>dmc1Δ</i>	SM	0.4	1.3	234	1.7	0.3
<i>dmc1Δ rfa2-A_x</i>	SM	1.0	2.4	210	3.3	0.4
<i>dmc1Δ rfa2-D_x</i>	SM	1.4	2.4	211	3.5	0.6
<i>dmc1Δ rfa2-ΔN_x</i>	SM	1.9	1.0	206	2.9	2
WT	-	NA	NA	NA	59.2 +/- 2.6	NA
<i>dmc1Δ</i>	-	NA	NA	NA	4.4 +/- 3.8	NA
<i>dmc1Δ rfa2-A_x</i>	-	NA	NA	NA	5.5 +/- 3.1	NA
<i>dmc1Δ rfa2-D_x</i>	-	NA	NA	NA	2.9 +/- 1.3	NA
<i>dmc1Δ rfa2-ΔN_x</i>	-	NA	NA	NA	7.1 +/- 5.9	NA

All strains listed are RM96 genetic background derivatives. All strains were analyzed after 24 hours of sporulation at 30°C in shaker incubator. The same strains were sporulated in two different types of liquid sporulation media, CL SPM and SM (Appendix F). The last section (below double lines) shows the averages with standard deviation calculated with the data collected from the two different media types used.

Initial evidence for Rad53 modification

Typically, Rad53 is considered dispensable during meiosis as cells are still able to sporulate and form viable spores in the absence of the Rad53 adaptor protein, Rad9 (Lydall et al. 1996, Sweeney et al. 2005). Additionally, the role of Rad53 in arresting the cell cycle until breaks are repaired appears to be replaced by the meiosis-specific Mek1 that functions during the MI pachytene checkpoint to ensure inter-homolog repair bias. In a *dmc1Δ* strain, both Mek1 and Rad53 phosphorylation is observed by western blotting after meiotic DSB formation, albeit the phosphorylation observed for Rad53 is minimal and does not contribute to any delay in the

timing of the MI division (Cartagena-Lirola et al. 2008). Rad53 appears only to reach maximal phosphorylation (hyper-phosphorylation) if cells progress to MII with DNA damage where Rad53 does delay the MII division (Cartagena-Lirola et al. 2008). Thus, it appears Rad53 can only stop the cell cycle after homologous chromosome segregation in MI. Recent evidence has shown that the DNA damage checkpoint (through Mec1 and Rad53) may actually assist in maintaining meiotic commitment in the presence of a mitosis-inducing signal during MI (Ballew and Lacefield 2019).

The *rfa2* mutations did not have an obvious effect on cell cycle progression during MI. Because of the decreased number of tetrads in the *rfa2-ΔN_x* mutant, this may suggest that the MII (mitotic-like) division is the one that is affected by the *rfa2* mutations. Thus, it was investigated if any detectable modifications were occurring to Rad53 via western blotting. First SJH2-1 derivative strains were investigated using the same protein collected from the liquid sporulation time course shown above with corresponding sporulation efficiency (Table 4.6). Interestingly, 8 hours after transfer to sporulation media, Rad53 in both *rfa2-A_x* and *rfa2-ΔN_x* strains appears to be modified, however it is dissimilar from the species observed in the positive control for phosphorylated Rad53 (+Rad53; Figure 4.16). It has been attempted to recreate this blot with β-Me added to the protein samples for clearer distinguished protein species, however results have been unable to be reproduced.

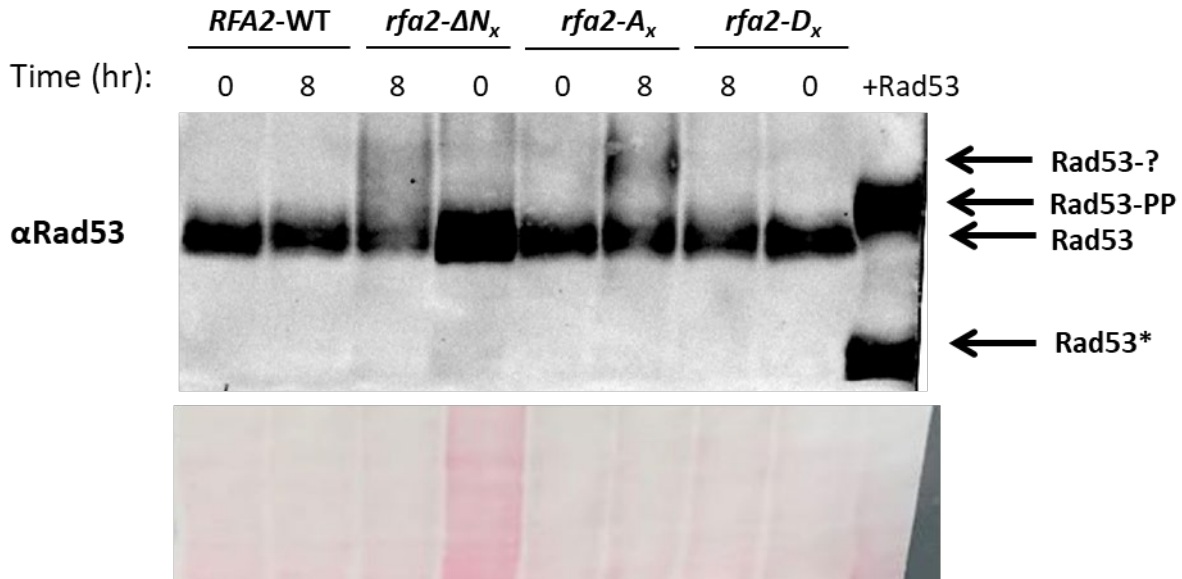


Figure 4.16. Analysis of Rad53 protein in SJH2-1 derivative strains

Western blot analysis of Rad53 protein at the indicated time (in hours, hr) during sporulation of the SJH2-1 background strains (left to right: *RFA2-WT*, *rfa2-ΔN_x*, *rfa2-A_x*, and *rfa2-D_x*). The +Rad53 control sample for Rad53 activation was obtained from Wendy Larson (TMW206, 12 hours after mitotic damage). Observed Rad53 species are indicated by arrows on right: unmodified Rad53 (Rad53), activated/phosphorylated Rad53 (Rad53-PP), Rad53 species detected at a higher molecular weight where modification is unknown (Rad53-?), and likely a degradation product occurring post- Rad53 activation (Rad53*). Ponceau staining was done to check for even loading and shown below the western blot. Methods specific to this blot: For each lane, 40 μg protein in 1X Laemmli buffer (no β-Me added) was loaded for SDS-PAGE. This western blot was developed with Pierce™ ECL 2 Western blotting substrate kit (Thermo Scientific) and imaged with the Storm 865 (GE Healthcare) imager.

The RM96 derivative strains were also investigated with the *dmc1Δ* derivative strains using protein collected from the liquid sporulation time course (utilizing CL SPM media) as shown above with the corresponding sporulation efficiency (Table 4.9). As stated above, Rad53 does appear to be minimally phosphorylated in a *dmc1Δ* strain (Cartagena-Lirola et al. 2008), which is observed in the *dmc1Δ RFA2-WT* strain at 8 hours and additional phospho-species may be present at 12 hours (Figure 4.17). In this blot it is unclear whether the *rfa2-A_x* and *rfa2-ΔN_x* strains are also showing minimal phosphorylation at 8 hours, or if this is potentially a background species observed due to a lighter haze observed above Rad53 detected in *RFA2-WT*

and *rfa2-D_x* strains. No definitive species are observed in the *dmc1Δ rfa2-A_x* and *dmc1Δ rfa2-D_x* strains. The *dmc1Δ rfa2-ΔN_x* strain may be more phosphorylated at 8 and 12 hours than in the *dmc1Δ* strain. This blot is not the best to draw major conclusions from due to the variability observed in the detected Rad53 species. Additional attempts have yet to be made to reproduce this blot.

After analysis of both blots, a simple conclusion is that Rad53 modification is difficult to detect in sporulating cells of these strain backgrounds; however, when Rad53 modifications are detected it is at later meiotic timepoints (likely corresponding to the MII division). To draw any major conclusions on Rad53 modifications occurring during sporulation of *rfa2* mutant strains, Rad53 modifications should be investigated in a higher, more-synchronously sporulating strain background as the amount of additional species observed may be increased and, because of synchrony, results might be more easily reproduced.

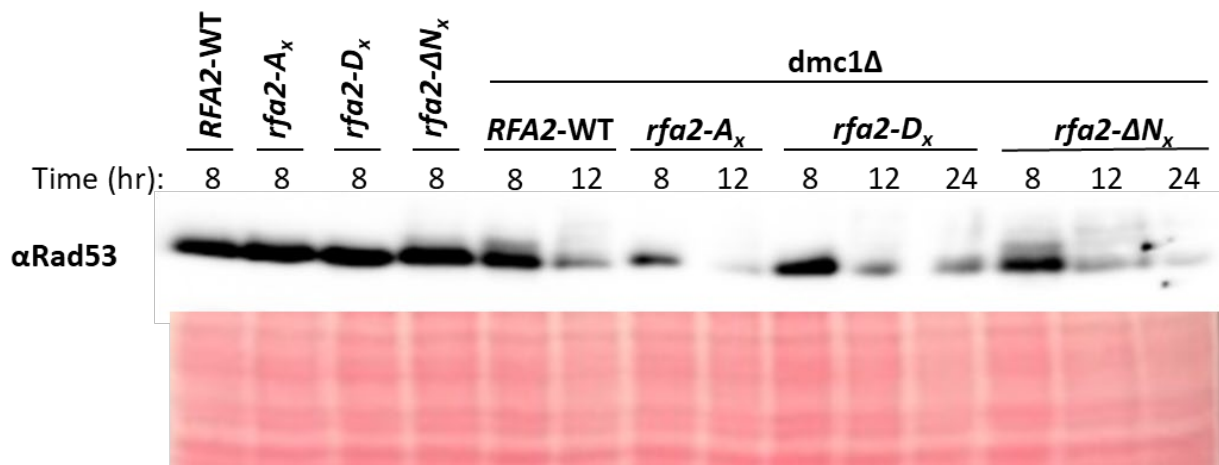


Figure 4.17. Analysis of Rad53 protein in RM96 derivative strains

Western blot analysis of Rad53 protein at the indicated time (in hours, hr) during sporulation of RM96 derivative strains. Ponceau staining was done to check for even loading and shown below the western blot. Methods specific for this blot: For each lane 30 μ L of protein in 1X Laemmli buffer + 4% β -Me was loaded for SDS-PAGE. This western blot was developed with SuperSignalTM West Pico PLUS Chemiluminescent western blotting substrate kit (Thermo Scientific) and image obtained with the myECLTM (Thermo Scientific) imager and myImageAnalysisTM software (Thermo Scientific).

Discussion

These results demonstrate that the Rfa2 NT is needed for efficient and timely progression through meiosis. The *rfa2-ΔN_x* mutant's reduction in sporulation and spore viability does not appear to be caused by an inability to perform meiotic DNA replication or homologous recombination in four-spore viable tetrads. While any effects the phospho-state of the N-terminus creates during meiosis are likely minimal since sporulation frequency of *rfa2-A_x* and *rfa2-D_x* strains are similar to wild-type and spore viability differences are only apparent with *rfa2-D_x* strains when viewing tetrad spore viability ratios.

After the discovery that Rfa2 phosphorylation occurring during meiosis is Ime2-dependent (Clifford et al. 2004), point mutations were made until it was uncovered that an *rfa2-S27A* mutation abolished Ime2-dependent phosphorylation (Clifford et al. 2005). Mass spectrophotometry data showed there could be up to three additional phospho-sites in amino acids 2-35 of the Rfa2 NT during meiosis (Clifford et al. 2005). Since our Rfa2 alanine extensive mutants, *rfa2-A_x*, have all serine and threonine residues in that interval mutated to alanine, we have eliminated the possibility for any other sites on the Rfa2 NT to become phosphorylated. Confirming data published for the *rfa2-S27A* mutant, our *rfa2-A_x* mutants appeared to be no different from wildtype when proceeding through meiosis. This data alone suggests that the phospho-state of the Rfa2 NT does not have much of an effect on the outcome of meiosis. It was therefore surprising to find that *rfa2-D_x* mutants produce approximately 10-30% fewer four-spore viable tetrads (Figure 4.9), which is discussed further on when considering cell-cycle regulatory data. A published study stated that cells (congenic to the SK-1 strain) containing a *rfa2-N40Δ* mutation (removal of the first 40 amino acids, similar to the removal of amino acids 3-37, *rfa2-ΔN_x*, used in this study) “were as efficient as wild-type in forming mature asci,” this is

clearly not the case in the three different strains (not of the SK-1 background) used in this study (Clifford et al. 2005). Furthermore, there was no data shown that supported the claim, so it is possible that there was not an immediately observed disparity in the strain background used, which lead to no further investigation. Sporulation data in this study was thoroughly investigated, in fact had we not discovered the tetrad:dyad ratio was severely decreased in the RM96 *rfa2-ΔN_x* strain after 4 days of sporulation (tetrad:dyad was 1.7, vs. 18.7 for wild-type), the percentage of sporulated cells (including both tetrads and dyads) in that experiment would have suggested that the mutant was similar to wild-type with the sporulation frequency at 35.2% compared to wild-type at 39.3% (Table 4.2).

All mitotic data gathered by the Haring lab group, including this study and current Baumgartner and Larson studies, indicate that *rfa2 NT* mutants control the time spent at a cell-cycle checkpoint (Ghospurkar et al. 2015b, Wilson 2018). This is evident from physiological and biochemical mitotic data, where *rfa2-D_x* mutants exit the G₂/M checkpoint faster which correlates with Rad53 dephosphorylation (deactivation). Whereas it is more difficult for *rfa2-ΔN_x* mutants to exit the G₂/M checkpoint observed by decreased adaptation frequency and appear more permanently arrested as cells maintain phosphorylated (activated) Rad53. This study confirms previous data using different strain backgrounds, as well as providing evidence for similar cell cycle regulation in diploid cells (Figures 4.6, 4.7).

During meiosis, Rad53 activation has been shown to occur only if breaks are unrepaired in the mitotic-like meiosis II division (Cartagena-Lirola et al. 2008). Thus, if there are unrepaired breaks after the first division *rfa2-D_x* mutants may cause deactivation of Rad53, allowing cells to complete meiosis with broken DNA which might explain the slight decrease in spore viability; however, something additional is likely occurring since wild-type Rfa2 is phosphorylated early

and thus also has the potential to cause deactivation of Rad53 in MII. The *rfa2-ΔN_x* mutants may be unable to alleviate arrest if breaks exist after the MI division, which may explain the increase in dyads and decrease in tetrads observed. Western blotting with meiotic protein revealed some modification may be occurring on Rad53 with both *rfa2-A_x* and *rfa2-ΔN_x* mutations; however, these results were not reproducible warranting exploration in higher, more-synchronously sporulating strains. A higher sporulating strain might increase the population of cells that appear to arrest (with modified/phosphorylated Rad53) after the MI division (as dyads), which would potentially increase the amount of modified Rad53 to consistently detectable levels. (For reference the population of dyads in the SJH2-1 background *rfa2-ΔN_x* strain was 4.6% at the end of the 26 hour liquid sporulation time course, which presents the possibility that the population of cells with modified Rad53 may be even less than 4.6% at 8 hours, Table 4.6 and Figure 4.16). Additionally, it may be better to explore the effects of *rfa2* mutations on Rad53 modification in a strain that does actually lead to hyper-phosphorylation of Rad53 during meiosis, as in *sae2Δ* cells (Cartagena-Lirola et al. 2008). Alternatively, if the inability to proceed through the MII division is due to activation of Rad53 permanently arresting the sporulating cells after the MI division (increasing dyads), then progression to tetrads of *rfa2-ΔN_x* strains may be rescued if Rad53 is unable to be recruited through use of a *rad9Δ* (Rad53 adaptor, (Sweeney et al. 2005). This method may in fact be better for directly implying a role for Rad53 in the increased dyad phenotype of *rfa2-ΔN_x*, as the population of dyads may be too low even in a higher, synchronously-sporulating strain to detect phosphorylated Rad53 species. Note: Deleting Rad9 was chosen instead of directly deleting Rad53 as it has been stated that *rad53Δsml1Δ* (*sml1Δ* is required to prevent lethality of *rad53Δ*) strains have impaired cell viability and mitotic cell cycle

progression that may prevent synchronization of cells for meiotic studies (Cartagena-Lirola et al. 2008).

A recent publication would suggest that although evidence for Rad53 modification has yet to be detected during MI, it may still have a role in ensuring proper chromosome segregation during MI (Ballew and Lacefield 2019). It was found that in performing return-to-growth from MI stages prior to the meiotic commitment point, chromosome mis-segregation events occurred in *rad53Δ* cells which lead to the formation of polyploid cells (Ballew and Lacefield 2019). Interestingly, cells failed to stay committed to meiosis only when both Rad53 (DNA Damage Checkpoint) and Bub2 (Spindle Assembly Checkpoint) were absent in the presence of a mitosis-inducing signal (Ballew and Lacefield 2019). This suggests that the DNA Damage Checkpoint and Spindle Assembly Checkpoint may function together to maintain meiotic commitment. Elucidating the function for these checkpoints during meiosis will be challenging, as the functions well-characterized in mitosis have, until recently, appeared to be dispensable prior to the mitotic-like MII division (Cartagena-Lirola et al. 2008, Attner and Amon 2012).

This recently published data and our mitotic data has led to the hypothesis that *rfa2* NT mutations may be similarly affecting Rad53 function during both mitosis and meiosis. Where the effect on Rad53 is easily distinguished by correlative differences in Rad53 modification and adaptation during mitosis. The effect of Rad53 during meiosis is more challenging to detect directly (by observing Rad53 modification in this study), however the indirect effects observed in this study (*rfa2-Dx* decreased viability, *rfa2-ΔNx* severely decreased tetrad:dyad ratio) can be explained by the mitotic observations. One may argue that the issue with this hypothesis is that *rfa2-Ax* mutants do not appear to have a problem completing both divisions, while mitotic data does show prolonged Rad53 activation, not unlike a *rfa2-ΔNx* mutant (Figure 4.6B). However,

mitotic data also shows that *rfa2-A_x* mutants adapt similarly to wildtype if no other adaptation deficiencies exist, which may explain why *rfa2-A_x* mutants do not appear to have a problem completing both divisions.

While spore viability reduction might be explained for *rfa2-D_x* mutants by extrapolating the observed effects on Rad53 during adaptation, spore viability of the *rfa2-ΔN_x* mutant is not as easily explained. Our data supports the idea that defective homologous recombination is not the reason for the reduction in spore viability occurring in *rfa2-D_x* mutants, or the more severe sporulation defects occurring in *rfa2-ΔN_x* mutants. However, the methods of analysis used are biased as they require spores to be viable, which means that enough recombination must have occurred to ensure spore viability. An unbiased analysis that does not require viable spores would involve the use of strains developed by Scott Keeney that contain spore-autonomous fluorescent constructs (Thacker et al. 2011). In these strains, tetrads are analyzed without spore dissection, which would allow one to determine if mis-segregation events or if reduced recombination is indeed responsible for producing inviable spores. It does seem unlikely that these mutations confer defects in HR as shown by the data presented in this study (Figures 4.11, 4.12; Tables 4.3, 4.4, 4.5), and when no HR defect is observed during mating-type switching (Appendix H).

However, if reduced recombination led to inviable spore formation in both *rfa2-D_x* and *rfa2-ΔN_x* mutants, this similarity may be explained by a difference in expression of repair genes that may have altered the ratio of Dmc1 to Rad51. RFA has been shown to bind to some upstream regulatory sequence (URS) elements (Singh and Samson 1995, Schramke et al. 2001, Gailus-Durner et al. 1997). RFA does not bind URS1 sites as well when Rfa2 is phosphorylated in a *set1Δ* mutant or when the Rfa2 NT is deleted, leading to increased expression of genes with

URS1 sites, such as *RAD51* and *CARI* (Schramke et al. 2001). There are also URS1 sites in meiotic genes, but *in vitro* analysis of the URS1 site of *HOP1* found that RFA did not seem to affect expression of these genes even though the URS1 site could be bound by RFA (Gailus-Durner et al. 1997). One could then envision a situation in which Rad51 expression is initially increased in *rfa2-D_x* and *rfa2-ΔN_x* mutants that would allow for more sister chromatid repair to occur. If more sister chromatid repair were occurring initially, additional breaks might be generated to increase the chance of crossover formation to ensure homologous chromosomes are tethered prior to the first division. This idea might be supported by the increase in genetic distance observed for the *CLY3-HIS2-CDC14* interval in both *rfa2-D_x* (7.5 cM) and *rfa2-ΔN_x* (10.0 cM) mutant strains compared to wild-type (5.3 cM). While this is an alternative explanation for what may be leading to a slight decrease in viability for *rfa2-D_x* mutants, this alone is unlikely to be causing *rfa2-ΔN_x* mutants to have both delayed/inhibited progression through divisions in addition to the severely reduced spore viability. Additionally, in meiosis Rad51 expression is downregulated through an Mek1 mechanism to allow Dmc1 to mediate interhomolog repair (Liu et al. 2014), so it is unclear whether the observed mitotic regulation of Rad51 (Schramke et al. 2001) would be able to occur during meiosis.

An alternative hypothesis to explain the sporulation defects of *rfa2-ΔN_x* mutants is that the Rfa2 NT is needed for direct interaction with Ime2. Clearly, Ime2 does interact with Rfa2 during meiosis, but this study and published work both suggest that it is not necessary for Ime2 to phosphorylate Rfa2 for successful completion of meiosis (*rfa2-A_x* cells sporulate like wild-type, Table 4.2, Figure 4.9) (Clifford et al. 2005). Just because the evidence of direct interaction (*i.e.*, phosphorylation) is absent in these mutants, does not mean that Ime2 cannot interact with altered Rfa2 N-termini. Thus, when the Rfa2 NT is missing, Ime2 may be unable to interact with

Rfa2 causing the apparent defects in sporulation in *rfa2-ΔN_x* mutants. As part of my hypothesis, Ime2 interaction with the Rfa2 NT may contribute to efficient activity of Ime2. If true, this would not be the first instance that a mutant protein has affected Ime2 activity, as demonstrated with *ids2* (other functions unknown) affecting Ime2-dependent transcription (Sia and Mitchell 1995).

In conclusion, the Rfa2 NT is required for proper progression through meiotic divisions, while the Rfa2 phospho-state does not appear to have any major effects on progression. The ideas proposed above should be explored further to directly determine if the failure of *rfa2-ΔN_x* mutant strains to remain committed to completing both meiotic divisions is due to a role of the Rfa2 NT that affects Rad53 activity similarly in mitosis and meiosis II.

Acknowledgements

Timothy Wilson made the two-step gene replacement plasmids, generated the TMW *rfa2* mutant strains, and initially tested TMW strain crosses by measuring sporulation efficiency, spore viability, and heteroallelic recombination frequencies. This initial analysis led to the divergence of this work (Wilson 2018). Courtney Karnopp generated the CMK strains. Brain Samuelson generated M2034α. Olivia Stiller generated the JKM139 *rfa2-ΔN_x* strain. Wendy Larson generated the diploid from which the allelism tester haploids were derived and provided a protein sample positive for Rad53 activation. Ally Christensen and Barbara Senger assisted with maintaining yeast master plates for tetrad analysis. Cris Hernandez completed a replicate Rfa2 western blot for the SJH2-1 derivatives. The NDSU Core Biology Facility provided: BD Accuri Flow cytometer, fluorescent microscope, and Storm 865/iBright FL1500 imager. The Wilkinson lab (John Wilkinson, Sujata Birua, and Sierra Giebel) permitted and assisted with use of the myECL™ (Thermo Scientific) imager and myImageAnalysis™ software (Thermo Scientific).

CHAPTER FIVE: RFA2 REGULATES MEC1 CHECKPOINT SIGNALING

In *Saccharomyces cerevisiae*, an irreparable DNA DSB causes cell cycle arrest by Mec1-dependent activation of the DNA damage checkpoint. Recently, Mec1 autophosphorylation at S1964 has been implicated in regulating DNA damage checkpoint signaling, specifically in appearing to control the delocalization of the Mec1-Ddc2 complex leading to cells exiting the checkpoint through checkpoint adaptation. Prior studies have shown that *rfa2 NT* mutations correlate with modification of checkpoint signaling, where phosphorylation appears to drive checkpoint adaptation. This study utilized *mec1-S1964 rfa2* double mutants to investigate this Rfa2 NT DNA damage response effect in conjunction with the recent Mec1 findings. The *rfa2* mutations that mimic or lead to early NT phosphorylation appear to rescue the adaptation-deficient *mec1-S1964A* mutant, while the *rfa2 NT* deletion mutant appears to reduce adaptation proficiency observed in the *mec1-S1964E* mutant. These results suggest that Rfa2 may regulate Mec1 checkpoint signaling, potentially by influencing Mec1-Ddc2 localization.

Introduction

Cells respond to DNA damage by activating the DNA damage response. In *Saccharomyces cerevisiae*, induction of an irreparable DSB activates the DNA damage response and leads to cell cycle arrest. After a DSB has occurred, the DNA ends at the break are resected resulting in ssDNA that RPA (RFA in yeast) binds (Zou et al. 2003). The sensor kinase Mec1 is recruited to the ssDNA in complex with Ddc2, by Ddc2-RPA interaction that leads to Mec1 activation (Nakada et al. 2005, Rouse and Jackson 2002, Deshpande et al. 2017). Mec1 phosphorylates SQ/TQ sites of downstream effectors, such as Rad53. Mec1-dependent phosphorylation of Rad53 promotes Rad53 auto-phosphorylation leading to the full activation of Rad53 and ultimately, cell cycle arrest (Lee et al. 1998, Pelliccioli et al. 2001, Kim et al. 1999,

Sanchez et al. 1996, Sweeney et al. 2005). Under circumstances where the DNA damage response (DDR) is activated and the break is able to be repaired, cells turn off the cell cycle checkpoint through a process termed checkpoint recovery (Lee et al. 2000). However, if the break is unable to be repaired, cells will eventually turn off the checkpoint by the phenomenon termed checkpoint adaptation in an effort to continue to survive (Lee et al. 1998, Lee et al. 2000).

RFA has been demonstrated to be phosphorylated in response to DNA damage. Mec1 has been shown to phosphorylate Rfa1-S178 and Rfa2-S122 in response to DNA damage during mitosis (Brush et al. 1996, Brush and Kelly 2000, Bartrand et al. 2004). Rfa2-S122 has also been shown to be phosphorylated by Mec1 after programmed DSB formation in meiosis (Brush et al. 2001, Bartrand et al. 2006). Phosphorylation of the Rfa2 NT has been observed at late time points following DNA damage and appears to be correlated with the disappearance of hyperphosphorylated (activated) Rad53 (Wilson 2018). Furthermore, an Rfa2 NT phospho-mimetic mutant (*rfa2-D_x*) promotes checkpoint adaptation in adaptation-deficient strain backgrounds (Ghospurkar et al. 2015b, Wilson 2018). These results support a role for the Rfa2 NT in modification of the DNA damage response.

Mec1's activity has been shown to be stimulated by several co-activators, which include Dpb11 (a Rad53 recruitment co-factor), Ddc1 (a component of the sliding clamp), and Dna2 (an endonuclease) after Mec1 is recruited to the site(s) of DNA damage (Majka et al. 2006b, Zou 2009, Navadgi-Patil and Burgers 2009, Navadgi-Patil and Burgers 2008, Wanrooij and Burgers 2015, Memisoglu et al. 2019). However, artificial recruitment of just the Mec1-Ddc2 complex and the sliding clamp has also been demonstrated to be sufficient to initiate the DNA damage response (Bonilla et al. 2008). The stability of the Mec1-Ddc2 complex appears to be dependent

on Mec1 kinase activity, while the delocalization of the complex appears to be dependent on Mec1 autophosphorylation (Memisoglu et al. 2019). These results hint that the Mec1-Ddc2 complex is most stable while Mec1 is actively phosphorylating downstream DDR effectors and once all the effectors have been activated, Mec1 auto-phosphorylates itself to promote the delocalization of the Mec1-Ddc2 complex from the break site. Thus, maintaining the DNA damage checkpoint appears to be largely dependent on the regulation of Mec1-Ddc2 complex localization.

In this study, *rfa2 NT* mutants previously shown to modify adaptation were used in the context of the adaptation-deficient *mec1-S1964A* mutation and the adaptation-proficient *mec1-S1964E/D* mutation. The *rfa2 NT* mutants modify adaptation of the *mec1-S1964* mutants in a similar manner to prior observations in other strain backgrounds, suggesting that the Rfa2 NT may modify the DDR by controlling Mec1-Ddc2 complex localization. Due to the ability of the phospho-mimetic *rfa2* mutant to restore adaptation in the *mec1-S1964A* mutant and that the *mec1-S1964E* mutant adaptation-proficiency is dependent on the Rfa2 NT, Rfa2 may have a more significant role in DDR modification than Mec1-Ddc2. Additionally, this role of Rfa2 may be Mec1-independent, since Rfa2 phosphorylation is not dependent on the autophosphorylation state of Mec1.

Materials and Methods

Yeast strains and plasmids

Yeast strains and plasmids used in this section are listed in Appendix A and Appendix C, respectively. EGY48 was used for homologous recombination cloning. TMW189 is the wild-type (JKM179/NMM104 derivative) containing pRS315-*RFA2* (*LEU2* selectable marker). TMW272, isogenic to TMW189 except for the *sm11Δ*, was used to generate the *mec1-S1964*

mutants by two-step gene replacement. TMW272 contains a chromosomal deletion of *RFA2*, thus contains pRS315-*RFA2* (*LEU2* selectable marker). TMW272 was chosen so that the *mec1-S1964* mutants could be generated by two-step gene replacement using the *URA3* gene.

Plasmids containing the *mec1-S1964* mutations were generated by cloning the genomic region of *MEC1* containing coding region for amino acids (aa)1650-2290 into the plasmid pAG416-GPD-ccdB followed by two site-directed mutagenesis reactions: one to remove CEN-ARS and the second to generate the mutations: *mec1-S1964A*, *mec1-S1964D*, *mec1-S1964E*. The specific steps taken are detailed in the following: To clone the *MEC1* DNA sequence corresponding to aa1650-2290, the region was amplified by PCR from JKM179 genomic DNA prepared by Trevor Baumgartner with the primers *mec1-aa1650-2290-FOR* and *mec1-aa1650-2290-REV* (Appendix D). Approximately 3 µg of pAG416-GPD-ccdB was digested with *KpnI* and *SacI* (New England Biolabs, NEB) to cut out GPD-ccdB for replacement with amplified *mec1-aa1650-2290*. EGY48 was transformed with digested plasmid and amplified product for *in vivo* homologous recombination cloning; pAG416-*mec1-aa1650-2290* was selected for on SD-Ura plates. A scrape of transformed EGY48 cells were taken and prepped for optimal plasmid recovery by following the yeast DNA isolation protocol without performing the RNaseA incubation. DH10B *Escherichia coli* cells were transformed by electroporation with the obtained DNA, since DH10B cells will die if they uptake any intact original pAG416-GPD-ccdB plasmid, while the desired cells containing the plasmid (pAG416-*mec1-aa1650-2290*) were selected for on LB+amp. DNA from candidate colonies was isolated and digested with *BglIII* (NEB) to confirm pAG416-*mec1-aa1650-2290*. To create an integrating vector, the confirmed candidate pAG416-*mec1-aa1650-2290* #6 was used in site-directed mutagenesis with the primer: Remove-ARS4-CEN6 (Appendix D). DNA from candidate colonies was isolated and digested with *PsiI*

(NEB) to confirm pAG406-*mec1*-aa1650-2290. To create plasmids containing *mec1-S1964* mutations the confirmed candidate pAG406-*mec1*-aa1650-2290 (pAMA29) was used in site-directed mutagenesis reactions with each of the following primers: *mec1-S1964A-SphI-F*, *mec1-S1964D-BclI-F*, *mec1-S1964E-PfeI-F* (Appendix D). T1 *ccdB Escherichia coli* cells were transformed with *DpnI* digested site-directed mutagenesis reactions and isolated colonies containing candidate *mec1* mutant plasmids were cultured, colony cracked, and digested with the appropriate enzyme (Table 5.1). Candidates for the *mec1-S1964D* mutation were PCR amplified with the primers *mec1-aa1650-2290-FOR* and *mec1-aa1650-2290-REV* (Appendix D) prior to digestion with *BclI*, due to methylation-sensitivity.

Table 5.1. Restriction enzyme information

Enzyme	Isoschizomer	Special Properties	Mutation
<i>SphI</i>	NA	NA	<i>mec1-S1964A</i>
<i>BclI</i>	NA	Does not cut methylated DNA	<i>mec1-S1964D</i>
<i>PfeI</i>	<i>TfiI</i>	65°C digest	<i>mec1-S1964E</i>

Enzymes listed. Isoschizomer listed only for enzymes that were used experimentally. Special properties contain information pertaining to enzyme activity. Mutation lists the *mec1* mutant in which the restriction site was generated.

MEC1 mutants were generated using two-step gene replacement in the haploid yeast strain TMW272 (See Figure 4.4 for two-step gene replacement technique). The pRS406 vectors generated above were digested with *SnaBI*, followed by TMW272 transformation with the digested vectors. Yeast containing the integration were selected for on SD-Ura (pop-ins). To stimulate pop-out of the wildtype *MEC1* gene with the *URA3* gene from the plasmid, cells were grown in YPD at 30°C overnight and then spread on 0.6-0.8 mg/mL 5-FOA plates. The *mec1* mutants (AMA253, AMA254, AMA257) were verified by PCR amplification of the region with the primers *mec1-aa1650-2290-FOR* and *mec1-aa1650-2290-REV*, followed by digestion with

the appropriate enzyme (Table 5.1), similar to how the pAG406-*mec1*-aa1650-2290-S1964D candidates were verified.

To use the *mec1*-S1964 mutant strains for plasmid shuffle with pRS315 vectors (*LEU2* selectable marker) to introduce *rfa2* mutations, competent TMW272 derivative (AMA253, AMA254, AMA257) cells were transformed with pJM132 (*URA3* selectable marker) and grown in SD-Ura media to maintain selective pressure for pJM132 while allowing for the loss of pRS315-*RFA2* (*LEU2* selectable marker).

After generation of *mec1*-S1964 mutants that contain the supplementary plasmid pJM132 (AMA258, AMA260, AMA262), plasmid shuffle was performed to generate *mec1 rfa2* double mutants. Briefly, transformation of competent cells introduced the *rfa2* mutations to *mec1*-S1964 mutant strains via plasmid (pRS315 derivatives; *LEU2* selectable marker), which then allowed for the wild-type pJM132 (*URA3* selectable marker) to be “shuffled” out of cells by negative selection on 5-FOA. The *rfa2* mutations generated by plasmid shuffle were: *rfa2*-A_x, *rfa2*-D_x, *rfa2*-ΔN_x, *rfa2*-H2NT, *rfa2*-K_xR, *rfa2*-S122A, *rfa2*-S238/240A, *rfa2*-S122A, S238/240A, and *rfa2*-S238/240D.

Checkpoint adaptation assay

The yeast strain JKM179, was designed to make an irreparable break at the *MAT* locus when HO endonuclease expression is induced by galactose. Thus, the JKM179 strain background provides for a way to study G₂/M checkpoint exit by adaptation as described previously (Lee et al. 1998). JKM179/NMM104/TMW272 derivatives were grown at least 14 hours overnight in liquid YP+Raf (1% yeast extract, 2% peptone, 2% raffinose) to reach an OD₆₀₀ of 0.6-1.0, before inducing expression of HO by adding galactose [2%]. 8 hours after galactose induction, 0.025 OD₆₀₀ equivalents of cells were sonicated and spread with glass beads to YP+Raf+Gal plates

(1% yeast extract, 2% peptone, 2% raffinose, 2% galactose, 2% agar). Cells were counted to determine the percentage of cells arrested at G₂/M checkpoint. Cells were counted again at 24 hours and 48 hours after galactose induction to determine the percentage of adapting cells. Cells were collected from liquid YP+Raf+Gal cultures at the timepoints indicated for western blotting. 2.5 OD₆₀₀ equivalents were collected for protein extraction by the Kushnirov method (Kushnirov 2000), while 5-10 OD₆₀₀ equivalents were collected for protein extraction by trichloroacetic acid (TCA) and acetone precipitation.

SDS-PAGE and western blotting for Rfa2 and Rad53

TMW189, TMW272, AMA253, and AMA254 were grown to exponential phase in liquid YPD in 30°C shaker incubator. Phleomycin (PHL) was added to cultures at 5 µg/mL. 2.5 OD₆₀₀ equivalents were collect at zero and 16 hours after damage.

Protein was extracted from PHL damaged cultures (TMW189, TMW272, AMA253, andAMA254) or liquid YP+Raf+Gal/adaptation cultures (same strains listed prior and TMW159) using the Kushnirov extraction method: cells were resuspended in 1 mL 0.3 M NaOH and incubated 5 minutes at room temperature, cells were pelleted and resuspended in 100 µL K-buffer (without β-Me, see Appendix F), then boiled for 3 minutes at 100 °C.

To detect Rfa2 protein, 20 µL of protein (K-buffer) with 4% β-Me added was separated on 15% (29:1) or 12% (150:1) resolving, 4% (37.5:1) stacking SDS-polyacrylamide gel by electrophoresis in 1X SDS buffer (Appendix F) and transferred to a nitrocellulose membrane at 0.04 Amp constant current for 16 hours overnight in transfer buffer (Appendix F). Membranes were Ponceau stained (0.5% Ponceau S, 5% acetic acid) and de-stained (1% acetic acid) to check for even loading. Membranes were blocked for 2 hrs with TBST buffer + 5 mM sodium fluoride + 1% bovine serum albumin (Appendix F). Primary anti-Rfa2 antibody was provided by Steven

Brill and used at 1:40000 in TBST buffer + 5mM sodium fluoride + 0.5% nonfat dry skim milk powder + 0.5% bovine serum albumin at 4°C for 12-14 hrs overnight on a platform shaker.

Secondary goat-anti-rabbit IgG-HRP antibody (Bethyl A120-101P) was used at 1:40000 in TBST buffer + 5mM sodium fluoride + 0.2% nonfat dry skim milk powder and incubated for 2 hrs at room temperature.

Cell samples collected at 10 OD₆₀₀ equivalents from liquid YP+Raf+Gal (checkpoint adaptation time courses) cultures for use in western blotting were extracted with TCA, precipitated by acetone washes, and resuspended in 1X Laemmli buffer (Cold Spring Harbor).

To detect Rad53 protein, protein was separated on 6% resolving (37.5:1 mono:bis) with 4% stacking (37.5:1) SDS-polyacrylamide gel by electrophoresis in 1X SDS buffer (Appendix F) and transferred to a nitrocellulose membrane at 0.04 Amp constant current for 16 hours overnight in transfer buffer (Appendix F). Membranes were Ponceau stained (0.5% Ponceau S, 5% acetic acid) and de-stained (1% acetic acid) to check for even loading. Membranes were blocked for 2 hrs with TBST buffer + 5 mM sodium fluoride + 1% bovine serum albumin (Appendix F). Primary anti-Rad53 antibody (Abcam ab104232) was used at 1:6000 in TBST buffer + 5mM sodium fluoride + 0.5% nonfat dry skim milk powder + 0.5% bovine serum albumin at 4°C for approximately 16 hrs overnight on a platform shaker. Secondary goat-anti-rabbit IgG-HRP antibody (Bethyl A120-101P) was used at 1:40000 in TBST buffer + 5mM sodium fluoride + 0.2% nonfat dry skim milk powder and incubated for 2 hrs at room temperature.

1X TBST + 5mM sodium fluoride was used for all washes (Appendix F). Western blots were developed using the PierceTM ECL 2 western blotting kit (Thermo Scientific) or the SuperSignalTM West Pico Plus Chemiluminescent substrate kit (Thermo Scientific). Images were

obtained by either: the Wilkinson laboratory myECL™ (Thermo Scientific) imager and myImageAnalysis™ software (Thermo Scientific) or the iBright FL1500 (Invitrogen) provided by the NDSU Core Facility. Specific details for each western blot provided in figure legend of the results section.

Results

Generation of integrating *mec1-S1964* mutant plasmids

Digested pAG416-GPD-ccdB and *mec1* sequence corresponding to aa1650-2290 was transformed into EGY48 for *in vivo* homologous recombination cloning to generate pAG416-*mec1*-aa1650-2290 plasmid candidates. Plasmid candidates were isolated and digested with *Bgl*III, generating two fragments (6508 bp and 207 bp; Figure 5.1). pAG416-GPD-ccdB is uncut by *Bgl*III, as it lacks *Bgl*III restriction sites, thus DNA may appear as three species: supercoiled, nicked circular, and linearized (Figure 5.1). Four candidates were confirmed as pAG416-*mec1*-aa1650-2290 (Figure 5.1).

To create an integrating vector to use for two-step gene replacement in yeast, site-directed mutagenesis was performed to remove the CEN-ARS sequence from pAG416-*mec1*-aa1650-2290. Candidates for pAG406-*mec1*-aa1650-2290 were digested with *Psi*I, as both the CEN-ARS sequence and a *Psi*I restriction site is lost, generating a 4218 bp fragment (Figure 5.2). Two candidates were confirmed as pAG406-*mec1*-aa1650-2290 (Figure 5.2).

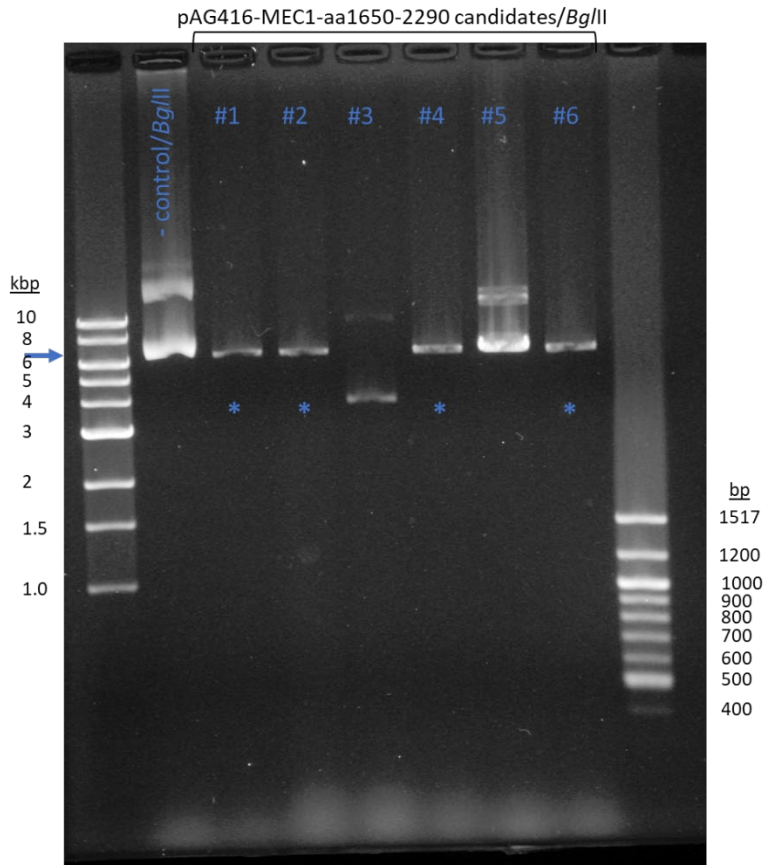


Figure 5.1. Confirmation of pAG416-mec1-aa1650-2290 candidates

DNA electrophoresed on a 1% agarose TAE gel. Serial cloner predicted fragments: pAG416-GPD-ccdB(- control)/Bg/II= uncut, pAG416-mec1-aa1650-2290/Bg/II= 6508 and 207 bp. The arrow indicates the approximate location of 6508 bp. * indicates correct candidate.

Site-directed mutagenesis reactions were set up using pAG406-mec1-aa1650-2290 to generate candidates containing either: *mec1-S1964A*, *mec1-S1964D*, and *mec1-S1964E*.

Candidate plasmids containing *mec1-S1964A* or *mec1-S1964E* were digested with *SphI* or *TfiI* respectively. Four candidates were identified as pAG406-mec1-aa1650-2290-S1964A (Figure 5.3) and six candidates were identified as pAG406-mec1-aa1650-2290-S1964E (Figure 5.4). Due to methylation-sensitivity, candidates for pAG406-mec1-aa1650-2290-S1964D were verified by first amplifying the *mec1* region by PCR, then digesting the PCR product with *BclI*. Six candidates were identified as pAG406-mec1-aa1650-2290-S1964D (Figure 5.5).

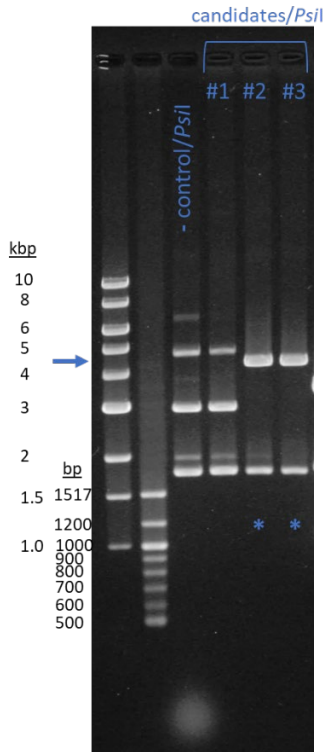


Figure 5.2. Confirmation of pAG406-mec1-aa1650-2290 candidates

DNA electrophoresed on a 1% agarose TAE gel. Serial cloner predicted fragments: pAG416-mec1-aa1650-2290/*PsiI*= 2950, 1782, 1768, and 215 bp, pAG406-mec1-aa1650-2290/*PsiI*= 4218, 1768, and 215 bp. The arrow indicates the approximate location of 4218 bp. * indicates correct candidate.

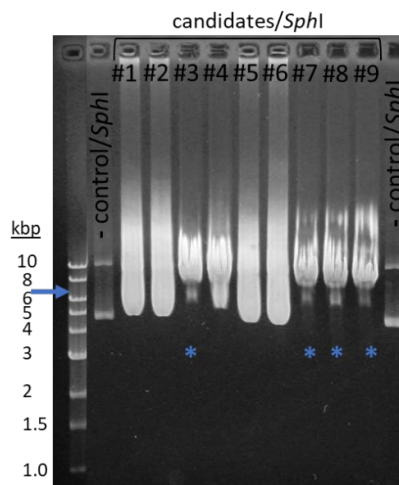


Figure 5.3. Confirmation of pAG406-mec1-aa1650-2290-S1964A candidates

DNA electrophoresed on a 1% agarose TAE gel. Serial cloner predicted fragments: pAG406-mec1-aa1650-2290/*SphI*= uncut, no restriction sites, pAG406-mec1-aa1650-2290-S1964A/*SphI*= linearized, 6201 bp. The arrow indicates the approximate location of 6201 bp. * indicates correct candidate.

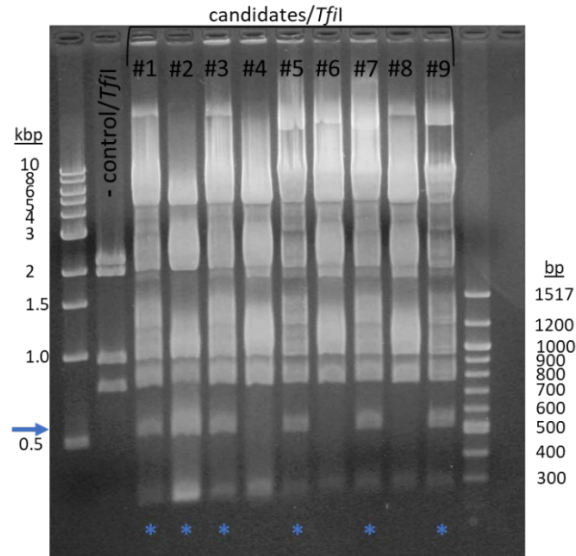


Figure 5.4. Confirmation of pAG406-mec1-aa1650-2290-S1964E candidates

DNA electrophoresed on a 1.5% agarose TAE gel. Serial cloner predicted fragments: pAG406-mec1-aa1650-2290/*TfiI*=2166, 1918, 956, 766, 255, and 140 bp, pAG406-mec1-aa1650-2290-S1964E/*TfiI*= 2166, 1918, 956, 518, 255, 248, and 140 bp. The arrow indicates the approximate location of 518 bp. * indicates correct candidate.

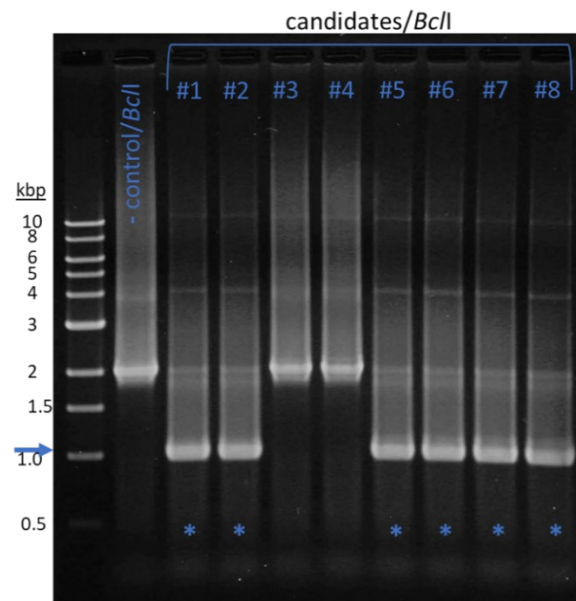


Figure 5.5. Confirmation of pAG406-mec1-aa1650-2290-S1964D candidates

DNA electrophoresed on a 1% agarose TAE gel. The *mec1* region was PCR amplified prior to digestion with *BclI*. Serial cloner predicted fragments: pAG406-mec1-aa1650-2290/*BclI*= 1993 bp, pAG406-mec1-aa1650-2290-S1964D= 1016 and 977 bp. The arrow indicates the approximate location of the doublet formed with the 1016 and 977 bp fragments. * indicates correct candidate.

The *mec1* mutants generated by two-step gene replacement with these plasmids were verified by PCR amplification then digestion with the appropriate enzyme, similar to how the pAG406-*mec1*-aa1650-2290-S1964D plasmid candidates were confirmed. The *mec1* mutants were generated in a JKM179-derived strain background to study checkpoint adaptation.

Rfa2 is phosphorylated during DNA damage by PHL and HO endonuclease in the *mec1-S1964* mutants

Mec1-S1964 has been demonstrated to be auto-phosphorylated, which has been correlated with adaptation (continuation of the cell cycle after arrest in response to irreparable DNA damage) phenotypes using *mec1* mutations that mimic phosphorylation (S1964D, S1964E) or prevent phosphorylation (S1964A) (Memisoglu et al. 2019). These *mec1-S1964* mutations have been shown to affect the outcome of adaptation with no intrinsic alterations to Mec1 activity; auto-phospho-mimetic mutants are adaptation-proficient while the non-phosphorylatable mutant is adaptation-deficient as shown by both microscopy and prolonged phosphorylation of the mitotic checkpoint effector kinase Rad53 (Memisoglu et al. 2019, Pellicioli et al. 2001).

The adaptation phenotypes corresponding to the phospho-state of Mec1-S1964 are similar to the adaptation phenotypes displayed by Rfa2 NT phospho-mutations. In which the non-phosphorylatable *rfa2* mutants (*rfa2-A_x*, *rfa2-ΔN_x*) reduce adaptation while the phospho-mimetic mutant (*rfa2-D_x*) promotes adaptation (Ghospurkar et al. 2015b, Wilson 2018). Typically the effects of the *rfa2* mutations on adaptation are most clearly observed in adaptation-deficient strains, in which *rfa2-A_x* and *rfa2-ΔN_x* further reduce adaptation while *rfa2-D_x* leads to adaptation proficiency in previously adaptation-deficient strains (Ghospurkar et al. 2015b, Wilson 2018). The *Homo sapiens* RPA2 NT is naturally phosphorylated early when it replaces

the Rfa2 NT (*rfa2-H2NT*) in yeast cells (Ghospurkar et al. 2015a, Wilson 2018). Cells containing *rfa2-H2NT* are adaptation-proficient and rescue adaptation of deficient strains as well as the rescue observed with the phospho-mimetic *rfa2-D_x* mutation (Wilson 2018) (Trevor Baumgartner unpublished data). An additional mutant whose NT is phosphorylated naturally is the “lysine-less” Rfa2 mutant, *rfa2-K_xR*, in which all 15 lysine residues are mutated to arginine to prevent ubiquitination, sumoylation, or other lysine-specific modifications (Wilson 2018) (Wendy Larson, Barbara Senger unpublished work). In cells containing *rfa2-K_xR*, Rfa2 appears to be phosphorylated to a greater extent than in wild-type cells and *rfa2-K_xR* promotes adaptation proficiency in adaptation-deficient strains similar to *rfa2-D_x* and *rfa2-H2NT* (Wendy Larson unpublished data).

Prior to studying the effects of *rfa2* mutations on the adaptation phenotype of *mec1-S1964* mutants, Rfa2 protein was observed under DNA damage conditions in the *mec1-S1964* mutants (Figure 5.6, 5.7). When double-strand breaks are generated by the DNA damaging agent phleomycin, there is no discernable difference in Rfa2 phosphorylation observed in *mec1-S1964A/E* mutants when compared to wild-type strains (Figure 5.6). When a single irreparable DSB is generated by HO endonuclease, Rfa2 phosphorylation is observed in all strain backgrounds (Figure 5.7).

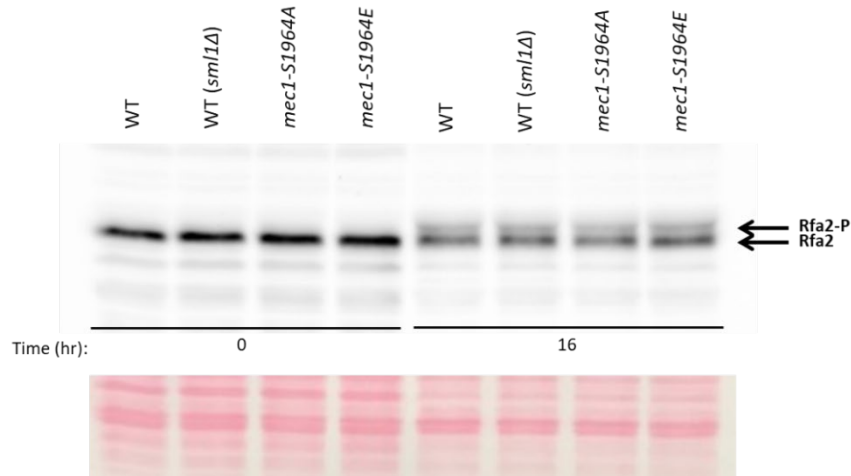


Figure 5.6. Rfa2 is phosphorylated after phleomycin treatment

Western blot analysis of Rfa2 protein collected at the times indicated (in hours, hr) after phleomycin treatment of *MEC1* (wildtype, WT) and *mec1* mutant strains. Arrows indicate the location of unmodified Rfa2 (Rfa2) and phosphorylated Rfa2 (Rfa2-P). Ponceau staining was performed to check for even loading and is shown below the blot. Note: all *mec1* mutant strains also contain the *smI1Δ* mutation. Methods specific for this blot: 20 uL of K-buffered samples + 4% B-Me was loaded into each lane for SDS-PAGE. Blot was developed with Pierce™ ECL 2 western blotting substrate kit (Thermo Scientific) and imaged with the myECL™ (Thermo Scientific) imager and myImageAnalysis™ software (Thermo Scientific).

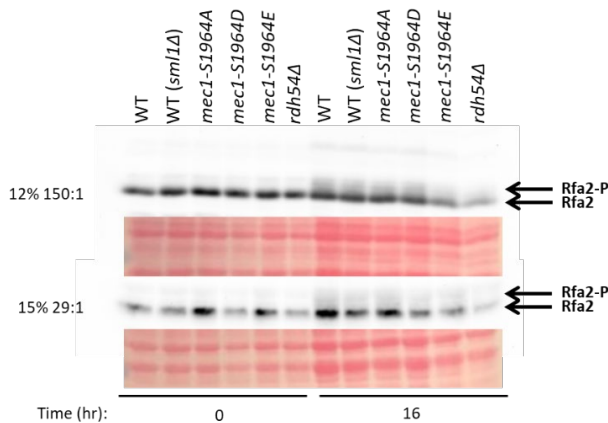


Figure 5.7. Rfa2 is phosphorylated after induction of HO endonuclease

Western blot analysis of Rfa2 protein collected at the times indicated (in hours, hr) after induction of HO endonuclease of *MEC1* (wildtype, WT) and *mec1* mutant strains. Arrows indicate the location of unmodified Rfa2 (Rfa2) and phosphorylated Rfa2 (Rfa2-P). Ponceau staining was performed to check for even loading and is shown below the blots. Note: all *mec1* mutant strains also contain the *smI1Δ* mutation. Methods specific for these blots: 20 uL of K-buffered samples + 4% B-Me was loaded into each lane for SDS-PAGE on either a 12% (150:1) or 15% (29:1) resolving SDS polyacrylamide gel, as labeled. Blots were developed with Pierce™ ECL 2 western blotting substrate kit (Thermo Scientific) and imaged with the myECL™ (Thermo Scientific) imager and myImageAnalysis™ software (Thermo Scientific).

Rfa2 mutations change the adaptation phenotype of *mec1-S1964* mutants

Observing Rfa2 phosphorylation in all *mec1* mutant strain backgrounds indicates that Rfa2 phosphorylation is independent from Mec1 auto-phosphorylation. This led to the generation of *mec1 rfa2* double mutants to analyze if the *rfa2* mutants can modify the adaptation phenotypes observed for the *mec1-S1964* mutants.

The checkpoint adaptation deficiency/proficiency of the respective *mec1-S1964* mutants generated are consistent with the published adaptation phenotypes (Figures 5.8, 5.9) (Memisoglu et al. 2019). All strains arrested following induction of the DSB, as observed by the high percentage of large-budded cells (cell cluster of 2) observed via light microscopy for each strain (Figure 5.8). The adaptation-deficient *mec1-S1964A* strain had 34% of cell clusters at 24 hours and 61% of cell clusters at 48 hours with 3 or more cells (*i.e.*, they had adapted, as continuation of cell cycle past G₂/M arrest results in the 2-cell cluster undergoing division to generate more cells in the cluster, Figure 5.8). The effects of the *rfa2* mutations on adaptation observed in the *mec1-S1964A* strain was consistent with the effects observed previously in other adaptation-deficient strains; adaptation was further reduced by *rfa2-A_x* and *rfa2-ΔN_x* mutations, while adaptation was rescued with *rfa2-D_x*, *rfa2-H2NT*, and *rfa2-K_xR* mutations (Figure 5.8A, Trevor Baumgartner unpublished data, Wendy Larson unpublished data) (Ghospurkar et al. 2015b, Wilson 2018). Additionally, the adaptation-proficient *mec1-S1964E* mutant (94% and 96% adapted at 24 and 48 hours, respectively) had a significant reduction in adaptation with the *rfa2-ΔN_x* mutation (51% and 64% adapted at 24 and 48 hours, respectively; Figure 5.8B).

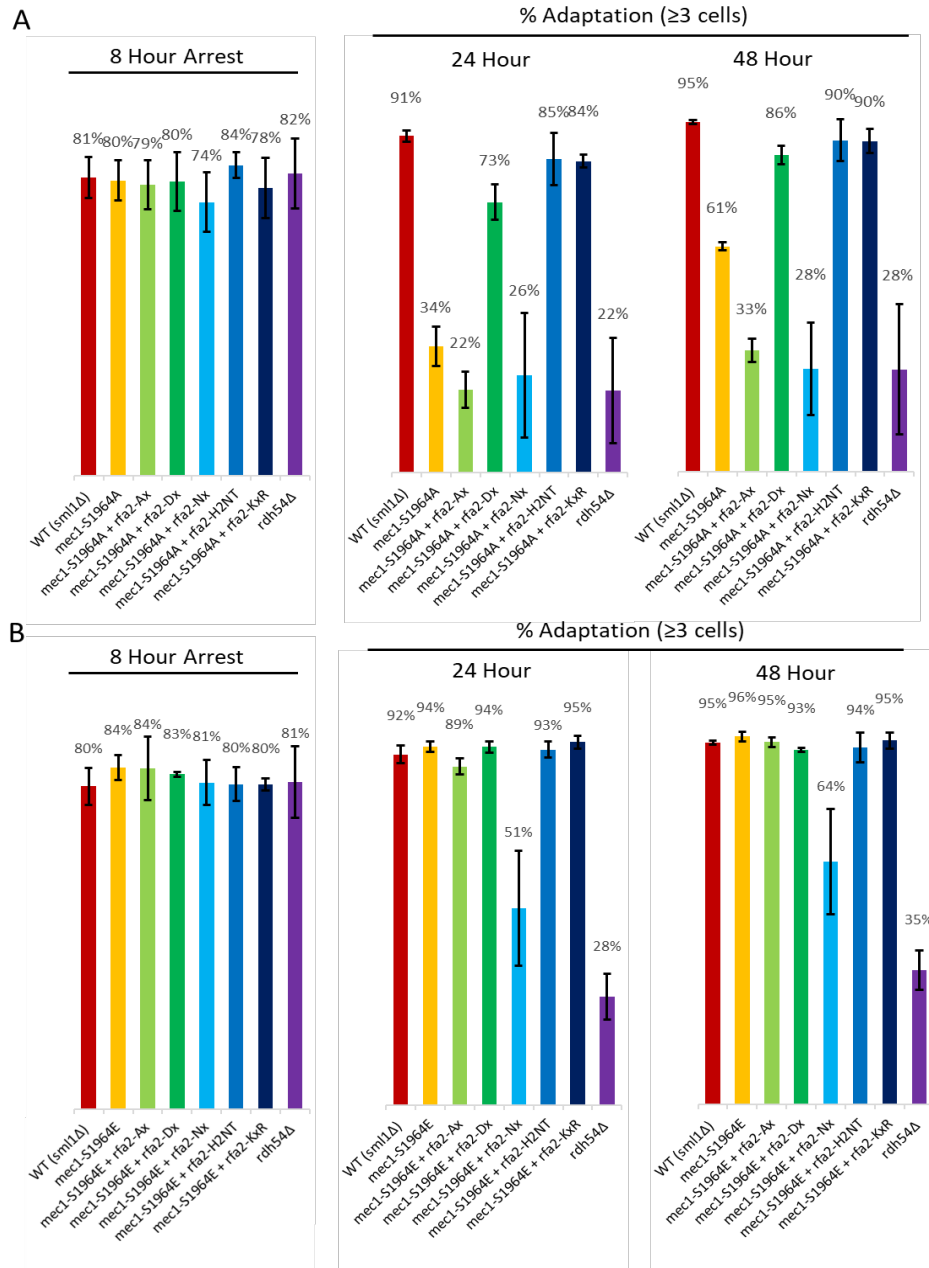


Figure 5.8. Adaptation phenotype of *mec1-S1964* mutants is modified by *rfa2* mutations

JKM179 derivative strains were analyzed via microscopy at 8, 24, and 48 hours following irreparable DSB induction. The percentage of arrested cells was determined by those appearing as a large-budded cell at 8 hours (8 Hour Arrest). The percentage of adapted cells was determined by those observed as clusters of 3 or more cells at 24 and 48 hours. Microscopic examination of cell cycle arrest and adaptation is shown for (A) *mec1-S1964A* mutants compared to the wild-type strain (WT (*sml1Δ*), TMW272) and the adaptation-deficient control, *rdh54Δ* (TMW159) and (B) *mec1-S1964E* mutants compared to the same controls as (A). Note: all *mec1* mutant strains also contain the *sml1Δ* mutation. Percentages reported are averages from 3 separate experiments, error bars indicate standard deviation. See Appendix J, Tables J1-J5 for statistical analyses performed on this data.

To observe the biochemical response during checkpoint arrest and adaptation Rad53 modification was investigated by western blot, due to variability in the 2 replicate experiments performed both blots are shown (Figure 5.9). Published data indicates that the *mec1-S1964A* mutant has prolonged Rad53 phosphorylation (activation) compared to the wild-type strain and the *mec1-S1964E* mutant (Memisoglu et al. 2019). Due to the *rfa2 NT* mutants' effect on Rad53 modification previously observed and the observed effect *rfa2* mutations had on the *mec1-S1964* mutants adaptation phenotype, it was hypothesized that differences in Rad53 modification would be observed between the *mec1-S1964* mutant and the *mec1-S1964 rfa2* double mutant. It was expected that *mec1-S1964A* mutant cells containing the *rfa2-D_x* mutation would have reduced Rad53 phospho-species at 24 hours (observe primarily unmodified Rad53) from *mec1-S1964A* mutant cells with wild-type *RFA2* and that *mec1-S1964E* mutant cells containing the *rfa2-ΔN_x* mutation would have increased Rad53 phospho-species at 24 hours. No differences were expected in observing hyper-activated Rad53 10 hours after irreparable DSB induction, since all strains appeared to arrest similarly at 8 hours under microscopic examination (Figure 5.8). These predictions were observed in the western blot from the first collection, although it is less clear that *mec1-S1964E rfa2-ΔN_x* cells have more Rad53 phospho-species than *mec1-S1964E* cells with wild-type *RFA2*, but this last lane also appears to have less total protein loaded (Figure 5.9, 1st collection). In the western blot produced from the second collection, the wild-type *RFA2* strain did not show as much hyper-activation at 10 hours as it had done in the first collection and when compared to *mec1-S1964A* mutants. Interestingly, the activated Rad53 species observed in *mec1-S1964E RFA2* mutant cells at 10 hours closely resembles the species observed in the wild-type *RFA2* strain and increased Rad53 phospho-species are observed when comparing *mec1-S1964E rfa2-ΔN_x* cells to *mec-S1964E RFA2* cells at both 10 and 24 hours (Figure 5.9, 2nd

collection). However, a decrease in Rad53 phospho-species is not clearly observed in *mec1-S1964A rfa2-D_x* cells when compared to *mec1-S1964A RFA2* cells (Figure 5.9, 2nd collection). Furthermore, the total protein loaded appears to vary considerably among lanes in the 2nd collection when compared to the 1st collection and it was expected that more drastic changes among the Rad53 phospho-species would be observed, so it is difficult to definitively state if any of these results are conclusive evidence to either support or reject the hypothesis (Figure 5.9). Overall, these results do lean towards supporting the hypothesis, however this experiment should be repeated for more conclusive evidence.

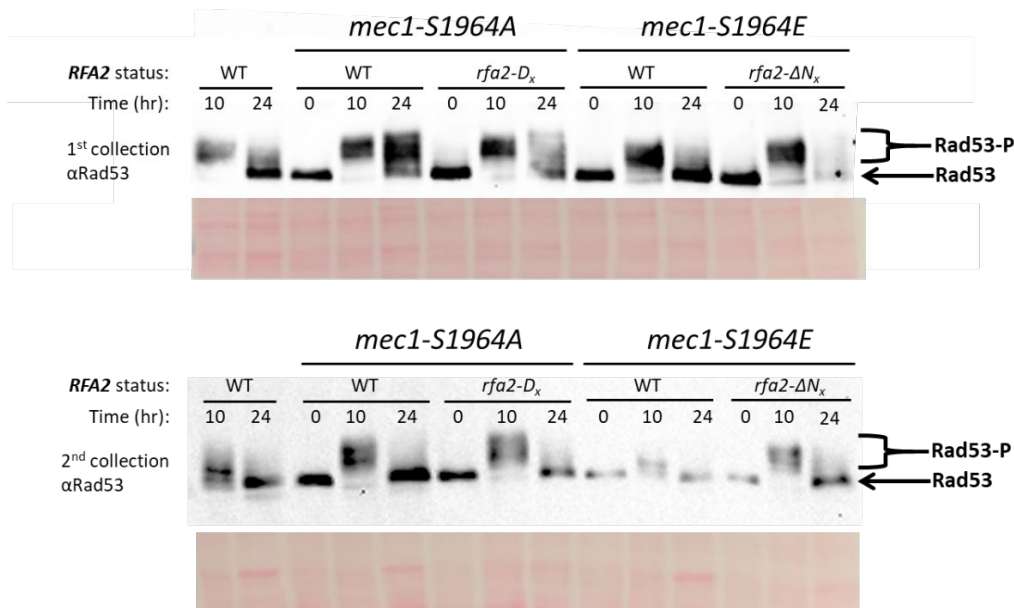


Figure 5.9. Rad53 western blots for *mec1-S1964 rfa2 NT* double mutants

Rad53 protein was analyzed via western blot following irreparable DSB induction at 0, 10, and 24 hours. The blots shown are from two separate experiments (1st collection and 2nd collection). The wild-type *RFA2* strain (WT (*sml1Δ*), TMW272) shows activated/phosphorylated Rad53 (bracket, Rad53-P) at 10 hours and primarily inactivated/dephosphorylated Rad53 (arrow, Rad53) at 24 hours. These Rad53 species are observed in the *mec1-S1964A/E* mutant strains containing either WT *RFA2*, *rfa2-D_x*, or *rfa2-ΔN_x*. Ponceau staining was performed to check for even loading and shown below each blot. Note: all *mec1* mutant strains also contain the *sml1Δ* mutation. Methods specific for this western blot: Each lane contained 40 μg of protein in Laemmli buffer + 4% β-Me separated on a 6% (37.5:1) resolving, 4% (37.5:1) stacking SDS PAGE gel. Blots were developed with the SuperSignalTM West Pico Plus Chemiluminescent substrate kit (Thermo Scientific) and imaged on the iBright FL1500 (Invitrogen) provided by the NDSU Core Facility.

The *rfa2* mutant effect on adaptation does not appear to be driven by Mec1-dependent phosphorylation of Rfa2 SQ sites

As shown, the Mec1 auto-phosphorylation state did not eliminate Rfa2 phosphorylation nor did the Mec1 auto-phosphorylation state prevent *rfa2* mutations from modifying adaptation (Figures 5.7, 5.8, 5.9). These results alone suggest that the *rfa2* mutant effect on adaptation is not driven by Mec1; however, “SQ” sites that may be targeted for phosphorylation by Mec1 exist in Rfa2. Therefore, these sites were mutated to investigate if adaptation of *mec1-S1964* mutants is influenced by modification of the Mec1 target sites. The “SQ” sites mutated were the known Mec1 target site, Rfa2-S122, and the potential “SQS” site, Rfa2-S238/240 (Figure 5.10).

```

1  MATYQPYNEYSSVTGGGFENSESRPGSGES 30
31  ETNTRVNTLTPVTIKQILESKQDIQDGPFV 60
61  SHNQELHHVCFVGVVRNITDHTANIFLTIE 90
91  DGTGQIEVRKWESEDANDLAAGNDSSGKGY 120
121 GQVAQQFEIGGYVKVFGALKEFGGKKNIQ 150
151 YAVIKPIDSFNEVLTHHLEVIKCHSIASGM 180
181 MKQPLESASNNNGQSLFVKDDNDTSSGSSP 210
211 LQRILEFCKKQCEGKDANSFAVPIPLISQS 240
241 LNLDETTNRNCCTTLTDQGFYPTFDDNNF 270
271  FAL

```

Figure 5.10. SQ motifs in Rfa2

Shown is the amino acid sequence for Rfa2 with amino acids highlighted for the known Mec1 target site for phosphorylation (Rfa2-S122) and the additional potential Mec1 target site (Rfa2-S238, following S of the SQS also mutated). These highlighted serine residues have been mutated to either A or D in the respective *rfa2* mutants.

The *rfa2-S122A/D* mutations have been demonstrated previously to be no more sensitive to DNA damage than the wild-type strain and have minimal to no detectable effect in adaptation-deficient strains (Ghospurkar et al. 2015b, Wilson 2018). While the *rfa2-S122* mutants do not affect DNA damage sensitivity when it is the only mutation, interestingly in the context of an *rfa2-D_x* strain containing either *rfa2-S122* mutation, the modified *rfa2-S122* (A or D) decreases the DNA damage sensitivity of *rfa2-D_x* (Appendix G, Figure G10). The *rfa2-S122D* mutation has also been demonstrated to increase the genetic distance of a single interval (out of the three

examined), suggesting a possible role in crossover formation/resolution (Bartrand et al. 2006). This published observation is the only significant phenotype previously reported for the *rfa2-S122D* mutation. While no striking differences have been observed between wild-type cells and cells containing an *rfa2-S122* mutation, it has been demonstrated that Mec1 phosphorylates this residue during the cell cycle and after DNA damage has occurred during both mitosis and meiosis (Brush and Kelly 2000, Bartrand et al. 2004, Brush et al. 1996, Bartrand et al. 2006).

There is no published data investigating Rfa2-S238/240 in the context of being a Mec1 target site for phosphorylation or otherwise. Therefore, the collaborative investigation of this site by Cristian Hernandez, Wendy Larson, and myself is novel. Two independent isolates confirmed to contain the *rfa2-S238/240A* mutation appear to be no more sensitive to DNA damaging agents than the wild-type strain (Appendix G, Figure G16). Rfa2 phospho-species are still observed in cells containing the single *rfa2-S238/240A* mutation and at least one phospho-species is observed in cells containing the double *rfa2-S122A, S238/240A* mutation (Figure 5.11).

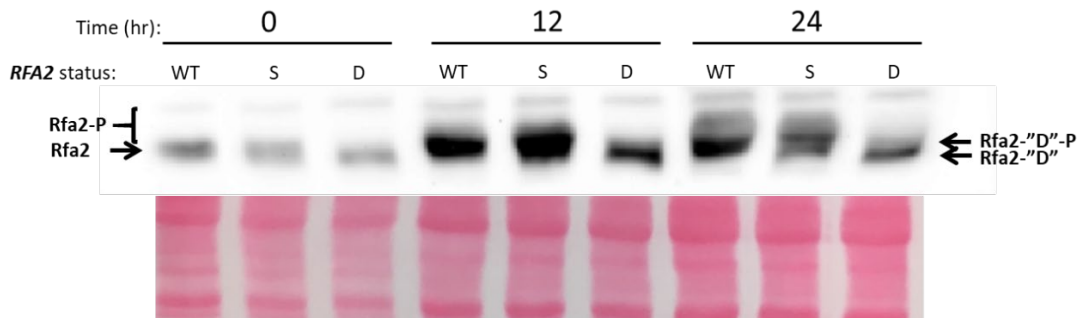


Figure 5.11. Rfa2 phosphorylation is detected in cells with mutations that eliminate Mec1 phosphorylation target sites

Rfa2 protein was analyzed via western blot in JKM179 derivative strains at 0, 12, and 24 hours after irreparable DSB induction. The *RFA2* status of strains analyzed were: WT = wild-type *RFA2*, S (single mutation) = *rfa2-S238/240A*, D (double mutation) = *rfa2-S122A, S238/240A*. The locations of wild-type Rfa2 species (left arrow and bracket) appearing after DNA damage are unmodified Rfa2 (left arrow) and phosphorylated Rfa2 species (Rfa2-P; bracket). The unmodified Rfa2-"D" (right, bottom arrow) mutant protein migrates faster than WT Rfa2 and an additional slower migratory species is observed (Rfa2-"D"-P; right, top arrow). Ponceau staining was performed to check for even loading and shown below the blot. This work was performed and duplicated by Cristian Hernandez.

The *rfa2-S238/240A* mutation does not appear to affect adaptation as the percentage of adapted cells (88.8/82.8%, 95.7/95.6%) are similar to the wild-type strain (78.8%, 93.8%) at 24 and 48 hours, respectively (Figure 5.12A). In the adaptation-deficient *rdh54Δ* strain, cells containing *rfa2-S238/240A* (36.9%, 44.4%) adapt similarly to cells containing wild-type *RFA2* (30.9%, 42.4%) at 24 and 48 hours, respectively (Figure 5.12B). It was interesting to see that in the adaptation-deficient *rdh54Δ* strain the *rfa2-S238/240D* mutation modestly increases the percentage of adapting cells (51.6%, 63.8%) compared to the *rdh54Δ* cells containing wild-type *RFA2* (30.9%, 42.4%) at 24 and 48 hours, respectively (Figure 5.12B). These results suggest that phosphorylated Rfa2-S238/240 may be able to influence adaptation; however, the non-phosphorylated state does not appear to have any effect. This is dissimilar from the decrease in adaptation observed in adaptation-deficient strains containing either of the non-phosphorylatable *rfa2 NT* mutations (*rfa2-A_x* or the *rfa2-ΔN_x*). In fact, these results exploring Rfa2-S238/240 are most similar to the results observed in prior investigations of Rfa2-S122 (Ghospurkar et al. 2015b, Wilson 2018).

In the *mecl* mutant strains that mimic the auto-phosphorylated state or the non-phosphorylated state, the effect of eliminating Mec1 target sites located in Rfa2 slightly modifies adaptation only in the adaptation-deficient *mecl-S1964A* strain background (Figure 5.13). The greatest difference is observed at 24 hours when 61% of *mecl-S1964A* cells containing the *rfa2-S238/240D* mutation adapt compared to the 43% observed of *mecl-S1964A* cells with wild-type *RFA2* (Figure 5.13A). However, by 48 hours all *mecl-S1964A rfa2* mutant strains are adapting within an 8% difference from the *mecl-S1964A RFA2* strain, which suggests that *rfa2-S238/240D* may promote cells to adapt earlier without increasing the total amount of cells that

adapt (Figure 5.13A). These results hint that the timing and potentially order in which Rfa2 residues become phosphorylated may be important regulators of cell cycle adaptation.

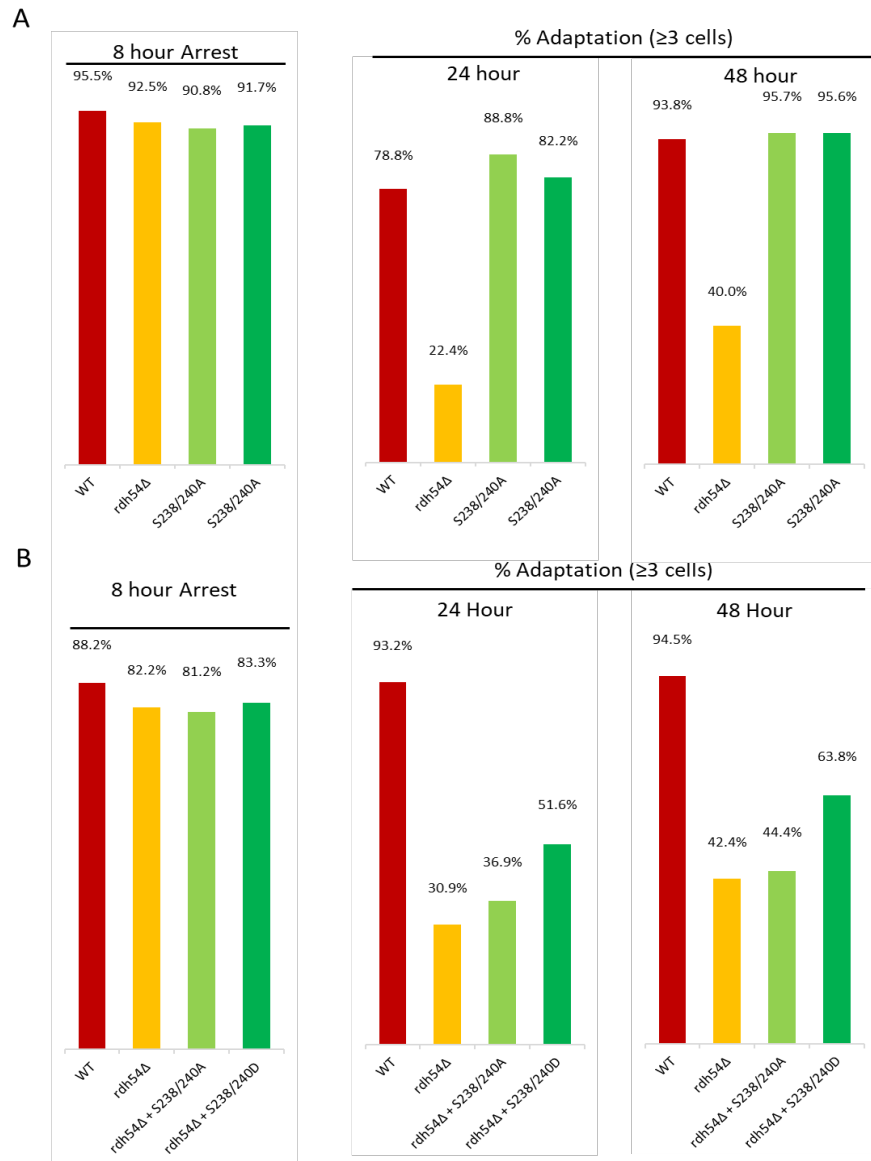


Figure 5.12. Adaptation of *rfa2*-*S238/240* mutants

JKM179 derivative strains were analyzed via microscopy at 8, 24, and 48 hours following irreparable DSB induction. The percentage of arrested cells was determined by those appearing as a large-budded cell at 8 hours (8 Hour Arrest). The percentage of adapted cells was determined by those observed as clusters of 3 or more cells at 24 and 48 hours. Microscopic examination of cell cycle arrest and adaptation is shown for (A) Two independent isolates containing *rfa2*-*S238/240A* assayed by Cris Hernandez and (B) Adaptation-deficient strain containing *rfa2*-*S238/240 A/D* mutation assayed by Wendy Larson. Both (A) and (B) contain the controls: NMM104 (wild-type *RFA2*, WT) and adaptation-deficient TMW159 (*rdh54Δ*). At least 450 cells were counted for each strain at each time. No replicates were performed.

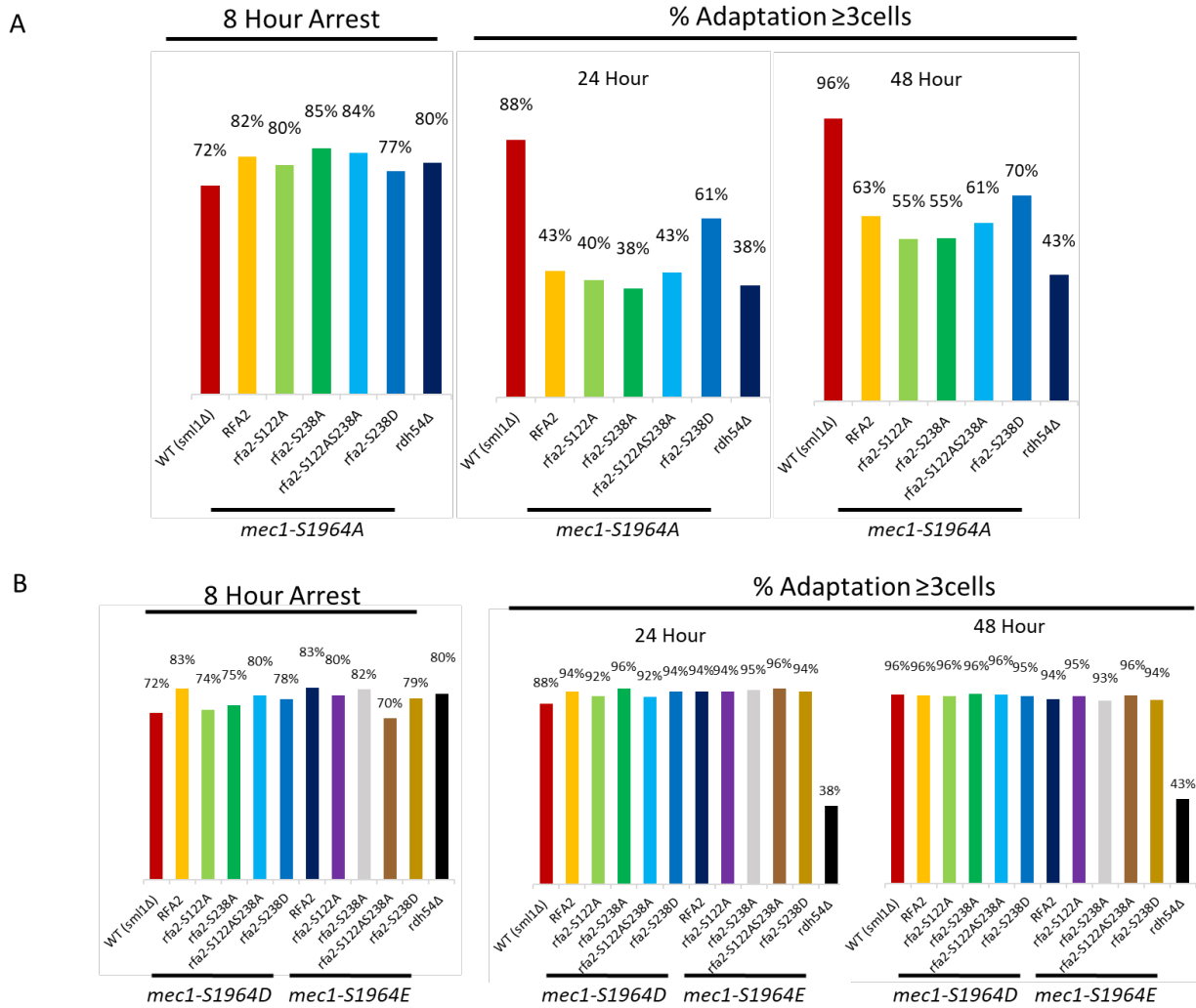


Figure 5.13. Mec1 target site mutations do not change adaptation proficiency

JKM179 derivative strains were analyzed via microscopy at 8, 24, and 48 hours following irreparable DSB induction. The percentage of arrested cells was determined by those appearing as a large-budded cell at 8 hours (8 Hour Arrest). The percentage of adapted cells was determined by those observed as clusters of 3 or more cells at 24 and 48 hours. Microscopic examination of cell cycle arrest and adaptation is shown for (A) *mec1-S1964A* mutants containing *RFA2* or *rfa2* Mec1 target site(s) mutations compared to the wild-type *RFA2* strain (WT (*sml1Δ*), TMW272) and the adaptation-deficient control, *rdh54Δ* (TMW159) and (B) *mec1-S1964D* and *mec1-S1964E* mutants containing *RFA2* or *rfa2* Mec1 target site(s) mutations compared to same controls as (A). At least 300 cells were counted for each strain at each time. No replicates were performed. Note: Labels for strains containing *rfa2-S238/240* mutations were simplified to *rfa2-S238* and all *mec1* mutant strains also contain the *sml1Δ* mutation.

Discussion

Turning off a DNA damage checkpoint to allow for either adaptation or recovery of the cell cycle will continue to be a highly studied research topic. Especially as the mechanism for adaptation, or continued cellular growth with persistent DNA damage, can be related to understanding how cancer might develop in human cells. Previous studies suggest that maintaining a cell cycle checkpoint relies on Mec1 activity localized at the DSB site by association with Ddc2 in complex (Pelliccioli et al. 2001, Clerici et al. 2001, Memisoglu et al. 2019)

Mec1 autophosphorylation has been implicated as playing a part in turning off the G₂/M DNA damage checkpoint during checkpoint adaptation (Memisoglu et al. 2019). Mec1-S1964 was identified as the site of autophosphorylation that under phospho-mimicry (*mec1-S1964D/E*) allows cells to adapt like wild-type (Memisoglu et al. 2019) (Figures 5.8, 5.9, 5.13). Whereas, the non-phosphorylated mimetic mutant (*mec1-S1964A*) appears to inhibit checkpoint adaptation by prolonged Ddc2-Mec1 localization at an irreparable break (Memisoglu et al. 2019), essentially allowing Mec1 to maintain the checkpoint (Pelliccioli et al. 2001). It was proposed that the autophosphorylation of Mec1 may be important for delocalization of the Mec1-Ddc2 complex at the break site, which leads to checkpoint exit by deactivation of Rad53 (Memisoglu et al. 2019, Pelliccioli et al. 2001). Interestingly, this study shows that the adaptation phenotypes of *mec1-S1964* mutants can be modified by *rfa2* mutations which suggests that Rfa2 may also function to control Mec1 localization/delocalization that ultimately leads to cell cycle checkpoint maintenance/exit (Figures 5.8, 5.9, 5.13; Table 5.2 for summary).

Table 5.2. Qualitative summary of *rfa2* mutant phenotypes

<i>RFA2</i> allele	Damage Sensitivity	Adaptation			
		<i>RDH54 MEC1</i>	<i>rdh54Δ</i>	<i>mec1-S1964A</i>	<i>mec1-S1964D/E</i>
<i>RFA2</i>	0	Proficient	Deficient	Deficient	Proficient
<i>rfa2-A_x</i>	0	Proficient/Reduced ^a	Deficient ^a	Deficient	Proficient
<i>rfa2-D_x</i>	+++	Proficient ^a	Proficient	Proficient	Proficient
<i>rfa2-ΔN_x</i>	+++	Deficient ^a	Deficient ^a	Deficient	Reduced
<i>rfa2-H2NT</i>	+	Proficient ^a	Proficient ^a	Proficient	Proficient
<i>rfa2-K_xR</i>	0 ^b	Proficient ^b	Proficient ^b	Proficient	Proficient
<i>rfa2-S122A</i>	0	Proficient ^a	Deficient ^a	Deficient	Proficient
<i>rfa2-S238/240A</i>	0	Proficient	Deficient	Deficient	Proficient
<i>rfa2-S122A, S238/240A</i>	ND	ND	ND	Deficient	Proficient
<i>rfa2-S238/240D</i>	ND	ND	Increased	Increased	Proficient

Scale for “Damage Sensitivity”: 0 = not sensitive, + = slightly sensitive, ++ = moderately sensitive, +++ = severely sensitive. Citations for data not shown in this study: ^a(Wilson 2018)

^bWendy Larson unpublished data. Adaptation proficiency data for *rfa2-A_x*, *rfa2-D_x*, and *rfa2-ΔN_x* in an otherwise wild-type strain also shown in Chapter 4. ND = No data.

Rfa2 NT mutants with natural early or hyper- phosphorylation (as observed in other studies with *rfa2-H2NT*, *rfa2-K_xR*; (Wilson 2018), Wendy Larson unpublished data) suggest that the timing and amount of phosphorylated Rfa2 may be driving factors in checkpoint adaptation, especially as Rfa2 phosphorylation (wild-type RFA2) is still observed in the *mec1-S1964A* mutant (Figures 5.6, 5.7), but only *rfa2-D_x*, *rfa2-H2NT*, and *rfa2-K_xR* are able to drive adaptation of the *mec1-S1964A* strain to near wild-type levels (Figure 5.8). Additionally, no Mec1-target site, real or putative, when mutated in Rfa2 (*rfa2-S122*, *rfa2-S238/240*, *rfa2-S122*, *S238/240*) influences adaptation to the same extent as the *Rfa2 NT* mutants (Figures 5.8, 5.13) (Wilson 2018). However, there is an increase in adaptation observed in the *mec1-S1964A* strain containing *rfa2-S238/240D* (Figure 5.13), which suggests that the mechanism for controlling checkpoint adaptation may still involve Mec1. This may be through an intricate feedback loop

between Rfa2 and Mec1/Mec1-mediation that ultimately controls checkpoint exit by the delocalization of Mec1 followed by deactivation of Rad53. It is also possible and not mutually exclusive that there may be a specific order/amount of Rfa2 phosphorylation that is required to get the full effect. Some Rfa2 phosphorylation is observed in a strain containing *rfa2-S122A, S238/240A* (Figure 5.11), which suggests that the Rfa2 NT can still be modified without Mec1 phosphorylating the Rfa2 SQ sites. If it can be shown that the Rfa2 NT is still modified in an *rfa2-S122D, S238/240D* mutant and that mutant shows a similar slight increase in adaptation to the *rfa2-S238/240D* mutant, this may further support that there is an order in which residues must be phosphorylated to promote adaptation. However, the best method to pursue to propose either timing or order of Rfa2 phosphorylation as key factors for checkpoint adaptation would be to analyze Rfa2 protein by mass spectrometry at different time intervals collected from checkpoint adaptation assays.

Shown in this study is the ability of *Rfa2 NT* mutants to override the adaptation phenotypes displayed by *mec1-S1964* mutants (Figures 5.8, 5.9, 5.13), suggesting that Mec1 activity may be regulated by Rfa2. Supported by results from the prior study of *mec1-S1964* mutants (Memisoglu et al. 2019), the current proposition is that the *Rfa2 NT* mutations may affect Mec1 localization. To provide further support for this hypothesis, Ddc2-Mec1 complex localization should be investigated in strains containing *rfa2* mutations.

Acknowledgements

Trevor Baumgartner provided JKM179 genomic DNA. Cristian (Cris) Hernandez generated the pRS315 *rfa2* mutant plasmids containing *rfa2-S238/240A* and performed the work shown in **Figure 5.11 and Figure 5.12A**. Wendy Larson generated the pRS315-*rfa2-S238/240D* plasmid, provided mini-prepped pRS315-*rfa2* mutant plasmids for me to generate *rfa2* mutants by plasmid shuffle, and performed the work shown in **Figure 5.12B**. The NDSU Core Biology facility provided the iBright FL1500 imager. Dr. Wilkinson and Wilkinson lab Sujata Birua and Sierra Giebel permitted and assisted with use of the myECL™ (Thermo Scientific) imager and myImageAnalysis™ software (Thermo Scientific).

CHAPTER 6: CONCLUDING DISCUSSION

The major focus of this dissertation was to investigate the role of Rfa2 during meiosis and the DNA damage response (DDR). The Rfa1 DBD-F domain was also investigated in relation to Rfa2. Rfa1 and Rfa2 comprise two out of the three subunits of the ssDNA binding complex in *Saccharomyces cerevisiae*, Replication Factor A (RFA). RFA is required for DNA replication, repair, recombination, and cell cycle regulation (Wold 1997, Lee et al. 1998, Soustelle et al. 2002, Ghospurkar et al. 2015b).

Chapter 3 demonstrates that DBD-F (Rfa1) participates in DNA-damage sensitive interactions with proteins identified in a yeast two-hybrid screen, that Rfa2 is phosphorylated in a DBD-F mutant (*rfa1-t11*), and that an Rfa2 phosphomimetic mutation increases the DNA damage sensitivity of cells with a defective checkpoint. Chapter 4 demonstrates that the Rfa2 NT is needed for meiotic progression and that the meiotic progression defect of *rfa2-ΔN_x* mutant cells is not due to an apparent defect in DNA replication or homologous recombination by the 4 different assessments of HR performed. Chapter 5 suggests that Rfa2 regulates Mec1 checkpoint signaling because mutations that mimic or lead to earlier phosphorylation of Rfa2 rescue the adaptation-deficient *mec1-S1964A* mutant that was proposed to be deficient by prolongment of Ddc2-Mec1 localization. Results of this dissertation suggest that Rfa2 phosphorylation alters the DNA damage response (DDR) more significantly than other proteins involved in DDR establishment/maintenance, such as components of the checkpoint clamp, Rad9 (Rad53 adaptor), and Mec1 (sensor kinase). While Rfa2 phosphorylation appears to have a more significant effect on the DDR, phosphorylation does not appear to be required in cells that do not have checkpoint deficiencies for a DDR response like wild-type cells during both mitosis and meiosis. However, the Rfa2 NT is required for proper progression through meiosis which suggests that the presence

of the Rfa2 NT may be necessary to prevent or alleviate Rad53 function during meiosis as it has been shown to do during a mitotic DDR. This discussion chapter focuses on the results of those research chapters along with work from the fields of RFA, the DNA damage response, and meiosis to propose a mechanism that links HR repair and cell cycle regulation involving both the Rfa2 NT and Rfa1 DBD-F and suggests future research that would support the proposed mechanism.

RFA during the DNA Damage Response and Meiosis

RFA involvement in transcription

RFA has been hypothesized previously to be involved in transcriptional regulation of repair genes due to binding of two upstream repressing sequence (URS) elements (Singh and Samson 1995). Further, *rfa2-ΔN40* (Rfa2 N-terminal deletion) and *set1Δ*-induced hyperphosphorylated Rfa2 have been demonstrated to increase gene expression of repair genes downstream of a URS site (Schramke et al. 2001). In human cells it has been suggested that RPA^{RFA} and ATR^{MEC1} may have a role in modulating the transcriptional response of the tumor suppressor p53 (TP53) during transcriptional stress or the DNA damage response (Ljungman 2007, Kaustov et al. 2006) TP53 has been previously identified to interact with DBD-F (Bochkareva et al. 2005, Li and Botchan 1993) and was also identified to interact with human DBD-F in the yeast two-hybrid screen performed in this study (Table 3.3). In addition to the identification of TP53, the yeast two-hybrid screen identified 5 other proteins with known involvement in transcription that interact with human DBD-F and one transcriptional regulator was identified to interact with yeast DBD-F (Tables 3.2, 3.3). As each protein identified had a DNA damage sensitive reduction in interaction with its respective DBD-F, this is additional

support for a role for RPA/RFA in transcription that may be modified under DNA damage conditions.

Appearance of phospho-Rfa2 correlated with time of Rad53 “deactivation”

It has been demonstrated previously that reappearance of unmodified Rad53 is correlated with the appearance of hyperphosphorylated Rfa2 (Wilson 2018). Additionally, phosphomimetic Rfa2 or Rfa2 mutants that are naturally phosphorylated earlier/more than wild-type Rfa2 promote checkpoint adaptation in adaptation-deficient strain backgrounds (Ghospurkar et al. 2015b, Wilson 2018). The Rfa2 NT appears to be required to alleviate checkpoint arrest; however, Rfa2 NT phosphorylation is only necessary for alleviation of a checkpoint when additional mutations exist since *rfa2-A_x* single mutants display similar phenotypes to wild-type. These prior results have been reiterated and similar effects have been observed in additional strains in this study (Figures 4.6, 4.7, 5.8, 5.9). This suggests that the status of the Rfa2 NT has the greatest impact on the outcome of a DDR checkpoint over at least all checkpoint proteins tested thus far.

Similar phenotypes of Rfa1-DBD-F (*rfa1-t11*) and Rfa2 (*rfa2-Dx*) mutations are likely caused by different, yet related mechanisms

The Rfa1-DBD-F mutant (*rfa1-t11*) has been demonstrated to have reduced recruitment of repair factors such as Mec1 and the checkpoint clamp (Chen et al. 1998, Umezumi et al. 1998, Soustelle et al. 2002, Seeber et al. 2016, Deshpande et al. 2017, Zou et al. 2003). The checkpoint established upon DNA damage in *rfa1-t11* mutant cells may be weaker since DBD-F may not be able to keep or recruit enough checkpoint proteins to the break to maintain a strong checkpoint response (Bonilla et al. 2008). The checkpoint may be further weakened after Rfa2 phosphorylation occurs in *rfa1-t11* cells (Wilson 2018) (Figure 3.3), since Rfa2 phosphorylation

has been demonstrated to promote checkpoint adaptation (Ghospurkar et al. 2015b, Wilson 2018) (Figures 4.6, 4.7, 5.8, 5.9). Thus, checkpoint adaptation observed in the *rfa1-t11* mutant may be a result of reduced interactions with checkpoint proteins plus the role of Rfa2 phosphorylation that leads to checkpoint exit.

It does not appear that the phenotypes of *rfa1* and *rfa2* mutants are caused by a resection defect (*i.e.*, not caused by a reduction/increase of repair factors on ssDNA as a result of how much RFA is present as it relates to the amount of resected DNA), because no striking difference in resection was observed between wild-type and each of the following mutants: *rfa1-t11*, *rfa2-A_x*, *rfa2-D_x*, *rfa2-ΔN_x*, and *rfa2-H2NT* in a qPCR assay measuring resection of the *MAT* locus 4 hours after break induction (Wilson 2018). Prior studies observing resection in an *rfa1-t11* mutant have either found no difference (Lee et al. 1998) or only subtle differences (Soustelle et al. 2002) in initial resection when compared to the wild-type strain. While resected fragments accumulate post 24 hours in the *rfa1-t11* mutant, this defect has been attributed to a defect in repair rather than a defect in resection per se (Soustelle et al. 2002). The defect in repair (specifically HR) occurring in the *rfa1-t11* mutant is supported by the reduced recombination frequency observed at the *ARG4* hot spot during meiosis (Soustelle et al. 2002) and during mating type switching (Umezu et al. 1998) (Appendix H).

Conversely, the *rfa2 NT* mutants examined do not have an apparent defect in HR repair (Figures 4.11, 4.12, Tables 4.3, 4.4, Appendix H). Rather, it is suggested that the *rfa2 NT* mutants may affect Ddc2-Mec1 localization due to the recent work implicating Mec1-S1964 autophosphorylation as a means to promote checkpoint adaptation by the delocalization of Ddc2-Mec1 (Memisoglu et al. 2019) and the demonstrated influence the *rfa2 NT* mutations have on *mec1-S1964* mutants during checkpoint adaptation (Figures 5.8, 5.9). Thus, it is proposed that

Rfa2 phosphorylation also promotes Ddc2 delocalization to physically affect the ability of Mec1 to localize to sites of damage, thereby affecting the downstream activation of Rad53.

Rfa2 phosphorylation may prevent Rad53 function during meiosis

Unlike mitosis, the Rfa2 NT is phosphorylated early by Ime2 (meiosis-specific kinase) during meiosis (Clifford et al. 2005). Mec1 and other mitotic checkpoint proteins have been demonstrated to maintain the MI meiotic arrest of *dmc1Δ* mutants and contribute to the formation of viable tetrads, which suggests that these mitotic checkpoint proteins also have a role during meiosis (Lydall et al. 1996). Interestingly, Rad9-Rad53 do not appear to have a checkpoint function during MI, rather the checkpoint roles they have during mitosis seem to be replaced by Hop1-Mek1 during MI to ensure interhomolog repair over sister chromatid repair (Lydall et al. 1996, Cartagena-Lirola et al. 2008, Hunter 2008, Carballo et al. 2008, Niu et al. 2007, Niu et al. 2005, Usui and Kanehara 2013). However, recent evidence has suggested that Rad53 may have a different role during MI in maintaining meiotic commitment (Ballew and Lacefield 2019).

Chapter 4 clearly demonstrates that the presence of the Rfa2 NT is needed for proper progression through meiotic divisions, because *rfa2-ΔN_x* mutants have a reduction in tetrad formation with increased dyads and severely reduced spore viability (Table 4.2, Figure 4.9, Appendix I: Table I3). The reduction in tetrad formation with an increase in dyads observed via light microscopy is supported by analysis of nuclear divisions which suggests that *rfa2-ΔN_x* mutants have issues in proceeding from MI through the MII division (Table 4.2, Figure 4.10B). This defect in progression through the mitotic-like MII is eerily similar to the mitotic checkpoint adaptation-deficiency of strains containing *rfa2-ΔN_x* that is observed physiologically by microscopy and biochemically by prolonged activation of Rad53 (Figures 4.6, 4.7, 5.8, 5.9) that prevents mitotic progression. Naturally, Rad53 modification was then investigated in meiotic

samples; however, Rad53 activation (phosphorylation) was not easily discernible in meiotic samples and detection of obvious modifications were not reproducible up to this point (Figure 4.16). Even though Rad53 activation (phosphorylation) was not readily detected in meiotic samples, it is possible that Rad53 is indeed functioning to interfere with proper procedure through meiosis in *rfa2-ΔN_x* mutants, because (1) it has been demonstrated that Rad53 phosphorylation is not detected when breaks are repairable (Pelliccioli et al. 2001) and (2) there appears to be a novel role for Rad53 in maintaining meiotic commitment (Ballew and Lacefield 2019). If missing the Rfa2 NT does allow for Rad53 to function as it does in mitosis, this also alludes that the repair bias of sporulating cells may not be strongly in favor of using homologous chromosomes for HR and could be allowing more sister chromatid repair in MI, leading to chromosome missegregation and the formation of inviable spores.

RFA removal from DNA

There is evidence to suggest that phosphorylated Rfa2 may be easier to remove from DNA. This evidence is a bit contradictory if taken without explanation. Studies that have investigated binding affinity of the human homolog RPA^{RFA} for DNA *in vitro* have found that phosphorylated/phospho-mimetic RPA2 has a decreased affinity for dsDNA but not ssDNA (Binz et al. 2003, Vassin, Wold and Borowiec 2004). Yeast data supports that phosphorylated Rfa2 may also have a decreased affinity for dsDNA by the work showing that URS1 sites are not bound as well by phosphorylated Rfa2 (Schramke et al. 2001).

One study that contradicts the above statements utilized *in vivo* damaged-induced phosphorylated RPA2 from mouse cell extracts to suggest a decreased affinity for ssDNA and replication factors (Fried et al. 1996). However, the later investigation by Vassin *et al.* has suggested that decreased affinity for ssDNA is not directly caused by phosphorylated RPA2,

since phospho-mimetic RPA2 binds ssDNA as well as wild-type RPA2 *in vitro* (Vassin et al. 2004). Rather it is suggested that *in vivo* it appears as though RPA2 has less affinity for ssDNA because phosphorylation modifies with which proteins RPA interacts and those proteins are ones that may promote the removal of RPA (Vassin et al. 2004, Wu et al. 2005) by virtue of them replacing RPA on ssDNA.

While no part of this work demonstrates that phosphorylated Rfa2 is easier to remove from DNA, what this work does show in Chapter 4 is that the *rfa2* mutants (*rfa2-Ax*, *rfa2-Dx*, *rfa2-ΔNx*) do not appear to have any major replication defect when compared to the wild-type RFA2 strain (Figure 4.10A). This implies that all mutants can interact with DNA well enough to facilitate DNA replication and therefore suggests that any defect the mutants might have involving DNA excludes replication processes.

Proposed Mechanism

Shown is the interaction between RFA, Mec1, and Rad53 that leads to establishment of a checkpoint (Figure 6.1). To allow for progression of the cell cycle, the following mechanism proposed essentially removes RFA from the ssDNA to limit Mec1 activity at the break site (Figures 6.2, 6.3). To achieve removal of RFA from ssDNA, Rfa2 is phosphorylated which promotes the recruitment of recombinases (Rad52/Rad51 in mitosis, Rad51/Dmc1 in meiosis). The loading of the recombinases onto ssDNA is proposed to be facilitated by DBD-F, this not only leads to the displacement of RFA but also physically places DBD-F in proximity with phosphorylated Rfa2 (Figure 6.2). While DBD-F is facilitating loading of recombinases it is unable to also interact with checkpoint proteins (such as Ddc2/Mec1, Figure 6.2). Once RFA is removed, DBD-F and phosphorylated Rfa2 are still near each other, so their interaction is promoted (Figure 6.3). This mechanism prevents DBD-F from interacting with other checkpoint

proteins still localized at the break site (*i.e.*, allows all checkpoint proteins to be removed from the DNA, since interactions occurring with RFA DBD-F to hold everything together, would now be completely inhibited, Figure 6.3).

During mitosis, the above mechanism promotes deactivation of the checkpoint, because the “activated” Rad53 pool is no longer maintained. When the checkpoint is active and maintained, additional, unmodified Rad53 is recruited to the break site and activated after interaction with Mec1 and other localized checkpoint proteins. During checkpoint adaptation or checkpoint exit, if Mec1 is no longer localized any additional, unmodified Rad53 recruited does not get activated. When new “active Rad53” is not added to the pool, the balance of activated Rad53 to inactivated Rad53 shifts towards inactivated Rad53 through dephosphorylation or degradation of the remaining activated Rad53.

During meiosis, the proposed mechanism is primed prior to programmed DNA damage by the act of phosphorylating Rfa2. It is proposed that this promotes faster recruitment of recombinases to replace RFA on ssDNA and/or limits the time Mec1 spends at the break site, both of which could help bias repair towards HR via homologous chromosomes and inhibit Rad53 from recognizing the damage and becoming activated during MI. Since additional mechanisms exist that also promote repair bias during meiosis and increase available HR proteins, Rfa2 phosphorylation may be a redundant mechanism to increase HR repair bias which is supported by the observation that Rfa2 phosphorylation appears dispensable. However, the Rfa2 NT is required for meiotic progression, suggesting that the presence of the NT may be necessary for timely removal of RFA from ssDNA to keep Rad53 from influencing repair during MI and/or alleviating Rad53-mediated arrest if breaks persist into MII. It is unknown what effects Rad53 may have on MI if it is “naturally” able to detect and influence repair during MI

(i.e., not in the context of Rad53 over expression, targeting to DSBs, nor in the presence of all other meiotic HR repair proteins) and how this might influence Mek1 activity. It is plausible that the interaction of Rad53 with DSBs increases the activity of Mek1 (since Mek1 may not be associated with these DSBs detected by Rad53), which might cause the generation of additional, unrepaired DSBs as the cell divides in MI, similarly to what has been observed with a more active version of Mek1 (Wu et al. 2010).

Future Directions

The following items are proposed to further test the validity of the proposed mechanism.

Investigate if Rad53 is the cause for the meiotic progression defect of *rfa2-ΔN_x* mutant cells by deleting Rad9, the Rad53 adaptor, to prevent recruitment of Rad53 to programmed DNA damage. Because if Rad53 activity is causing the meiotic progression defects of *rfa2-ΔN_x*, then preventing Rad53 from localizing to the DSB and becoming active might allow for a normal meiosis. Thus, *rad9Δ rfa2-ΔN_x* double mutants should proceed through meiosis like wild-type cells. Chromosome dynamics of *rfa2-ΔN_x* mutant cells undergoing meiosis should also be examined to determine if there is any apparent defect in chromosome segregation leading to the formation of inviable spores. Additionally, it could be investigated whether *rfa2-ΔN_x* cells have unrepaired DSBs after the MI division.

Interestingly, *rad52Δ* (codes for Rad52 protein in the Rad51 recombination pathway) cells are adaptation-proficient unless combined with another adaptation-proficient mutation, *rfa1-t11* (Lee et al. 2003). While Rad52 is required for Rad51-mediated DSB repair, it is unclear whether *in vivo* replacement of RFA with Rad51 (with no repair) requires Rad52. *In vitro* curtain assays suggest this may be possible since Rad51 is able to replace RFA on ssDNA (Gibb et al. 2014). These prior data support the idea that Rfa2 phosphorylation might promote recruitment of

HR repair proteins, while Rfa1 DBD-F may be required for loading HR repair proteins. This idea may be further supported if adaptation-deficient *rad51Δ* mutant cells are unable to be rescued by the *rfa2-D_x* mutation. If the Rad51 recombinase replacing RFA on the DNA is key for how the *rfa2-D_x* mutation is promoting adaptation in adaptation-deficient strains, then the *rad51Δ rfa2-D_x* mutant should remain adaptation-deficient. Additionally, if this replacement of RFA changes the amount of time the Ddc2-Mec1 is able to detect a DSB by localization, investigating Ddc2-Mec1 localization in *rfa2* mutants during checkpoint adaptation might reveal that the amount of time Ddc2-Mec1 is localized is contingent on the Rfa2 NT (prolonged localization with the *rfa2-ΔN_x* mutation and shortened localization with the *rfa2-D_x* mutation).

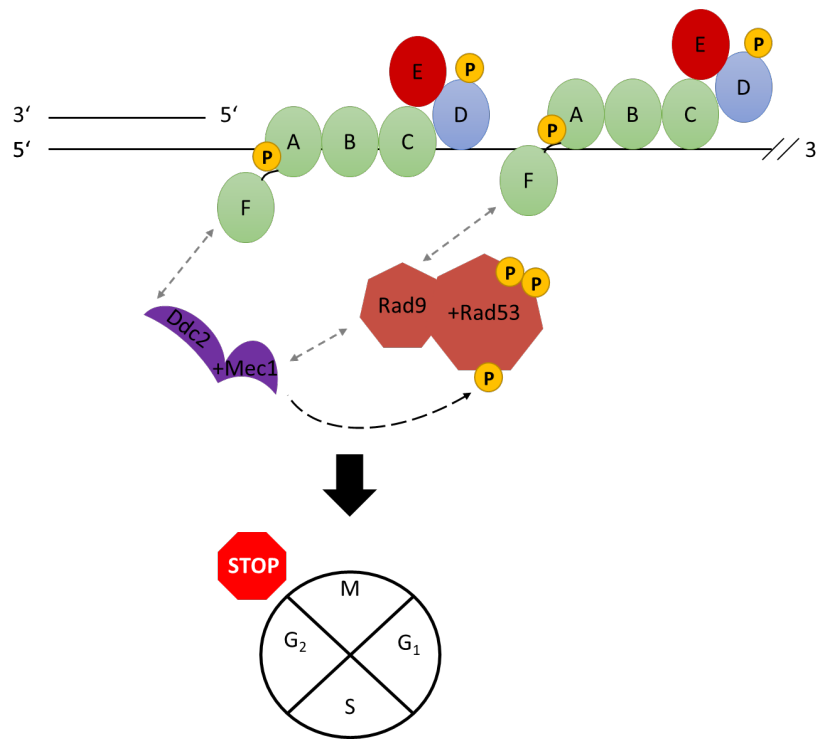


Figure 6.1. Model for interaction between RFA, Mec1, and Rad53 to stop the cell cycle
 Demonstrates that Mec1 is localized to the break site by Ddc2-RFA(DBD-F) interaction. Rad9-Rad53 is also localized to the break site by Rad9-DBD-F interaction, shown with an adjacent RFA complex. After Mec1-Rad9 interaction, Mec1 phosphorylates Rad53, which primes Rad53 for auto-phosphorylation leading to activated Rad53 to stop the cell cycle at the G₂/M checkpoint during mitosis. Also depicted are Mec1-dependent phospho-groups on RFA, Rfa1-S178 and Rfa2-S122.

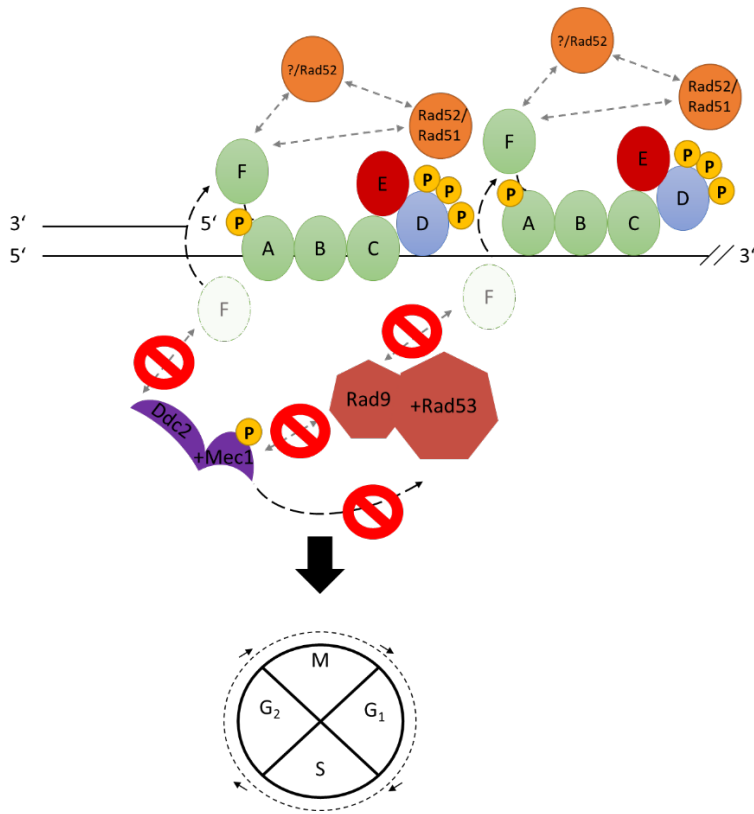


Figure 6.2. Model that promotes removal of RFA from ssDNA, limiting Mec1 activity

When Rfa2 is phosphorylated and Mec1 is auto-phosphorylated: Mec1 is unable to remain at the break site due to the recruitment of recombinases (During meiosis Rad51 and Dmc1, not shown for simplicity) which are subsequently loaded by DBD-F facilitation. Once RFA is replaced on ssDNA, DBD-F interacts with phosphorylated Rfa2 to prevent any additional interactions with Ddc2-Mec1. Because Mec1 is no longer present, additional Rad53 does not get activated and previously activated Rad53 is either dephosphorylated or ubiquitinated for degradation, leading to the continuation of the cell cycle. Also depicted is Mec1-S1964 phosphorylation implicated as an influence on Ddc2-Mec1 localization (Memisoglu et al. 2019).

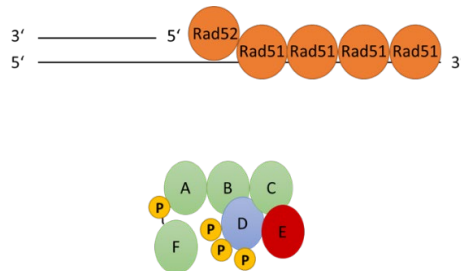


Figure 6.3. Model that prevents DBD-F from additional interactions with repair proteins once RFA is displaced

DBD-F interacts with phosphorylated Rfa2, this makes DBD-F unable to interact with repair proteins, such as: Ddc2-Mec1, Rad9-Rad53, Sgs1-Dna2, the clamp loader (Rad24, Rfc2-5), or the clamp (Rad17-Ddc1-Mec3).

REFERENCES

- Arunkumar, A. I., M. E. Stauffer, E. Bochkareva, A. Bochkarev & W. J. Chazin (2003) Independent and coordinated functions of replication protein A tandem high affinity single-stranded DNA binding domains. *J Biol Chem*, 278, 41077-82.
- Attner, M. A. & A. Amon (2012) Control of the mitotic exit network during meiosis. *Mol Biol Cell*, 23, 3122-32.
- Bae, K. H., H. S. Kim, S. H. Bae, H. Y. Kang, S. Brill & Y. S. Seo (2003) Bimodal interaction between replication-protein A and Dna2 is critical for Dna2 function both in vivo and in vitro. *Nucleic Acids Res*, 31, 3006-15.
- Ballew, O. & S. Lacefield (2019) The DNA Damage Checkpoint and the Spindle Position Checkpoint Maintain Meiotic Commitment in *Saccharomyces cerevisiae*. *Curr Biol*, 29, 449-460.e2.
- Bao, Z., H. Xiao, J. Liang, L. Zhang, X. Xiong, N. Sun, T. Si & H. Zhao (2015) Homology-Integrated CRISPR-Cas (HI-CRISPR) System for One-Step Multigene Disruption in *Saccharomyces cerevisiae*. *ACS Synthetic Biology*, 4, 585-594.
- Bartrand, A. J., D. Iyasu & G. S. Brush (2004) DNA stimulates Mec1-mediated phosphorylation of replication protein A. *J Biol Chem*, 279, 26762-7.
- Bartrand, A. J., D. Iyasu, S. M. Marinco & G. S. Brush (2006) Evidence of meiotic crossover control in *Saccharomyces cerevisiae* through Mec1-mediated phosphorylation of replication protein A. *Genetics*, 172, 27-39.
- Bastin-Shanower, S. A. & S. J. Brill (2001) Functional analysis of the four DNA binding domains of replication protein A. The role of RPA2 in ssDNA binding. *J Biol Chem*, 276, 36446-53.
- Belanger, K. D., A. L. Griffith, H. L. Baker, J. N. Hansen, L. A. Kovacs, J. S. Seconi & A. C. Strine (2011) The karyopherin Kap95 and the C-termini of Rfa1, Rfa2, and Rfa3 are necessary for efficient nuclear import of functional RPA complex proteins in *Saccharomyces cerevisiae*. *DNA Cell Biol*, 30, 641-51.
- Benjamin, K. R., C. Zhang, K. M. Shokat & I. Herskowitz (2003) Control of landmark events in meiosis by the CDK Cdc28 and the meiosis-specific kinase Ime2. *Genes Dev*, 17, 1524-39.
- Binz, S. K., Y. Lao, D. F. Lowry & M. S. Wold (2003) The phosphorylation domain of the 32-kDa subunit of replication protein A (RPA) modulates RPA-DNA interactions. Evidence for an intersubunit interaction. *J Biol Chem*, 278, 35584-91.
- Bishop, D. K., D. Park, L. Xu & N. Kleckner (1992) DMC1: a meiosis-specific yeast homolog of *E. coli recA* required for recombination, synaptonemal complex formation, and cell cycle progression. *Cell*, 69, 439-56.
- Bochkarev, A., R. A. Pfuetzner, A. M. Edwards & L. Frappier (1997) Structure of the single-stranded-DNA-binding domain of replication protein A bound to DNA. *Nature*, 385, 176-81.
- Bochkareva, E., L. Kaustov, A. Ayed, G. S. Yi, Y. Lu, A. Pineda-Lucena, J. C. Liao, A. L. Okorokov, J. Milner, C. H. Arrowsmith & A. Bochkarev (2005) Single-stranded DNA mimicry in the p53 transactivation domain interaction with replication protein A. *Proc Natl Acad Sci U S A*, 102, 15412-7.

- Bochkareva, E., S. Korolev, S. P. Lees-Miller & A. Bochkarev (2002) Structure of the RPA trimerization core and its role in the multistep DNA-binding mechanism of RPA. *Embo j*, 21, 1855-63.
- Bolte, M., P. Steigemann, G. H. Braus & S. Irniger (2002) Inhibition of APC-mediated proteolysis by the meiosis-specific protein kinase Ime2. *Proc Natl Acad Sci U S A*, 99, 4385-90.
- Bonilla, C. Y., J. A. Melo & D. P. Toczyski (2008) Colocalization of sensors is sufficient to activate the DNA damage checkpoint in the absence of damage. *Mol Cell*, 30, 267-76.
- Brill, S. J. & B. Stillman (1991) Replication factor-A from *Saccharomyces cerevisiae* is encoded by three essential genes coordinately expressed at S phase. *Genes Dev*, 5, 1589-600.
- Brush, G. S., D. M. Clifford, S. M. Marinco & A. J. Bartrand (2001) Replication protein A is sequentially phosphorylated during meiosis. *Nucleic Acids Res*, 29, 4808-17.
- Brush, G. S. & T. J. Kelly (2000) Phosphorylation of the replication protein A large subunit in the *Saccharomyces cerevisiae* checkpoint response. *Nucleic Acids Res*, 28, 3725-32.
- Brush, G. S., D. M. Morrow, P. Hieter & T. J. Kelly (1996) The ATM homologue MEC1 is required for phosphorylation of replication protein A in yeast. *Proc Natl Acad Sci U S A*, 93, 15075-80.
- Cannavo, E., P. Cejka & S. C. Kowalczykowski (2013) Relationship of DNA degradation by *Saccharomyces cerevisiae* exonuclease 1 and its stimulation by RPA and Mre11-Rad50-Xrs2 to DNA end resection. *Proc Natl Acad Sci U S A*, 110, E1661-8.
- Carballo, J. A. & R. S. Cha (2007) Meiotic roles of Mec1, a budding yeast homolog of mammalian ATR/ATM. *Chromosome Res*, 15, 539-50.
- Carballo, J. A., A. L. Johnson, S. G. Sedgwick & R. S. Cha (2008) Phosphorylation of the axial element protein Hop1 by Mec1/Tel1 ensures meiotic interhomolog recombination. *Cell*, 132, 758-70.
- Cartagena-Lirola, H., I. Guerini, N. Manfrini, G. Lucchini & M. P. Longhese (2008) Role of the *Saccharomyces cerevisiae* Rad53 checkpoint kinase in signaling double-strand breaks during the meiotic cell cycle. *Mol Cell Biol*, 28, 4480-93.
- Cartagena-Lirola, H., I. Guerini, V. Viscardi, G. Lucchini & M. P. Longhese (2006) Budding Yeast Sae2 is an In Vivo Target of the Mec1 and Tel1 Checkpoint Kinases During Meiosis. *Cell Cycle*, 5, 1549-59.
- Cejka, P., E. Cannavo, P. Polaczek, T. Masuda-Sasa, S. Pokharel, J. L. Campbell & S. C. Kowalczykowski (2010) DNA end resection by Dna2-Sgs1-RPA and its stimulation by Top3-Rmi1 and Mre11-Rad50-Xrs2. *Nature*, 467, 112-116.
- Chan, S. P., D. I. Kao, W. Y. Tsai & S. C. Cheng (2003) The Prp19p-associated complex in spliceosome activation. *Science*, 302, 279-82.
- Chen, C., K. Umezū & R. D. Kolodner (1998) Chromosomal rearrangements occur in *S. cerevisiae* rfa1 mutator mutants due to mutagenic lesions processed by double-strand-break repair. *Mol Cell*, 2, 9-22.
- Chen, H., M. Lisby & L. S. Symington (2013) RPA coordinates DNA end resection and prevents formation of DNA hairpins. *Mol Cell*, 50, 589-600.
- Chen, X., R. Gaglione, T. Leong, L. Bednorz, T. de Los Santos, E. Luk, M. Airola & N. M. Hollingsworth (2018) Mek1 coordinates meiotic progression with DNA break repair by directly phosphorylating and inhibiting the yeast pachytene exit regulator Ndt80. *PLoS Genet*, 14, e1007832.

- Cheng, X., O. Jobin-Robitaille, P. Billon, R. Buisson, H. Niu, N. Lacoste, N. Abshiru, V. Côté, P. Thibault, S. J. Kron, P. Sung, C. J. Brandl, J. Y. Masson & J. Côté (2018) Phospho-dependent recruitment of the yeast NuA4 acetyltransferase complex by MRX at DNA breaks regulates RPA dynamics during resection. *Proc Natl Acad Sci U S A*, 115, 10028-10033.
- Cho, S. W., S. Kim, Y. Kim, J. Kweon, H. S. Kim, S. Bae & J. S. Kim (2014) Analysis of off-target effects of CRISPR/Cas-derived RNA-guided endonucleases and nickases. *Genome Res*, 24, 132-41.
- Chu, D. B., T. Gromova, T. A. C. Newman & S. M. Burgess (2017) The Nucleoporin Nup2 Contains a Meiotic-Autonomous Region that Promotes the Dynamic Chromosome Events of Meiosis. *Genetics*, 206, 1319-1337.
- Chu, S., J. DeRisi, M. Eisen, J. Mulholland, D. Botstein, P. O. Brown & I. Herskowitz (1998) The transcriptional program of sporulation in budding yeast. *Science*, 282, 699-705.
- Clerici, M., D. Mantiero, G. Lucchini & M. P. Longhese (2005) The *Saccharomyces cerevisiae* Sae2 protein promotes resection and bridging of double strand break ends. *J Biol Chem*, 280, 38631-8.
- Clerici, M., V. Paciotti, V. Baldo, M. Romano, G. Lucchini & M. P. Longhese (2001) Hyperactivation of the yeast DNA damage checkpoint by TEL1 and DDC2 overexpression. *Embo j*, 20, 6485-98.
- Clifford, D. M., S. M. Marinco & G. S. Brush (2004) The meiosis-specific protein kinase Ime2 directs phosphorylation of replication protein A. *J Biol Chem*, 279, 6163-70.
- Clifford, D. M., K. E. Stark, K. E. Gardner, S. Hoffmann-Benning & G. S. Brush (2005) Mechanistic insight into the Cdc28-related protein kinase Ime2 through analysis of replication protein A phosphorylation. *Cell Cycle*, 4, 1826-33.
- Cloud, V., Y. L. Chan, J. Grubb, B. Budke & D. K. Bishop (2012) Rad51 is an accessory factor for Dmcl-mediated joint molecule formation during meiosis. *Science*, 337, 1222-5.
- Cong, L., F. A. Ran, D. Cox, S. Lin, R. Barretto, N. Habib, P. D. Hsu, X. Wu, W. Jiang, L. A. Marraffini & F. Zhang (2013) Multiplex genome engineering using CRISPR/Cas systems. *Science*, 339, 819-23.
- Conrad, M. N., A. M. Dominguez & M. E. Dresser (1997) Ndj1p, a meiotic telomere protein required for normal chromosome synapsis and segregation in yeast. *Science*, 276, 1252-5.
- de la Torre-Ruiz, M. A., C. M. Green & N. F. Lowndes (1998) RAD9 and RAD24 define two additive, interacting branches of the DNA damage checkpoint pathway in budding yeast normally required for Rad53 modification and activation. *Embo j*, 17, 2687-98.
- Deshpande, I., A. Seeber, K. Shimada, J. J. Keusch, H. Gut & S. M. Gasser (2017) Structural Basis of Mec1-Ddc2-RPA Assembly and Activation on Single-Stranded DNA at Sites of Damage. *Mol Cell*, 68, 431-445.e5.
- Dirick, L., L. Goetsch, G. Ammerer & B. Byers (1998) Regulation of meiotic S phase by Ime2 and a Clb5,6-associated kinase in *Saccharomyces cerevisiae*. *Science*, 281, 1854-7.
- Ellison, V. & B. Stillman (2003) Biochemical characterization of DNA damage checkpoint complexes: clamp loader and clamp complexes with specificity for 5' recessed DNA. *PLoS Biol*, 1, E33.
- Fan, J. & N. P. Pavletich (2012) Structure and conformational change of a replication protein A heterotrimer bound to ssDNA. *Genes Dev*, 26, 2337-47.

- Foiani, M., E. Nadjar-Boger, R. Capone, S. Sagee, T. Hashimshoni & Y. Kassir (1996) A meiosis-specific protein kinase, Ime2, is required for the correct timing of DNA replication and for spore formation in yeast meiosis. *Mol Gen Genet*, 253, 278-88.
- Fried, L. M., C. Koumenis, S. R. Peterson, S. L. Green, P. van Zijl, J. Allalunis-Turner, D. J. Chen, R. Fishel, A. J. Giaccia, J. M. Brown & C. U. Kirchgesner (1996) The DNA damage response in DNA-dependent protein kinase-deficient SCID mouse cells: replication protein A hyperphosphorylation and p53 induction. *Proc Natl Acad Sci U S A*, 93, 13825-30.
- Fu, Y., J. A. Foden, C. Khayter, M. L. Maeder, D. Reyon, J. K. Joung & J. D. Sander (2013) High-frequency off-target mutagenesis induced by CRISPR-Cas nucleases in human cells. *Nat Biotechnol*, 31, 822-6.
- Fu, Y., J. D. Sander, D. Reyon, V. M. Cascio & J. K. Joung (2014) Improving CRISPR-Cas nuclease specificity using truncated guide RNAs. *Nat Biotechnol*, 32, 279-284.
- Gailus-Durner, V., C. Chintamaneni, R. Wilson, S. J. Brill & A. K. Vershon (1997) Analysis of a meiosis-specific URS1 site: sequence requirements and involvement of replication protein A. *Mol Cell Biol*, 17, 3536-46.
- Galgoczy, D. J. & D. P. Toczyski (2001) Checkpoint adaptation precedes spontaneous and damage-induced genomic instability in yeast. *Mol Cell Biol*, 21, 1710-8.
- Ghospurkar, P. L. 2015. Characterization of RPA2 N-Terminal Function in the DNA Damage Response in *Saccharomyces cerevisiae*. In *Chemistry and Biochemistry*, 201. Fargo, North Dakota: North Dakota State University of Agriculture and Applied Science.
- Ghospurkar, P. L., T. M. Wilson, S. Liu, A. Herauf, J. Steffes, E. N. Mueller, G. G. Oakley & S. J. Haring (2015a) Phosphorylation and cellular function of the human Rpa2 N-terminus in the budding yeast *Saccharomyces cerevisiae*. *Exp Cell Res*, 331, 183-99.
- Ghospurkar, P. L., T. M. Wilson, A. L. Severson, S. J. Klein, S. K. Khaku, A. P. Walther & S. J. Haring (2015b) The DNA damage response and checkpoint adaptation in *Saccharomyces cerevisiae*: distinct roles for the replication protein A2 (Rfa2) N-terminus. *Genetics*, 199, 711-27.
- Gibb, B., L. F. Ye, S. C. Gergoudis, Y. Kwon, H. Niu, P. Sung & E. C. Greene (2014) Concentration-dependent exchange of replication protein A on single-stranded DNA revealed by single-molecule imaging. *PLoS One*, 9, e87922.
- Gomes, X. V. & M. S. Wold (1996) Functional domains of the 70-kilodalton subunit of human replication protein A. *Biochemistry*, 35, 10558-68.
- Grushcow, J. M., T. M. Holzen, K. J. Park, T. Weinert, M. Lichten & D. K. Bishop (1999) *Saccharomyces cerevisiae* checkpoint genes MEC1, RAD17 and RAD24 are required for normal meiotic recombination partner choice. *Genetics*, 153, 607-20.
- Guillemain, G., E. Ma, S. Mauger, S. Miron, R. Thai, R. Guerois, F. Ochsenein & M. C. Marsolier-Kergoat (2007) Mechanisms of checkpoint kinase Rad53 inactivation after a double-strand break in *Saccharomyces cerevisiae*. *Mol Cell Biol*, 27, 3378-89.
- Haring, S. J., G. R. Halley, A. J. Jones & R. E. Malone (2003) Properties of natural double-strand-break sites at a recombination hotspot in *Saccharomyces cerevisiae*. *Genetics*, 165, 101-14.
- Haring, S. J., T. D. Humphreys & M. S. Wold (2010) A naturally occurring human RPA subunit homolog does not support DNA replication or cell-cycle progression. *Nucleic Acids Res*, 38, 846-58.

- Hassold, T. & P. Hunt (2001) To err (meiotically) is human: the genesis of human aneuploidy. *Nat Rev Genet*, 2, 280-91.
- Hegnauer, A. M., N. Hustedt, K. Shimada, B. L. Pike, M. Vogel, P. Amsler, S. M. Rubin, F. van Leeuwen, A. Guénolé, H. van Attikum, N. H. Thomä & S. M. Gasser (2012) An N-terminal acidic region of Sgs1 interacts with Rpa70 and recruits Rad53 kinase to stalled forks. *Embo j*, 31, 3768-83.
- Herskowitz, I., & R. E. Jensen (1991) Putting the HO gene to work: practical uses for mating-type switching. *Methods Enzymol*, 194, 132-46.
- Honigberg, S. M. & K. Purnapatre (2003) Signal pathway integration in the switch from the mitotic cell cycle to meiosis in yeast. *J Cell Sci*, 116, 2137-47.
- Hunter, N. (2008) Hop1 and the meiotic DNA-damage response. *Cell*, 132, 731-2.
- Jinek, M., K. Chylinski, I. Fonfara, M. Hauer, J. A. Doudna & E. Charpentier (2012) A programmable dual-RNA-guided DNA endonuclease in adaptive bacterial immunity. *Science*, 337, 816-21.
- Kantake, N., T. Sugiyama, R. D. Kolodner & S. C. Kowalczykowski (2003) The recombination-deficient mutant RPA (rfa1-t11) is displaced slowly from single-stranded DNA by Rad51 protein. *J Biol Chem*, 278, 23410-7.
- Kaustov, L., G. S. Yi, A. Ayed, E. Bochkareva, A. Bochkarev & C. H. Arrowsmith (2006) p53 transcriptional activation domain: a molecular chameleon? *Cell Cycle*, 5, 489-94.
- Keelagher, R. E., V. E. Cotton, A. S. Goldman & R. H. Borts (2011) Separable roles for Exonuclease I in meiotic DNA double-strand break repair. *DNA Repair (Amst)*, 10, 126-37.
- Keeney, S. (2008) Spo11 and the Formation of DNA Double-Strand Breaks in Meiosis. *Genome Dyn Stab*, 2, 81-123.
- Keeney, S., C. N. Giroux & N. Kleckner (1997) Meiosis-specific DNA double-strand breaks are catalyzed by Spo11, a member of a widely conserved protein family. *Cell*, 88, 375-84.
- Kim, C., R. O. Snyder & M. S. Wold (1992) Binding properties of replication protein A from human and yeast cells. *Mol Cell Biol*, 12, 3050-9.
- Kim, H. S. & S. J. Brill (2003) MEC1-dependent phosphorylation of yeast RPA1 in vitro. *DNA Repair (Amst)*, 2, 1321-35.
- Kim, S. T., D. S. Lim, C. E. Canman & M. B. Kastan (1999) Substrate specificities and identification of putative substrates of ATM kinase family members. *J Biol Chem*, 274, 37538-43.
- Klapholz, S., C. S. Waddell & R. E. Esposito (1985) The role of the SPO11 gene in meiotic recombination in yeast. *Genetics*, 110, 187-216.
- Koehn, D. R., S. J. Haring, J. M. Williams & R. E. Malone (2009) Tethering recombination initiation proteins in *Saccharomyces cerevisiae* promotes double strand break formation. *Genetics*, 182, 447-58.
- Krokan, H. E. & M. Bjørås (2013) Base excision repair. *Cold Spring Harb Perspect Biol*, 5, a012583.
- Kushnirov, V. V. (2000) Rapid and reliable protein extraction from yeast. *Yeast*, 16, 857-60.
- Lax, C. & S. Fogel (1978) Novel interallelic complementation at the his1 locus of yeast. *Genetics*, 90, 501-16.
- Lee, J. Y., J. B. Steinfeld, Z. Qi, Y. Kwon, P. Sung & E. C. Greene (2017) Sequence imperfections and base triplet recognition by the Rad51/RecA family of recombinases. *J Biol Chem*, 292, 11125-11135.

- Lee, S. E., J. K. Moore, A. Holmes, K. Umezu, R. D. Kolodner & J. E. Haber (1998) Saccharomyces Ku70, mre11/rad50 and RPA proteins regulate adaptation to G2/M arrest after DNA damage. *Cell*, 94, 399-409.
- Lee, S. E., A. Pelliccioli, J. Demeter, M. P. Vaze, A. P. Gasch, A. Malkova, P. O. Brown, D. Botstein, T. Stearns, M. Foiani & J. E. Haber (2000) Arrest, adaptation, and recovery following a chromosome double-strand break in Saccharomyces cerevisiae. *Cold Spring Harb Symp Quant Biol*, 65, 303-14.
- Lee, S. E., A. Pelliccioli, A. Malkova, M. Foiani & J. E. Haber (2001) The Saccharomyces recombination protein Tid1p is required for adaptation from G2/M arrest induced by a double-strand break. *Curr Biol*, 11, 1053-7.
- Lee, S. E., A. Pelliccioli, M. B. Vaze, N. Sugawara, A. Malkova, M. Foiani & J. E. Haber (2003) Yeast Rad52 and Rad51 recombination proteins define a second pathway of DNA damage assessment in response to a single double-strand break. *Mol Cell Biol*, 23, 8913-23.
- Lengsfeld, B. M., A. J. Rattray, V. Bhaskara, R. Ghirlando & T. T. Paull (2007) Sae2 is an endonuclease that processes hairpin DNA cooperatively with the Mre11/Rad50/Xrs2 complex. *Mol Cell*, 28, 638-51.
- Leroy, C., S. E. Lee, M. B. Vaze, F. Ochsenbein, R. Guerois, J. E. Haber & M. C. Marsolier-Kergoat (2003) PP2C phosphatases Ptc2 and Ptc3 are required for DNA checkpoint inactivation after a double-strand break. *Mol Cell*, 11, 827-35.
- Li, R. & M. R. Botchan (1993) The acidic transcriptional activation domains of VP16 and p53 bind the cellular replication protein A and stimulate in vitro BPV-1 DNA replication. *Cell*, 73, 1207-21.
- Li, S., Z. Xu, J. Xu, L. Zuo, C. Yu, P. Zheng, H. Gan, X. Wang, L. Li, S. Sharma, A. Chabes, D. Li, S. Wang, S. Zheng, J. Li, X. Chen, Y. Sun, D. Xu, J. Han, K. Chan, Z. Qi, J. Feng & Q. Li (2018) Rtt105 functions as a chaperone for replication protein A to preserve genome stability. *Embo j*, 37.
- Lisby, M., J. H. Barlow, R. C. Burgess & R. Rothstein (2004) Choreography of the DNA damage response: spatiotemporal relationships among checkpoint and repair proteins. *Cell*, 118, 699-713.
- Liu, Y., W. A. Gaines, T. Callender, V. Busygina, A. Oke, P. Sung, J. C. Fung & N. M. Hollingsworth (2014) Down-regulation of Rad51 activity during meiosis in yeast prevents competition with Dmc1 for repair of double-strand breaks. *PLoS Genet*, 10, e1004005.
- Liu, Y., S. Vaithiyalingam, Q. Shi, W. J. Chazin & S. S. Zinkel (2011) BID binds to replication protein A and stimulates ATR function following replicative stress. *Mol Cell Biol*, 31, 4298-309.
- Ljungman, M. (2007) The Transcription Stress Response. *Cell Cycle*, 6, 2252-2257.
- Lydall, D., Y. Nikolsky, D. K. Bishop & T. Weinert (1996) A meiotic recombination checkpoint controlled by mitotic checkpoint genes. *Nature*, 383, 840-3.
- Majka, J., S. K. Binz, M. S. Wold & P. M. Burgers (2006a) Replication protein A directs loading of the DNA damage checkpoint clamp to 5'-DNA junctions. *J Biol Chem*, 281, 27855-61.
- Majka, J., A. Niedziela-Majka & P. M. Burgers (2006b) The checkpoint clamp activates Mec1 kinase during initiation of the DNA damage checkpoint. *Mol Cell*, 24, 891-901.

- Maleki, S., M. J. Neale, C. Arora, K. A. Henderson & S. Keeney (2007) Interactions between Mei4, Rec114, and other proteins required for meiotic DNA double-strand break formation in *Saccharomyces cerevisiae*. *Chromosoma*, 116, 471-86.
- Malkova, A., F. Klein, W. Y. Leung & J. E. Haber (2000) HO endonuclease-induced recombination in yeast meiosis resembles Spo11-induced events. *Proc Natl Acad Sci U S A*, 97, 14500-5.
- Mallory, J. C., V. I. Bashkirov, K. M. Trujillo, J. A. Solinger, M. Dominska, P. Sung, W. D. Heyer & T. D. Petes (2003) Amino acid changes in Xrs2p, Dun1p, and Rfa2p that remove the preferred targets of the ATM family of protein kinases do not affect DNA repair or telomere length in *Saccharomyces cerevisiae*. *DNA Repair (Amst)*, 2, 1041-64.
- Malone, R. E., S. Kim, S. A. Bullard, S. Lundquist, L. Hutchings-Crow, S. Cramton, L. Lutfiyya & J. Lee (1994) Analysis of a recombination hotspot for gene conversion occurring at the HIS2 gene of *Saccharomyces cerevisiae*. *Genetics*, 137, 5-18.
- Manfrini, N., I. Guerini, A. Citterio, G. Lucchini & M. P. Longhese (2010) Processing of meiotic DNA double strand breaks requires cyclin-dependent kinase and multiple nucleases. *J Biol Chem*, 285, 11628-37.
- Maniar, H. S., R. Wilson & S. J. Brill (1997) Roles of replication protein-A subunits 2 and 3 in DNA replication fork movement in *Saccharomyces cerevisiae*. *Genetics*, 145, 891-902.
- Mao-Draayer, Y., A. M. Galbraith, D. L. Pittman, M. Cool & R. E. Malone (1996) Analysis of meiotic recombination pathways in the yeast *Saccharomyces cerevisiae*. *Genetics*, 144, 71-86.
- Maréchal, A., J. M. Li, X. Y. Ji, C. S. Wu, S. A. Yazinski, H. D. Nguyen, S. Liu, A. E. Jiménez, J. Jin & L. Zou (2014) PRP19 transforms into a sensor of RPA-ssDNA after DNA damage and drives ATR activation via a ubiquitin-mediated circuitry. *Mol Cell*, 53, 235-246.
- Maréchal, A. & L. Zou (2015) RPA-coated single-stranded DNA as a platform for post-translational modifications in the DNA damage response. *Cell Res*, 25, 9-23.
- Mason, A. C., S. J. Haring, J. M. Pryor, C. A. Staloch, T. F. Gan & M. S. Wold (2009) An alternative form of replication protein a prevents viral replication in vitro. *J Biol Chem*, 284, 5324-31.
- Melo, J. A., J. Cohen & D. P. Toczyski (2001) Two checkpoint complexes are independently recruited to sites of DNA damage in vivo. *Genes Dev*, 15, 2809-21.
- Memisoglu, G., M. C. Lanz, V. V. Eapen, J. M. Jordan, K. Lee, M. B. Smolka & J. E. Haber (2019) Mec1(ATR) Autophosphorylation and Ddc2(ATRIP) Phosphorylation Regulates DNA Damage Checkpoint Signaling. *Cell Rep*, 28, 1090-1102.e3.
- Mier, P., A. J. Pérez-Pulido & M. A. Andrade-Navarro (2018) Automated selection of homologs to track the evolutionary history of proteins. *BMC Bioinformatics*, 19, 431.
- Mika, S. & B. Rost (2006) Protein-Protein Interactions More Conserved within Species than across Species. *PLOS Computational Biology*, 2, e79.
- Mimitou, E. P., S. Yamada & S. Keeney (2017) A global view of meiotic double-strand break end resection. *Science*, 355, 40-45.
- Mitchell, A. P., S. E. Driscoll & H. E. Smith (1990) Positive control of sporulation-specific genes by the IME1 and IME2 products in *Saccharomyces cerevisiae*. *Mol Cell Biol*, 10, 2104-10.

- Moreau, S., J. R. Ferguson & L. S. Symington (1999) The nuclease activity of Mre11 is required for meiosis but not for mating type switching, end joining, or telomere maintenance. *Mol Cell Biol*, 19, 556-66.
- Moreau, S., E. A. Morgan & L. S. Symington (2001) Overlapping functions of the *Saccharomyces cerevisiae* Mre11, Exo1 and Rad27 nucleases in DNA metabolism. *Genetics*, 159, 1423-33.
- Murakami, H. & S. Keeney (2008) Regulating the formation of DNA double-strand breaks in meiosis. *Genes Dev*, 22, 286-92.
- Nakada, D., Y. Hirano, Y. Tanaka & K. Sugimoto (2005) Role of the C terminus of Mec1 checkpoint kinase in its localization to sites of DNA damage. *Mol Biol Cell*, 16, 5227-35.
- Nakada, D., K. Matsumoto & K. Sugimoto (2003) ATM-related Tel1 associates with double-strand breaks through an Xrs2-dependent mechanism. *Genes Dev*, 17, 1957-62.
- Navadgi-Patil, V. M. & P. M. Burgers (2008) Yeast DNA replication protein Dpb11 activates the Mec1/ATR checkpoint kinase. *J Biol Chem*, 283, 35853-9.
- (2009) A tale of two tails: activation of DNA damage checkpoint kinase Mec1/ATR by the 9-1-1 clamp and by Dpb11/TopBP1. *DNA Repair (Amst)*, 8, 996-1003.
- Neale, M. J., M. Ramachandran, E. Trelles-Sticken, H. Scherthan & A. S. Goldman (2002) Wild-type levels of Spo11-induced DSBs are required for normal single-strand resection during meiosis. *Mol Cell*, 9, 835-46.
- Ngo, G. H., L. Balakrishnan, M. Dubarry, J. L. Campbell & D. Lydall (2014) The 9-1-1 checkpoint clamp stimulates DNA resection by Dna2-Sgs1 and Exo1. *Nucleic Acids Res*, 42, 10516-28.
- Niu, H., X. Li, E. Job, C. Park, D. Moazed, S. P. Gygi & N. M. Hollingsworth (2007) Mek1 kinase is regulated to suppress double-strand break repair between sister chromatids during budding yeast meiosis. *Mol Cell Biol*, 27, 5456-67.
- Niu, H., L. Wan, B. Baumgartner, D. Schaefer, J. Loidl & N. M. Hollingsworth (2005) Partner choice during meiosis is regulated by Hop1-promoted dimerization of Mek1. *Mol Biol Cell*, 16, 5804-18.
- Niwa, O., M. Shimanuki & F. Miki (2000) Telomere-led bouquet formation facilitates homologous chromosome pairing and restricts ectopic interaction in fission yeast meiosis. *Embo j*, 19, 3831-40.
- Oakley, G. G., K. Tillison, S. A. Opiyo, J. G. Glanzer, J. M. Horn & S. M. Patrick (2009) Physical interaction between replication protein A (RPA) and MRN: involvement of RPA2 phosphorylation and the N-terminus of RPA1. *Biochemistry*, 48, 7473-81.
- Oude Blenke, E., M. J. Evers, E. Mastrobattista & J. van der Oost (2016) CRISPR-Cas9 gene editing: Delivery aspects and therapeutic potential. *J Control Release*, 244, 139-148.
- Pak, J. & J. Segall (2002) Regulation of the premiddle and middle phases of expression of the NDT80 gene during sporulation of *Saccharomyces cerevisiae*. *Mol Cell Biol*, 22, 6417-29.
- Pan, J., M. Sasaki, R. Kniewel, H. Murakami, H. G. Blitzblau, S. E. Tischfield, X. Zhu, M. J. Neale, M. Jasin, N. D. Socci, A. Hochwagen & S. Keeney (2011) A hierarchical combination of factors shapes the genome-wide topography of yeast meiotic recombination initiation. *Cell*, 144, 719-31.
- Pelliccioli, A., S. E. Lee, C. Lucca, M. Foiani & J. E. Haber (2001) Regulation of *Saccharomyces* Rad53 checkpoint kinase during adaptation from DNA damage-induced G2/M arrest. *Mol Cell*, 7, 293-300.

- Peng, R., G. Lin & J. Li (2016) Potential pitfalls of CRISPR/Cas9-mediated genome editing. *Febs j*, 283, 1218-31.
- Piya, G., E. N. Mueller, H. K. Haas, P. L. Ghospurkar, T. M. Wilson, J. L. Jensen, C. L. Colbert & S. J. Haring (2015) Characterization of the interaction between Rfa1 and Rad24 in *Saccharomyces cerevisiae*. *PLoS One*, 10, e0116512.
- Prinz, S., A. Amon & F. Klein (1997) Isolation of COM1, a new gene required to complete meiotic double-strand break-induced recombination in *Saccharomyces cerevisiae*. *Genetics*, 146, 781-95.
- Prugar, E., C. Burnett, X. Chen & N. M. Hollingsworth (2017) Coordination of Double Strand Break Repair and Meiotic Progression in Yeast by a Mek1-Ndt80 Negative Feedback Loop. *Genetics*, 206, 497-512.
- Pungartnik, C., J. Picada, M. Brendel & J. A. Henriques (2002) Further phenotypic characterization of pso mutants of *Saccharomyces cerevisiae* with respect to DNA repair and response to oxidative stress. *Genet Mol Res*, 1, 79-89.
- Richardson, C., N. Horikoshi & T. K. Pandita (2004) The role of the DNA double-strand break response network in meiosis. *DNA Repair (Amst)*, 3, 1149-64.
- Robison, J. G., J. Elliott, K. Dixon & G. G. Oakley (2004) Replication protein A and the Mre11.Rad50.Nbs1 complex co-localize and interact at sites of stalled replication forks. *J Biol Chem*, 279, 34802-10.
- Roeder, G. S. (1997) Meiotic chromosomes: it takes two to tango. *Genes Dev*, 11, 2600-21.
- Ross, L. O., R. Maxfield & D. Dawson (1996) Exchanges are not equally able to enhance meiotic chromosome segregation in yeast. *Proc Natl Acad Sci U S A*, 93, 4979-83.
- Rouse, J. & S. P. Jackson (2002) Lcd1p recruits Mec1p to DNA lesions in vitro and in vivo. *Mol Cell*, 9, 857-69.
- Sanchez, Y., B. A. Desany, W. J. Jones, Q. Liu, B. Wang & S. J. Elledge (1996) Regulation of RAD53 by the ATM-like kinases MEC1 and TEL1 in yeast cell cycle checkpoint pathways. *Science*, 271, 357-60.
- Schindler, K., K. R. Benjamin, A. Martin, A. Boglioli, I. Herskowitz & E. Winter (2003) The Cdk-activating kinase Cak1p promotes meiotic S phase through Ime2p. *Mol Cell Biol*, 23, 8718-28.
- Schindler, K. & E. Winter (2006) Phosphorylation of Ime2 regulates meiotic progression in *Saccharomyces cerevisiae*. *J Biol Chem*, 281, 18307-16.
- Schramke, V., H. Neecke, V. Brevet, Y. Corda, G. Lucchini, M. P. Longhese, E. Gilson & V. Geli (2001) The set1Delta mutation unveils a novel signaling pathway relayed by the Rad53-dependent hyperphosphorylation of replication protein A that leads to transcriptional activation of repair genes. *Genes Dev*, 15, 1845-58.
- Seeber, A., A. M. Hegnauer, N. Hustedt, I. Deshpande, J. Poli, J. Eglinger, P. Pasero, H. Gut, M. Shinohara, K. P. Hopfner, K. Shimada & S. M. Gasser (2016) RPA Mediates Recruitment of MRX to Forks and Double-Strand Breaks to Hold Sister Chromatids Together. *Mol Cell*, 64, 951-966.
- Shinohara, A., S. Gasior, T. Ogawa, N. Kleckner & D. K. Bishop (1997) *Saccharomyces cerevisiae* recA homologues RAD51 and DMC1 have both distinct and overlapping roles in meiotic recombination. *Genes to cells : devoted to molecular & cellular mechanisms*, 2, 615-629.
- Shinohara, A., H. Ogawa & T. Ogawa (1992) Rad51 protein involved in repair and recombination in *S. cerevisiae* is a RecA-like protein. *Cell*, 69, 457-70.

- Shinohara, M., S. L. Gasiior, D. K. Bishop & A. Shinohara (2000) Tid1/Rdh54 promotes colocalization of rad51 and dmc1 during meiotic recombination. *Proc Natl Acad Sci U S A*, 97, 10814-9.
- Shinohara, M., K. Sakai, T. Ogawa & A. Shinohara (2003) The mitotic DNA damage checkpoint proteins Rad17 and Rad24 are required for repair of double-strand breaks during meiosis in yeast. *Genetics*, 164, 855-65.
- Shinohara, M. & A. Shinohara (2013) Multiple pathways suppress non-allelic homologous recombination during meiosis in *Saccharomyces cerevisiae*. *PLoS One*, 8, e63144.
- Shiotani, B., H. D. Nguyen, P. Håkansson, A. Maréchal, A. Tse, H. Tahara & L. Zou (2013) Two distinct modes of ATR activation orchestrated by Rad17 and Nbs1. *Cell Rep*, 3, 1651-62.
- Sia, R. A. & A. P. Mitchell (1995) Stimulation of later functions of the yeast meiotic protein kinase Ime2p by the IDS2 gene product. *Mol Cell Biol*, 15, 5279-87.
- Singh, K. K. & L. Samson (1995) Replication protein A binds to regulatory elements in yeast DNA repair and DNA metabolism genes. *Proc Natl Acad Sci U S A*, 92, 4907-11.
- Sollier, J., W. Lin, C. Soustelle, K. Suhre, A. Nicolas, V. Geli & C. de La Roche Saint-Andre (2004) Set1 is required for meiotic S-phase onset, double-strand break formation and middle gene expression. *Embo j*, 23, 1957-67.
- Soustelle, C., M. Vedel, R. Kolodner & A. Nicolas (2002) Replication protein A is required for meiotic recombination in *Saccharomyces cerevisiae*. *Genetics*, 161, 535-47.
- Sternberg, S. H. & J. A. Doudna (2015) Expanding the Biologist's Toolkit with CRISPR-Cas9. *Mol Cell*, 58, 568-74.
- Stuart, D. & C. Wittenberg (1998) CLB5 and CLB6 are required for premeiotic DNA replication and activation of the meiotic S/M checkpoint. *Genes Dev*, 12, 2698-710.
- Sung, P. (1997) Yeast Rad55 and Rad57 proteins form a heterodimer that functions with replication protein A to promote DNA strand exchange by Rad51 recombinase. *Genes Dev*, 11, 1111-21.
- Sweeney, F. D., F. Yang, A. Chi, J. Shabanowitz, D. F. Hunt & D. Durocher (2005) *Saccharomyces cerevisiae* Rad9 acts as a Mec1 adaptor to allow Rad53 activation. *Curr Biol*, 15, 1364-75.
- Symington, L. S., R. Rothstein & M. Lisby (2014) Mechanisms and regulation of mitotic recombination in *Saccharomyces cerevisiae*. *Genetics*, 198, 795-835.
- Thacker, D., I. Lam, M. Knop & S. Keeney (2011) Exploiting spore-autonomous fluorescent protein expression to quantify meiotic chromosome behaviors in *Saccharomyces cerevisiae*. *Genetics*, 189, 423-39.
- The UniProt, C. (2018) UniProt: a worldwide hub of protein knowledge. *Nucleic Acids Research*, 47, D506-D515.
- Umezumi, K., N. Sugawara, C. Chen, J. E. Haber & R. D. Kolodner (1998) Genetic analysis of yeast RPA1 reveals its multiple functions in DNA metabolism. *Genetics*, 148, 989-1005.
- Usui, T. & Y. Kanehara (2013) Elevated Rad53 kinase activity influences formation and interhomolog repair of meiotic DNA double-strand breaks in budding yeast. *Biochem Biophys Res Commun*, 441, 593-9.
- Usui, T., H. Ogawa & J. H. Petrini (2001) A DNA damage response pathway controlled by Tel1 and the Mre11 complex. *Mol Cell*, 7, 1255-66.
- Vassin, V. M., M. S. Wold & J. A. Borowiec (2004) Replication protein A (RPA) phosphorylation prevents RPA association with replication centers. *Mol Cell Biol*, 24, 1930-43.

- Vaze, M. B., A. Pelliccioli, S. E. Lee, G. Ira, G. Liberi, A. Arbel-Eden, M. Foiani & J. E. Haber (2002) Recovery from Checkpoint-Mediated Arrest after Repair of a Double-Strand Break Requires Srs2 Helicase. *Molecular Cell*, 10, 373-385.
- Wan, L. & J. Huang (2014) The PSO4 protein complex associates with replication protein A (RPA) and modulates the activation of ataxia telangiectasia-mutated and Rad3-related (ATR). *J Biol Chem*, 289, 6619-26.
- Wanrooij, P. H. & P. M. Burgers (2015) Yet another job for Dna2: Checkpoint activation. *DNA Repair (Amst)*, 32, 17-23.
- Wellinger, R. J. & V. A. Zakian (2012) Everything you ever wanted to know about *Saccharomyces cerevisiae* telomeres: beginning to end. *Genetics*, 191, 1073-105.
- Wilson, T. M. 2018. Biochemical and Functional Characterization of Rpa2 N-Terminal Phosphorylation during DNA Repair and Checkpoint Adaptation in *Saccharomyces cerevisiae*. In *Chemistry and Biochemistry*, 275. Fargo, North Dakota: North Dakota State University of Agriculture and Applied Science.
- Wold, M. S. (1997) Replication protein A: a heterotrimeric, single-stranded DNA-binding protein required for eukaryotic DNA metabolism. *Annu Rev Biochem*, 66, 61-92.
- Wu, H. Y., H. C. Ho & S. M. Burgess (2010) Mek1 kinase governs outcomes of meiotic recombination and the checkpoint response. *Curr Biol*, 20, 1707-16.
- Wu, X., Z. Yang, Y. Liu & Y. Zou (2005) Preferential localization of hyperphosphorylated replication protein A to double-strand break repair and checkpoint complexes upon DNA damage. *Biochem J*, 391, 473-80.
- Wyka, I. M., K. Dhar, S. K. Binz & M. S. Wold (2003) Replication Protein A Interactions with DNA: Differential Binding of the Core Domains and Analysis of the DNA Interaction Surface. *Biochemistry*, 42, 12909-12918.
- Xu, L., M. Ajimura, R. Padmore, C. Klein & N. Kleckner (1995) NDT80, a meiosis-specific gene required for exit from pachytene in *Saccharomyces cerevisiae*. *Mol Cell Biol*, 15, 6572-81.
- Xu, L., B. M. Weiner & N. Kleckner (1997) Meiotic cells monitor the status of the interhomolog recombination complex. *Genes Dev*, 11, 106-18.
- Xu, X., S. Vaithiyalingam, G. G. Glick, D. A. Mordes, W. J. Chazin & D. Cortez (2008) The basic cleft of RPA70N binds multiple checkpoint proteins, including RAD9, to regulate ATR signaling. *Mol Cell Biol*, 28, 7345-53.
- Yoo, E., B. U. Kim, S. Y. Lee, C. H. Cho, J. H. Chung & C. H. Lee (2005) 53BP1 is associated with replication protein A and is required for RPA2 hyperphosphorylation following DNA damage. *Oncogene*, 24, 5423-30.
- Zakharyevich, K., Y. Ma, S. Tang, P. Y. Hwang, S. Boiteux & N. Hunter (2010) Temporally and biochemically distinct activities of Exo1 during meiosis: double-strand break resection and resolution of double Holliday junctions. *Mol Cell*, 40, 1001-15.
- Zhang, Q., H. L. Xing, Z. P. Wang, H. Y. Zhang, F. Yang, X. C. Wang & Q. J. Chen (2018) Potential high-frequency off-target mutagenesis induced by CRISPR/Cas9 in *Arabidopsis* and its prevention. *Plant Mol Biol*, 96, 445-456.
- Zhou, H., M. Zhou, D. Li, J. Manthey, E. Lioutikova, H. Wang & X. Zeng (2017) Whole genome analysis of CRISPR Cas9 sgRNA off-target homologies via an efficient computational algorithm. *BMC Genomics*, 18, 826.
- Zhu, Z., W. H. Chung, E. Y. Shim, S. E. Lee & G. Ira (2008) Sgs1 helicase and two nucleases Dna2 and Exo1 resect DNA double-strand break ends. *Cell*, 134, 981-94.

- Zou, L. (2009) Checkpoint Mec-tivation comes in many flavors. *Mol Cell*, 36, 734-5.
- Zou, L. & S. J. Elledge (2003) Sensing DNA damage through ATRIP recognition of RPA-ssDNA complexes. *Science*, 300, 1542-8.
- Zou, L., D. Liu & S. J. Elledge (2003) Replication protein A-mediated recruitment and activation of Rad17 complexes. *Proc Natl Acad Sci U S A*, 100, 13827-32.

APPENDIX A. HAPLOID YEAST STRAINS

Stock #	Strain Name	Genotype	Source
Y-185	EGY48	<i>MATa tryp1 his3 ura3 leu2Δ::6 LexAop-LEU2</i>	(Ghospurkar 2015)
Kit	EGY194	<i>MATa tryp1 his3 ura3 leu2Δ::4 LexAop-LEU2</i>	(Ghospurkar 2015)
Y-7	RMY122-A	<i>MATa leu2-3, 122 trp1-1 can1-100 ura3-1 his3-11,15 rad5-535 rfa1Δ ::TRP1 rfa2Δ ::TRP1 + pJM132</i>	(Ghospurkar 2015)
Y-008	B9B-A	<i>MATa ade3 cyhr HIS2 his5-2 leu1-c LEU2 TRP1 trp5-20 ura1 URA3</i>	Malone Lab
Y-009	B9B-α	<i>MATa ade3 cyhr HIS2 his5-2 leu1-c LEU2 TRP1 trp5-20 ura1 URA3</i>	Malone Lab
Y-198/460	JKM179	<i>MATa ura3-52 lys5 trp1::hisG leu2-3,112 ade1-100 ade3::GAL-HO hoΔ hmrΔ::ADE1 hmlΔ::ADE1</i>	(Lee et al. 1998)
Y-190	AWY097	Isogenic derivative of JKM179 except <i>rfa2-ΔN_x</i>	Andre Walther
Y-207	TMW311	Isogenic derivative of RMY122-A except pRS313- <i>RFA1</i> pRS315- <i>RFA2</i>	(Wilson 2018, Ghospurkar et al. 2015b)
Y-208	TMW312	Isogenic derivative of RMY122-A except pRS313- <i>rfa1-t11</i> and pRS315- <i>RFA2</i>	(Wilson 2018, Ghospurkar et al. 2015b)
Y-209	TMW313	Isogenic derivative of RMY122-A except pRS313- <i>RFA1</i> and pRS315- <i>rfa2-D_x</i>	(Wilson 2018, Ghospurkar et al. 2015b)
Y-210	TMW314	Isogenic derivative of RMY122-A except pRS313- <i>RFA1</i> and pRS315- <i>rfa2-A_x</i>	(Wilson 2018, Ghospurkar et al. 2015b)
Y-211	TMW315	Isogenic derivative of RMY122-A except pRS313- <i>RFA1</i> and pRS315- <i>rfa2-ΔN_x</i>	(Wilson 2018, Ghospurkar et al. 2015b)
Y-229	NMM101	Isogenic derivative of JKM179 except <i>rfa1Δ::kanMX</i> and pJM132	Nolan Miles
Y-232	NMM104	Isogenic derivative of JKM179 except <i>rfa2Δ::kanMX</i> and pJM132	Nolan Miles

Stock #	Strain Name	Genotype	Source
Y-249	JKM139	<i>MATa ura3-52 lys5 trp1::hisG leu2-3,112 ade1-100 ade3::GAL-HO hoΔ hmrΔ::ADE1 hmlΔ::ADE1</i>	(Lee et al. 1998)
Y-763	RM96-15A-390	<i>MATa his2-390 leu2-1 met2-1 trp1-1 ura3-13</i>	(Mao-Draayer et al. 1996)
Y-287	RM26-26C-A	Isogenic to RM26-26C, except <i>MATa</i>	Brian Samuelson
Y-288	K264-10D- α	Isogenic to K264-10D, except <i>MATa</i>	Brian Samuelson
Y-290	M2034 α	Isogenic derivative of RM96-15A-390 except <i>MATa</i>	Brian Samuelson
Y-779	RM96-15A-0C1	Isogenic derivative of RM96-15A-390 except <i>his2-390</i> , Δc	(Haring et al. 2003)
Y-780	RM182-55C-C1	<i>MATa ade2-1 ade5 can1^r cdc14^{ts} cly3ts his2-Δc lys2-1 ura3-1</i>	(Haring et al. 2003)
Y-341	CMK001	Isogenic derivative of RM96-15A-0C1 except <i>rfa2-A_x</i>	Courtney Karnopp
Y-343	CMK003	Isogenic derivative of RM96-15A-0C1 except <i>rfa2-D_x</i>	Courtney Karnopp
Y-345	CMK005	Isogenic derivative of RM96-15A-0C1 except <i>rfa2-ΔN_x</i>	Courtney Karnopp
Y-351	CMK011	Isogenic derivative of RM182-55C-C1 except <i>rfa2-ΔN_x</i>	Courtney Karnopp
Y-362	RM26-26C	<i>MATa ade2-1 ade5 can^r CYH^S his1 HIS7 leu1-12 lys2-1 trp5-2 ura3-1</i>	(Koehn et al. 2009)
Y-363	TMW302	Isogenic derivative of RM26-26C except <i>rfa2-A_x</i>	Timothy Wilson
Y-365	TMW304	Isogenic derivative of RM26-26C except <i>rfa2-ΔN_x</i>	Timothy Wilson
Y-366	TMW305	Isogenic derivative of RM26-26C except <i>rfa2-cDNA</i>	Timothy Wilson
Y-367	K264-10D	<i>MATa ade2-1 CAN^S cyh^r HIS1 his7-1 leu1-c lys2-2 met13-c trp5-c tyr1-2 ura3-1</i>	(Koehn et al. 2009)
Y-368	TMW307	Isogenic derivative of K264-10D except <i>rfa2-A_x</i>	Timothy Wilson
Y-370	TMW309	Isogenic derivative of K264-10D except <i>rfa2-ΔN_x</i>	Timothy Wilson
Y-371	TMW310	Isogenic derivative of K264-10D except <i>rfa2-cDNA</i>	Timothy Wilson

Stock #	Strain Name	Genotype	Source
Y-380	TMW159	Isogenic derivative of NMM104 except <i>rdh54Δ::natMX</i> (contains pJM132)	Timothy Wilson
Y-385	AMA122	Isogenic derivative of K264-10D except <i>rfa2-D_x</i>	This study
Y-396	AMA124	Isogenic derivative of RM182-55C-C1 except <i>rfa2-D_x</i>	This study
Y-398	AMA126	Isogenic derivative of RM182-55C-C1 except <i>rfa2-A_x</i>	This study
Y-450	TAB113	Isogenic derivative of NMM104 except pRS315- <i>rfa2-D_x</i> -S122A (no longer containing pJM132)	Timothy Wilson, Trevor Baumgartner
Y-451	TAB114	Isogenic derivative of NMM104 except pRS315- <i>rfa2-D_x</i> -S122D (no longer containing pJM132)	Timothy Wilson, Trevor Baumgartner
Y-452	TAB115	Isogenic derivative of NMM104 except pRS315- <i>rfa2-A_x</i> -S122A (no longer containing pJM132)	Timothy Wilson, Trevor Baumgartner
Y-453	TAB116	Isogenic derivative of NMM104 except pRS315- <i>rfa2-A_x</i> -S122D (no longer containing pJM132)	Timothy Wilson, Trevor Baumgartner
Y-456	AWY016	Isogenic derivative of JKM139 except <i>rfa2-D_x</i>	Andre Walther
Y-458	AWY019	Isogenic derivative of JKM179 except <i>rad9Δ rfa2-A_x</i>	Andre Walther
Y-462	AWY033	Isogenic derivative of JKM179 except <i>rad9Δ</i>	Andre Walther
Y-464	AWY035	Isogenic derivative of JKM179 except <i>rad17Δ</i>	Andre Walther
Y-466	AWY040	Isogenic derivative of JKM179 except <i>rad17Δ rfa2-D_x</i>	Andre Walther
Y-470	AWY045	Isogenic derivative of JKM179 except <i>rad9Δ rfa2-D_x</i>	Andre Walther
Y-472	AWY092	Isogenic derivative of JKM179 except <i>rfa2-A_x</i>	Andre Walther
Y-474	AWY096	Isogenic derivative of JKM179 except <i>rfa2-D_x</i>	Andre Walther
Y-476	AWY114	Isogenic derivative of JKM179 except <i>mec3Δ</i>	Andre Walther
Y-478	AWY200	Isogenic derivative of JKM179 except <i>mec3Δ rfa2-D_x</i>	Andre Walther

Stock #	Strain Name	Genotype	Source
Y-482	AWY201	Isogenic derivative of JKM179 except <i>mec3Δ rfa2-A_x</i>	Andre Walther
Y-488	AWY194	Isogenic derivative of JKM139 except <i>rfa2-A_x</i>	Andre Walther
Y-499	AMA135	Isogenic derivative of JKM179 except <i>rad17Δ rfa2-A_x</i>	This study
Y-501	AMA137	Isogenic derivative of JKM179 except <i>rad52Δ rfa2-A_x</i>	This study
Y-503	AMA139	Isogenic derivative of JKM179 except <i>rad52Δ rfa2-D_x</i>	This study
Y-551	TMW189	Isogenic derivative of NMM104 except pRS315-RFA2 (no longer containing pJM132)	Timothy Wilson
Y-552	TMW190	Isogenic derivative of NMM104 except pRS315-rfa2-D _x (no longer containing pJM132)	Timothy Wilson, (Ghospurkar et al. 2015b)
Y-553	TMW191	Isogenic derivative of NMM104 except pRS315-rfa2-A _x (no longer containing pJM132)	Timothy Wilson, (Ghospurkar et al. 2015b)
Y-554	TMW192	Isogenic derivative of NMM104 except pRS315-rfa2-N _x (no longer containing pJM132)	Timothy Wilson
Y-582	TMW206	Isogenic derivative of NMM104 except pRS315-rfa2-A _{M1+2} (no longer containing pJM132)	Timothy Wilson
Y-599	AMA141	Isogenic derivative of RM26-26C except <i>rfa2-D_x</i> (no longer containing pJM132)	This study
Y-671	TMW247	Isogenic derivative of NMM104, except contains <i>rdh54Δ::natMX</i> and pRS315-RFA2 (no longer containing pJM132)	Timothy Wilson
Y-696	TMW272	Isogenic derivative of NMM104, except contains <i>sml1Δ::hphNT</i> and pRS315-RFA2 (no longer containing pJM132)	Timothy Wilson
Y-725	AMA145	Isogenic derivative of K264-10D except <i>spo11Δ::kanMX</i> . Isogenic to M403spo11Δ.7.	This study
Y-727	AMA147	Isogenic derivative of JKM139 except <i>rfa2-ΔN_x</i>	This study

Stock #	Strain Name	Genotype	Source
Y-729	AMA149	Isogenic derivative of RM26-26C except <i>spo11Δ::kanMX</i> . Isogenic to M163spo11Δ.5.	This study
Y-732	AMA152	Isogenic derivative of RM26-26C except <i>sae2Δ::hphNT</i>	This study
Y-734	AMA154	Isogenic derivative of K264-10D except <i>sae2Δ::hphNT</i>	This study
Y-772	AMA161	Isogenic to K264-10D except <i>dmc1Δ::hphNT</i>	This study
Y-776	AMA165	Isogenic to RM26-26 C except <i>ndt80Δ::natMX</i>	This study
Y-778	AMA167	Isogenic to K264-10D except <i>ndt80Δ::natMX</i>	This study
Y-781	AMA168	Isogenic to RM26-26C except <i>dmc1Δ::hphNT</i>	This study
Y-816	WAL105	Isogenic derivative of NMM101 except pRS315-RFA1 (no longer containing pJM132)	Wendy Larson
Y-817	WAL105	Isogenic derivative of NMM101 except pRS315-rfa1-t11 (no longer containing pJM132)	Wendy Larson
Y-841	AMA188	Isogenic to AMA168 except <i>rfa2-A_x</i>	This study
Y-843	AMA190	Isogenic to AMA168 except <i>rfa2-D_x</i>	This study
Y-845	AMA192	Isogenic to AMA165 except <i>rfa2-D_x</i>	This study
Y-846	AMA193	Isogenic to AMA161 except <i>rfa2-A_x</i>	This study
Y-849	AMA196	Isogenic to AMA167 except <i>rfa2-A_x</i>	This study
Y-852	AMA199	Isogenic to AMA167 except <i>rfa2-D_x</i>	This study
Y-854	AMA201	Isogenic to AMA167 except <i>rfa2-ΔN_x</i>	This study
Y-855	AMA202	Isogenic to AMA145 except <i>rfa2-A_x</i>	This study
Y-858	AMA205	Isogenic to AMA145 except <i>rfa2-ΔN_x</i>	This study
Y-879	AMA210	Isogenic to AMA154 except <i>MATa</i>	This study
Y-882	AMA213	Isogenic to AMA152 except <i>MATa</i>	This study
Y-896	AMA216	Isogenic to AMA168 except <i>rfa2-ΔN_x</i>	This study
Y-897	AMA217	Isogenic to AMA161 except <i>rfa2-ΔN_x</i>	This study
Y-898	AMA218	Isogenic to AMA165 except <i>rfa2-A_x</i>	This study
Y-900	AMA220	Isogenic to AMA165 except <i>rfa2-ΔN_x</i>	This study
Y-902	AMA222	Isogenic to AMA149 except <i>rfa2-D_x</i>	This study
Y-904	AMA224	Isogenic to AMA152 except <i>rfa2-ΔN_x</i>	This study

Stock #	Strain Name	Genotype	Source
Y-907	AMA227	Isogenic to AMA154 except <i>rfa2-A_x</i>	This study
Y-908	AMA228	Isogenic to AMA154 except <i>rfa2-D_x</i>	This study
Y-909	AMA229	Isogenic to AMA154 except <i>rfa2-ΔN_x</i>	This study
Y-911	AMA231	Isogenic to AMA152 except <i>rfa2-A_x</i>	This study
Y-913	AMA233	Isogenic to AMA149 except <i>rfa2-A_x</i>	This study
Y-917	AMA237	Isogenic to AMA152 except <i>rfa2-D_x</i>	This study
Y-920	AMA240	Isogenic to AMA161 except <i>rfa2-D_x</i>	This study
Y-927	AMA242	Isogenic to AMA149 except <i>rfa2-ΔN_x</i>	This study
Y-928	AMA243	Isogenic to AMA145 except <i>rfa2-D_x</i>	This study
Y-937	CAH017	Isogenic to NMM104 except pRS315- <i>rfa2-S238/240A</i> , isolate #4	Cristian Hernandez
Y-938	CAH018	Isogenic to NMM104 except pRS315- <i>rfa2-S238/240A</i> , isolate #9	Cristian Hernandez
Y-967	AMA253	Isogenic to TMW272 except <i>mecI-S1964A</i> (contains pRS315- <i>RFA2</i> ; <i>LEU2</i> selectable marker)	This study
Y-968	AMA254	Isogenic to TMW272 except <i>mecI-S1964E</i> (contains pRS315- <i>RFA2</i> ; <i>LEU2</i> selectable marker)	This study
Y-999	AMA257	Isogenic to TMW272 except <i>mecI-S1964D</i> (contains pRS315- <i>RFA2</i> ; <i>LEU2</i> selectable marker)	This study
Y-1000	AMA258	Isogenic to AMA253, except contains pJM132 (<i>URA3</i> selectable marker) and lost pRS315- <i>RFA2</i>	This study
Y-1002	AMA260	Isogenic to AMA254, except contains pJM132 (<i>URA3</i> selectable marker) and lost pRS315- <i>RFA2</i>	This study
Y-1010	AMA262	Isogenic to AMA257, except contains pJM132 (<i>URA3</i> selectable marker) and lost pRS315- <i>RFA2</i>	This study
Y-1042	AMA264	Isogenic to AMA253, except contains pRS315- <i>rfa2-A_x</i>	This study
Y-1043	AMA265	Isogenic to AMA253, except contains pRS315- <i>rfa2-D_x</i>	This study
Y-1044	AMA266	Isogenic to AMA253, except contains pRS315- <i>rfa2-ΔN_x</i>	This study
Y-1045	AMA267	Isogenic to AMA253, except contains pRS315- <i>rfa2-H2NT</i>	This study

Stock #	Strain Name	Genotype	Source
Y-1046	AMA268	Isogenic to AMA253, except contains pRS315- <i>rfa2-K_xR_x</i>	This study
Y-1047	AMA269	Isogenic to AMA253, except contains pRS315- <i>rfa2-S122A</i>	This study
Y-1048	AMA270	Isogenic to AMA253, except contains pRS315- <i>rfa2-S238/240A</i>	This study
Y-1049	AMA271	Isogenic to AMA253, except contains pRS315- <i>rfa2-S122A-S238/240A</i>	This study
Y-1050	AMA272	Isogenic to AMA253, except contains pRS315- <i>rfa2-S238/240D</i>	This study
Y-1051	AMA273	Isogenic to AMA257, except contains pRS315- <i>rfa2-A_x</i>	This study
Y-1052	AMA274	Isogenic to AMA257, except contains pRS315- <i>rfa2-D_x</i>	This study
Y-1053	AMA275	Isogenic to AMA257, except contains pRS315- <i>rfa2-ΔN_x</i>	This study
Y-1054	AMA276	Isogenic to AMA257, except contains pRS315- <i>rfa2-H2NT</i>	This study
Y-1055	AMA277	Isogenic to AMA257, except contains pRS315- <i>rfa2-K_xR_x</i>	This study
Y-1056	AMA278	Isogenic to AMA257, except contains pRS315- <i>rfa2-S122A</i>	This study
Y-1057	AMA279	Isogenic to AMA257, except contains pRS315- <i>rfa2-S238/240A</i>	This study
Y-1058	AMA280	Isogenic to AMA257, except contains pRS315- <i>rfa2-S122A-S238/240A</i>	This study
Y-1059	AMA281	Isogenic to AMA257, except contains pRS315- <i>rfa2-S238/240D</i>	This study
Y-1060	AMA282	Isogenic to AMA254, except contains pRS315- <i>rfa2-A_x</i>	This study
Y-1061	AMA283	Isogenic to AMA254, except contains pRS315- <i>rfa2-D_x</i>	This study
Y-1062	AMA284	Isogenic to AMA254, except contains pRS315- <i>rfa2-ΔN_x</i>	This study
Y-1063	AMA285	Isogenic to AMA254, except contains pRS315- <i>rfa2-H2NT</i>	This study
Y-1064	AMA286	Isogenic to AMA254, except contains pRS315- <i>rfa2-K_xR_x</i>	This study
Y-1065	AMA287	Isogenic to AMA254, except contains pRS315- <i>rfa2-S122A</i>	This study

Stock #	Strain Name	Genotype	Source
Y-1066	AMA288	Isogenic to AMA254, except contains pRS315- <i>rfa2-S238/240A</i>	This study
Y-1067	AMA289	Isogenic to AMA254, Isogenic to AMA257, except contains pRS315- <i>rfa2-S122A-S238/240A</i>	This study
Y-1068	AMA290	Isogenic to AMA254, Isogenic to AMA257, except contains pRS315- <i>rfa2-S238/240D</i>	This study
Y-1069	SJH2-390T-2-1A	*Dissected from SJH2-390T <i>MATa ADE3 cyh^r his2-390 HIS5 leu1-c LEU2 trp1-1 trp5-20 ura1 URA3</i>	This study
Y-1070	SJH2-390T-2-8C	*Dissected from SJH2-390T <i>MATa ADE3 his2-390 HIS5 LEU1 leu2-1 trp1-1 trp5-20 ura1 URA3</i>	This study
Y-1079	WAL199	Isogenic to TMW159 except contains pRS315- <i>rfa2-S238/240D</i>	Wendy Larson
Y-1086	WAL206	Isogenic to TMW159 except contains pRS315- <i>rfa2-S238/240A</i>	Wendy Larson
	M403.SPST5.1	Isogenic derivative of K264-10D except <i>Cas9-natMX</i> insertion at <i>SPO11</i> locus in addition to wild-type <i>SPO11</i>	Barbara Senger
	M403.SPST6.1	Isogenic derivative of K264-10D except <i>Cas9-natMX</i> insertion at <i>SPO11</i> locus in addition to wild-type <i>SPO11</i>	Barbara Senger
	M403.SPST9.1	Isogenic derivative of K264-10D except <i>Cas9-natMX</i> insertion at <i>SPO11</i> locus in addition to wild-type <i>SPO11</i>	Barbara Senger
	M163.SPST5.1	Isogenic derivative of RM26-26C except <i>Cas9-natMX</i> insertion at <i>SPO11</i> locus in addition to wild-type <i>SPO11</i>	Barbara Senger
	M163.SPST6.1	Isogenic derivative of RM26-26C except <i>Cas9-natMX</i> insertion at <i>SPO11</i> locus in addition to wild-type <i>SPO11</i>	Barbara Senger
	M163.SPST9.1	Isogenic derivative of RM26-26C except <i>Cas9-natMX</i> insertion at <i>SPO11</i> locus in addition to wild-type <i>SPO11</i>	Barbara Senger
	M163spo11Δ.5	Isogenic derivative of RM26-26C except <i>spo11Δ::kanMX</i>	This study
	M403spo11Δ.7	Isogenic derivative of K264-10D except <i>spo11Δ::kanMX</i>	This study

Stock #	Strain Name	Genotype	Source
	M403spo11Δ::Cas9 -natMX 2-1	Isogenic derivative of K264-10D except <i>spo11Δ::kanMXΔ::Cas9-natMX</i>	This study
	M163spo11Δ::Cas9 -natMX 1-2	Isogenic derivative of RM26-26C except <i>spo11Δ::kanMXΔ::Cas9-natMX</i>	This study

APPENDIX B. DIPLOID YEAST STRAINS

Strain Name	Cross	Relevant Genotype(s)
JSJ1	JKM139 x JKM179	WT
RM96	K264-10D x RM26-26C	WT
SJH2-1	RM96-15A-0C1 x RM182-55C-C1	<i>his2-390,ΔC/his2-ΔC</i> RFA2/RFA2 (WT)
SJH2-390T	B9B-A x M2034α	<i>HIS2/his2-390 ura1/URA1</i>
AMA100	M403.SPST5.1 x M163.SPST5.1	Isogenic to RM96, except <i>Cas9-natMX/Cas9-natMX</i> addition
AMA101	M403.SPST5.1 x M163.SPST6.1	Isogenic to RM96, except <i>Cas9-natMX/Cas9-natMX</i> addition
AMA102	M403.SPST5.1 x M163.SPST9.1	Isogenic to RM96, except <i>Cas9-natMX/Cas9-natMX</i> addition
AMA103	M403.SPST6.1 x M163.SPST5.1	Isogenic to RM96, except <i>Cas9-natMX/Cas9-natMX</i> addition
AMA104	M403.SPST6.1 x M163.SPST6.1	Isogenic to RM96, except <i>Cas9-natMX/Cas9-natMX</i> addition
AMA105	M403.SPST6.1 x M163.SPST9.1	Isogenic to RM96, except <i>Cas9-natMX/Cas9-natMX</i> addition
AMA106	M403.SPST9.1 x M163.SPST5.1	Isogenic to RM96, except <i>Cas9-natMX/Cas9-natMX</i> addition
AMA107	M403.SPST9.1 x M163.SPST6.1	Isogenic to RM96, except <i>Cas9-natMX/Cas9-natMX</i> addition
AMA108	M403.SPST9.1 x M163.SPST9.1	Isogenic to RM96, except <i>Cas9-natMX/Cas9-natMX</i> addition
AMA109	M403spo11Δ.7 x M163spo11Δ.5	Isogenic to RM96, except <i>spo11Δ::kanMX</i>
AMA110	K264-10D x RM26-26C <i>spo11Δ::Cas9-natMX</i>	Isogenic to RM96, except <i>SPO11/spo11Δ::Cas9-natMX</i>
AMA111	M403spo11Δ::Cas9-natMX 2-1 x RM26-26C	Isogenic to RM96, except <i>spo11Δ::Cas9-natMX/SPO11</i>
AMA112	M403spo11Δ.7 x M163spo11Δ::Cas9-natMX 1-2	Isogenic to RM96, except <i>spo11Δ::kanMX/spo11Δ::Cas9-natMX</i>
AMA113	M403spo11Δ::Cas9-natMX 2-1 x M163spo11Δ.5	Isogenic to RM96, except <i>spo11Δ::Cas9-natMX/spo11Δ::kanMX</i>
AMA114	M403spo11Δ::Cas9-natMX 2-1 x M163spo11Δ::Cas9-natMX 1-2	Isogenic to RM96, except <i>spo11Δ::Cas9-natMX/spo11Δ::Cas9-natMX</i>

Strain Name	Cross	Relevant Genotype(s)
AMA116	CMK005 x CMK011	Isogenic to SJH2-1, except <i>rfa2-ΔN_x/Δrfa2-N_x</i>
AMA118	TMW307 x TMW302	Isogenic to RM96, except <i>rfa2-A_x/rfa2-A_x</i>
AMA120	TMW309 x TMW304	Isogenic to RM96, except <i>rfa2-ΔN_x/Δrfa2-N_x</i>
AMA121	TMW310 x TMW305	Isogenic to RM96, except <i>rfa2-cDNA/rfa2-cDNA</i>
AMA129	CMK001 x AMA126	Isogenic to SJH2-1, except <i>rfa2-A_x/rfa2-A_x</i>
AMA131	CMK003 x AMA124	Isogenic to SJH2-1, except <i>rfa2-D_x/rfa2-D_x</i>
AMA172	AMA145 x AMA149	Isogenic to RM96, except <i>spo11Δ::kanMX</i> , Isogenic to AMA109 (generated from new haploid strains)
AMA176	AMA152 x AMA154	Isogenic to RM96, except <i>sae2Δ::hphNT</i>
AMA180	AMA161 x AMA168	Isogenic to RM96, except <i>dmc1Δ::hphNT</i>
AMA184	AMA167 x AMA165	Isogenic to RM96, except <i>ndt80Δ::natMX</i>
AMA206	AMA122 x AMA141	Isogenic to RM96, except <i>rfa2-D_x/rfa2-D_x</i>
AMA244	AMA193 x AMA188	Isogenic to AMA180, except <i>rfa2-A_x/rfa2-A_x</i>
AMA245	AMA240 x AMA190	Isogenic to AMA180, except <i>rfa2-D_x/rfa2-D_x</i>
AMA246	AMA217 x AMA216	Isogenic to AMA180, except <i>rfa2-ΔN_x/rfa2-ΔN_x</i>
AMA247	AMA196 x AMA218	Isogenic to AMA184, except <i>rfa2-A_x/rfa2-A_x</i>
AMA248	AMA199 x AMA192	Isogenic to AMA184, except <i>rfa2-D_x/rfa2-D_x</i>
AMA249	AMA201 x AMA220	Isogenic to AMA184, except <i>rfa2-ΔN_x/rfa2-ΔN_x</i>
AMA293	AWY194 x AWY092	Isogenic to JSJ1, except <i>rfa2-A_x/rfa2-A_x</i>
AMA295	AWY016 x AWY096	Isogenic to JSJ1, except <i>rfa2-D_x/rfa2-D_x</i>
AMA297	AMA147 x AWY097	Isogenic to JSJ1, except <i>ΔN_x/Δrfa2-N_x</i>
AMA299	AMA202 x AMA233	Isogenic to AMA172, except <i>rfa2-A_x/rfa2-A_x</i>
AMA300	AMA243 x AMA222	Isogenic to AMA172, except <i>rfa2-D_x/rfa2-D_x</i>

Strain Name	Cross	Relevant Genotype(s)
AMA301	AMA205 x AMA242	Isogenic to AMA172, except <i>rfa2-ΔN_x</i> / <i>rfa2-ΔN_x</i>
AMA302	AMA227 x AMA231	Isogenic to AMA176, except <i>rfa2-A_x</i> / <i>rfa2-A_x</i>
AMA303	AMA228 x AMA237	Isogenic to AMA176, except <i>rfa2-D_x</i> / <i>rfa2-D_x</i>
AMA304	AMA229 x AMA224	Isogenic to AMA176, except <i>rfa2-ΔN_x</i> / <i>rfa2-ΔN_x</i>

APPENDIX C. PLASMIDS

Stock #	Plasmid Name	Plasmid Genotype/Description	Source
B-99	pRS313- <i>RFA1</i>	pRS313- <i>RFA1</i> (wild-type); centromeric vector with <i>HIS3</i> and amp ^r selectable marker	(Ghospurkar et al. 2015b)
B-101	pRS313- <i>rfa1-11</i>	pRS313- <i>rfa1-11</i> ; centromeric vector with <i>HIS3</i> and amp ^r selectable marker	(Ghospurkar et al. 2015b)
B-108	pAW07	pRS315- <i>rfa2</i> -WT(cDNA); centromeric vector with <i>LEU2</i> and amp ^r selectable marker	Andre Walther
B-109	pAW08	pRS315- <i>rfa2</i> -D _x ; centromeric vector with <i>LEU2</i> and amp ^r selectable marker	Andre Walther
B-110	pAW09	pRS315- <i>rfa2</i> -A _x ; centromeric vector with <i>LEU2</i> and amp ^r selectable marker	Andre Walther
B-111	pAW10	pRS315- <i>rfa2</i> -ΔN _x ; centromeric vector with <i>LEU2</i> and amp ^r selectable marker	Andre Walther
B-112	pJM132	(pRS416 derived) centromeric vector containing wild-type <i>RFA1</i> , <i>RFA2</i> , and <i>RFA3</i> genes expressed from their native promoters; <i>URA3</i> and amp ^r selectable markers	(Maniar, Wilson and Brill 1997)
B-128	pGAL-HO	pGAL-HO; <i>HO</i> endonuclease expressed from <i>GAL</i> promoter	(Herskowitz and Jensen 1991)
B-?	pKKW1	contains <i>kanMX</i> cassette, PCR amplified from for one-step gene replacement	Kit Wong
B-423	pAG416-GPD- <i>ccdB</i>	pRS416 vector backbone; <i>URA3</i> , <i>camr</i> ^r and amp ^r selectable markers	Susan Lindquist (Addgene 14148)
B-751	pAMH1	pRS315- <i>rfa2</i> -H2NT; <i>LEU2</i> and amp ^r selectable markers (pAW10 derivative)	Anna Herauf (Ghospurkar et al. 2015a)
B-833	pAML1	pEG202K-LexA-RPA1-F; human RPA1-F yeast two hybrid vector	Alexis Larson
B-894	pJM132-RPA2-RPA3-RPA1- <i>kanMX</i>	cRPA; canonical RPA containing RPA2, <i>kanMX</i> and amp ^r selectable markers	Padmaja Ghospurkar
B-895	pJM132-Rpa4-RPA3-RPA1- <i>kanMX</i>	aRPA; alternative RPA containing Rpa4, <i>kanMX</i> and amp ^r selectable markers	Padmaja Ghospurkar
B-939	pPLG62	pSJH18-34K, pSJH18-34 amp ^r selectable marker replaced by <i>kan</i> ^r	Padmaja Ghospurkar
B-1005	pRS315- <i>rfa2</i> -S122A	pRS315- <i>rfa2</i> -S122A; <i>LEU2</i> and amp ^r selectable markers	Timothy Wilson

Stock #	Plasmid Name	Plasmid Genotype/Description	Source
B-1007	pTMW01	pRS306-rfa2-WT(cDNA); integrating vector for 2-step gene replacement; <i>URA3</i> and amp ^r selectable markers	Timothy Wilson
B-1008	pTMW02	pRS306-rfa2-D _x ; integrating vector for 2-step gene replacement; <i>URA3</i> and amp ^r selectable markers	Timothy Wilson
B-1009	pTMW03	pRS306-rfa2-A _x ; integrating vector for 2-step gene replacement; <i>URA3</i> and amp ^r selectable markers	Timothy Wilson
B-1010	pTMW04	pRS306-rfa2-ΔN _x ; integrating vector for 2-step gene replacement; <i>URA3</i> and amp ^r selectable markers	Timothy Wilson
B-1049	pCRCT	Plasmid containing iCas9, tracrRNA, and crRNA cassette with lacZ to screen for target sequence insertion; <i>URA3</i> and amp ^r selectable markers	Zehua Bao (Addgene)
B-1053	pCas9Nat-9	pCas9Nat-9, precursor plasmid to pST+ST-5	Barbara Senger
B-1055	pSP+ST-5	pSP+ST-5; plasmid containing <i>Cas9-natMX</i> , in which <i>Cas9</i> has <i>SPO11</i> promoter and terminator sequences	Barbara Senger
B-1093	pJAB001a	pEG202K-LexA-Rfa1-F	Jason Balster
B-1132	pNPT2	pRS315-rfa1-t11; <i>LEU2</i> and amp ^r selectable markers	Noelle Torrence
B-1134	pAMA1	pScCas9#13, <i>Saccharomyces cerevisiae</i> codon optimized Cas9 containing a frameshift mutation in ScCas9-1 G-block (G-32) used as a vector for reinsertion of ScCas9-1; contains tracrRNA, and crRNA cassette with lacZ to screen for target sequence insertion; <i>URA3</i> and amp ^r selectable markers	This study
B-1177	pCRT-ScCas9.1	Corrected <i>ScCas9</i> identified by RA from BIOC 474/674 2017 class; contains tracrRNA, and crRNA cassette with lacZ to screen for target sequence insertion; <i>URA3</i> and amp ^r selectable markers; contains an additional <i>BsaI</i> site introduced by codon optimization	BIOC 474/674 2017 class
B-1179	pAMA6	ScCas9 Q1; contains <i>ScCas9</i> , tracrRNA, and crRNA cassette with lacZ to screen for target sequence insertion; <i>URA3</i> and amp ^r selectable markers	This study

Stock #	Plasmid Name	Plasmid Genotype/Description	Source
B-1180	pAMA7	ScCas9 Q2; contains <i>ScCas9</i> , <i>tracrRNA</i> , and <i>crRNA</i> cassette with <i>lacZ</i> to screen for target sequence insertion; <i>URA3</i> and <i>amp^r</i> selectable markers	This study
B-1181	pAMA8	ScCas9 Q3; contains <i>ScCas9</i> , <i>tracrRNA</i> , and <i>crRNA</i> cassette with <i>lacZ</i> to screen for target sequence insertion; <i>URA3</i> and <i>amp^r</i> selectable markers	This study
B-1182	pAMA9	ScCas9 P3; contains <i>ScCas9</i> , <i>tracrRNA</i> , and <i>crRNA</i> cassette with <i>lacZ</i> to screen for target sequence insertion; <i>URA3</i> and <i>amp^r</i> selectable markers	This study
B-1183	pAMA10	ScCas9 P4; contains <i>ScCas9</i> , <i>tracrRNA</i> , and <i>crRNA</i> cassette with <i>lacZ</i> to screen for target sequence insertion; <i>URA3</i> and <i>amp^r</i> selectable markers	This study
B-1192	pWAL020	pRS315-RFA1; <i>LEU2</i> and <i>amp^r</i> selectable markers	Wendy Larson
B-1198	pBLS015	pRS315-rfa2-K _x R _x ; <i>LEU2</i> and <i>amp^r</i> selectable markers	Barbara Senger/Wendy Larson
B-1232	pCAH001	pRS315-rfa2-S238/240A; <i>LEU2</i> and <i>amp^r</i> selectable markers	Cristian Hernandez
B-1238	pCAH002	pRS315-rfa2-S122A-S238/240A; <i>LEU2</i> and <i>amp^r</i> selectable markers	Cristian Hernandez
B-1240	pAMA18	pAG416-mec1-aa1650-2290, derived from pAG416-GPD-ccdB, GPD-ccdB is removed and contains <i>MEC1</i> -aa1650-2290; isolate #4	This study
B-1241	pAMA19	pAG416-mec1-aa1650-2290, derived from pAG416-GPD-ccdB, GPD-ccdB is removed and contains <i>MEC1</i> -aa1650-2290; isolate #6	This study
B-1251	pAMA29	pAG-406-mec1-aa1650-2290, derived from pAMA18, by CEN-ARS removal through site-directed mutagenesis	This study
B-1252	pAMA30	pAG-406-mec1-aa1650-2290-S1964A, derived from pAMA29 by site-directed mutagenesis with <i>mec1</i> -S1964A-SphI-F	This study
B-1256	pAMA34	pAG-406-mec1-aa1650-2290-S1964E, derived from pAMA29 by site-directed mutagenesis with <i>mec1</i> -S1964E-PfeI-F	This study

Stock #	Plasmid Name	Plasmid Genotype/Description	Source
B-1260	pWAL021	pRS315-rfa2-S238/240D; <i>LEU2</i> and amp ^r selectable markers	Wendy Larson
B-1263	pAMA38	pAG-406-mec1-aa1650-2290-S1964D, derived from pAMA29 by site-directed mutagenesis with mec1-S1964D-BclI-F	This study
B-1281	pAMA41	cRPA + ScDBD-F; canonical RPA (cRPA) containing RPA2, RPA1-DBD-F has been replaced with the <i>Saccharomyces cerevisiae</i> Rfa1-DBD-F, <i>kanMX</i> and amp ^r selectable markers; derived from pJM132-RPA2-RPA3-RPA1-kanMX	This study
B-1282	pAMA42	cRPA + ScDBD-F+L; canonical RPA (cRPA) containing RPA2, RPA1-DBD-F+L has been replaced with the <i>Saccharomyces cerevisiae</i> Rfa1-DBD-F+L, <i>kanMX</i> and amp ^r selectable markers; derived from pJM132-RPA2-RPA3-RPA1-kanMX	This study
B-1283	pAMA43	aRPA + ScDBD-F; alternative RPA (aRPA) containing Rpa4, RPA1-DBD-F has been replaced with the <i>Saccharomyces cerevisiae</i> Rfa1-DBD-F, <i>kanMX</i> and amp ^r selectable markers; derived from pJM132-Rpa4-RPA3-RPA1-kanMX	This study
B-1284	pAMA44	aRPA + ScDBD-F+L; alternative RPA (aRPA) containing Rpa4, RPA1-DBD-F+L has been replaced with the <i>Saccharomyces cerevisiae</i> Rfa1-DBD-F+L, <i>kanMX</i> and amp ^r selectable markers; derived from pJM132-Rpa4-RPA3-RPA1-kanMX	This study

APPENDIX D. PRIMERS

Stock #	Primer Name	Sequence	Purpose
O-000	PRIMER-F	AAAAAAAAAAAAAAAAAAAA AAAAAAAAAAAAAAAAAAAA	Amplification
O-194	RAD52-F	TTG GCG TCT GTA TCA TCT GCT TGC	Amplification of <i>RAD52</i> locus; this study <i>rad52Δ::TRP1</i>
O-195	RAD52-R	CAA TGA ACC TAA GGA TTC CGC TG	Amplification of <i>RAD52</i> locus; this study <i>rad52Δ::TRP1</i>
O-198	RAD17-F	GAT GGT ACT GGA TGG AGC AC	Amplification of <i>RAD17</i> locus; this study <i>rad17Δ::LEU2</i>
O-199	RAD17-R	GTT GTC GGT GCC TCC GTT G	Amplification of <i>RAD17</i> locus; this study <i>rad17Δ::LEU2</i>
O-300	Remove-ARS4-CEN6	TAA TGT CAT GAT AAT AAT GGT TTC TTA GAC GTC AGG TGG CAC TTT TCG GGG AAA TGT GCG	Used in site-directed mutagenesis to remove the autonomously replicating sequence (origin of replication) and centromeric regions.
O-338/ O-767/ O-1165	RFA2-UP-FOR	TAG CAA TTC CTT TGG CCT CGA TGA GCT TCC	Amplification of <i>RFA2</i> locus
O-339/ O-768/ O-1166	RFA2-DOWN-REV	GAT AAA ACC CTG GTC AGT CAA GGT CGT AC	Amplification of <i>RFA2</i> locus
O-547	pJG4-5-TOF1-FOR	ATT ATG CCT CTC CCG AAT TCA TGT CTG CTG ATT TGC AAC A	External <i>TOF1</i> locus primer; for gene deletion confirmation
O-548	pJG4-5-TOF1-REV	GAA GTC CAA AGC TTC TCG AGT CAA TCA TCA CTA TCA CCT T	External <i>TOF1</i> locus primer; for gene deletion confirmation
O-650	pJG4-5-UP-Sequence	GAT CCA GCC TGA CTG GCT GAA ATC GAA TGG	Used for sequencing Y2H prey vectors
O-701	kanMX4-UP-REV	GAT TGT CGC ACC TGA TTG CCC GAC	Internal <i>kanMX</i> cassette primer; for gene deletion confirmation

Stock #	Primer Name	Sequence	Purpose
O-702	kanMX4-DOWN-FOR	AGT CGT CAC TCA TGG TGA TTT CTC	Internal <i>kanMX</i> cassette primer; for gene deletion confirmation
O-759	SPO11-UP-FOR	TTG TTC GAG AGT CAT ATC AAT GAC	Upstream <i>SPO11</i> forward primer
O-755	Cas9-NAT-UP-REV	TTT TCA TGG TAC GCC ACC TCG TCC	Internal upstream <i>Cas9-natMX</i> Reverse primer
O-756	Cas9-NAT-DOWN-FOR	TTC GTC GTC CGA TTC GTC GTC GG	Internal downstream <i>Cas9-natMX</i> forward primer
O-760	SPO11-DOWN-REV	GTG GTT AGT ACA CAT CGT TGT GGC	Downstream <i>SPO11</i> reverse primer
O-765	SPO11-DELTA-NATMX-F	CCT TAA GAT TTT ACG ATT TAC TAA GTT CAC CTT CTC GAC ATG GAG GCC CAG AAT AC	Forward primer used to delete <i>SPO11</i> with either <i>natMX</i> or <i>kanMX</i> cassette
O-766	SPO11-DELTA-NATMX-R	AAA CAT TTT TTA TAA AGC AAC AGC TCC CAT TCT TAT CAG TAT AGC GAC CAG CAT TC	Reverse primer used to delete <i>SPO11</i> with either <i>natMX</i> or <i>kanMX</i> cassette
O-787	SPO11-UP-FOR-LONG	CTA GAC CCA TGA ATT ACT TCG TGG	Further upstream <i>SPO11</i> forward primer
O-788	SPO11-DOWN-REV-LONG	TCT ATA ACC TAC ACC ATT AGT AGC C	Further downstream <i>SPO11</i> reverse primer
O-871	hphN-1406-1465-F	CGT CTG GAC CGA TGG CTG TGT AGA AGT ACT CGC CGA TAG TGG AAA CCG ACG CCC CAG CAC	Internal <i>hphNT</i> cassette primer; for gene deletion confirmation
O-872	hphN-915-975-R	CGC ACT GAC GGT GTC GTC CAT CAC AGT TTG CCA GTG ATA CAC ATG GGG ATC AGC AAT CGC	Internal <i>hphNT</i> cassette primer; for gene deletion confirmation
O-889	pCRT-ScCas9-F	ATT AGA AAG AAA GCA TAG CAA TCT AAT CTA AGT TTT CTA GAT GGA CAA GAA GTA CTC TAT	Used to amplify G-32 ScCas9 G-block #1

Stock #	Primer Name	Sequence	Purpose
O-904	ScCas9-2,4-R	TTC GAT CAA TGG TCT CTT TGT CGA CCA AAG CCT TCA ACA AAG TCA AGT CTT GGT GGT GTT	Used to amplify G- 32 ScCas9 G-block #1
O-905	ScCas9-2,4-F	TTG TTG AAG GCT TTG GTC GAC AAA GAG ACC ATT GAT CGA AAC TAA CGG TGA AAC TGG TGA	Used to amplify G- 36 ScCas9 G-block #5
O-906	pCRT-ScCas9-R-NEW	ACT ATA AAT CGT AAA GAC ATA AGA GAT CCG CCT ATC ATT AAA CCT TTC TCT TCT TCT TTG	Used to amplify G- 36 ScCas9 G-block #5
O-907	ScCas9-1-R	AGT CAA GTC TTG GTG GTG TTC GTC GTA TCT	Used to amplify G- 32 ScCas9 G-block #1
O-908	ScCas9-2-F	TCT AAG GAC ACT TAC GAC GAC GAC TTG GAC	Used to amplify G- 33 ScCas9 G-block #2
O-909	ScCas9-2-R	CTT CAA CAA GTC GTG GTA AGT ACC CAA AGA	Used to amplify G- 33 ScCas9 G-block #2
O-910	ScCas9-3-F	GGT ATG AGA AAG CCA GCT TTC TTG TCT GGT	Used to amplify G- 34 ScCas9 G-block #3
O-911	ScCas9-3-R	ACC TCT GTT CTT GTC AGA TCT AGT CAA AAC	Used to amplify G- 34 ScCas9 G-block #3
O-912	ScCas9-4-F	CAC CCA GTT GAA AAC ACT CAA TTG CAA AAC	Used to amplify G- 35 ScCas9 G-block #4
O-913	ScCas9-4-R	GTA CTT CTT TGG GTC CCA GTC CTT CTT TCT	Used to amplify G- 35 ScCas9 G-block #4
O-935	LEU2-up-rev	CAAAACGGCATCAGCCTTC T	Internal <i>LEU2</i> cassette primer; for gene deletion confirmation
O-936	LEU2-down-for	TCAACCCTATCGCCACTATC	Internal <i>LEU2</i> cassette primer; for gene deletion confirmation

Stock #	Primer Name	Sequence	Purpose
O-937	TRP1-up-rev	CAAGTATTTTCGGAGTGCCT G	Internal <i>TRP1</i> cassette primer; for gene deletion confirmation
O-938	TRP1-down-for	CGATTTCTGACTGGGTTGGA	Internal <i>TRP1</i> cassette primer; for gene deletion confirmation
O-941	mec3-up-for	TTATAAAACATCGAACATG T	External <i>MEC3</i> locus primer; for gene deletion confirmation
O-942	mec3-down-rev	CAAATTTAAAAAGTTTCCTA	External <i>MEC3</i> locus primer; for gene deletion confirmation
O-943	rad9-up-for	ACCTCAAGGGGAAGTGTC A	External <i>RAD9</i> locus primer; for gene deletion confirmation
O-944	rad9-down-rev	TGTCGTCCCAGTACTCAACT	External <i>RAD9</i> locus primer; for gene deletion confirmation
O-945	rad17-up-for	GACAATTGATCTTTTTGAGA	External <i>RAD17</i> locus primer; for gene deletion confirmation
O-946	rad17-down-rev	GCCGAAGTTACTATCGAAG A	External <i>RAD17</i> locus primer; for gene deletion confirmation
O-947	rad52-up-for	TCTTGTCACAATGATCAAA A	External <i>RAD52</i> locus primer; for gene deletion confirmation
O-948	rad52-down-rev	AAAATCAATTATGGTCAGA A	External <i>RAD52</i> locus primer; for gene deletion confirmation
O-991	pCRT-ScCas9- Corrected(FS7)-ScaI-F	GTT TTC TAG ATG GAC AAG AAA TAC TCT ATC GGT TTG GAC ATC GGT ATC AAC TCT GTT GGT	Used by BIOC474/674 2017 to correct mutations in a pCRT-ScCas9 candidate by site- directed mutagenesis

Stock #	Primer Name	Sequence	Purpose
O-992	pCRT-ScCas9-Corrected(M161T)-NdeI-F	AGA TTG ATC TAC TTG GCT TTG GCT CAT ATG ATC AAG TTC AGA GGT CAC TTC TTG ATC GAA	Used by BIOC474/674 2017 to correct mutations in a pCRT-ScCas9 candidate by site-directed mutagenesis
O-1069	REM-XTRA-BsaI-pCRT-ScCas9-F	CAC TTT GGC TAA CGG TGA AAT CAG AAA AAG ACC ATT GAT CGA AAC TAA CGG TGA AAC TGG	Used in site-directed mutagenesis to remove the extra <i>BsaI</i> site in pCRT-ScCas9.1 (RA)
O-1200	<i>mec1</i> -aa1650-2290-FOR	GCG CGC GTA ATA CGA CTC ACT ATA GGG CGA ATT GGG ATT ATC GAA TGG AAC GTA TTG GGG	Amplification of <i>MEC1</i> gene from coding region corresponding to aa 1650-2290
O-1201	<i>mec1</i> -aa1650-2290-REV	CGC AAT TAA CCC TCA CTA AAG GGA ACA AAA GCT GGA GCC AAC GTG ACT TCA CTA GAC TTC	Amplification of <i>MEC1</i> gene from coding region corresponding to aa 1650-2290
O-1202	<i>mec1</i> -S1964A-SphI-F	AGC ATA TTT TAG AAA AGT ATA GAC AGC ATG CGC AAA ATC CTC ATG ATC TAG TTT CTA GTG	Used in site-directed mutagenesis to create <i>mec1-S1964A</i>
O-1203	<i>mec1</i> -S1964D-BclI-F	AGC ATA TTT TAG AAA AGT ATA GAC AAC ATG ATC AAA ATC CTC ATG ATC TAG TTT CTA GTG	Used in site-directed mutagenesis to create <i>mec1-S1964D</i>
O-1204	<i>mec1</i> -S1964E-PfeI-F	AGC ATA TTT TAG AAA AGT ATA GAC AAC ATG AGC AGA ATC CTC ATG ATC TAG TTT CTA GTG	Used in site-directed mutagenesis to create <i>mec1-S1964E</i>

APPENDIX E. IDT G-BLOCKS

Stock #	G-block Name	Sequence	Purpose
G-000	FRAGMENT	AAAAAAAAAAAAAAAAAAAAAAAAA AAAAAAAAAAAAAAAAAAAAAAAAA AAAAAAAAA	Amplification
G-23	rpal-rfa1-DBD-F-Linker	TTATCACTTTAAGTTCTACACGTA AAACAAAACACTATTCCTCTTCTT ATTACGGTAAAGGCGAAACCAGC AAGAAGACCAGATTATACTTACA AGAGATGAGCAGTGTTCACCTTT CGAGGGGCGATTTTCATAGCATC TTCACCAATAAGCAAAGGTACGA TAATCCCACCGGTGGCGTTTATC AAGTTTATAACACCAGGAAATCT GATGGGGCTAACAGCAACAGAA AGAATTTGATCATGATTTCCGAT GGTATTTACCATATGAAGGCTCT GTTGAGAAACCAAGCTGCATCCA AGTTCCAGTCAATGGAACTACAA AGGGGTGATATCATTTCGCGTGAT AATTGCAGAACCTGCTATTGTCA GGGAAAGAAAGAAATACGTTT	Replacement of <i>Saccharomyces cerevisiae</i> RFA1 F-linker domain with <i>Homo sapiens</i> RPA1 F-linker domain
G-24	rpal-rfa1-DBD-F	ACTATTCCTCTTATTACGGT AAAGGCGAAACCAGCAAGAAGA CCAGATTATACTTACAAGAGATG AGCAGTGTTCACCTTTTCGAGGGG CGATTTTCATAGCATCTTCACCAA TAAGCAAAGGTACGATAATCCCA CCGGTGGCGTTTATCAAGTTTATA ACACCAGGAAATCTGATGGGGCT AACAGCAACAGAAAGAATTTGAT CATGATTTCCGATGGTATTTACCA TATGAAGGCTCTGTTGAGAAACC AAGCTGCATCCAAGTTCCAGTCA ATGGAACACTACAAAGGGGTGATAT CATTCGCGTGATAATTGCAGAAC CTGCTATTGTCAGGGAAAGAAAG AAATACGTTCTTTTAGTAGATGA CTTTGAGTTGGTCCAGTCG	Replacement of <i>Saccharomyces cerevisiae</i> RFA1 F-domain with <i>Homo sapiens</i> RPA1 F-domain
G-32	ScCas9-1	ATGGACAAGAAGTACTCTATCGG TTTGGACATCGGTAATACTCTGT TGGTTGGGCTGTTATCACTGACG AATACAAGGTTCCATCTAAGAAG TTCAAGGTTTTGGGTAACACTGA CAGACACTCTATCAAGAAGAACT	Creation of <i>Saccharomyces cerevisiae</i> codon optimized Cas9

Stock #	G-block Name	Sequence	Purpose
		TGATCGGTGCTTTGTTGTTGCGACT CTGGTGAAACTGCTGAAGCTACT AGATTGAAGAGAACTGCTAGAAG AAGATACTAGAAAGAAAGAAC AGAATCTGTTACTTGCAAGAAAT CTTCTCTAACGAAATGGCTAAGG TTGACGACTCTTTCTTCCACAGAT TGGAAGAATCTTTCTTGGTTGAA GAAGACAAGAAGCACGAAAGAC ACCCAATCTTCGGTAACATCGTT GACGAAGTTGCTTACCACGAAAA GTACCCAATCTTACTACTTGA GAAAGAAGTTGGTTGACTCTACT GACAAGGCTGACTTGAGATTGAT CTACTTGGCTTTGGCTCACATGAT CAAGTTCAGAGGTCACTTCTTGA TCGAAGGTGACTTGAACCCAGAC AACTCTGACGTTGACAAGTTGTT CATCCAATTGGTTCAAACCTTACA ACCAATTGTTTGAAGAAAACCCA ATCAACGCTTCTGGTGGTTGACGCT AAGGCTATCTTGTCTGCTAGATTG TCTAAGTCTAGAAGATTGGAAAA CTTGATCGCTCAATTGCCAGGTG AAAAGAAGAACGGTTTGTTCGGT AACTTGATCGCTTTGTCTTTGGGT TTGACTCCAACTTCAAGTCTAA CTTCGACTTGGCTGAAGACGCTA AGTTGCAATTGTCTAAGGACACT TACGACGACGACTTGGACAACCT GTTGGCTCAAATCGGTGACCAAT ACGCTGACTTGTCTTGGCTGCTA AGAACTTGTCTGACGCTATCTTGT TGTCTGACATCTTGAGAGTTAAC ACTGAAATCACTAAGGCTCCATT GTCTGCTTCTATGATCAAGAGAT ACGACGAACACCACCAAGACTTG ACT	
G-33	ScCas9-2	TCTAAGGACACTTACGACGACGA CTTGGACAACCTGTTGGCTCAA TCGGTGACCAATACGCTGACTTG TTCTTGGCTGCTAAGAAGTGTCT GACGCTATCTTGTGTCTGACATC TTGAGAGTTAACTGAAATCAC TAAGGCTCCATTGTCTGCTTCTAT	Creation of <i>Saccharomyces cerevisiae</i> codon optimized <i>Cas9</i>

Stock #	G-block Name	Sequence	Purpose
G-34	ScCas9-3	GATCAAGAGATACGACGAACACC ACCAAGACTTGACTTTGTTGAAG GCTTTGGTTAGACAACAATTGCC AGAAAAGTACAAGGAAATCTTCT TCGACCAATCTAAGAACGGTTAC GCTGGTTACATCGACGGTGGTGC TTCTCAAGAAGAATTTTACAAGT TCATCAAGCCAATCTTGGAAAAG ATGGACGGTACTGAAGAATTGTT GGTTAAGTTGAACAGAGAAGACT TGTTGAGAAAGCAAAGAACTTTC GACAACGGTTCTATCCCACACCA AATCCACTTGGGTGAATTGCACG CTATCTTGAGAAGACAAGAAGAC TTCTACCCATTCTTGAAGGACAA CAGAGAAAAGATCGAAAAGATCT TGACTTTCAGAATCCCATACTAC GTTGGTCCATTGGCTAGAGGTAA CTCTAGATTTCGCTTGGATGACTA GAAAGTCTGAAGAACTATCACT CCCTGGAACTTCGAAGAAGTTGT TGACAAGGGTGCTTCTGCTCAAT CTTTCATCGAAAGAATGACTAAC TTCGACAAGAACTTGCCAAACGA AAAGGTTTTGCCAAAGCACTCTT TGTTGTACGAATACTTCACTGTTT ACAACGAATTGACTAAGGTTAAG TACGTTACTGAAGGTATGAGAAA GCCAGCTTCTTGTCTGGTGAACA AAAGAAGGCTATCGTTGACTTGT TGTTCAAGACTAACAGAAAGGTT ACTGTTAAGCAATTGAAGGAAGA CTACTTCAAGAAGATCGAATGTT TCGACTCTGTTGAAATCTCTGGTG TTGAAGACAGATTCAACGCTTCT TTGGGTACTIONACCACGACTTGTTG AAG GGTATGAGAAAGCCAGCTTTCTT GTCTGGTGAACAAAAGAAGGCTA TCGTTGACTTGTTGTTCAAGACTA ACAGAAAGGTTACTGTTAAGCAA TTGAAGGAAGACTACTTCAAGAA GATCGAATGTTTCGACTCTGTTGA AATCTCTGGTGTGTAAGACAGAT TCAACGCTTCTTTGGGTACTIONACC	Creation of <i>Saccharomyces cerevisiae</i> codon optimized <i>Cas9</i>

Stock #	G-block Name	Sequence	Purpose
G-35	ScCas9-4	ACGACTTGTTGAAGATCATCAAG GACAAGgacttcctggataacgaagaaatgaa gacattttggaagatattgtttgaccctgacattgttga aGACAGAGAAATGATCGAAGAAA GATTGAAGACTTACGCTCACTTG TTCGACGACAAGGTTATGAAGCA ATTGAAGAGAAGAAGATACTG GTTGGGGTAGATTGTCTAGAAAG TTGATCAACGGTATCAGAGACAA GCAATCTGGTAAGACTATCTTGG ACTTCTTGAAGTCTGACGGTTTCG CTAACAGAACTTCATGCAATTG ATCCACGACGACTCTTTGACTTTC AAGGAAGACATCCAAAAGGCTCA AGTTTCTGGTCAAGGTGACTCTTT GCACGAACACATCGCTAACTTGG CTGGTTCTCCAGCTATCAAGAAG GGTATCTTGCAAACGTTAAGGT TGTTGACGAATTGGTTAAGGTTA TGGGTAGACACAAGCCAGAAAAC ATCGTTATCGAAATGGCTAGAGA AAACCAAACACTCAAAAAGGGTC AAAAGAACTCTAGAGAAAGAAT GAAGAGAATCGAAGAAGGTATC AAGGAATTGGGTTCTCAAATCTT GAAGGAACACCCAGTTGAAAACA CTCAATTGCAAAACGAAAAGTTG TACTTGTACTACTTGCAAAACGG TAGAGACATGTACGTTGACCAAG AATTGGACATCAACAGATTGTCT GACTACGACGTTGACCACATCGT TCCACAATCTTTCTTGAAGGACG ACTCTATCGACAACAAGGTTTTG ACTAGATCTGACAAGAACAGAGG T CACCCAGTTGAAAACACTCAATT GCAAAACGAAAAGTTGTAAGTTGT ACTACTTGCAAAACGGTAGAGAC ATGTACGTTGACCAAGAATTGGA CATCAACAGATTGTCTGACTACG ACGTTGACCACATCGTTCCACAA TCTTTCTTGAAGGACGACTCTATC GACAACAAGGTTTTGACTAGATC TGACAAGAACAGAGGTAAGTCTG ACAACGTTCCATCTGAAGAAGTT	Creation of <i>Saccharomyces cerevisiae</i> codon optimized Cas9

Stock #	G-block Name	Sequence	Purpose
G-36	ScCas9-5	GTTAAGAAGATGAAGAACTACTG GAGACAATTGTTGAACGCTAAGT TGATCACTCAAAGAAAGTTCGAC AACTTGACTAAGGCTGAAAGAGG TGGTTTGTCTGAATTGGACAAGG CTGGTTTCATCAAGAGACAATTG GTTGAAACTAGACAAATCACTAA GCACGTTGCTCAAATCTTGGACT CTAGAATGAACACTAAGTACGAC GAAAACGACAAGTTGATCAGAGA AGTTAAGGTTATCACTTTGAAGT CTAAGTTGGTTTCTGACTTCAGAA AGGACTTCCAATTCTACAAGGTT AGAGAAATCAACAACTACCACCA CGCTCACGACGCTTACTTGAACG CTGTTGTTGGTACTGCTTTGATCA AGAAGTACCCAAAGTTGGAATCT GAATTTGTTTACGGTGACTACAA GGTTTACGACGTTAGAAAGATGA TCGCTAAGTCTGAACAAGAAATC GGTAAGGCTACTGCTAAGTACTT CTTCTACTCTAACATCATGAACTT CTTCAAGACTGAAATCACTTTGG CTAACGGTGAAATCAGAAAGAGA CCATTGATCGAAACTAACGGTGA AACTGGTGAAATCGTTTGGGACA AGGGTAGAGACTTCGCTACTGTT AGAAAGGTTTTGTCTATGCCACA AGTTAACATCGTTAAGAAGACTG AAGTTCAAACCTGGTGGTTTCTCTA AGGAATCTATCTTGCCAAAGAGA AACTCTGACAAGTTGATCGCTAG AAAGAAGGACTGGGACCCAAAG AAGTAC ACTAACGGTGAAACTGGTGAAT CGTTTGGGACAAGGGTAGAGACT TCGCTACTGTTAGAAAGGTTTTGT CTATGCCACAAGTTAACATCGTT AAGAAGACTGAAGTTCAAACCTGG TGGTTTCTCTAAGGAATCTATCTT GCCAAAGAGAACTCTGACAAGT TGATCGCTAGAAAGAAGGACTGG GACCCAAAGAAGTACGGTGGTTT CGACTCTCCAACCTGTTGCTTACTC TGTTTTGGTTGTTGCTAAGGTTGA	Creation of <i>Saccharomyces cerevisiae</i> codon optimized Cas9

Stock #	G-block Name	Sequence	Purpose
		AAAGGGTAAGTCTAAGAAGTTGA AGTCTGTTAAGGAATTGTTGGGT ATCACTATCATGGAAAGATCTTC TTTCGAAAAGAACCCAATCGACT TCTTGGAAGCTAAGGGTTACAAG GAAGTTAAGAAGGACTTGATCAT CAAGTTGCCAAAGTACTCTTTGTT CGAATTGGAAAACGGTAGAAAG AGAATGTTGGCTTCTGCTGGTGA ATTGCAAAGGGTAACGAATTGG CTTTGCCATCTAAGTACGTAACT TCTTGTAAGTTGGCTTCTCACTACG AAAAGTTGAAGGGTTCTCCAGAA GACAACGAACAAAAGCAATTGTT CGTTGAACAACACAAGCACTACT TGGACGAAATCATCGAACAAATC TCTGAATTTTCTAAGAGAGTTATC TTGGCTGACGCTAACTTGGACAA GGTTTTGTCTGCTTACAACAAGC ACAGAGACAAGCCAATCAGAGA ACAAGCTGAAAACATCATCCACT TGTTCACTTTGACTAACTTGGGTG CTCCAGCGGCTTCAAGTACTTCG ACACTACTATCGACAGAAAGAGA TACTTCTACTAAGGAAGTTTTG GACGCTACTTTGATCCACCAATCT ATCACTGGTTTGTACGAACTAG AATCGACTTGTCTCAATTGGGTG GTGACTCTAGAGCTGACCCAAAG AAGAAGAGAAAGGTT	

APPENDIX F. RECIPES

Media

YPD (Yeast Peptone Dextrose)

10 g Dextrose

10 g Peptone

5 g Yeast Extract

Bring up to 500 mL volume with ddH₂O. For plates add 10 g Agar to media bottle.

Autoclave at 121°C for 20 min.

YPD dissection plates

10 g Peptone

5 g Yeast Extract

450 mL volume with ddH₂O

Add 10 g Agar to media bottle

Autoclave at 121°C for 20 min.

Add 50 mL 20% Dextrose immediately after autoclaving, then pour thin (Hot media will make it easier to pour thin plates).

YP- (Yeast Peptone)

10 g Peptone

5 g Yeast Extract

Add volume of ddH₂O to equal 500 mL after addition of desired sugars (volume= 500mL – sugar volume). For plates add 10 g Agar to media bottle.

Autoclave at 121°C for 20 min.

This is “sugar-less” media. Made to add filter sterilized sugars (20% Galactose/Gal, 20% Raffinose/Raf) after autoclaving. If making plates, cool before adding sugars.

SD (- selective nutrient; Synthetic Dextrose)

10 g Dextrose

3.35 g Yeast N2 base with ammonium sulfate and without supplements (amino acids and amino bases)

X g Supplement (that includes all nutrients, except the selective nutrient; - selective nutrient)

Bring up to 500 mL volume with ddH₂O. For plates add 10 g Agar to media bottle. Autoclave at 121°C for 20 min.

For SD + Cyh: Make SD + Com media, after autoclaving and cooling to 60°C, add 0.5 mL of 1 mg/mL filter sterilized Cycloheximide dissolved in ddH₂O.

For SD + Can: Make SD – Arg media, after autoclaving and cooling to 60°C, add 0.5 mL of 6 mg/mL filter sterilized canavanine dissolved in ddH₂O. For SD + Can + Cyh: To SD + Can add 0.5 mL of 1 mg/mL filter sterilized Cycloheximide dissolved in ddH₂O.

For SD + Thialysine: Make SD – Lys media, after autoclaving and cooling to 60°C, add 0.5 mL of 50 mg/mL filter sterilized L- thialysine dissolved in ddH₂O.

SRG-His-Trp-Ura-Leu+X-gal (Synthetic Raffinose Galactose; For yeast two-hybrid)

3.35 g Yeast Nitrogen Base with ammonium sulfate and without amino acids

0.3 g -HTUL supplement

325 mL volume with ddH₂O

Add 10 g Agar to media bottle

Buffering solution: prepared separately, 3 g monobasic sodium phosphate +7 g dibasic sodium phosphate in 100 mL volume with ddH₂O

Autoclave both at 121°C for 20 min. Cool, then add buffering solution to media.

Add 50 mL 20% Galactose (Gal/G) and 25 mL 20% Raffinose (Raf/R)

Add 0.4 mL 100 mg/mL X-gal (in N,N-dimethylformamide)

5-FOA (5-Fluoroorotic Acid)

10 g Dextrose

3.35 g Yeast N2 base with ammonium sulfate and without supplements (amino acids and amino bases)

0.39 g COM supplement

25 mg uracil

20 mg adenine

500 mL volume with ddH₂O

(For plates add 10 g Agar to media bottle)

Autoclave at 121°C for 20 min. Cool to 60°C, add appropriate volume of 100 mg/mL 5-FOA (dissolved in DMSO, warmed) to reach desired concentration of media.

SPO (Sporulation) plate media

10 g Potassium Acetate

0.195 g COM supplement (1/2)

500 mL volume with ddH₂O

Use Acetic Acid to pH= 6.8

Add 10 g Bacto Agar to media bottle

Autoclave at 121°C for 20 min.

YPA (Yeast extract, Peptone, potassium Acetate; liquid)

5 g Potassium Acetate

10 g Peptone

5 g Yeast Extract

Bring up to 500 mL volume with ddH₂O.

Autoclave at 121°C for 20 min.

SPO (liquid SPOrulation media) *Haring lab previously utilized recipe

10 g Potassium Acetate

0.195g Com Supplement (1/2)

500 mL volume with ddH₂O

Use Acetic Acid to pH= 6.8

Autoclave at 121°C for 20 min.

CL-SPM (Cartagena-Lirola Sporulation Media, liquid) *(Cartagena-Lirola et al. 2006, Cartagena-Lirola et al. 2008)

0.3 g Potassium Acetate (0.3%)

100 mL volume with ddH₂O

Autoclave at 121°C for 20 min. Add 100 µL 20% Raffinose (0.02%) after cooling.

ESPM (Extra potassium acetate SPorulation Media, liquid) *(Schindler et al. 2003)

1 g Potassium Acetate (1%)

100 mL volume with ddH₂O

Autoclave at 121°C for 20 min. Add 100 µL 20% Raffinose (0.02%) after cooling.

SM (Schindler sporulation Media, liquid) *(Schindler et al. 2003)

2 g Potassium Acetate (2%)

1 mg Adenine (10 µg/mL)

0.5 mg Histidine (5 µg/mL)

3.0 mg Leucine (30 µg/mL)

0.75 mg Lysine (7.5 µg/mL)

1 mg Tryptophan (10 µg/mL)

0.5 mg Uracil (5 µg/mL)

Bring up to 100 mL volume with ddH₂O.

Autoclave at 121°C for 20 min.

LB (Luria-Bertani)

5 g Tryptone

2.5 g Yeast Extract

2.5 g Sodium Chloride

250 μ L 2M Sodium Hydroxide

500 mL volume with ddH₂O

(For plates add 10 g Agar to media bottle)

Autoclave at 121°C for 20 min. If adding antibiotics, cool to 60°C, add appropriate volume of antibiotic stock to reach desired concentration in media.

Western Blotting Reagents

Protein sample buffers

1.5X Laemmli buffer

62.5 mL ddH₂O

18 mL 4X Tris-HCl/SDS (pH 6.8)

15 mL glycerol

3 g SDS

1.5 mL 10 mg/mL or 1% Bromophenol blue

Dilute 1.5X Laemmli buffer to 1X Laemmli buffer with ddH₂O. Add desired β -Me to samples immediately prior to loading.

Kushnirov(K) buffer

89 mL ddH₂O

12 mL 4X Tris-HCl/SDS (pH 6.8)

5 mL glycerol

2 g SDS

250 μ L 10 mg/mL or 1% Bromophenol blue

Add 4% β -Me to samples immediately prior to loading.

SDS-PAGE gel buffers

4X Tris-HCl/SDS pH 8.8

45.5 g Tris base dissolved in 150 mL ddH₂O

Adjust pH to 8.8 with 1N HCl

Bring volume up to 250 mL with ddH₂O

Filter sterilize buffer.

Then add 1 g SDS to filtered buffer. Store at 4°C.

4X Tris-HCl/SDS pH 6.8

6.05 g Tris base dissolved in 40 mL ddH₂O

Adjust pH to 6.8 with 1N HCl

Bring volume up to 100 mL with ddH₂O. Filter sterilize buffer.

Add 0.4 g SDS to filtered buffer. Store at 4°C.

SDS electrophoresis buffers

5X SDS

15.1 g Tris base

72.0 g Glycine

5.0 g SDS

Bring up to 1 L with ddH₂O. Dilute to 1X before use, store at 4°C.

1X SDS

200 mL 5X SDS

800 mL ddH₂O

Transfer buffer

20X Transfer buffer

150.14 g Glycine

24.23 g Tris base

Bring up to 1 L with ddH₂O. Store at room temperature.

1X Transfer buffer

50 mL 20X Transfer buffer

100 mL Methanol

850 mL ddH₂O

For best results prepare on day of use, chill buffer prior to setting up transfer.

Western blot wash buffer

10X TBS

24.2 g Tris base

80 g NaCl

900 mL ddH₂O

Adjust pH to 7.6 with HCl

Bring up to 1 L with ddH₂O. Autoclave at 121°C for 20 min.

TBST wash buffer

100 mL 10X TBS

900 mL ddH₂O

3 mL Tween-20

For TBST + NaF, add 10 mL 0.5M NaF

APPENDIX G. SUPPLEMENTARY FIGURES

Agarose Gels

Verification of AWY mutant strains used in Chapter 3

The JKM179 derivatives (AWY strains) provided by Andre Walther and utilized in the spot assays shown in Chapter 3 were genotyped by PCR for *rfa2* mutant status and for *geneΔ::selectable marker*. *RFA2* extensive alanine/aspartate mutations (*rfa2-A_x*, *rfa2-D_x*) were confirmed as mutants by PCR length (utilizing the primers RFA2-UP-FOR and RFA2-DOWN-REV) then PCR products were sequenced utilizing the primer RFA2-UP-FOR by Eton Biosciences to confirm *rfa2-A_x/rfa2-D_x* (Appendix D). Due to the absence of the intron in *rfa2* mutant strains, wild-type and potential mutant strains are easily distinguished by size, shown is a representation of verification of *rfa2* mutant status (Figure G1). PCR was performed to confirm gene deletions by insertion of the selectable marker (*geneΔ::selectable marker*), for the following: *rad52Δ::TRP1*, *tof1Δ::hphNT*, *rad9Δ::kanMX*, *rad17Δ::LEU2*, *mec3Δ::TRP1* with appropriate primers (Appendix D). As the directionality of each selectable marker (insertion) was unknown, four separate reactions were prepared so that regardless of direction, the insertion could be confirmed by PCR product produced from the upstream and downstream PCR (2/4 reactions per direction of the insertion). Additionally, PCR product can only be produced (in 2/4 reactions) if the insertion has correctly integrated. In the verifications of *geneΔ::selectable marker*, there should be PCR product produced in either the two outside lanes or the two inside lanes (Figure G2).

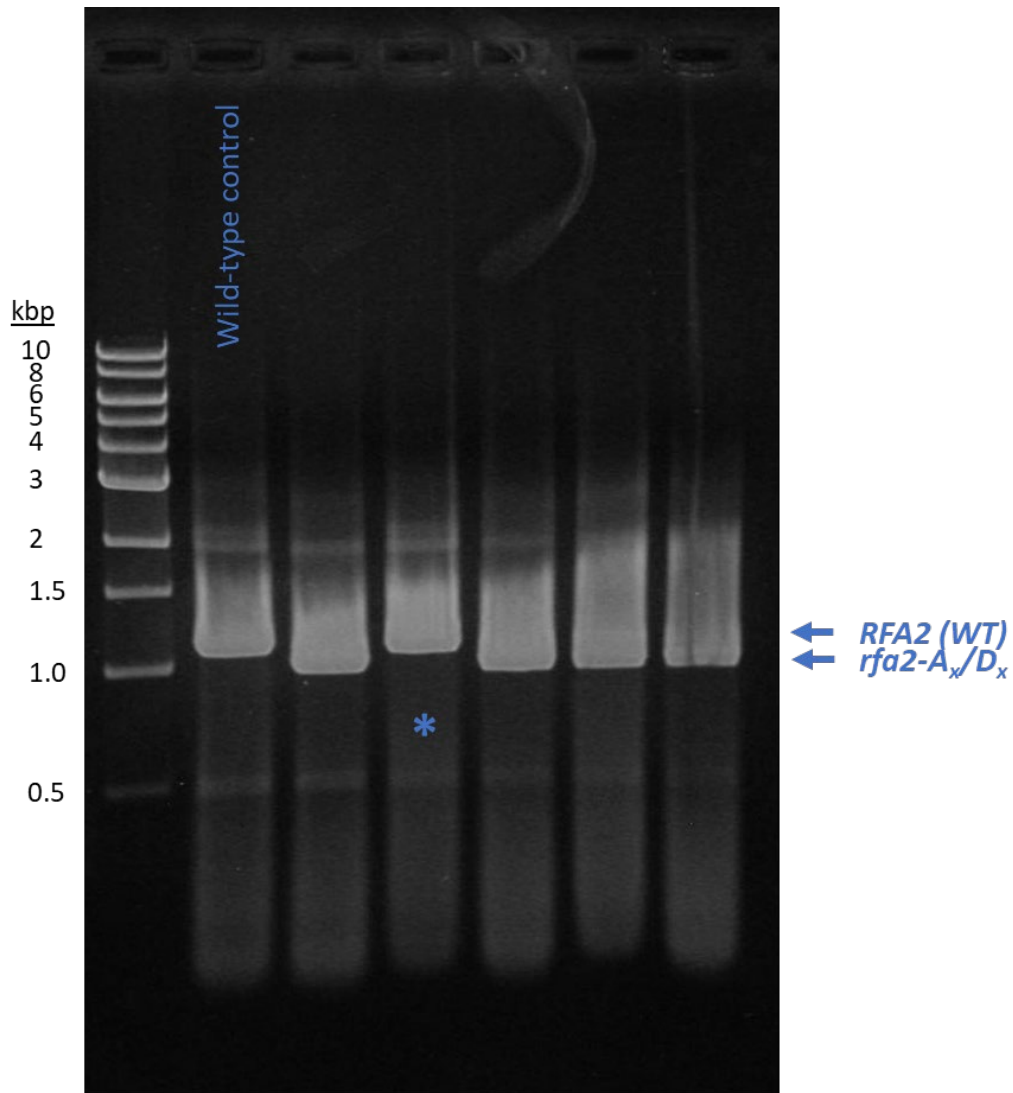


Figure G1. Verification of *rfa2* mutant status

DNA electrophoresed on a 1% agarose TAE gel instead of the typically used 1.5% agarose for *rfa2* PCR. Indicated by arrows are the approximate sizes of the PCR products produced. Shown is a wild-type strain as a control. Predicted fragment sizes generated using Serial Cloner: *RFA2*= 1106 bp, *rfa2-A_x/D_x* = 998 bp. *Denotes a strain identified as wild-type by PCR length.

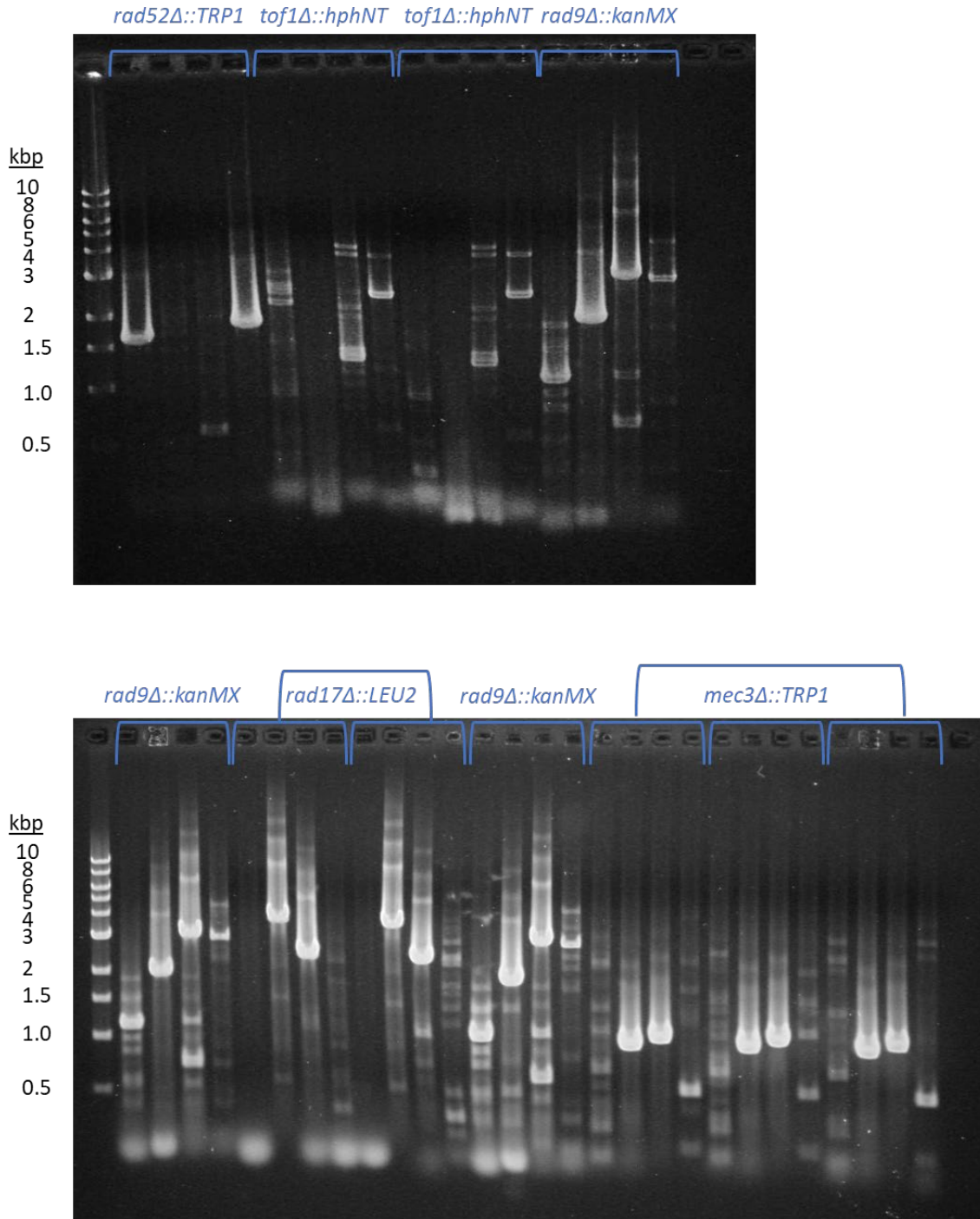


Figure G2. Verification of *geneΔ::selectable marker*

DNA electrophoresed on a 1% agarose TAE gel. For each set of 4 reactions performed for each *geneΔ::selectable marker* candidate, PCR product can only be produced (in 2/4 reactions) if the insertion has correctly integrated. To confirm, product should be present in either the two outside lanes or the two inside lanes.

Verification of AMA mutant strains used in Chapter 3 and generated as collaborate effort

Correct *rad17Δ::LEU2* and *rad52Δ::TRP1* mutants (AMA135 – AMA140) were made by *in vivo* HR cloning. The selectable marker was PCR amplified from verified *rad17Δ::LEU2* and *rad52Δ::TRP1* strains using the primers: RAD52-F, RAD52-R, RAD17-F, RAD17-R, respectively (Appendix D). The PCR products were transformed by lithium acetate transformation into competent confirmed JKM179 derivatives that contained the desired *RFA2* mutation and selected for on appropriate media (SD-Leu or SD-Trp). These AMA mutants were PCR confirmed utilizing the same primers and method as the above AWY mutants, only the correct insertion set of primers was used to verify *rad52Δ::TRP1* (Figure G3).

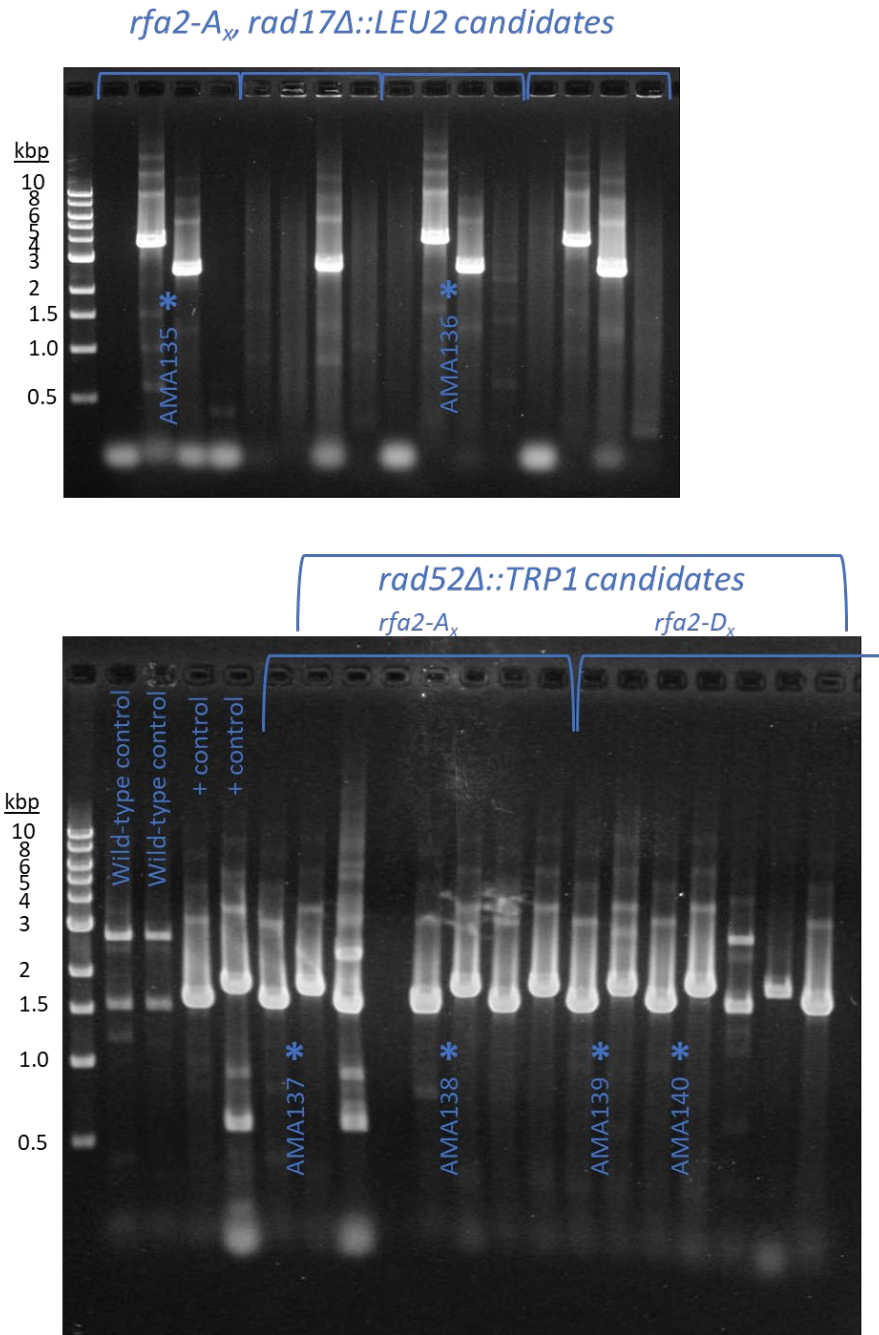


Figure G3. Verification of AMA generated strains

DNA electrophoresed on a 1% agarose TAE gel. For each set of 4 reactions performed for each *rad17Δ::LEU2* candidate, PCR product can only be produced (in 2/4 reactions) if the insertion has correctly integrated. To confirm *rad17Δ::LEU2*, product should be present in either the two outside lanes or the two inside lanes. For each *rad52Δ::TRP1* candidate, only the correct insertion set of primers was used to verify *rad52Δ::TRP1*, thus two consecutive lanes were used for each strain and both lanes must produce product to confirm *rad52Δ::TRP1*. Wild-type and positive control used for comparison. *For both gels shown, denotes candidate and name for permanent collection between the two lanes used to confirm.

DNA Damage Spot Assays

Integrated *rfa2* mutants (JKM179 vs. JKM139)

As part of a collaborate effort with Andre Walther, Stuart Haring, Timothy Wilson, Trevor Baumgartner; I performed this DNA damage spot assay to compare variability of DNA damage sensitivity between the nearly isogenic JKM179 and JKM139 strain backgrounds (Figure G4). The JKM179 wild-type strain appears to be less sensitive than the JKM139 wild-type strain. There may be subtle differences observed between the two strain backgrounds with the same *rfa2* mutation (AWY strains, Appendix A), but the overall sensitivity is very similar (Figure G4).

Integrated *rfa2* mutants vs. plasmid-based *rfa2* mutants (JKM179 vs NMM104)

As part of a collaborate effort with Andre Walther, Stuart Haring, Timothy Wilson, Trevor Baumgartner; I performed this DNA damage spot assay to compare variability of DNA damage sensitivity between JKM179 derivative strains (AWY strains, Appendix A) in which *rfa2* mutations are integrated or plasmid-based (Figure G5). The JKM179-derived NMM104 strain contains a genomic deletion of *RFA2* (*rfa2* Δ) and the supplemental pJM132 plasmid so that it may be used to generate *rfa2* mutants by plasmid shuffle (i.e. plasmid-based *rfa2* mutants, TMW strains, Appendix A). Subtle differences are observed between integrated and plasmid-based *rfa2* mutations on all plates, generally it appears that the plasmid-based *rfa2* mutations confer a minimal increase in growth, making these strains slightly less sensitive to DNA damaging agents (Figure G5).

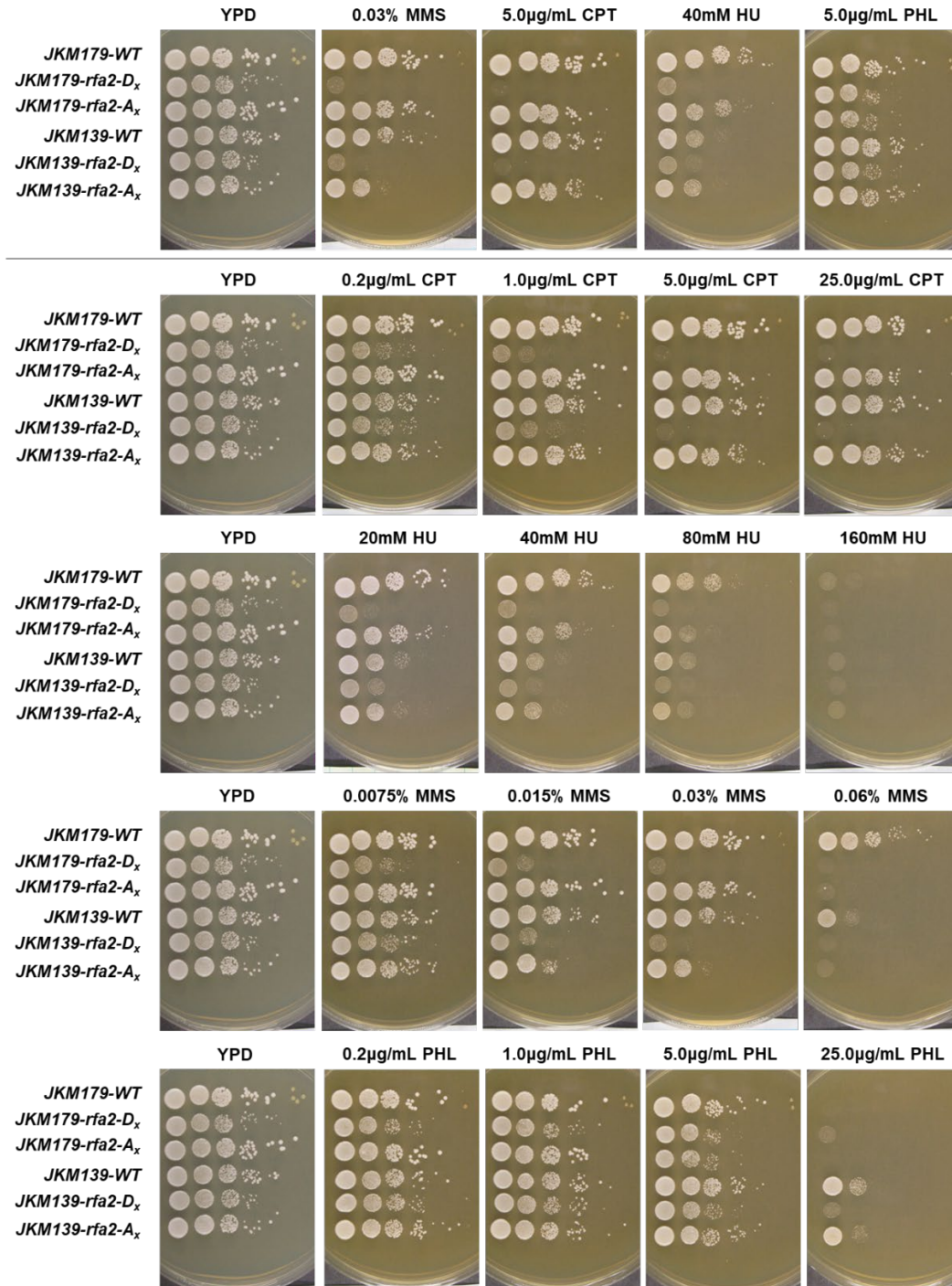


Figure G4. DNA damage assay for JKM179 vs. JKM139 mutants

Cells were grown in YPD at 30°C in shaker incubator overnight. Cell cultures were initially diluted to 1×10^7 cells/mL, which were used to create five additional 1:10 serial dilutions. 5 μ L of each dilution was spotted on YPD media or YPD media containing genotoxic agents at various concentrations (labeled).

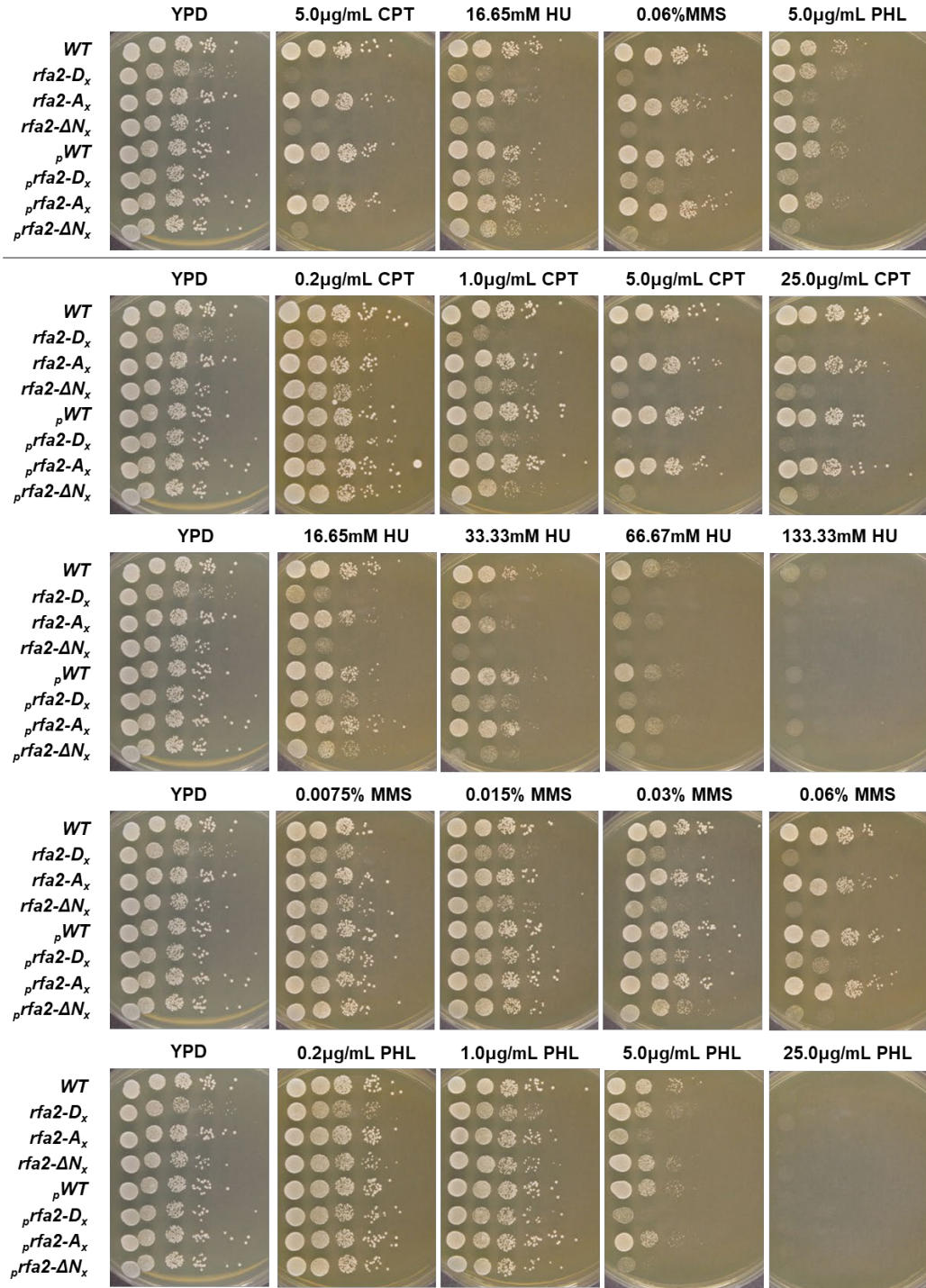


Figure G5. DNA damage assay for integrated vs. plasmid-based *rfa2* mutants

Cells were grown in YPD at 30°C in shaker incubator overnight. Cell cultures were initially diluted to 1×10^7 cells/mL, which were used to create five additional 1:10 serial dilutions. 5 μ L of each dilution was spotted on YPD media or YPD media containing genotoxic agents at various concentrations (labeled).

Checkpoint protein deletions (*rad9Δ*, *rad17Δ*, *mec3Δ*) with *rfa2* phospho-mutants

These DNA damaging agent spot assays were performed as part of Chapter 3 (Figures G6-G9). Set 1 and Set 2 were performed as two separate replicates of the experiment. A different isolate was used for each strain to perform each set. All strains used were JKM179 derivatives (AWY092, AWY096, AWY019, AWY033, AWY035, AWY040, AWY45, AWY114, AWY200, AWY201, AMA135) and wild-type JKM179. Both sets of spot assays were performed on the range of concentrations of DNA damaging agents (CPT, HU, MMS, and PHL) as labeled (Figures G6-G9). Selected images from Set 2 were used to create Figure 3.4 in Chapter 3. See “Results” in Chapter 3 for further commentary on experimental observations.

Plasmid based *rfa2* mutants with S122A/D (NMM104)

This was the first spot assay I performed, so note that minor variability and crooked rows may be due to inexperience. Strains used were provided by Timothy Wilson, however strains listed for the double mutants (*rfa2 NT* + *S122* mutations) will be found as “TAB” strains in Appendix A as those strains were put into the permanent collection by Trevor Baumgartner. This spot assay was performed as a duplicate experiment of the graduate rotation student Srinivasulu Dasanna. The *rfa2-S122A* or *rfa2-S122D* mutations do not seem to have any additive effect on the N-terminal phospho-mimetic mutations (*rfa2-D_x/rfa2-A_x*) as the double mutants containing either of the *rfa2-S122* mutations (*rfa2-S122A* or *rfa2-S122D*) display similar sensitivity to the DNA damaging agents shown (Figure G10). However, the timing of phosphorylation of Rfa2-S122 might contribute to DNA damage sensitivity only in the phospho-mimetic (*rfa2-D_x*) mutant strain as the single *rfa2-D_x* mutant always appears more sensitive than the double mutants (*rfa2-D_x* containing either *S122A/D*; Figure G10).

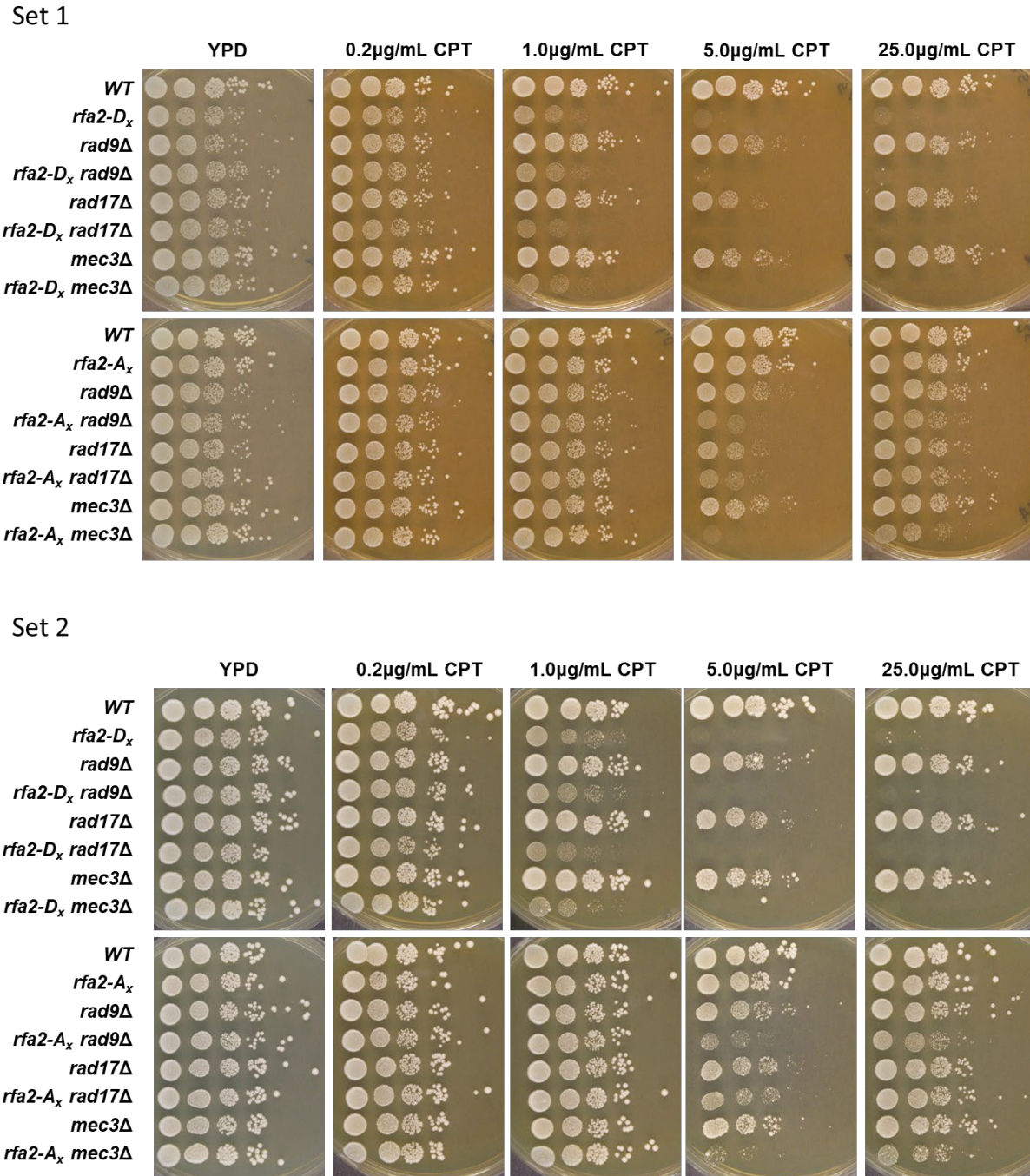
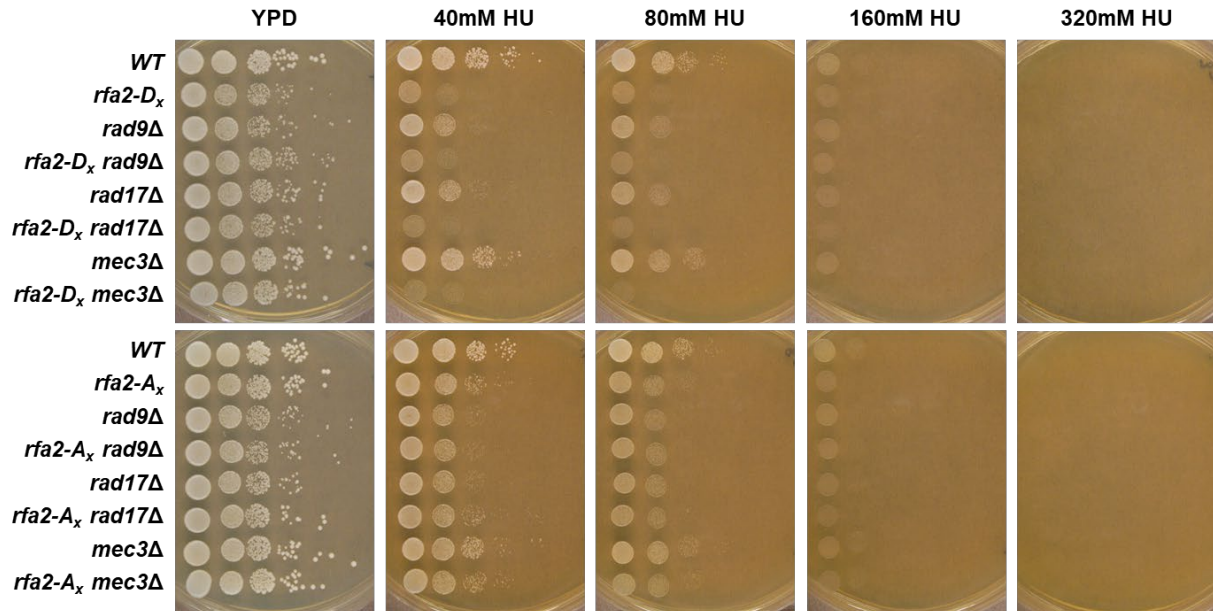


Figure G6. Sensitivity of checkpoint protein mutants on concentrations of CPT

Cells were grown in YPD at 30°C in shaker incubator overnight. Cell cultures were initially diluted to 1×10^7 cells/mL, which were used to create five additional 1:10 serial dilutions. 5 µL of each dilution was spotted on YPD media or YPD media containing camptothecin (CPT) at various concentrations (labeled).

Set 1



Set 2

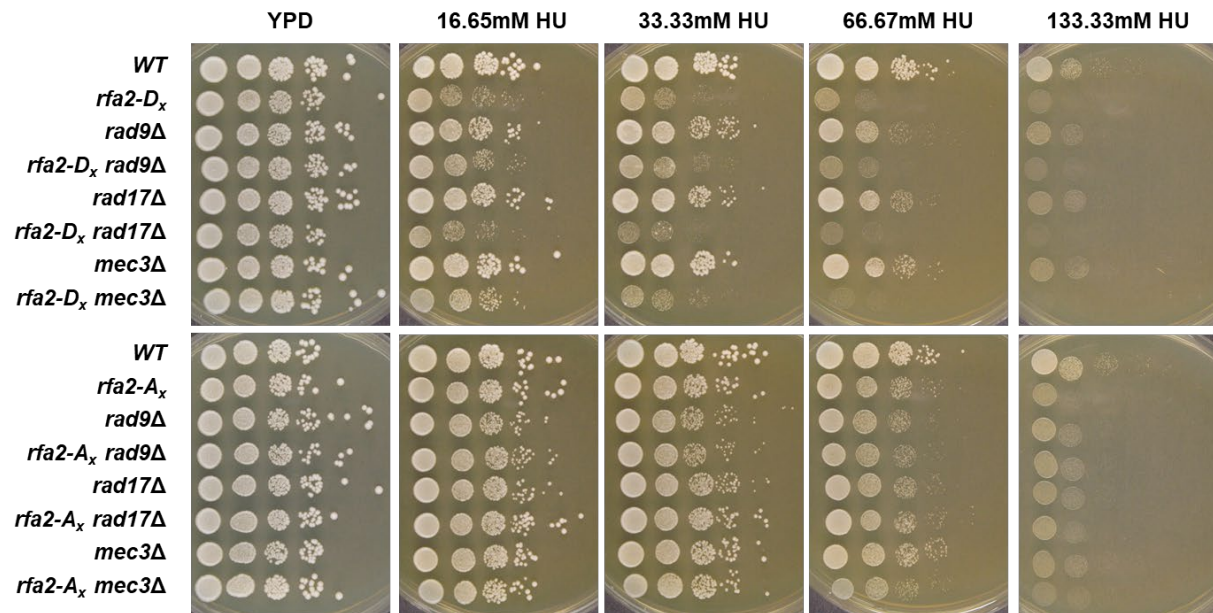
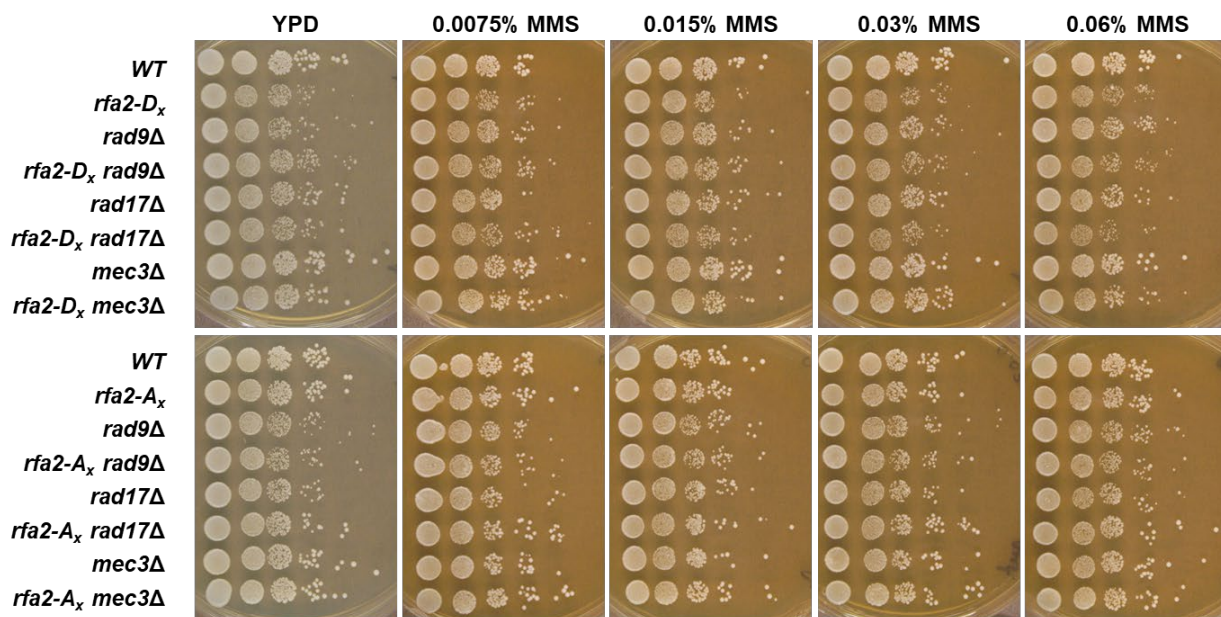


Figure G7. Sensitivity of checkpoint protein mutants on concentrations of HU

Cells were grown in YPD at 30°C in shaker incubator overnight. Cell cultures were initially diluted to 1×10^7 cells/mL, which were used to create five additional 1:10 serial dilutions. 5 μ L of each dilution was spotted on YPD media or YPD media containing hydroxyurea (HU) at various concentrations (labeled).

Set 1



Set 2

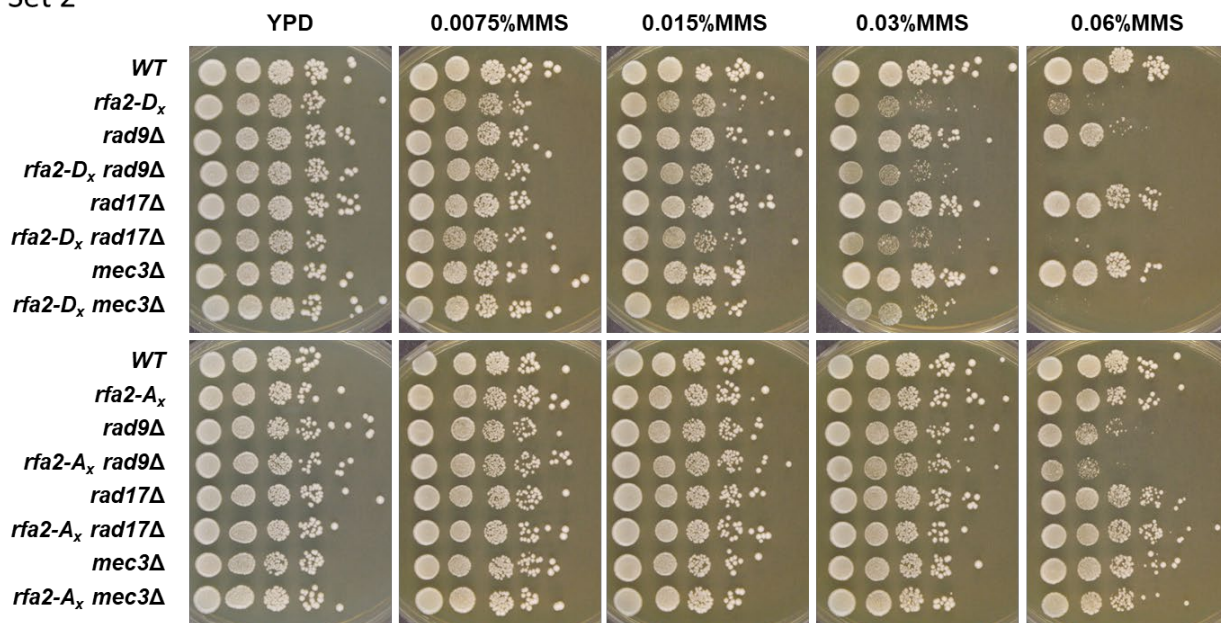
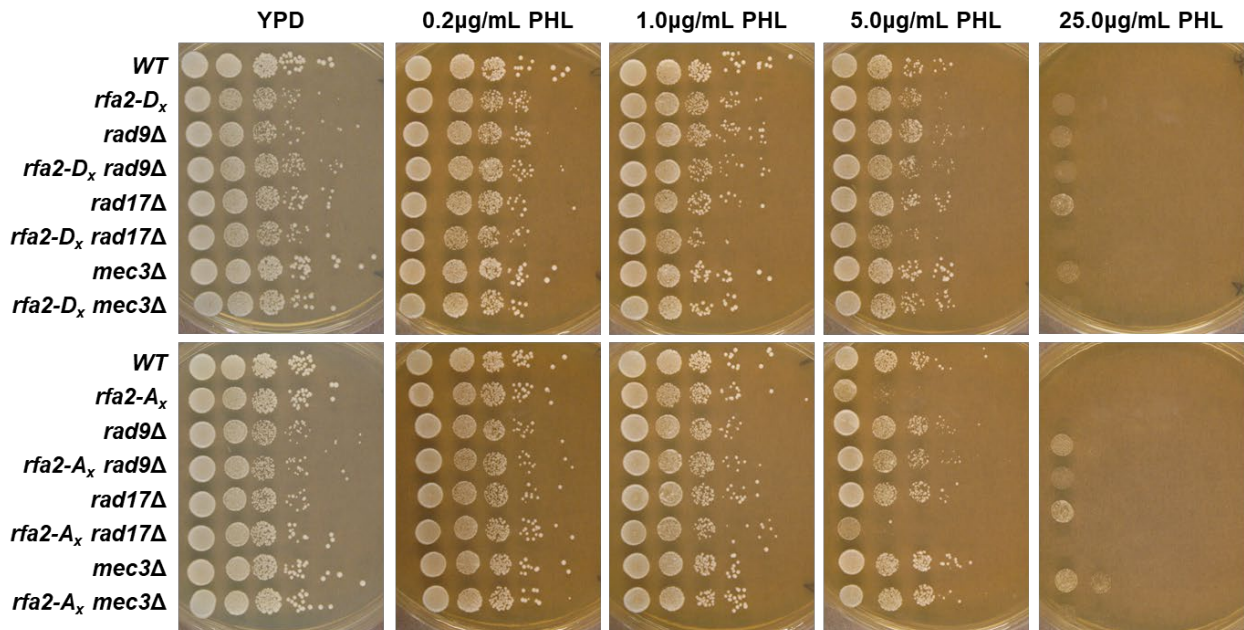


Figure G8. Sensitivity of checkpoint protein mutants on concentrations of MMS

Cells were grown in YPD at 30°C in shaker incubator overnight. Cell cultures were initially diluted to 1×10^7 cells/mL, which were used to create five additional 1:10 serial dilutions. 5 μ L of each dilution was spotted on YPD media or YPD media containing methyl methane sulfonate (MMS) at various concentrations (labeled).

Set 1



Set 2

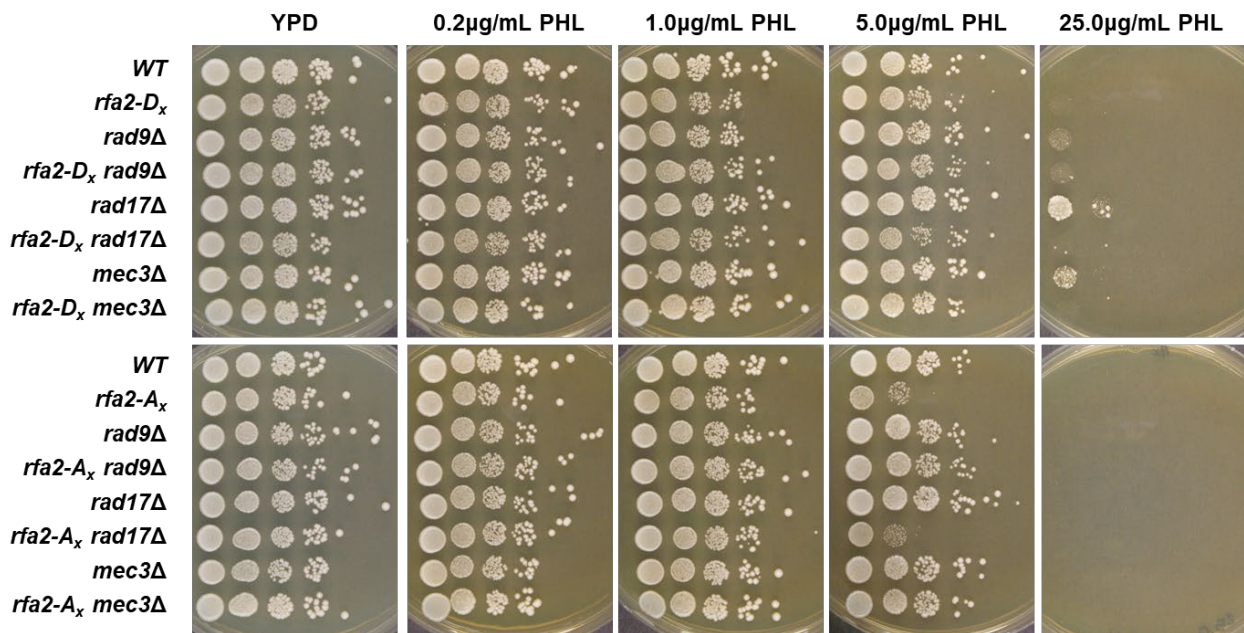


Figure G9. Sensitivity of checkpoint protein mutants on concentrations of PHL

Cells were grown in YPD at 30°C in shaker incubator overnight. Cell cultures were initially diluted to 1×10^7 cells/mL, which were used to create five additional 1:10 serial dilutions. 5 µL of each dilution was spotted on YPD media or YPD media containing phleomycin (PHL) at various concentrations (labeled).

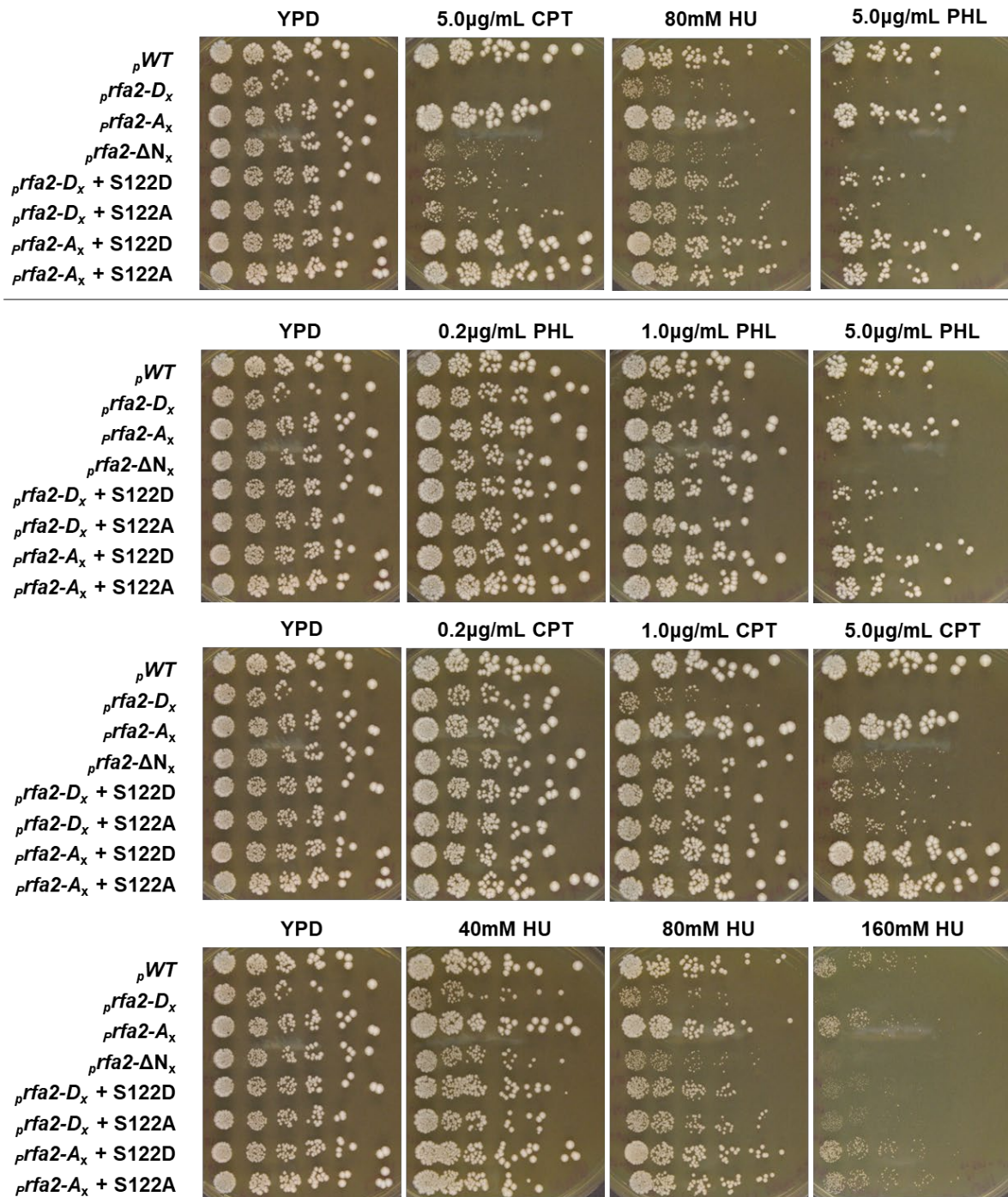


Figure G10. DNA damage assay for *rfa2* mutants

Cells were grown in YPD at 30°C in shaker incubator overnight. Cell cultures were initially diluted to 2.43×10^5 cells/mL, which were used to create five additional 1:3 serial dilutions. 5 μL of each dilution was spotted on YPD media or YPD media containing genotoxic agents at various concentrations (labeled). Plates were incubated for 4 days at 30°C before pictures were taken.

Meiotic Rfa2 NT mutant strains

These DNA damaging agent spot assays were performed as part of Chapter 4 (G11-G15). Set 1 and Set 2 were performed as two separate replicates of the experiment. A different isolate was used for each strain to perform each set. The strain background for each mutant is denoted. Both sets of spot assays were performed on the range of concentrations of DNA damaging agents (CPT, HU, MMS, and PHL) shown in these appendix figures (Figures G11-G15). Selected images were used to create Figure 4.8 in Chapter 4. See “Results” in Chapter 4 for further commentary on experimental observations.

Investigation of *rfa2-S238/240A* strain sensitivity by Cristian Hernandez

This DNA damaging agent spot assay was performed by Cristian Hernandez to investigate the DNA damage sensitivity of the *rfa2-S238/240A* strain (Figure G16). All strains utilized were of the JKM179 genetic background, derived from NMM104. This spot assay was included to show that cells containing *rfa2-S238/240A* were no more sensitive to DNA damaging agents than wild-type cells. See reference in “Results” of Chapter 5.

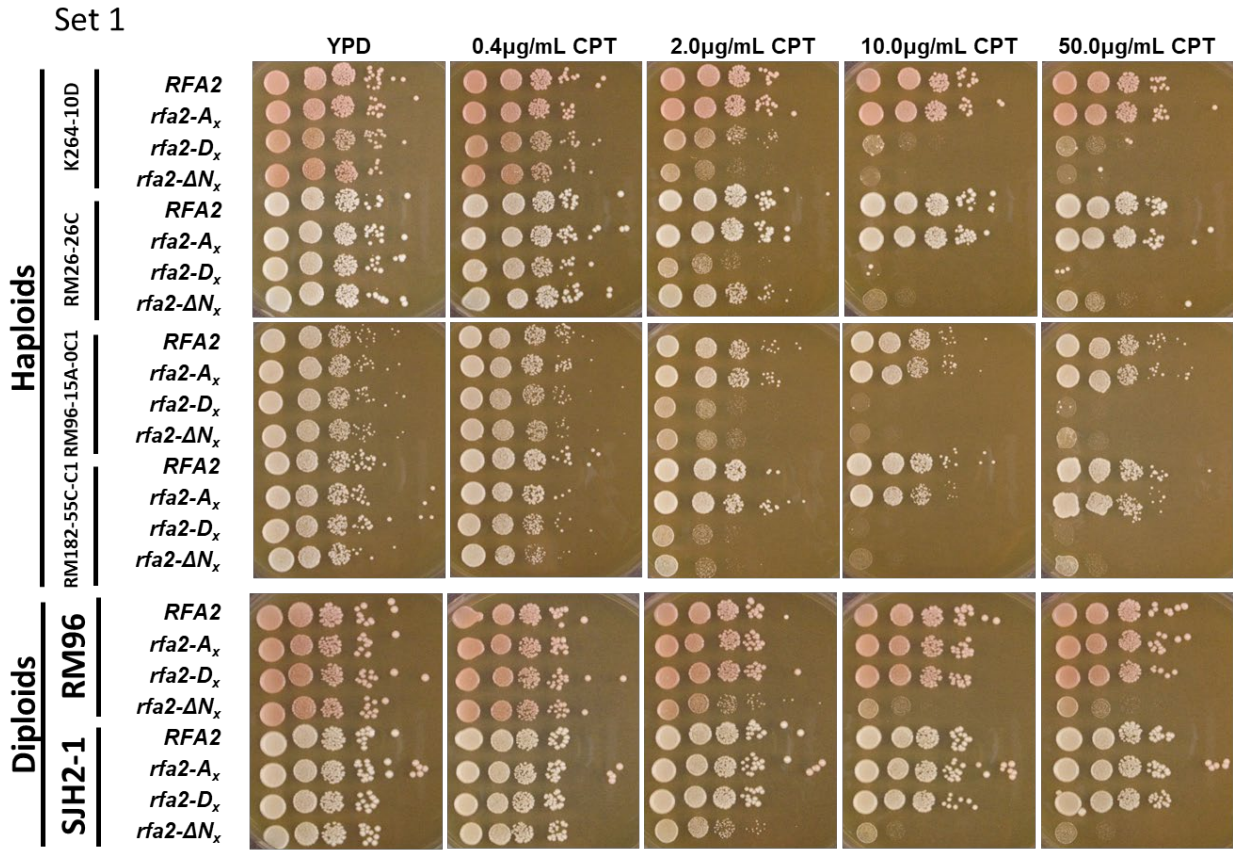


Figure G11. Sensitivity of meiotic strain mutants on CPT- Set 1

Cells were grown in YPD at 30°C (or 24°C for temperature sensitive strains) in shaker incubator overnight. Cell cultures were initially diluted to 1×10^7 cells/mL, which were used to create five additional 1:10 serial dilutions. 5 µL of each dilution was spotted on YPD media or YPD media containing camptothecin (CPT) at various concentrations (labeled). After 2 days of incubation at the appropriate temperature, pictures were taken.

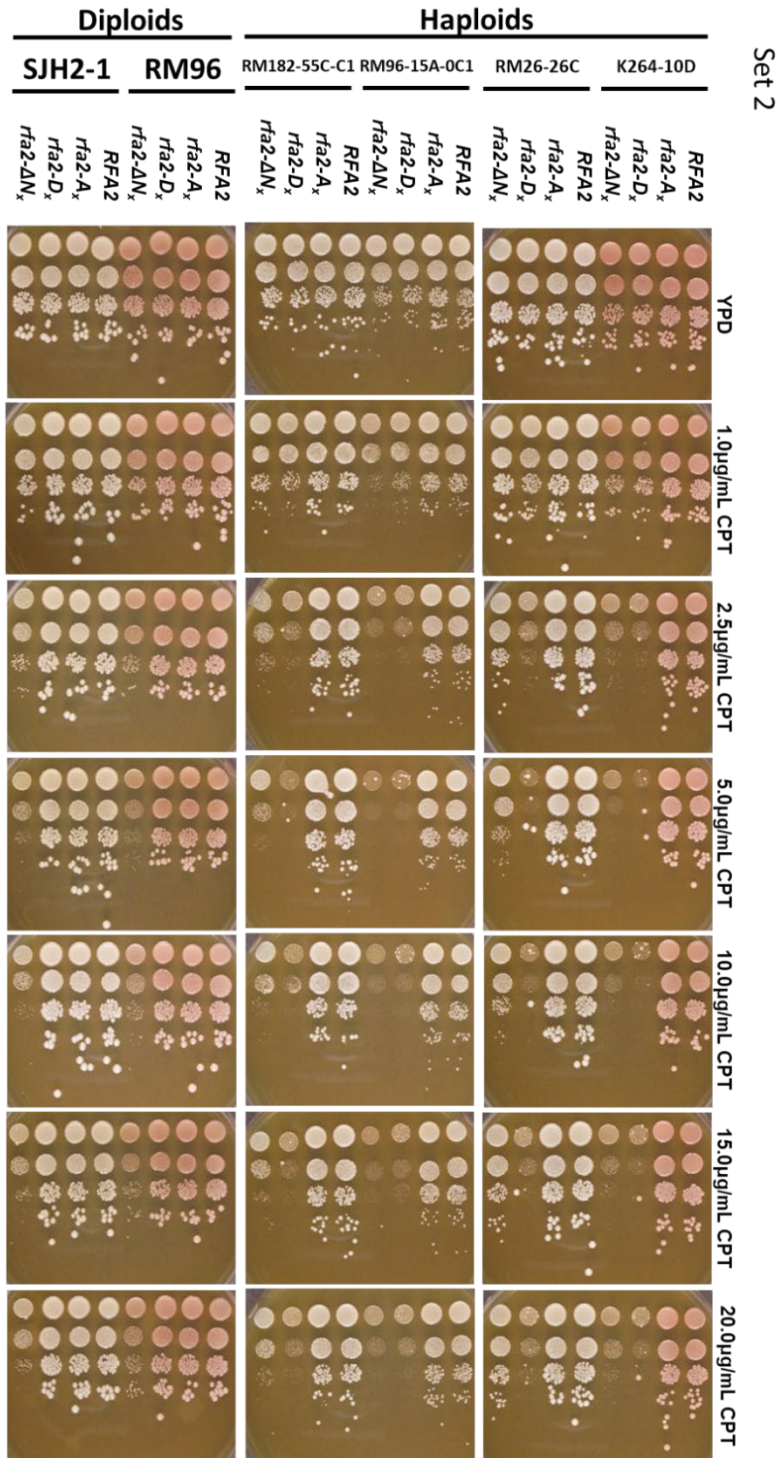


Figure G12. Sensitivity of meiotic strain mutants on CPT- Set 2

Cells were grown in YPD at 30°C (or 24°C for temperature sensitive strains) in shaker incubator overnight. Cell cultures were initially diluted to 1×10^7 cells/mL, which were used to create five additional 1:10 serial dilutions. 5 μ L of each dilution was spotted on YPD media or YPD media containing camptothecin (CPT) at various concentrations (labeled). After 2 days of incubation at the appropriate temperature, pictures were taken.

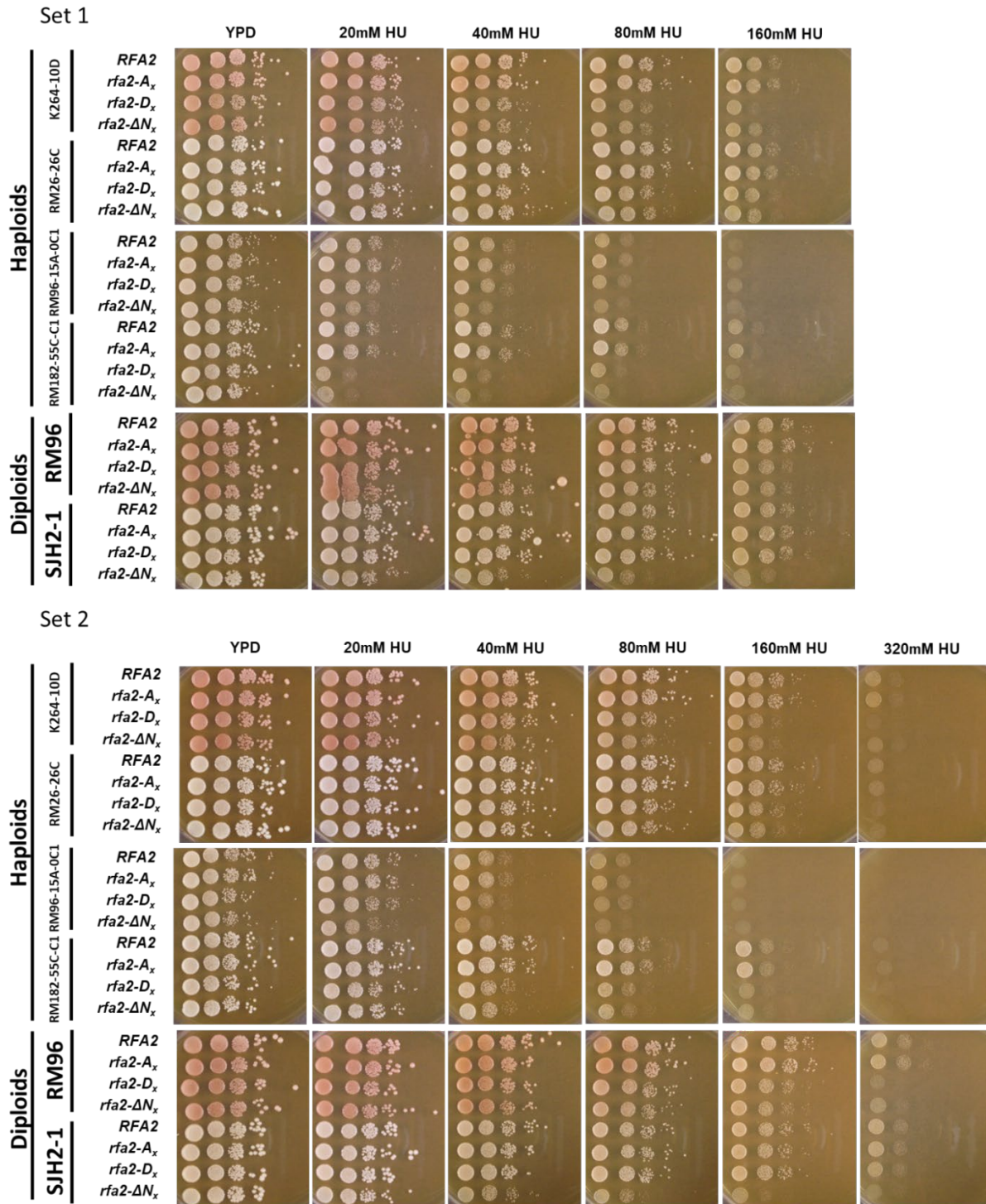


Figure G13. Sensitivity of meiotic strain mutants on HU

Cells were grown in YPD at 30°C (or 24°C for temperature sensitive strains) in shaker incubator overnight. Cell cultures were initially diluted to 1×10^7 cells/mL, which were used to create five additional 1:10 serial dilutions. 5 μ L of each dilution was spotted on YPD media or YPD media containing hydroxyurea (HU) at various concentrations (labeled). After 2 days of incubation at the appropriate temperature, pictures were taken.

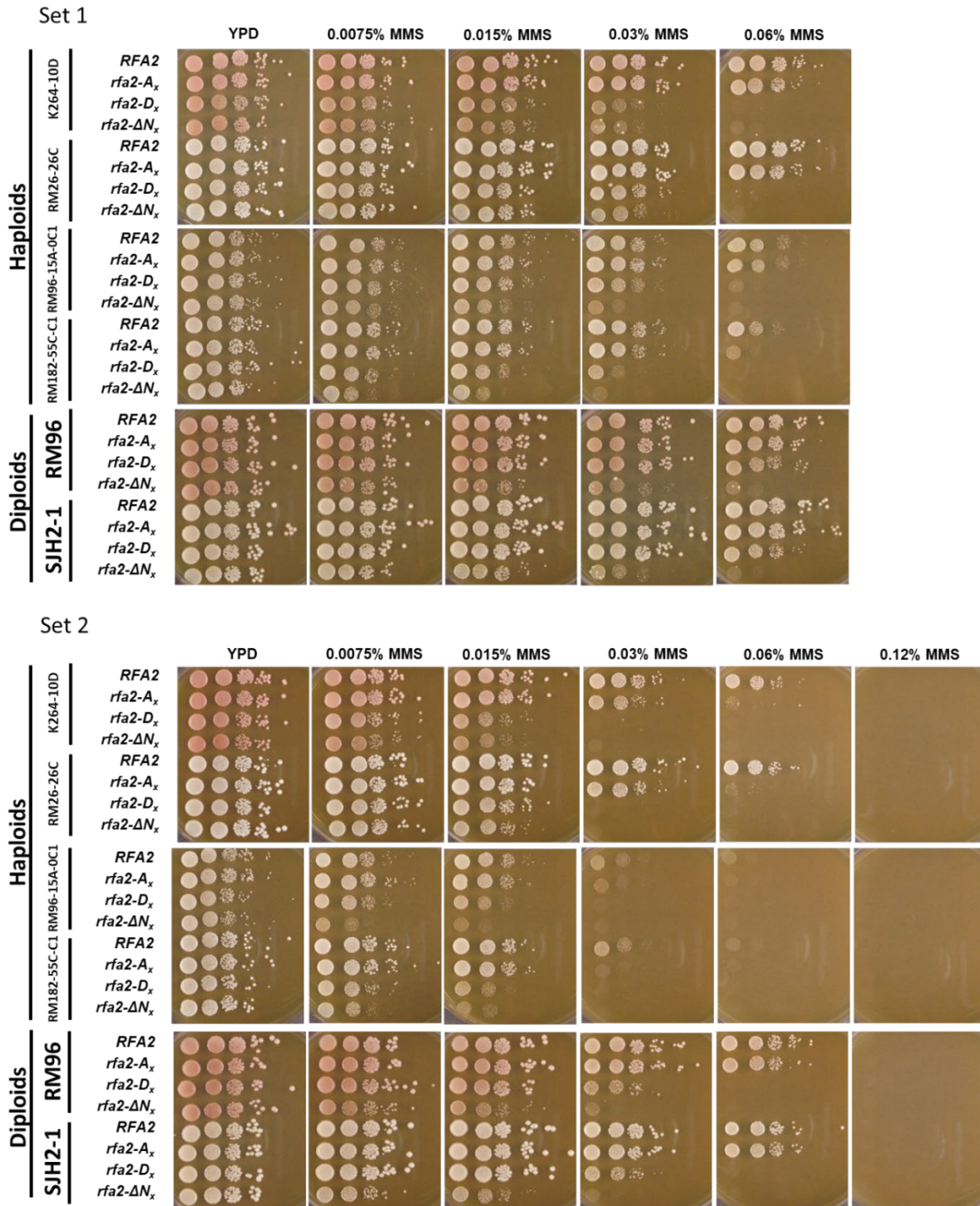


Figure G14. Sensitivity of meiotic strain mutants on MMS

Cells were grown in YPD at 30°C (or 24°C for temperature sensitive strains) in shaker incubator overnight. Cell cultures were initially diluted to 1×10^7 cells/mL, which were used to create five additional 1:10 serial dilutions. 5 μ L of each dilution was spotted on YPD media or YPD media containing methyl methane sulfonate (MMS) at various concentrations (labeled). After 2 days of incubation at the appropriate temperature, pictures were taken.

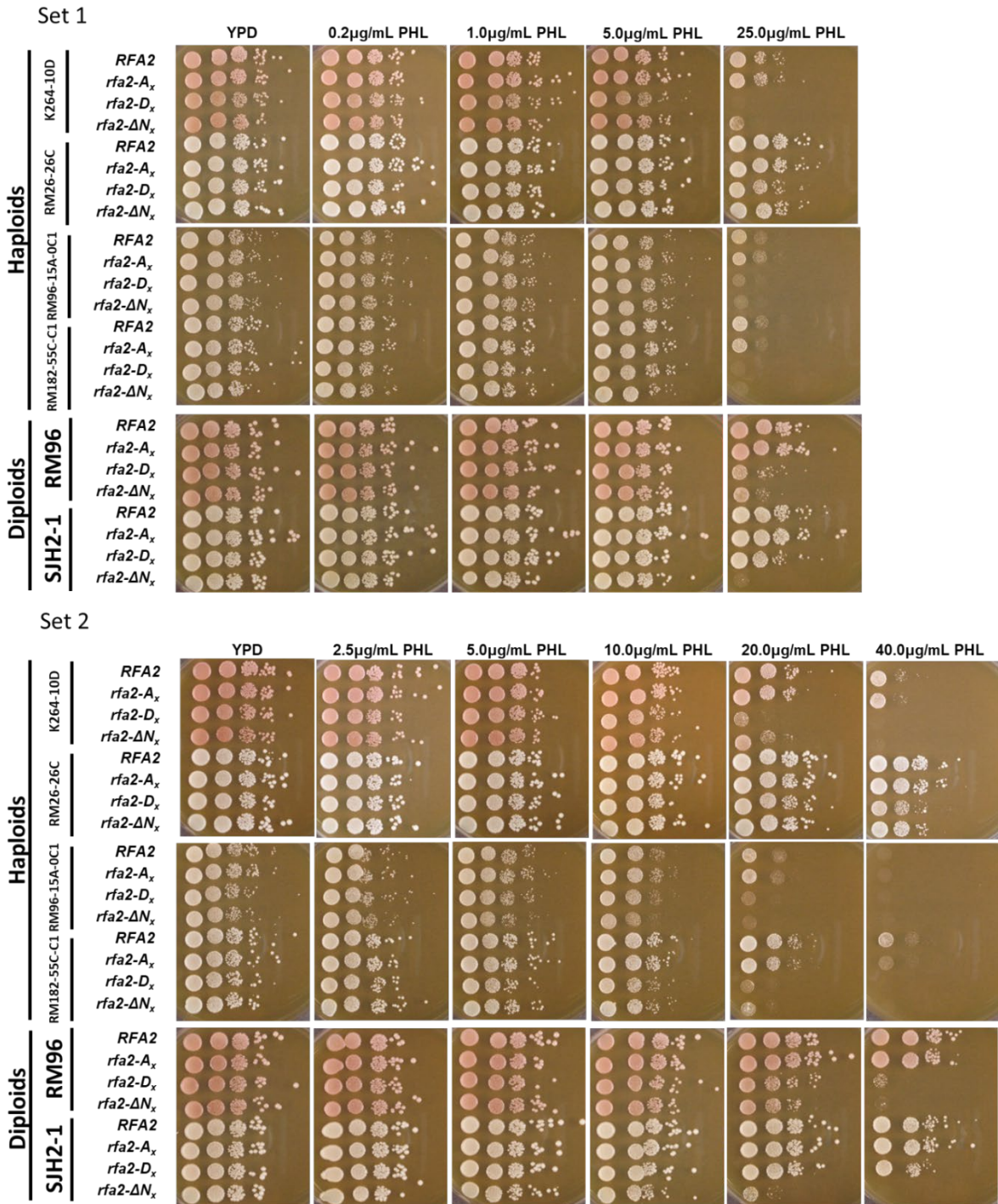


Figure G15. Sensitivity of meiotic strain mutants on PHL

Cells were grown in YPD at 30°C (or 24°C for temperature sensitive strains) in shaker incubator overnight. Cell cultures were initially diluted to 1 x 10⁷ cells/mL, which were used to create five additional 1:10 serial dilutions. 5 µL of each dilution was spotted on YPD media or YPD media containing phleomycin (PHL) at various concentrations (labeled). After 2 days of incubation at the appropriate temperature, pictures were taken.

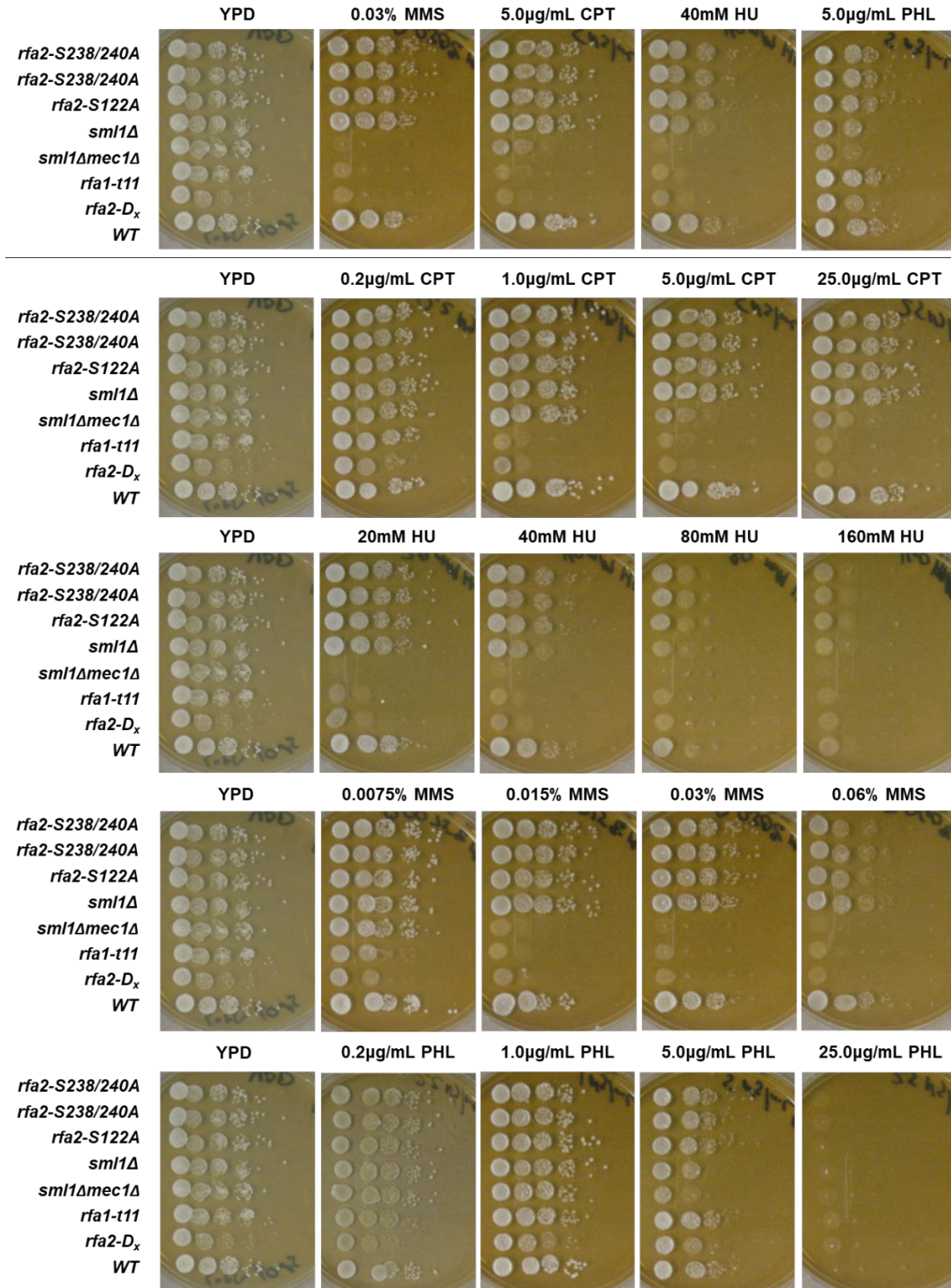


Figure G16. Investigation of *rfa2-S238/240A* DNA damage sensitivity
 5 μ L of each cell culture serial dilution was spotted on YPD media or YPD media containing genotoxic agents at various concentrations (labeled). Work performed by Cristian Hernandez.

APPENDIX H. MATING-TYPE SWITCHING ASSAY

Strains containing *rfa2* mutations or the *rfa1-t11* mutation were investigated in their ability to perform mating type switching. This assay was performed to analyze if any mutation might impair repair by homologous recombination. As the *rfa1-t11* mutation has been shown to have a defect in homologous recombination, this strain was used as a control.

Methods

Yeast strains and plasmids

RMY122-A background derivative strains containing plasmid-based *rfa2* mutations or the *rfa1-t11* mutation were transformed with the plasmid, pGAL-HO (Appendix C), in order to induce expression of HO endonuclease to cleave the MAT locus. B9B-A and B9B- α were used to as mating-type testers.

Mating-type switching

RMY122-A derivative strains containing pGAL-HO were grown in YPD to exponential phase before inoculating S-Ura+Raf and grown for at least 16 hrs in 30°C shaker incubator. 2% Galactose was added to cultures to induce expression of HO endonuclease for 2-3 hours. Cells were diluted to OD₆₀₀=0.0005. From each strain's dilution, volumes of 50 μ L, 100 μ L, and 200 μ L were plated to SD-Ura to retain pGAL-HO and grown at 30°C for 3 days. Colonies were picked from spread plates to YPD patch master plates and grown at 30°C for 2 days. Patch master plates were then replica plated to YPD media to mate with B9B-A/B9B- α for 2 days at 30°C. The mated plates were then replica plated to SD-Ade and grown at 30°C for 2 days to determine the mating type of the original patch.

Patch scoring and analysis

Patches that grew on SD-Ade when mated with B9B-A/B9B- α were determined to be the opposite mating type. As only a B9B-A/ α crossed with RMY122-A will be able to grow on SD-Ade due to genetic complementation of the *ade3* and *ade* (*ade1/2*; generates red pigment) mutations, respectively. Patches that grew on SD-Ade when mated with both mating types were determined to be mixed patches. Mixed patches were excluded from the analysis of calculating frequencies of each mating type, where frequency = # of mating type / # of (*MATa* + *MAT α*). Instead mixed patches were analyzed separately by determining frequency of mixed patches out of the total patches, where frequency = # of mixed patches / # of (homogenous + mixed) for each strain. To compare all strains ability to switch mating types (from *MATa* to *MAT α*) to each other, the frequency of wild-type switching was set to 1 by dividing by frequency of *MAT α* by itself and thus dividing the frequency of all other strains by that of wild-type strain.

Results

The *rfa1-t11* mutant was found to have a homologous recombination deficiency, consistent with previous reports (Soustelle et al. 2002, Umezu et al. 1998), reduced to 27.8% of the wild-type (WT) frequency for switching mating types from *MATa* to *MAT α* (Table A1). The frequency of switching from *MATa* to *MAT α* was nearly identical to WT in all *rfa2* mutants examined (99.3%, 93.8%, 105.4%; Table H1).

The frequency of mixed mating type patches was compared for all strains to that of the wild-type strain (Table A2). Interestingly, the frequency of mixed patches was nearly identical to wild-type in only the *rfa2-A_x* mutant strain, with the frequency of mixed patches in *rfa2-D_x* (66.7%) and *rfa2- ΔN_x* (40.2%) mutant strains at approximately half that of wild-type, while the *rfa1-t11* strain was the most severely reduced from the wild-type strain (12.7%; Table H2). The

appearance of mixed patches is interesting as generating a mixed patch could have resulted from a cell that has duplicated its DNA (2 chromatids each containing the *MATa* locus) but has not yet divided when only one of the chromatids is broken and repaired. After one chromatid has switched mating types then the cell divides, leaving a colony behind that contains half of each mating type. In nature, it is optimal for a yeast cell to be able to mate so that diploid spores can be formed; spore formation is a more resilient mechanism to protect DNA to ensure it is passed on to another generation.

Table H1. Mating type switching analysis

Strain	Relevant Genotype	Total Patches	Frequency of <i>MATα</i> (#)	Frequency of <i>MATa</i> (#)	Frequency compared to wild-type
RMY122-A	WT	419	0.578 (242)	0.422 (177)	1
-	<i>rfa1-t11</i>	193	0.161 (31)	0.839 (162)	0.278
-	<i>rfa2-Ax</i>	422	0.573 (242)	0.427 (180)	0.993
-	<i>rfa2-Dx</i>	443	0.542 (240)	0.458 (203)	0.938
-	<i>rfa2-ΔNx</i>	465	0.609 (283)	0.391 (182)	1.054

All strains listed are RMY122-A derivatives. All strains were analyzed for selective diploid growth after 2 days at 30°C. Patches displaying only one mating type are included in this table's calculations. Frequency is compared to wild-type, where wild-type frequency is set equal to 1 and all other strains' frequency is divided by the wild-type frequency.

Table H2. Mating type switching analysis of mixed mating type patches

Strain	Relevant Genotype	Total Patches	Frequency of mixed patches (#)	Frequency compared to wild-type
RMY122-A	WT	499	0.160 (80)	1
-	<i>rfa1-t11</i>	197	0.020 (4)	0.127
-	<i>rfa2-Ax</i>	494	0.146 (72)	0.909
-	<i>rfa2-Dx</i>	496	0.107 (53)	0.667
-	<i>rfa2-ΔNx</i>	497	0.064 (32)	0.402

All strains listed are RMY122-A derivatives. All strains were analyzed for selective diploid growth after 2 days at 30°C. Mixed patches contained cells that appeared to mate with both mating types. Frequency is compared to wild-type, where wild-type frequency is equal to 1 and all other strains' frequency is divided by the wild-type frequency.

Acknowledgements

This mating-type switching assay was a graduate rotation student project. Methods were performed by Mary (Maggie) Lenertz, except for patch scoring and analysis.

APPENDIX I. CHAPTER 4 SUPPLEMENTARY TABLES

Data Referenced in Methods

Testing liquid sporulation media for RM96 derivative diploids

See Appendix F for all media recipes. RM96 cells were grown to oversaturation in YPD. As 3 different medias were to be tested, (3) 50 mL flasks containing 10 mL of YPA were each inoculated with RM96 cells to 1.0 OD₆₀₀. Cells were incubated in YPA at 30°C in shaker incubator for 17 hours, spun down, aspirated, and resuspended in 10 mL of either CL-SPM, ESPM, or SM. After 24 hours of liquid sporulation, each culture's sporulation efficiency and spore viability were determined. Sporulation efficiency was calculated as the addition of tetrads and dyads observed divided by the total number of cells counted on an Olympus microscope. To determine spore viability, cells were treated with zymolyase in 1M sorbitol, then dissected using an Olympus microscope onto YPD plates. Spore viability was calculated as the number of viable spores divided by the total number of spores dissected onto YPD.

Results of the sporulation test shown in Table II. SM media had the highest sporulation efficiency and spore viability of the medias tested. CL-SPM was the media commonly used throughout this thesis (especially found to be best for sporulating SJH2-1 derivative strains) and was second highest for sporulation efficiency but had the lowest spore viability.

Table II. Sporulation test of three different liquid sporulation medias

Media	Tetrads	Dyads	Vegetative Cells	Total Cells	% Sporulation	% Viability (# of total spores)
CL-SPM	90	25	126	241	47.7%	83.8% (80)
ESPM	73	4	141	218	35.3%	91.2% (68)
SM	118	4	105	227	53.7%	95.8% (72)

The wild-type RM96 strain was used to test three different liquid sporulation medias: CL-SPM, ESPM, and SM (Appendix F). All strains were analyzed after 24 hours of liquid sporulation at 30°C in shaker incubator.

Liquid sporulation in SM is high for all RM96 derivative strains after 45 hours

See Appendix F for all media recipes. RM96 derivative cells were sporulated two different ways: on solid media and in liquid media (Table I2). To sporulate cells on solid media, cells were replica-plated to SPO media. To sporulate cells in liquid, cells were grown to oversaturation in YPD, then used to inoculate 10 mL of YPA to an OD₆₀₀ of 1.0. Cells were incubated in YPA at 30°C in shaker incubator for 23 hours, spun down, aspirated, and resuspended in 10 mL of SM. Cells were analyzed after 45 hrs in liquid sporulation media. Interestingly, after 45 hrs, sporulation is high for all *rfa2* mutants, even *rfa2-ΔNx*, however the tetrad:dyad ratio remains the lowest. The liquid sporulated cells were used for determining the meiotic heteroallelic recombination frequency in Chapter 4.

Table I2. Sporulation on solid spo vs. liquid SM media

Relevant Genotype	Media	Tetrads	Dyads	Vegetative Cells	Total Cells	% Sporulation	Tetrad:Dyad
<i>RFA2</i>	SPO	80	2	146	228	36.0	40
<i>rfa2-Ax</i>	SPO	78	2	134	214	37.4	39
<i>rfa2-Dx</i>	SPO	87	4	128	219	41.6	21.8
<i>rfa2-ΔNx</i>	SPO	30	15	173	218	20.6	2
<i>RFA2</i>	SM	117	19	107	243	56.0	6.2
<i>rfa2-Ax</i>	SM	89	26	117	232	49.6	3.4
<i>rfa2-Dx</i>	SM	105	24	124	253	51.0	4.8
<i>rfa2-ΔNx</i>	SM	91	39	110	240	54.2	2.3

RM96 derivative diploid strains were grown on SPO (solid) or in SM (liquid; Appendix F). All strains grown on SPO were analyzed after 4 days of sporulation at 30°C. All strains grown in SM were analyzed after 45 hours of liquid sporulation at 30°C in shaker incubator. All strains analyzed were counted on the same day.

Data Referenced in Results

Spore viability of Rfa2 N-terminal mutants from multiple genetic backgrounds

This data was collected to assemble the graphs shown in Figure 4.9, as the differences in tetrad spore viability is more apparent when shown as a figure rather than in a table. Shown as a figure however excludes the number of tetrads examined and the percentage of total viable spores, so those are also included in the table below (Table I3). See “Results” in Chapter 4 for further commentary on experimental observations.

Table I3. Spore viability of Rfa2 NT mutants in multiple genetic backgrounds

Strain Background	Relevant Genotype	Days ^a	Viable: Inviable					# Tetrads Examined	% Spore Viability
			4:0	3:1	2:2	1:3	0:4		
JSJ1	<i>RFA2</i>	4	31	6	2	0	0	39	93.6
	<i>rfa2-A_x</i>		36	3	1	0	0	40	96.9
	<i>rfa2-D_x</i>		27	6	5	0	0	38	89.5
	<i>rfa2-ΔN_x</i>		20	12	5	0	1	38	82.9
RM96	<i>RFA2</i>	4	95	11	10	0	1	117	92.5
	<i>rfa2-A_x</i>		104	10	4	0	0	118	96.2
	<i>rfa2-D_x</i>		87	22	10	0	0	119	91.2
	<i>rfa2-ΔN_x</i>		39	43	20	16	2	120	71.0
RM96	<i>RFA2</i>	7	55	5	0	0	0	60	97.9
	<i>rfa2-A_x</i>		54	4	2	0	0	60	96.7
	<i>rfa2-D_x</i>		34	21	4	1	0	60	86.7
	<i>rfa2-ΔN_x</i>		20	14	12	10	2	58	67.2
SJH2-1	<i>RFA2</i>	4	333	223	79	20	14	669	81.4
	<i>rfa2-A_x</i>		347	199	61	20	6	633	84.0
	<i>rfa2-D_x</i>		349	322	165	43	12	891	76.7
	<i>rfa2-ΔN_x</i>		70	202	308	304	137	1,021	44.2

^a Number of days incubated at 30°C on solid sporulation media. The viable: inviable spore ratio was recorded for each tetrad dissected. The total number of tetrads examined is listed for each strain. The overall percentage of spore viability was determined from the total number of viable spores and the total number of spores dissected.

APPENDIX J. STATISTICAL ANALYSIS OF CHAPTER 5 DATA

The following tables contain the statistical analyses performed on the cell cycle arrest and checkpoint adaptation data presented in Chapter 5, Figure 5.8.

Table J1. Statistical analysis of mutant cellular arrest compared to wild-type arrest

Relevant strain genotype	Mean (%)	Variance (%)	Observations	P (one-tail)	P (two-tail)
WT (<i>sml1Δ</i>)	80.7	± 0.31	3	NA	NA
<i>rdh54Δ</i>	81.7	± 0.90	3	0.444	0.888
<i>mec1-S1964A</i>	79.8	± 0.30	3	0.426	0.852
<i>mec1-S1964A rfa2-A_x</i>	78.7	± 0.44	3	0.353	0.706
<i>mec1-S1964A rfa2-D_x</i>	79.6	± 0.64	3	0.425	0.851
<i>mec1-S1964A rfa2-ΔN_x</i>	73.9	± 0.64	3	0.148	0.297
<i>mec1-S1964A rfa2-H2NT</i>	83.9	± 0.12	3	0.229	0.458
<i>mec1-S1964A rfa2-K_xR</i>	77.8	± 0.66	3	0.321	0.642
WT (<i>sml1Δ</i>)	79.9	± 0.21	3	NA	NA
<i>rdh54Δ</i>	80.9	± 0.79	3	0.438	0.875
<i>mec1-S1964E</i>	84.5	± 0.10	3	0.113	0.226
<i>mec1-S1964E rfa2-A_x</i>	84.3	± 0.61	3	0.231	0.461
<i>mec1-S1964E rfa2-D_x</i>	82.9	± 0.004	3	0.190	0.381
<i>mec1-S1964E rfa2-ΔN_x</i>	80.9	± 0.31	3	0.417	0.834
<i>mec1-S1964E rfa2-H2NT</i>	80.4	± 0.18	3	0.445	0.889
<i>mec1-S1964E rfa2-K_xR</i>	80.3	± 0.02	3	0.451	0.901

Statistical analysis was performed in Microsoft Excel using the t-test for two-sample comparison assuming unequal variances.

Table J2. Statistical analysis of adaptation at 24 hours of all mutants compared to wild-type

Relevant strain genotype	Mean (%)	Variance (%)	Observations	P (one-tail)	P (two-tail)
WT (<i>sml1Δ</i>)	91.3	± 0.02	3	NA	NA
<i>rdh54Δ</i>	22.1	± 2.05	3	0.007	0.014
<i>mec1-S1964A</i>	34.2	± 0.29	3	0.002	0.003
<i>mec1-S1964A rfa2-A_x</i>	22.4	± 0.24	3	0.001	0.002
<i>mec1-S1964A rfa2-D_x</i>	73.3	± 0.23	3	0.013	0.026
<i>mec1-S1964A rfa2-ΔN_x</i>	26.3	± 2.83	3	0.011	0.022
<i>mec1-S1964A rfa2-H2NT</i>	85.0	± 0.50	3	0.136	0.273
<i>mec1-S1964A rfa2-K_xR</i>	84.4	± 0.03	3	0.004	0.007
WT (<i>sml1Δ</i>)	91.9	± 0.05	3	NA	NA
<i>rdh54Δ</i>	28.4	± 0.37	3	0.0002	0.0004
<i>mec1-S1964E</i>	93.9	± 0.02	3	0.138	0.277
<i>mec1-S1964E rfa2-A_x</i>	88.7	± 0.04	3	0.076	0.151
<i>mec1-S1964E rfa2-D_x</i>	93.9	± 0.02	3	0.149	0.299
<i>mec1-S1964E rfa2-ΔN_x</i>	51.5	± 2.26	3	0.022	0.044
<i>mec1-S1964E rfa2-H2NT</i>	93.1	± 0.05	3	0.265	0.530
<i>mec1-S1964E rfa2-K_xR</i>	95.1	± 0.03	3	0.064	0.127

Statistical analysis was performed in Microsoft Excel using the t-test for two-sample comparison assuming unequal variances.

Table J3. Statistical analysis of adaptation at 24 hours of all *mec1 rfa2* mutants compared to the *mec1* mutant containing wild-type *RFA2*

Relevant strain genotype	Mean (%)	Variance (%)	Observations	P (one-tail)	P (two-tail)
<i>mec1-S1964A</i>	34.2	± 0.29	3	NA	NA
<i>rdh54Δ</i>	22.1	± 2.05	3	0.133	0.266
<i>mec1-S1964A rfa2-A_x</i>	22.4	± 0.24	3	0.024	0.048
<i>mec1-S1964A rfa2-D_x</i>	73.3	± 0.23	3	0.0004	0.0007
<i>mec1-S1964A rfa2-ΔN_x</i>	26.3	± 2.83	3	0.261	0.521
<i>mec1-S1964A rfa2-H2NT</i>	85.0	± 0.50	3	0.0003	0.0006
<i>mec1-S1964A rfa2-K_xR</i>	84.4	± 0.03	3	0.002	0.004
<i>mec1-S1964E</i>	93.9	± 0.02	3	NA	NA
<i>rdh54Δ</i>	28.4	± 0.37	3	0.001	0.003
<i>mec1-S1964E rfa2-A_x</i>	88.7	± 0.04	3	0.018	0.035
<i>mec1-S1964E rfa2-D_x</i>	93.9	± 0.02	3	0.480	0.960
<i>mec1-S1964E rfa2-ΔN_x</i>	51.5	± 2.26	3	0.020	0.040
<i>mec1-S1964E rfa2-H2NT</i>	93.1	± 0.05	3	0.314	0.628
<i>mec1-S1964E rfa2-K_xR</i>	95.1	± 0.03	3	0.201	0.403

Statistical analysis was performed in Microsoft Excel using the t-test for two-sample comparison assuming unequal variances.

Table J4. Statistical analysis of adaptation at 48 hours of all mutants compared to wild-type

Relevant strain genotype	Mean (%)	Variance (%)	Observations	P (one-tail)	P (two-tail)
WT (<i>sml1Δ</i>)	94.8	± 0.004	3	NA	NA
<i>rdh54Δ</i>	27.7	± 3.13	3	0.011	0.022
<i>mec1-S1964A</i>	61.1	± 0.01	3	0.00001	0.00002
<i>mec1-S1964A rfa2-A_x</i>	32.9	± 0.10	3	0.0004	0.0009
<i>mec1-S1964A rfa2-D_x</i>	86.0	± 0.06	3	0.014	0.027
<i>mec1-S1964A rfa2-ΔN_x</i>	27.9	± 1.57	3	0.006	0.012
<i>mec1-S1964A rfa2-H2NT</i>	89.9	± 0.33	3	0.137	0.274
<i>mec1-S1964A rfa2-K_xR</i>	89.6	± 0.11	3	0.056	0.112
WT (<i>sml1Δ</i>)	94.9	± 0.004	3	NA	NA
<i>rdh54Δ</i>	35.2	± 0.28	3	0.001	0.003
<i>mec1-S1964E</i>	96.4	± 0.02	3	0.075	0.151
<i>mec1-S1964E rfa2-A_x</i>	95.0	± 0.02	3	0.457	0.915
<i>mec1-S1964E rfa2-D_x</i>	92.9	± 0.003	3	0.007	0.013
<i>mec1-S1964E rfa2-ΔN_x</i>	63.7	± 1.90	3	0.030	0.060
<i>mec1-S1964E rfa2-H2NT</i>	93.6	± 0.15	3	0.316	0.632
<i>mec1-S1964E rfa2-K_xR</i>	95.4	± 0.04	3	0.361	0.722

Statistical analysis was performed in Microsoft Excel using the t-test for two-sample comparison assuming unequal variances.

Table J5. Statistical analysis of adaptation at 48 hours of all *mec1 rfa2* mutants compared to the *mec1* mutant containing wild-type *RFA2*

Relevant strain genotype	Mean (%)	Variance (%)	Observations	P (one-tail)	P (two-tail)
<i>mec1-S1964A</i>	61.1	± 0.01	3	NA	NA
<i>rdh54Δ</i>	27.7	± 3.13	3	0.041	0.083
<i>mec1-S1964A rfa2-A_x</i>	32.9	± 0.10	3	0.002	0.005
<i>mec1-S1964A rfa2-D_x</i>	86.0	± 0.06	3	0.0003	0.0006
<i>mec1-S1964A rfa2-ΔN_x</i>	27.9	± 1.57	3	0.022	0.045
<i>mec1-S1964A rfa2-H2NT</i>	89.9	± 0.33	3	0.007	0.013
<i>mec1-S1964A rfa2-K_xR</i>	89.6	± 0.11	3	0.002	0.005
<i>mec1-S1964E</i>	96.5	± 0.02	3	NA	NA
<i>rdh54Δ</i>	35.2	± 0.28	3	0.001	0.003
<i>mec1-S1964E rfa2-A_x</i>	95.0	± 0.02	3	0.118	0.237
<i>mec1-S1964E rfa2-D_x</i>	92.9	± 0.003	3	0.011	0.022
<i>mec1-S1964E rfa2-ΔN_x</i>	63.7	± 1.90	3	0.027	0.055
<i>mec1-S1964E rfa2-H2NT</i>	93.6	± 0.15	3	0.176	0.351
<i>mec1-S1964E rfa2-K_xR</i>	95.4	± 0.04	3	0.253	0.506

Statistical analysis was performed in Microsoft Excel using the t-test for two-sample comparison assuming unequal variances.